THERMODYNAMICS LABORATORY
AEROSPACE AND MECHANICAL ENGINEERING DEPARTMENT
UNIVERSITY OF LIEGE

Contribution to the Characterization of Piston Expanders for their Use in Small-Scale Power Production Systems

A Thesis

Submitted to the Faculty of Applied Sciences

of the

University of Liège (Belgium)

by

Jean-François Oudkerk

In partial fulfillment of the requirements for the degree

of

Doctor of Applied Sciences

Liège, August 2016

Acknowledgements

I would like to thank Prof. Vincent Lemort who gave me the opportunity to work in his team and to do this thesis. I'm grateful for his encouragement, his trust and all what I learned from him.

I would also like to thank all the people I had the chance to work with during these years. A large part of this work would not have been possible without the help, trust and involvement of Thierry Carrette, Pierre Detré and Thomas Briamont from Coretec and Remi Daccord, Julien Melis and Antoine Darmedru.

Thank you to all my colleagues from the Thermodynamics Laboratory for their help, their support, the team spirit and all the enjoyment we had together. Special thanks to Richard Labenda, Bernard Loly and José Concha for their work on test benches and their numerous sound advices.

I also want to thank all my friends to be there in good and hard times, special thanks go to "La Chaîne" for their presence during this thesis.

I thank my mother and Jean for their sacrifices, unwavering support and love. Finally, a very special word of thanks to Marie for her encouragement and help.

Abstract

Piston expanders are well suited for small scale power generation (<50kW) using heat engines such as Ericsson engine or Organic Rankine Cycle (ORC) system. Both systems offer the possibility to use renewable energy sources and are increasingly considered in light of the economic and environmental context. This thesis aims at contributing to the knowledge and the development of piston expanders by presenting modeling, simulation and experimental investigations.

Two types of piston engine models are proposed. The first type (denoted as “detailed”) describes the shaft angle (or time) evolution of the state of the fluid in the control volume limited by the cylinder wall and the piston. The second type of model (denoted as “semi-empirical”) is based on theoretical indicator diagram. A calibration process is proposed and applied with the measurement collected on two different expanders.

The detailed model is first used to simulate an Ericsson engine. The simulations allow for the optimization of the pressure ratio, the determination of the ratio between the swept volumes of the expander and the compressor, the computation of the valve timing and the evaluation of the potential performances.

The main modifications made to turn an available Internal Combustion Engine (ICE) into an Ericsson engine are described. This prototype is then tested but did not run as expected. The identified reasons are a too high leakage rate, a too large cut-off ratio and a too low expander supply temperature. These three features led to insufficient pressure. Nevertheless, a compressor is used to rise the pressure up to 7 bar in order to test the expander part. This expander shows a maximal isentropic efficiency of 59% at 600 RPM with a pressure ratio of 5.

A swash-plate expander integrated into an ORC using R245fa is also investigated in a wide range of operating conditions. Performance maps in terms of pressure ratio and rotational speed are given. Maximal reached isentropic efficiency is 54% at 2500 RPM for a pressure ratio of 10.5.

Experimental results obtained on both expanders are analyzed with the same methodology to assess the importance of each source of losses. This methodology is based on the disaggregation of the isentropic efficiency into different factors. Each of these factors represents one source of losses. In-cylinder pressure measurements are performed in order to measure mechanical losses. Leakage effects are simulated with the detailed model.

Finally, an Ericsson engine-based m-CHP unit and an ORC-based m-CHP unit using the swash-plate expander are simulated with the validated semi-empirical model. Ericsson engine system shows a 6.5% electrical efficiency while the ORC system shows en efficiency of 8.2%. For both systems, possible improvements are simulated. It is shown, among other things, that the benefit of an increase of the built-in volume is limited by the decrease of the mechanical efficiency.

Contents

Nomenclature

AU	Overall heat transfer coefficient [W/K]
A_v	Valve flow cross section area [m]
B	Connecting rod length [mm]
$\dot{C}$	Heat capacity flow [W/K]
C_d	Flow coefficient [-]
CF	Clearance factor [-]
CO	Cut-off ratio [-]
C_p	Mean piston speed [m/s]
c_p	Constant pressure specific heat capacity [J/(K.kg)]
c_v	Constant volume specific heat capacity [J/(K.kg)]
D	Bore diameter [m]
D_s	Valve stem diameter [m]
D_v	Valve head diameter [m]
D_{vi}	Valve inner seat diameter diameter [m]
e	Fuel CO2 specific emission [kgCO2/MWh]
$\dot{E}_{out}$	Net outlet energy flow [W]
$fmep$	Friction mean effective pressure [bar]
h	Specific enthalpy [J/kg]
h_c	Convective heat transfer coefficient [W/(K.m²)]
$\dot{H}_{in}$	Net inlet enthalpy flow [W]
$imep$	Indicated mean effective pressure [bar]
L	Piston stroke [m]
LHV	Lower heating value [W/kg]
L_v	Valve lift [m]
$\dot{M}$	Mass flow rate [kg/s]
m	Mass [kg]
$MARE$	Mean Relative Error [%]
N	Rotational speed [Hz]
n_{cyl}	Number of cylinders [-]
Nu	Nusselt number [-]
P	Pressure [Pa]
PES	Primary Energy Saving [%]
Pr	Prandtl number [-]
$\dot{Q}$	Heat power [W]
Ra	Rayleight number [-]]
Re	Reynolds number [-]
R_p	Pressure ratio [-]
r_T	Temperature ratio [-]
$r_{v,in,cp}$	Compression built-in volume ratio [-]
$r_{v,in,exp}$	Expansion built-in volume ratio [-]
t	Time [s]
u	Specific internal energy [J/kg]
V	Inlet closing or cut-off volume [m³]
v	Specific volume [m³/kg]
V_0	Clearance volume [m³]
V_{tot}	Volume total [m³]
$\dot{W}$	Mechanical or electrical power [W]
W	Work [J]

Greek symbols

ϵ_{in}	Diagram factor [-]
ϵ_s	Isentropic efficiency [-]
$\epsilon_{sp,in}$	Specific diagram factor
η	Efficiency [-]
γ	Isentropic ratio [-]
ω	Rotational speed [°/s]
ϕ	Filling factor [-] or Volume ratio [-]
ϕ_{in}	Internal filling factor [-]
ϕ_l	Leakages filling factor [-]
ρ	Density [kg/m³]
σ	Standard deviation
θ	Shaft angle [°]

Subscripts

a	Air
amb	Ambient
$CCGT$	Combined Cycle Gas Turbine
cd	Condensing or Condenser
CHP	Combined heat and power
cor	Corrected
cp	Compressor
$crit$	Critic
$down$	Downstream
EC	Exhaust closing
el	Electric
EO	Exhaust opening
ev	Evaporating or Evaporator
ex	Exhaust
exp	Expander
g	Saturated gases
hx	Heat exchanger

IC	Inlet closing
IC	Inter cooler
in	Indicated or Internal
s	Entropy [J/(kg.K)]
S_{co2}	CO2 Saving [kgCO2/MWhe]
T	Temperature [°C] or torque [N.m]
IO	Inlet opening
l	Saturated liquid
$leak$	Leakage
$loss$	Losses
m	Mechanical
mf	Mechanical friction
min	Minimum
n	Net
opt	Optimal
out	Out or Outdoor
pp	Pump or Pinch-Point
ref	Reference
reg	Regenerator
s	Isentropic
sc	Sub cooling
sh	Shaft
sh	Super heating
su	Supply
th	Theoretical or Thermic
thr	Nozzle throat
up	Upstream
w	Wall or Water
wf	Working fluid

Acronyms

BTC	Bottom Dead Center
CCGT	Combined Cycle Gas Turbine
CHP	Combined Heat and Power
HTF	Heat Transfer Fluid
IC	Inter Cooler
ICE	Internal Combstion Engine
IPCC	Intergovernmental Panel on Climate Change
ORC	Organic Rankine Cycle
PV	Pressure Volume
RC	Rankine Cycle
TDC	Top Dead Center
WHR	Waste Heat Recovery

Chapter 1: Introduction

Contents

1. Context

From an economic point of view, the rise of energy price over the last 20 years has pushed our society to consume energy more and more rationally. For this purpose, new and more efficient systems are in development such as waste heat recovery, cogeneration or use of solar energy.

Moreover, before 2003, the European electricity market was subject to a regulated natural monopoly. Since 2004 for the professional sector and 2007 for private individuals, the electricity and gas markets have been liberalized (SPF Economie 2008). This liberalization has given the opportunity to everyone connected to the electricity grid to produce and sell electricity. Consequently, today, everyone can make profitable a distributed electricity production such as photovoltaic panels or CHP unit.

Another important purpose is the energetic dependence. Indeed, the European Union meets 50 % of its energy needs with importation and this ratio will reach 70 % in 2030 if the trend is maintained (Comission Européenne 2006). This strong dependency on exporting countries could lead to a lack of supply and a more accentuated price rise.

Another observation is that, in this beginning of 21st century, environmental and energetic concerns have never been so strong. Indeed, the fossil energy resources are in depletions and their use leads to a pollution of the environment. Table 1-1 summarizes the situation of the world fossil fuels reserves (these numbers have to be considered as orders of magnitude given the incertitude linked to this matter).

Table 1-1: World fossil fuels reserves (AFH2 2007)

	Proven world reserve [Gtep]	Annual consumption [Gtep]	Duration (at current consumption rate) [year]
Oil	~140	3.9	~40
Natural gas	~160	2.4	~60
Coal	~600	2.8	~200

Concerning the pollution associated to the use of fossil fuels, CO2 emissions are generally the first concern. Indeed, according to the IPCC, greenhouse gas emissions are leading to climate change, which will cause dramatic consequences for the planet such as melt of ice sheet, rise of sea level, increase of natural disasters frequency and negative impacts on biodiversity. Among greenhouse gases, CO2 is the principal one and 84% of its emissions are attributed to the energy sector (Quadrelli and Peterson 2007).

Hence, the necessity to reduce fossil fuels consumption and emissions of greenhouse gases has been pointed out for several years. This necessity led to international treaties such as the Kyoto protocol in 1997 (AFH2 2007). This one aims for the stabilization of the greenhouse gases to the 1990 level. More recently, in 2015, the COP21 took place in Paris where 195 states agreed to limit the increase in global average temperature below 2°C compared to pre-industrial level by reducing greenhouse gas emission. Each country has to publish its contribution depending on their specificities and constraints.

In order to improve the situation in Europe, several regulations and directives concerning the rational use of energy and pollutant emissions give some guidelines and constraints to the Member States. For example, directive 2010/31/UE concern the buildings energetic performance and constrains Member States to ensure a feasibility study on high efficiency system (such as CHP) to be performed for each new building. The directive 2004/8/CE gives a common framework for high efficiency cogeneration and constrains States to publish reports on the state of this sector and to encourage it. The regulation (EC) No 715/2007 fixes the rules to measure pollutant emissions and maximal values of these emissions. In a more general way, the decision No 406/2009/EC gives the contribution of each Member State in order to respect commitments in terms of reduction of greenhouse gases.

Through this context analysis, it can be concluded that alternatives to the current energy sources and conversion systems are needed in terms of economic and environmental purposes. To push forward this energetic transition, authorities have started to put in place incentives, regulations and frameworks. Moreover, profitable opportunities can be found in this energetic challenge.

2. Motivation of the work

The analyses of economic, environmental and political contexts show the need to develop more efficient use of energy as well as to shift from fossil fuels to renewable energy sources. In this scope, small-scale Ericsson engine and Rankine Cycle (RC) or Organic Rankine Cycle (ORC) are interesting and gain more and more interest. Indeed, both systems are external combustion engines and then show the advantage to allow the small scale (<50 kW) production of electricity by using renewable heat sources such as biomass, solar and geothermal especially for CHP application. Another main application is the recovery of heat loss from industrial processes and from automotive and truck Internal Combustion Engines (ICE).

While large-scale ORC plants use turbomachines as expansion machines, volumetric expanders such as scroll, screw or piston machines are often preferred for small-scale applications. In the same way, the Ericsson engine operates with the same thermodynamic cycle as the gas turbine (the Brayton cycle) but uses piston machines instead of turbomachinery. Indeed, according to several studies, volumetric expanders are more suited for small-scale application because of their lower rotational speed. In a general way, the similarity concept using specifics speed (Ns) and diameter (Ds) gives boundaries between technologies of expansion machine (Baljé 1962). This concept is illustrated by the Ds-Ns diagram shown in Figure 1-1 where efficiency maps are plotted for turbo machinery and volumetric machines. This diagram shows that volumetric machines such as pistons expanders are suited for low specific rotational speeds, while turbines have good efficiency at high specific speed. As specific speed is proportional to the square root of the volume flow rate, low specific speed means low volume flow capacity and small-scale power.

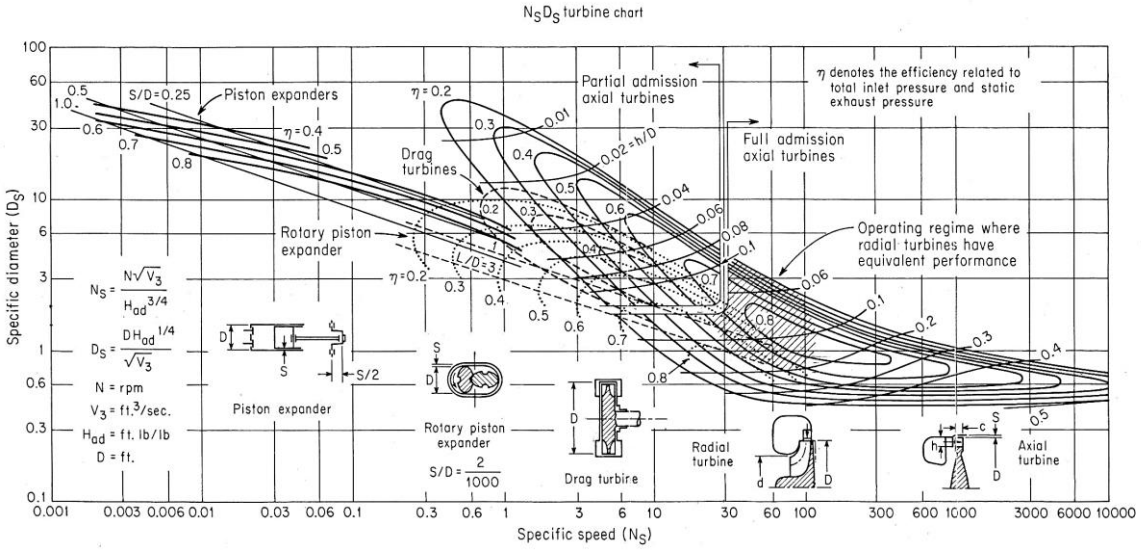

Figure 1-1: Specific speed and diameter diagram (Baljé 1962)

In addition to the low rotational speed, volumetric expanders have the advantages to handle high pressure ratio and the ability to ingest liquid droplets. On the other hand, they are generally bulkier than turbines. Recently, a lot of researches and developments have been carried out on positive displacement machines for small-scale applications. Most of these works deal with scroll, screw, piston and vane types. Among these different expander types, piston type shows some advantages such as larger built-in volume ratio, high robustness and high achievable supply pressure and temperature. For these different reasons, piston expanders are more and more considered for ORC and , especially for micro-CHP applications and for waste heat recovery in mobile applications. However, there is a lack of modern scientific literature with experimental work focusing on piston expander used in ORC . Indeed, most of the experimental publications focus on the system level and did not enter in detail concerning the losses affecting the expander. Moreover, less publications can be found on piston expanders compared to other type of volumetric engines. For example, in (Quoilin 2015), a database of 954 publications from 1972 to 2015 on ORC from Elsevier, Sage, ASME and MDPI relates 51 publications specifically on volumetric expanders. From these 51 publications, only 4 are related to piston expanders while 23 deal with scroll expanders and 11 with screw expanders. Regarding Ericsson engines, only 3 modern experimental campaigns have been found in the literature by the author (an exhaustive literature review will be presented in Chapter 2).

Consequently, the main objective of this thesis is to characterize operation of modern piston expanders used in ORC and Ericsson engines through the identification and quantification of losses and potential improvements. Other objectives are to propose efficient ways to model piston expanders for simulation in thermal systems and to evaluate performance of CHP-applications using such technologies.

3. Overview

The present thesis is organized as follows:

Chapter 2 summarizes the state-of-the-art of piston expanders and their use in Ericsson engines and Rankine cycle systems. The piston expander is described in terms of working principle, mechanical design, thermodynamic aspects and performance indicators. Then Ericsson engine and Rankine cycle system basic principles are recalled and a review of the use of piston expanders for these applications is presented.

Chapter 3 presents two simulation models. The first model, more detailed, is based on the evolution over one revolution of the state of the working fluid in the control volume defined by the cylinder. The second model, denoted as a "semi-empirical" model, is based on the theoretical indicator diagram. Both are 0D model but the first one is time dependent and uses a detailed geometrical description while the second uses lumped parameters.

Chapter 4 describes the experimental work done by the author in the context of a project aiming at developing an Ericsson engine by modifying an existing ICE. First, the detailed simulation model is used to design main geometrical parameters. Then, the modifications made on the ICE to build the prototype are presented. Finally, experimental results are exploited to analyse the performance and the losses of the expander part of the engine and to validate the models presented in Chapter 3.

Chapter 5 presents the experimental investigation performed on a swash plate piston expander integrated into an ORC system. Isentropic efficiency and shaft power maps are established with the measurements. Then, as in Chapter 4, analyses of the different sources of losses are presented and models are validated.

Chapter 6 aims at evaluating performance of cogeneration systems. The first system is based on an Ericsson engine with the piston machine tested in Chapter 4 while the second system uses an ORC system with the piston expander tested in Chapter 5. Evaluation of CHP efficiencies is obtained by simulation with the help of the semi-empirical models validated with the experimental results.

4. References

AFH2. 2007. “Situation Mondiale de l’Energie.” Mémento de l’Hydrogène Fiche 2.1. Association Française de l’Hydrogène.

Baljé, O. E. 1962. “A Study on Design Criteria and Matching of Turbomachines: Part A—Similarity Relations and Design Criteria of Turbines.” *Journal of Engineering for Power* 84 (1): 83. doi:10.1115/1.3673386.

Comissoin Européenne. 2006. “Attitudes Au Sujet de L’énergie.” Eurobaromètre Spécial.

Quadrelli, R., and S. Peterson. 2007. “The Energy–climate Challenge: Recent Trends in CO2 Emissions from Fuel Combustion.” *Energy Policy* 35 (11): 5938–52. doi:10.1016/j.enpol.2007.07.001.

Quoilin, S. 2015. “Keynote Lecture: Past and Current Research Trends in ORC Power Systems.” In *3rd International Conference on ORC Power Systems*. Brussels, Belgium. http://orbi.ulg.ac.be/handle/2268/186850.

SPF Economie. 2008. “Projet d’Etude Sur Les Perspectives d’Approvisionement En Electricité.” Belgique: Bureau Fédéral du Plan.

Chapter 2: Piston expanders and their use in Rankine cycle and Ericsson heat engines

Contents

1. Introduction

The piston expander, or reciprocating expander, is one of the major types of positive displacement expander. This type of machine converts the energy contained in a pressurized fluid into mechanical energy by increasing the volume of a working chamber and then, decreasing the pressure of the fluid.

The piston expander is among the oldest displacement machines. It has been largely used during the Industrial Revolution and up to the beginning of the 20th century. There is currently a large regain of interest for piston expanders in small-scale application such as Ericsson engine and Rankine cycle systems used for micro-CHP, solar application and waste heat recovery on internal combustion engines (see literature review in section 3.2 and 4.2). Piston expanders actually show some advantages over other expansion machines, such as larger built-in volume ratio, high achievable operating pressures and temperatures, their ability to ingest liquid and low rotational speeds.

2. Piston expander description

2.1. Working principle

Reciprocating expanders use one or several pistons moving inside cylinders from the top dead center (TDC) to the bottom dead center (BTC) with a reciprocating motion. The cylinder has some openings by which the working fluid can enter and leave the cylinder. In order to explain the working principle of such expander, a theoretical pressure-volume diagram, called “indicator diagram”, is shown in Figure 2-1. This diagram shows the six steps of the expansion process.

At initial position 1, the piston is at the TDC and the volume is clearance volume V_0. At this point, the inlet ports opens and the piston starts its down-stroke. The pressurized fluid enters into the cylinder until the inlet port closes. The volume at this moment is the cut-off volume and is generally described by the cut-off ratio defined as the ratio between the inlet closing volume (V_{IC}) and the total volume (V_{tot}).

$$CO = \frac{V_{IC}}{V_{tot}} \quad (2\text{-}1)$$

Then, at position 2, inlet and exhaust ports are both closed and the expansion of the fluid begins. Indeed, the volume in the cylinder increases while the piston continues his down-stroke, leading to a decrease of the pressure. This process takes part until the piston reaches the BTC at which the volume is maximal (V_{tot}). The built-in volume ratio is defined as the ratio between the volumes at the end and at the beginning of the expansion. Depending on pressure ratio applied to the expander and on the built-in expansion volume ratio, the pressure at the end of expansion process is either higher (under expansion), equal, or lower (over expansion) than the exhaust pressure.

$$r_{v,in,exp} = \frac{V_{tot}}{V_{IC}} = \frac{1}{CO} \quad (2\text{-}2)$$

When the piston reached the BDC (point 3), the exhaust port opens and some fluid leaves or enters the cylinder (depending whether the pressure is respectively higher or lower than the exhaust pressure) until

pressure inside the cylinder reaches the exhaust pressure. At this position, the piston starts its up-stroke and pushes out the remaining fluid. This exhaust process occurs until the exhaust ports are closed.

At position 5, the exhaust ports closes and the inlet port remains closed. From this position, the piston continues is up-stroke towards the TDC and the fluid is compressed. This compression phase lasts until the piston reaches the TDC. The built-in compression ratio is defined as the ratio between the volumes at the beginning and at the end of the compression. These two volumes are respectively the exhaust closing volume (V_{EC}) and the clearance volume (V_0).

$$r_{v,in,cp} = \frac{V_{EC}}{V_0} \qquad (2\text{-}3)$$

Similarly to the expansion process, three different situations may occur at the end of compression process: pressure is higher (over compression), equal or lower (under compression) than the supply pressure.

When the piston is back to the TDC, inlet port opens and some fluid enters or leaves the cylinder, respectively in the case of under or over compression, until the pressure in the cylinders is equal to the supply pressure.

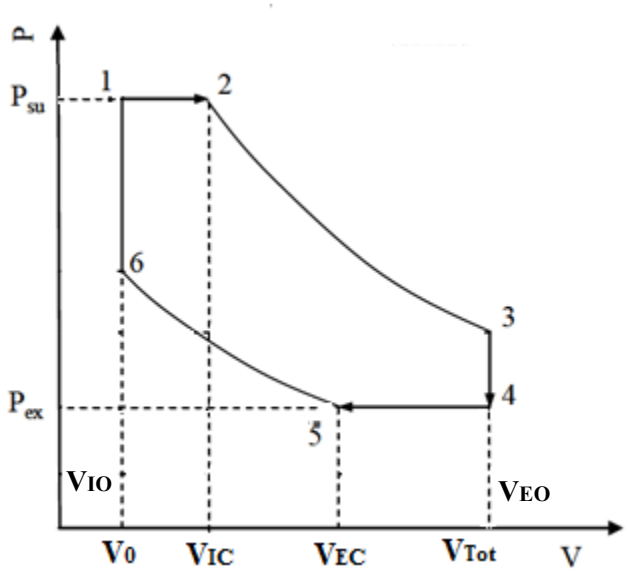

Figure 2-1: Theoretical indicator diagram of a piston expander

This description of the working principle of piston expander shows that four main geometrical parameters allow describing the theoretical indicator diagram: the total displacement V_{tot}; the clearance volume V_0; the inlet closing volume V_{IC} and the exhaust closing volume V_{EC}. As it will be shown latter, these parameters determine the power and mass flow rate of the expander.

It should be noted that in practice, the inlet valve can open before the piston reaches the TDC and the inlet opening volume V_{IO} can be different than the clearance volume. In the same way, the exhaust valve can open before the piston reaches the BDC and the exhaust opening volume V_{EO} can be different of the total displacement. This anticipation of the opening of the ports can be done in order to reduce the pressure

drop or can be a consequence of the type of valves used, as with piston-controlled exhaust port where $V_{EO} = V_{EC}$.

2.2.Mechanical design

Different types of piston expander exist and are characterized by their mechanical design. Reciprocating expanders differ by:

- The mechanism used to convert the reciprocating motion into a rotating motion
- The type of valves and their location
- The action of the fluid upon the piston, simple or double acting

2.2.1. Reciprocating motion conversion system

The reciprocating motion of the piston is not easy to use directly and is more often converted into a rotational motion. In order to do this, two main mechanisms are used: crank train or swash/wobble plate. The crank train mechanism is composed of a camshaft and connecting rods connected to the piston pins and the crank pins. This system is the one used in internal combustion engines (ICE). In axial piston machine, the pistons are disposed in parallel and around the shaft. The rotational motion of the shaft is converted into a reciprocating motion with the help of tilted plate connected to the pistons rods. The rods are either fixed to this plate with ball joints or are sliding on the plate and linked to it with cams. In the former system, the plate has an oscillating movement and is called “wobble plate”. In the second system, the plate rotates and is called “swash plate”. For the wobble plate, the oscillation movement induced by a Z-shaft or by a second tilted plate (see Figure 2-3). Axial piston machines are often used as compressors in mobile air conditioning applications and are more compact than crank train piston machines.

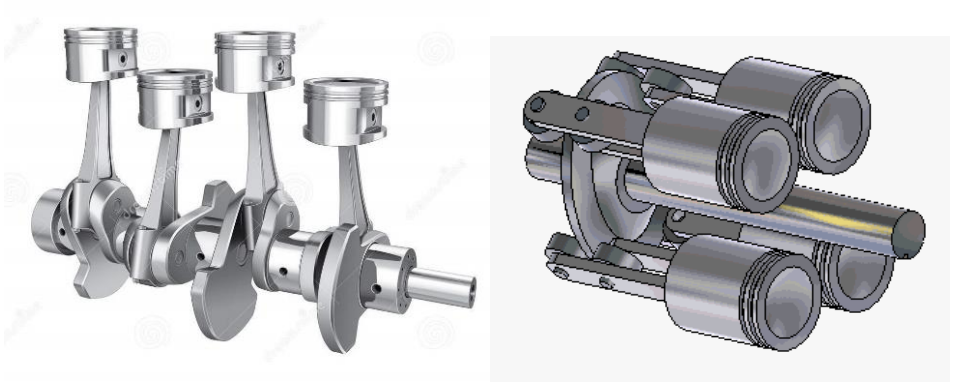

Figure 2-2: Reciprocating to rotational motion system conversion. Crankshaft on the left and swash-plate on the right.

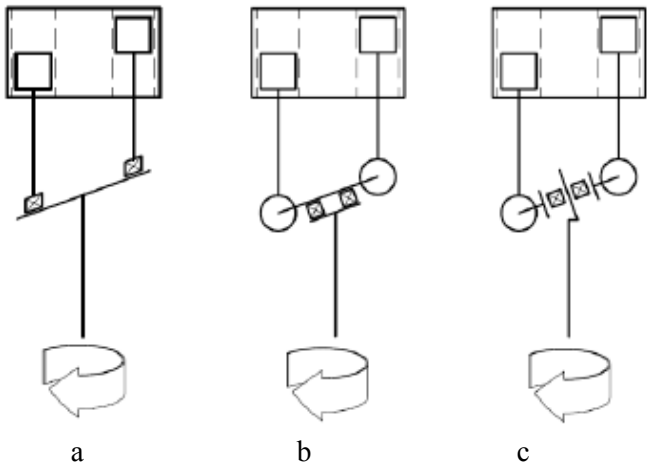

Figure 2-3: Axial piston mechanism: a) swash plate, b) wobble plate with sliding plate, c) wobble plate with Z-shaft (Grip 2009)

Some piston expanders are classified as "free-piston" engines. In this configuration, the reciprocating motion of the pistons is directly used to activate a piston compressor (e.g. in Ericsson engine (Mikalsen and Roskilly 2012) or in CO2 compression cycle (Heyl and Quack 1999)) or to produce electricity with a linear generator. This configuration has less moving parts in contact and hence less friction losses.

2.2.2. Types of valves

Unlike in piston compressors, the pressure gradient across the expander is in the opposite direction to the fluid flow. Consequently, check valves cannot be used and the opening and closing of the ports have to be actuated. This actuation system makes the expander more complex and then less robust and leads to additional losses.

As explained above, the inlet and exhaust closing and opening volumes define the operating cycle of the piston expander. So it is the timing of the valves, i.e. the moments at which the vales open and close, that determines important geometrical parameters such as the cut-off ratio and the built-in compression ratio.

Different types of valves and actuation systems can be used. The main types are poppet valves (as in fours stroke ICE), piston-controlled ports (as in small two stroke ICE), rotary valves and sliding valves (Figure 2-4). The valves are usually mechanically actuated but sometimes electrical actuation is used, for example with solenoid valves, to easily control and modify the timing of the valves. Poppet valves are generally actuated with a camshaft and the profile and the position of the cams defined the timing. Since piston-controlled ports are closed and opened by the piston covering and uncovering the ports, they do not need an actuation system and are then simpler and avoid valve train mechanical losses. The timing is fixed by the position of the port along the cylinder and the opening and closing is always symmetrical with respect to top dead center. With rotary valves, the timing can be modified by modifying the rotational speed of the valve. An effective way to control the opening duration of a port is to use two valves in series and to adjust the opening overlap.

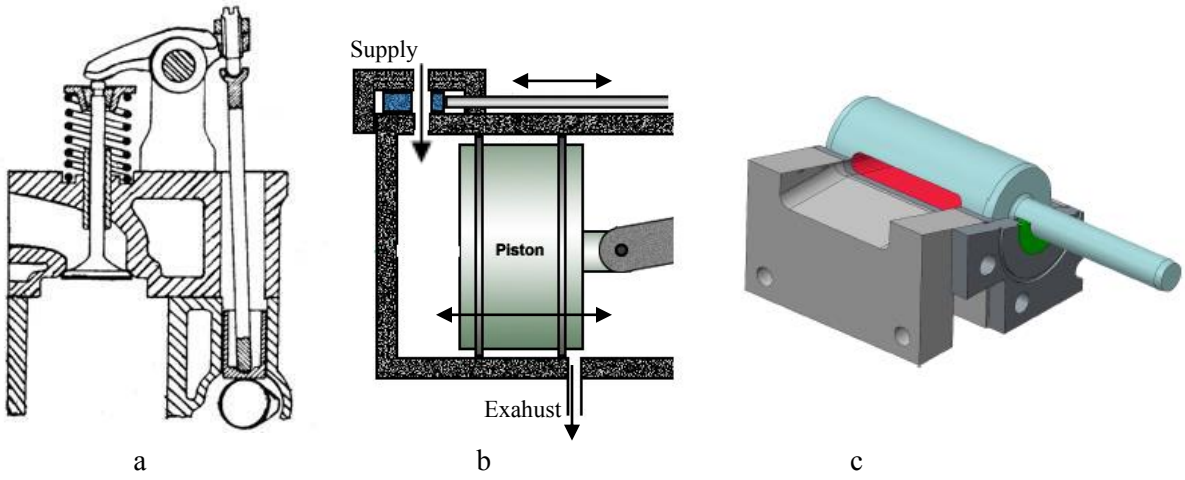

Figure 2-4: Types of valve: a) poppet valve, b) supply sliding valve and piston-controlled exhaust port, c) rotary valve (Wronski 2015)

The location of supply and exhaust valves can differ, determining the flow configuration. In crossflow engine, both supply and exhaust valves are located close or on the cylinder head. In uniflow expander, the supply port is close to the cylinder head while the exhaust port is close to the bottom of the cylinder and is in general a piston-controlled exhaust port (see Figure 2-4). Some engines, denoted as multiflow, combined the two systems with an exhaust port close to the cylinder head and another close to the cylinder bottom. The advantage of the uniflow configuration is that the cylinder head is not cooled down during the exhaust process, leading to a higher wall temperature and less risk of condensation (if vapor is used as working fluid) during supply process.

2.2.3. Double acting piston expander

In some expanders, the fluid acts alternatively on the two faces of the piston in the same cylinder. This configuration is denoted as double acting and leads to a more compact engine as two expansion processes occur in one cylinder.

2.3. Thermodynamic aspect and losses

2.3.1. Losses

Several sources of losses affect the performance of piston expanders. These sources are under/over expansion and compression, pressure drops across the ports, heat transfers, leakages and mechanical losses. These losses affect the power delivered by the expander and the mass flow rate it displaces.

- *Under/over expansion and compression*

Figure 2-5 shows the comparison between the ideal, the theoretical and the actual indicator diagrams. In the ideal case, the pressures at the end of the expansion and the compression processes are equal to the exhaust and the supply pressures respectively and no pressure drop or other losses affect the expansion process. This case represents a fully isentropic evolution of the fluid through the machine. In practice, the

pressure ratio rarely matches with internal built-in expansion and compression ratios leading to under- or over-expansion and compression losses. The theoretical diagram shows the effect of under-expansion and compression, which tends to decrease the area under the indicator diagram and thus the indicated power.

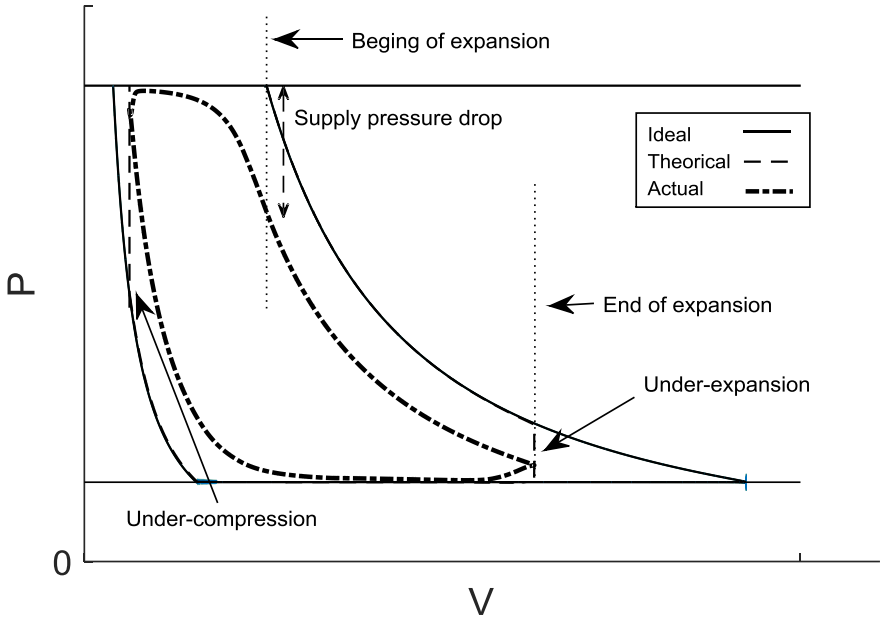

Figure 2-5: Comparison between ideal, theoretical and actual indicator diagram

- *Pressure drop*

Pressure drop result from flow restrictions through the valves. Supply pressure drop tend to decrease the pressure at the beginning of expansion phase and exhaust pressure drop to increase the pressure during the compression process. Moreover, at the end of expansion and compression, the equalization of the pressure in case of under expansion and compression is not sudden as in the theoretical diagram. As shown in Figure 2-5, these effects deform the indicator diagram and reduce the indicated power. Pressure drops also tend to decrease the mass flow rate displaced by the expander.

- *Heat transfer*

As the temperature of the fluid is different from the temperature of the cylinder wall and piston head, a heat exchange occurs. The wall temperature is lower than the fluid supply temperature (unless if the cylinder is heated by an external hot source in order to approach an isothermal expansion) leading to a cooling down of the fluid and then a possible increase in the mass flow rate. This supply cooling down can lead to condensation if vapor is used. Condensation of the vapor can reduce significantly the in-cylinder pressure and then reduce the power. During the exhaust process, the wall temperature can be either higher or lower than the fluid temperature and heating-up or cooling-down can occur. In the absence of condensation, heat transfer does not have significant impact on the indicated work and affect mostly the exhaust temperature.

- *Leakages*

Leakages occur when a pressure difference is applied to a leakages path. Leakage paths result from clearances between mechanical parts of the expander and depend on the mechanical design. In piston expanders, fluid can leak along the supply valve from the admission manifold to the cylinder. As this leak flow enters the cylinder, it contributes to the indicated power but still constitutes a loss as the fluid is throttled before entering the cylinder. Another leakage path is clearance between the piston rings and the cylinder wall. This leakage flow leaves the cylinder and then tends to decreases the indicated power. Some fluid can also by-pass the cylinder through clearances such as along supply valves stems. Leakages increase the mass flow rate and thus decrease the specific work.

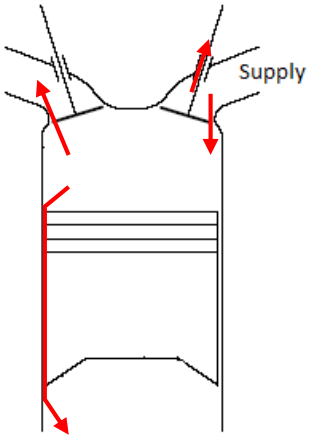

Figure 2-6: Main leakages paths

- *Mechanical friction losses*

Friction losses appear between moving parts in contact. In piston expanders, the main friction forces appear in the piston-cylinder assembly, the bearings of the crank train or swash plate system and in the valve trains. The magnitude of the friction forces depends on the friction coefficient which depends on the lubrication regime. Three different types of regime of lubricated friction exist, according to the oil film thickness between the two sliding part: boundary, hydrodynamic and mixt. In boundary regime, the oil film is too small to prevent solid-to-solid contact between surfaces. In hydrodynamic regime, the oil film separates completely the two surfaces. The mixed regime is the transition between the boundary and hydrodynamic lubrication. These three regimes can be illustrated by the Stribeck diagram (see Figure 2-7) where the friction coefficient is plotted in terms of the dimensionless parameter $\mu.U/\sigma$, where μ is the dynamic viscosity of the lubricant, U is the relative velocity of the two surfaces and σ is the load. In boundary regime, friction is higher and independent on the relative speed of the two surfaces while in hydrodynamic regime, the friction force increases with the speed. Friction losses depend also on the load applied to the moving parts and then on the pressure in the cylinder. However, in hydrodynamic regime, the friction power does not depend significantly on the load.

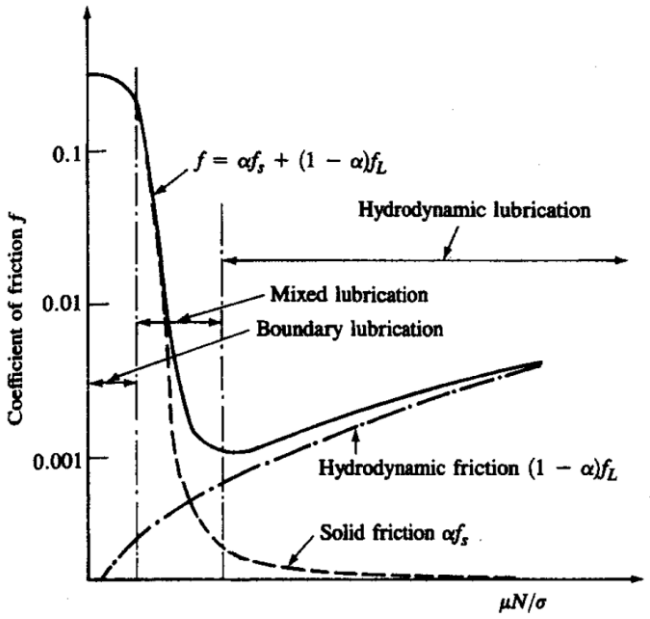

Figure 2-7: Stribeck diagram (Heywood 1988)

Figure 2-8 shows an ICE motored engine breakdown test results. The graphic shows the evolution of the different sources of mechanical losses in terms of engine speed. According to (Heywood 1988), the piston assembly accounts for 50% of total mechanical losses, the valve train for 25%, the crankshaft bearings for 10% and the auxiliaries for 15%.

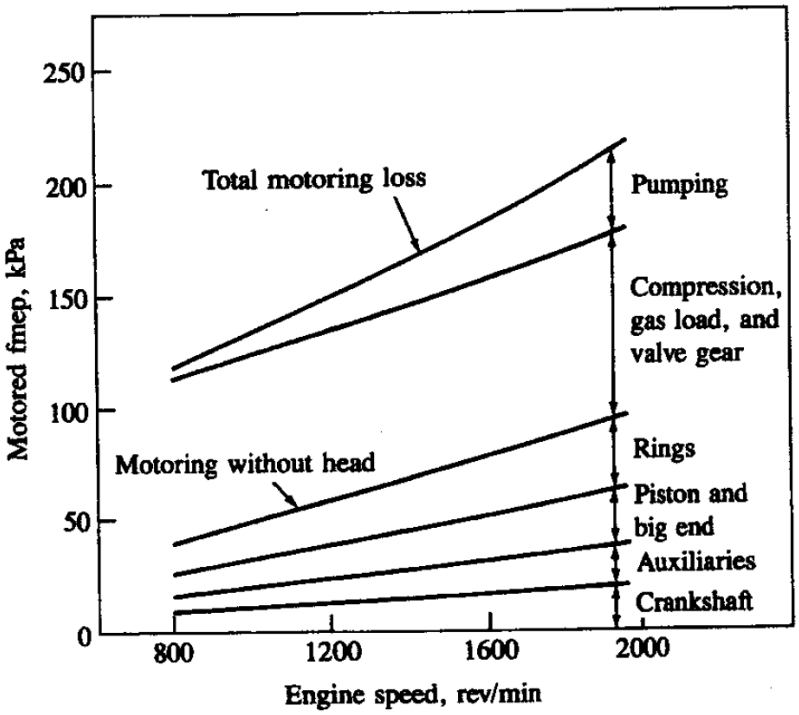

Figure 2-8: Friction losses in ICE (Heywood 1988)

2.3.2. Mass flow rate

The theoretical mass flow rate is the mass flow rate associated with the theoretical indicator diagram. Then, according to Figure 2-1, the mass entering into the cylinder is the difference between the masses at point 2 and point 6 or point 5 as the system is a closed system during step 5-6. The theoretical mass flow rate is then given by:

$$\dot{M}_{th} = n_{cyl}.N.\left(V_{IC}.\rho_{IC,th} - V_{EC}.\rho_{ex}\right) \quad (2\text{-}4)$$

where n_{cyl} is the number of cylinders, N the rotational speed and $\rho_{IC,th}$ and ρ_{ex} the densities of the fluid at the end of the supply process and exhaust thermodynamic states. The state of the fluid at the end of the admission process differs from the one at the supply because of the mixing of the new fluid charge and the fluid remaining in the clearance volume.

As explained above, losses affect the theoretical mass flow rate. Indeed, pressure drops tend to decrease it while leakages and heat transfer tends to increase it. Actual mass flow rate entering the expander can be expressed by:

$$\dot{M} = \dot{M}_{in} + \dot{M}_{leak} = n_{cyl}.N.(V_{IC}.\rho_{IC} - V_{IO}.\rho_{IO}) + \dot{M}_{leak} \quad (2\text{-}5)$$

where $\dot{M}_{in}$ is the internal mass flow rate, $\dot{M}_{leak}$ the lumped leakage flow rate, V_{IO} is the inlet open volume and ρ_{IC} and ρ_{IO} the density of the fluid in the cylinder at inlet closing and opening volume and. ρ_{IC} differs from $\rho_{IC,th}$ because of supply pressure drop and heat transfer.

2.3.3. Indicated and mechanical power

The indicated work is defined has the work delivered by the fluid to the piston. This indicated work is given by the area enclosed in the PV diagram. This area is obtained by integrating the pressure curve of the PV diagram:

$$W_{in} = \oint P.dV \quad (2\text{-}6)$$

The corresponding indicated power is given by the product of the rotational speed (in Hz) and the indicated work:

$$\dot{W}_{in} = N.W_{in} \quad (2\text{-}7)$$

Considering the theoretical PV diagram (Figure 2-1), theoretical indicated work is the sum of the suction work, expansion work, discharge work and compression work. It can be expressed by:

$$W_{in,th} = P_{su}.(V_{IC} - V_0) + V_{IC}.\rho_{su}.\left(u_{su} - u_{in,exp}\right) - P_{ex}.(V_{Tot} - V_{EC}) - V_{EC}.\rho_{EC}.\left(u_{in,cp} - u_{EC}\right) \quad (2\text{-}8)$$

where u is the internal specific energy and subscript in, exp and in, cp represent the state of the fluid at the end of the internal expansion and compression respectively.

In order to quantify the indicated work decrease caused by the irreversiblies, the diagram factor (in reference to the indicator diagram) is defined as the ratio between the actual indicated work and theoretical indicated work:

$$\epsilon_{in} = \frac{\dot{W}_{in}}{\dot{W}_{in,th}} \quad (2\text{-}9)$$

Due to friction losses, all the indicated power is not available at the expander shaft. The shaft power is obtained by substracting the mechanical losses:

$$\dot{W}_{sh} = \dot{W}_{in} - \dot{W}_{loss,mec} = N.2.\pi.T_{sh} \quad (2\text{-}10)$$

where $T_{sh}$is the shaft torque.

To quantify these mechanical losses, the mechanical efficiency is defined as:

$$\eta_m = \frac{\dot{W}_{sh}}{\dot{W}_{in}} = \frac{\dot{W}_{in} - \dot{W}_{loss,mec}}{\dot{W}_{in}} \quad (2\text{-}11)$$

2.4.Performances indicators

2.4.1. Volumetric performance

As for volumetric compressor, the volumetric performance of positive displacement expander is evaluated with the ratio between the actual and theoretical mass flow rate (called filling factor):

$$\phi = \frac{\dot{M}}{\dot{M}_{th}} \quad (2\text{-}12)$$

However, unlike in compressors, the leakage flows is in the same direction as internal flow and tends to increase the total mass flow and then the filling factor. So, the effects of the leakages and of the pressure drops are antagonist. Moreover, supply cooling down can also lead to an increase in the entering fluid mass flow rate. These different antagonist effects make the analysis of the filling factor difficult. To better understand the separate effect of leakages, the filling factor can be disaggregated into two parts:

$$\phi = \frac{\dot{M}}{\dot{M}_{th}} = \frac{\dot{M}}{\dot{M}_{in}} . \frac{\dot{M}_{in}}{\dot{M}_{th}} = \phi_l . \phi_{in} \quad (2\text{-}13)$$

In this equation, ϕ_l is the leakage filling factor and quantifies the effect of the leakages. ϕ_{in} is the internal filling factor and quantifies the effect of supply pressure drop and heat transfer. The leakage filling factor is greater than one while the internal filling factor is smaller than unity if pressure drops are predominant.

2.4.2. Energy conversion efficiency

In order to assess the performance of expansion machine, the produced power is compared to the power produced for a reference fluid evolution in the same operating conditions (supply condition and exhaust pressure) and with the same mass flow rate. The reference evolution is an isentropic evolution (adiabatic

and reversible) and the ratio between the actual power and the isentropic power is defined as the isentropic efficiency. Considering the indicated power, the indicated isentropic efficiency is given by:

$$\epsilon_{s,in} = \frac{\dot{W}_{in}}{\dot{W}_s} = \frac{\dot{W}_{in}}{\dot{M}.(h_{su} - h_{ex,s})} = \frac{\dot{W}_{in}}{\dot{M}.\Delta h_s} \quad (2\text{-}14)$$

where $h_{ex,s}$ is the specific enthalpy at the exhaust of the isentropic expansion. Alternatively, considering the shaft power, the shaft isentropic efficiency is:

$$\epsilon_{s,sh} = \frac{\dot{W}_{sh}}{\dot{W}_s} = \frac{\dot{W}_{sh}}{\dot{W}_{in}} \frac{\dot{W}_{in}}{\dot{M}.\Delta h_s} = \eta_m . \epsilon_{s,in} \quad (2\text{-}15)$$

As for the filling factor, the shaft isentropic efficiency can be disaggregated to assess the relative impact of each source of losses:

$$\epsilon_{s,sh} = \frac{\dot{W}_{sh}}{\dot{m}.\Delta h_s} = \frac{\dot{W}_{sh}}{\dot{W}_{in}} \frac{\dot{W}_{in}}{\dot{W}_{in,th}} \frac{\dot{W}_{in,th}}{\dot{M}_{th}.\Delta h_s} \frac{\dot{M}_{th}}{\dot{M}_{in}} \frac{\dot{M}_{in}}{\dot{M}} = \eta_m . \epsilon_{in} . \epsilon_{s,th} . \frac{1}{\phi_{in}} . \frac{1}{\phi_l} \quad (2\text{-}16)$$

All the factors of this decomposition have already been defined, except the theoretical isentropic efficiency $\epsilon_{s,th}$, which quantifies the under or over expansion and compression losses. As explained above, the mechanical efficiency η_m quantifies the mechanical losses and the diagram factor ϵ_{in} quantifies the impact of pressure and heat transfer losses on indicated work (and on indicated diagram, hence its name). The last two factors account for the impact of losses on the mass flow rate.

In equation (2-16), two terms account for pressure drops and heat transfer effect: diagram factor ϵ_{in} and internal filling factor ϕ_{in}. Then, the effect of pressure drop and heat transfer on isentropic efficiency is given by:

$$\epsilon_{sp,in} = \frac{\epsilon_{in}}{\phi_{in}} = \frac{\dot{W}_{in}}{\dot{M}_{in}} . \frac{\dot{M}_{th}}{\dot{W}_{in,th}} = \frac{w_{in}}{w_{in,th}} \quad (2\text{-}17)$$

and corresponds to the ratio between indicated and theoretical specific works and it will be called “specific diagram factor”. It is interesting to note that, as internal filling factor is more often smaller than unity, it tends to increase the isentropic efficiency. However, this increase does not come from an improvement but from the reduction of the mass flow rate used to compute the isentropic efficiency.

This disaggregation allows the evaluation of the impact of the different source of losses and the comparison of different volumetric expanders. The values of these losses factors can be obtained by experimentation and/or modeling. Theoretical isentropic efficiency is always determined by modeling. Mechanical efficiency and diagram factor can be measured if in-cylinder pressure measurements are available to compute indicated work. Finally, as leakages are difficult to measure, it is more convenient to simulate them to obtain leakage and internal filling factor.

2.4.3. Compactness

In order to quantify the compactness of a piston expander, the delivered power can be divided by the displaced volume. As shown in equation (2-18), the compactness is the product of the rotational speed, of the diagram factor and of the ratio between the theoretical indicated work and the displaced volume.

This last factor has the dimensional unit of a pressure and is called “theoretical indicated mean effective pressure”. Regarding the equation (2-18), the diagram factor can be considered as a compactness efficiency.

$$C_{ness} = \frac{\dot{W}_{sh}}{V_{tot}} = \frac{W_{sh}}{W_{in}} \frac{W_{in}}{W_{in,th}} . \frac{W_{in,th}}{V_{tot}} . N = \eta_m . \epsilon_{in} . imep_{th} . N = \eta_m . imep . N = smep . N \quad (2\text{-}18)$$

As for the theoretical indicated mean effective pressure, the “indicated mean effective pressure” and “shaft mean effective pressure” can be defined:

$$smep = \frac{W_{sh}}{V_{tot}} = \eta_m . imep = \eta_m . \epsilon_{in} . imep_{th} \quad (2\text{-}19)$$

Considering equations (2-18) and (2-19) , the compactness can be expressed as:

$$C_{ness} = \eta_m . imep . N = smep . N \quad (2\text{-}20)$$

In the same way, mechanical losses is sometime expressed as “friction mean effective pressure”:

$$fmep = \frac{W_{loss}}{V_{tot}} \quad (2\text{-}21)$$

3. Ericsson engine

3.1. Working principle

The Ericsson engine is an externally heated piston engine. The working fluid is generally air so it is classified as a hot air engine. A schematic representation of an Ericsson engine is shown in Figure 2-9. It shows that the fluid enters the compression cylinder (Cp) where it is compressed. Then, the fluid exits the compressor to enter the heater. There, it receives an amount of thermal energy and its temperature rises. Finally, the fluid expands into the expander (Exp) to produce mechanical energy. Improvement of the engine can be made by adding a recuperator that recovers the heat available at the exhaust of the expander to preheat the fluid before it enters the heater. It is also possible to introduce a heat exchanger to cool the fluid that leaves the expander before driving it to the compressor, so that the engine works in a closed loop.

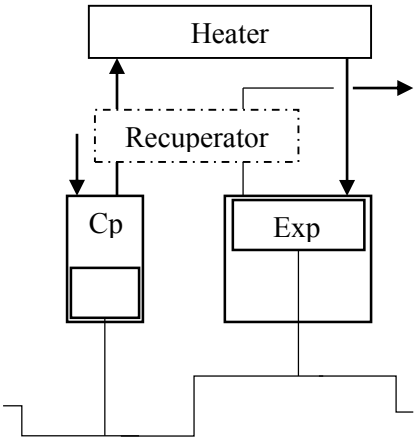

Figure 2-9: Schematic representation of an Ericsson engine

Contrary to what its name suggests, the best theoretical cycle to describe an Ericsson engine is the Brayton cycle and not the Ericsson cycle. Indeed, the Ericsson cycle is made up of two isobaric and two isothermal processes (Figure 2-10). However, in an Ericsson engine, the heat transfers between the heat source/sink and the working fluid take place in dedicated heat exchangers and not in the cylinders. Then, the Brayton cycle, consisting of two isobaric and two isentropic processes, used to describe gas turbines, is more suitable. In this sense, the Ericsson engine is a gas turbine where turbomachines are replaced by volumetric engines (Bonnet, Alaphilippe, and Stouffs 2005).

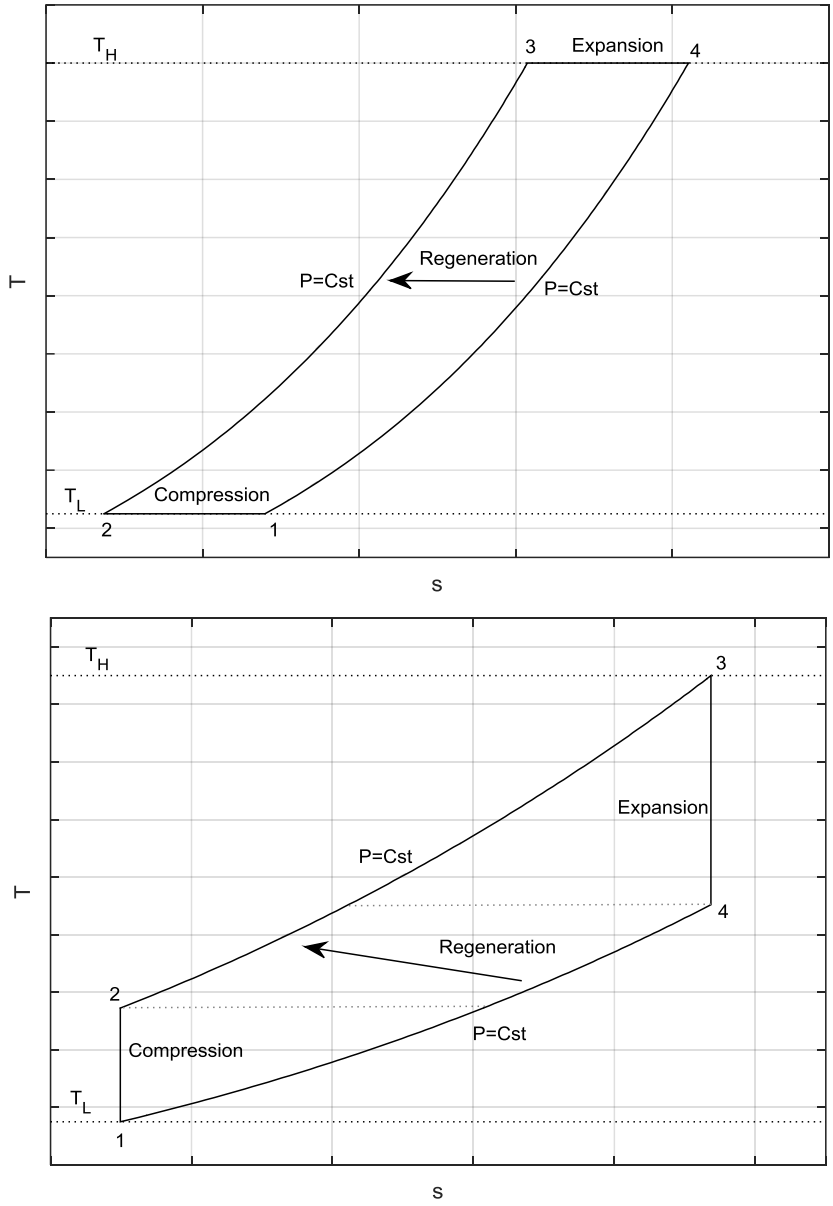

Figure 2-10: T-s diagram of ideal Ercisson (up) and Brayton (down) cycle

For this type of engine, the pressure ratio is defined as the ratio between the pressure in the heater and the engine supply/exhaust pressure. The temperature ratio is defined as the ratio between the temperature at the exhaust of the heater and the temperature at the supply of the engine.

Figure 2-11 shows the thermal efficiency of the simple ideal Brayton cycle and of the ideal regenerative cycle in terms of pressure ratio and for different temperature ratios. The simple cycle efficiency is independent on the temperature ratio and increases with the pressure ratio. The ideal regenerative cycle efficiency is maximal for a pressure equal to one, but the delivered power is null for this pressure ratio and decreases until reaching the simple cycle efficiency. At this point, the expander exhaust temperature is

equal to the compressor exhaust temperature and the recuperator becomes pointless. The higher the temperature ratio the higher the regenerative efficiency.

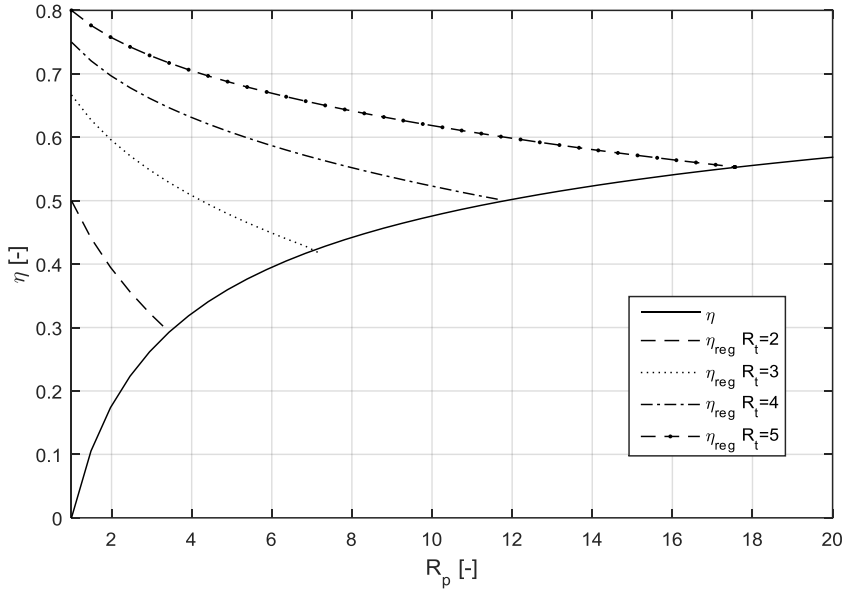

Figure 2-11: Cycle efficiency of the ideal Brayton cycle in terms of pressure ratio for different temperature ratios

However, the compression and the expansion processes are not isentropic in an actual Brayton cycle. Therefore the cycle efficiency is affected by the isentropic efficiency of the compressor and the expander. Figure 2-12 shows regenerative and simple cycle efficiencies in terms of pressure ratio and for different temperature ratios. It can be seen that, when the compression and the expansion are not isentropic:

- there is an optimum pressure ratio for both efficiencies
- the optimal pressure ratio is lower for the regenerative cycle efficiency
- both efficiencies increase with temperature ratio

The efficiency of the actual Brayton cycle is much lower than the one of an ideal cycle and is very sensitive to the compressor/expander isentropic efficiency. Indeed, for an expander supply temperature of 800°C the optimal regenerative efficiency drops from 30% to 5% when the isentropic efficiency drops from 80% to 60%.

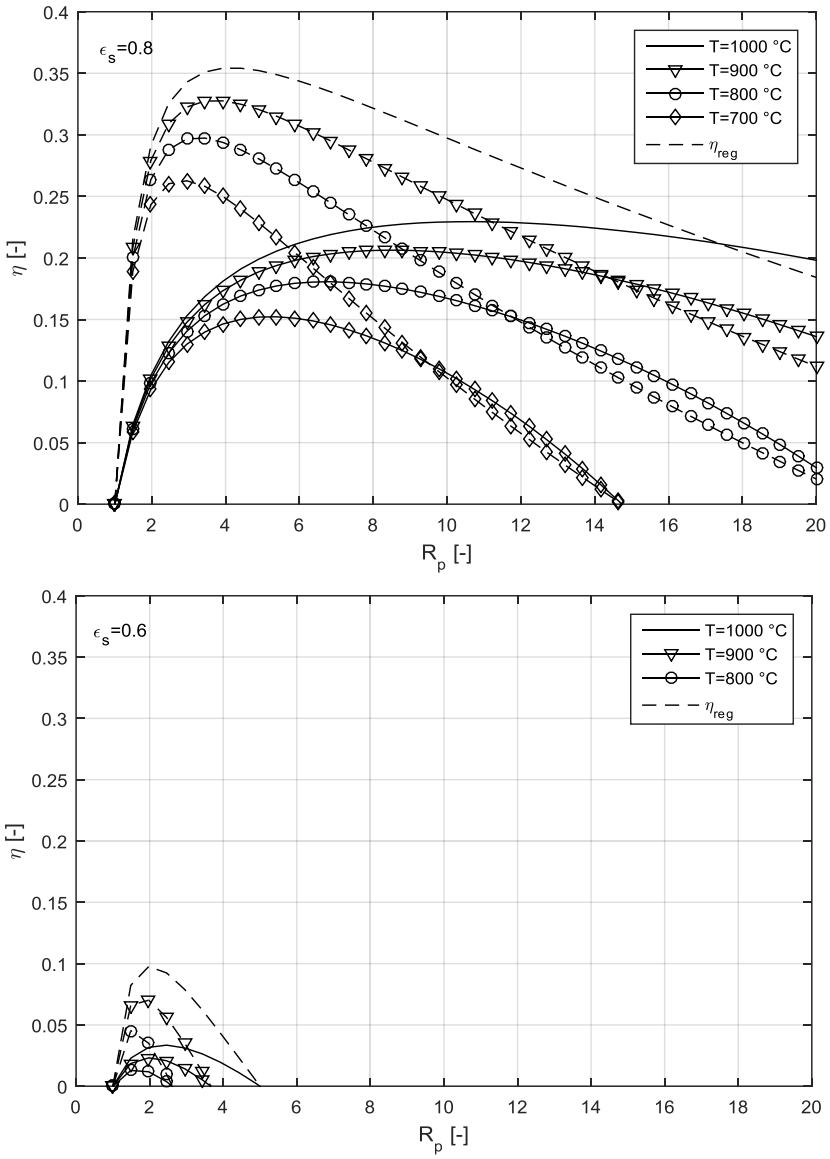

Figure 2-12: Efficiency of the Brayton cycle in term of pressure, with compression and expansion isentropic efficiency of 0.8 (up) and 0.6 (down) and for different expander supply temperature

3.2. Previous work on Ericsson engine

The first Ericsson engine was designed and built by John Ericsson in 1833. In 1853 he built another engine with a power of 220 kW to propel a ship. Then, J. Ericsson designed a smaller engine of 600W, which was the first mass-produced engine with 3000 pieces produced between 1855 and 1860. Later, steam engines and ICE replaced hot air engines. However, the Ericsson engine has recently regained interest for application such as biomass cogeneration.

Blank and Wu (1996) (Blank and Wu 1998) proposed to use an Ericsson engine based on theoretical Ericsson cycle with perfect regeneration and with a pressure ratio of 2.64. The engine would be used with

heat sources of temperatures varying between 630°C and 1230°C or in space application, with radiant heat exchanges with the sun as heat source and outer space as heat sink.

Brzeski and Kazimierski (2001) tested an Ericsson engine (denoted as externally heated valve engine (EHVE)) with cylinder of 432.8 cm³ for both compressor and expander (ratio=1). The engine run in a closed cycle, higher temperature is between 550 and 800°C, high and low pressures are around 26 bar and 8 bar respectively and rotational speed ranges from 360 to 720 RPM. Two small volumes (about the volume of the expansion cylinder) heaters are used alternatively. This system allows higher cut-off but needs very high heat transfers rate. The engine had just enough power to overcome frictions because of too low heat flow. Then, in the continuity of this work, Wojewoda and Kazimierski (2010) proposed to use one larger heater (3 to 5 times the volume of the expansion cylinder) with recirculating blower to improve heat transfer, shorter cut-off and a ratio between the volume of the expander and the volume of the compressor larger than one. The total cylinders volume of the expander and compressor are $V_{tot,exp}$=428 cm³ and $V_{tot,cp}$=323 cm³ respectively (ratio=1.33). The simulation results show high and low pressures of around 95 bar and 16 bar respectively with an operating temperature around 900°C. The study concludes that simulated performances are equivalent to those that would be obtained with a Stirling engine.

Stouffs (2002) considered using Ericsson engine to valorize energy sources such as biomass, biogas, hot gases and, in particular, syngas from waste thermolysis, not adapted to be burnt into ICE. The authors proposed to use double acting piston expander and compressor and to connect in series the volumes of the compressor to achieve a multistage compression. A fast design lead to a 100 kW engine with total expander swept volume of 0.145 m³ and compressor swept volume of 0.0627 m³ and 0.0278 m³ (ratio of 2.3). Maximal values of 800°C, 6 bar, 500 RPM and 8 m/s as high temperature, high pressure, rotational speed and mean piston speed respectively are considered. The system is expected to produce 113 kW of mechanical power.

Bell and Partridge (2003) proposed to use an Ericsson engine for domestic CHP (1-5 kW). The influence of the swept volume ratio (ratio between swept volume of expander and compressor of the engine), pressure ratio, pressure drop and leakages on thermal efficiency are used to give guideline for the design. A maximum operating temperature of 1000°C is considered and pressure ratio ranges from 6 to 8. In the continuity of the work of Bell et al., Allen (2008) adapted a four cylinders 2.5 L diesel engine to work as an Ericsson engine by modifying the cylinders heads. Two cylinders were used for the expander and one for the compressor. During the experimental campaign, several modification were made following different issues such as unstable combustion, damage to valve gear, investigation on valve timing … Pressure and temperature up to 4 bar and 870°C were achieved but the engine only self-sustained and no net power was produced. The author pointed out the importance of low friction for good efficiency of the Ericsson engine and to maximize the IMEP to increase mechanical efficiency. Because of the lower operating pressure compared to ICE, the authors proposed to use a single gas ring and an oil control ring.

Several other studies considered the use of Ericsson engine for domestic CHP. Moss, Roskilly, and Nanda (2005) proposed to directly burn natural gases in the air used as working fluid for CHP of 5 kW. The authors preconized a pressure ratio of 7.5, a rotational speed of 1000 RPM, leading to expander and compressor cylinders capacities of 4650 cm3 and 1770 cm³ respectively (ratio=2.6). Bonnet, Alaphilippe, and Stouffs (2005) performed parametric study on heat exchanger efficiency and energy, exergetic and

cost analysis on a 10 kW CHP. A maximal rotational speed of 1000 RPM and a mean piston speed of 8 m/s are considered. The expander swept volume is 2200 cm³ and the compressor swept volume is 957 cm³ (ratio=2.3). The expander inlet pressure and temperature are 6 bar and 800°C respectively. The authors concluded that a profitability of the system is possible considering the price of the French energy suppliers. Mikalsen and Roskilly (2012) proposed to use free piston engine for a 4.5 kW CHP. The swept volumes of the expander and compressor are 773 cm³ and 386 cm³ (ratio=2). Expander and compressor are directly connected and electricity is produced with a linear generator. Operating temperature and pressure are 800°C and 5.9 bar. Creyx et al. (2013) studied the influence of incomplete expansion and compression on the energetic performances of an Ericsson engine used for micro-CHP with operating temperature and pressure ranging between 400-650°C and 5-8 bar. Later, the authors presented a test bench of expansion part and biomass furnace (Creyx 2015). The expansion part of the Ericsson engine is made with a 160 cm³ mono-cylinder expander with adapted distribution system. The engine is designed to run with the operating condition aforementioned and for rotational speed of 100-1400 RPM. In the publication, only mechanical losses are assessed by electrically driving the engine and no test under operating conditions is performed. Lontsi et al. (2013) performed dynamic simulation for a 1.6 kW CHP. Swept volumes are 226 cm³ for the compressor and 425 m³ for the expander (ratio 1.88). Pressure ratio of 4, temperature of 800°C and rotational speed of 480 RPM are considered.

Alaphilippe, Bonnet, and Stouffs (2007) considered the coupling of a parabolic trough solar concentrator and a 733W Ericsson engine in order to convert solar energy into electricity. A pressure ratio of 3 is considered to maximize the global efficiency of the system and a maximal operating temperature of 722°C is expected.

Touré (2010) tested a 650 cm³ expander prototype fed by a commercial compressor. Operating temperature during the test varied from 300°C to 500°C, pressure ratio was about 3.5 and maximal 950 RPM corresponding to a mean piston speed of 4.1 m/s. The expander produced between 0.3 and 1kW with a mechanical efficiency of 87% independent of the speed and isentropic efficiency varied from 40% to 75%. In the continuity of this work, Fula, Stouffs, and Sierra (2013) proposed a dynamic model and the study of the influence on the in-cylinder heat transfer. Simulation showed that heat transfers affect exhaust temperatures but not so much the performance of the compressor and expander.

Galindo, Serrano, et al. (2015) studied the possibility of a WHR system for a car with a Brayton cycle. Piston compressor and expander were selected because turbines or roots machines would show a too high rotational speed.

In conclusion, the Ericsson engine is generally considered because of its externally heated feature leading to the possibility of using a large panel of fuels. The different theoretical and experimental studies are summarized in Table 2-1. The major application considered for this hot air engine is micro-CHP. Operating temperature ranges between 300°C and 1000°C but is more often about 800°C, the pressure ratio is between 3 and 8 and low rotational speeds seem to be preferred (500-1500 RPM). Most of the studies consider an open cycle and a volume ratio around 2. Among the 14 studies, only 3 report experimental results and none of them relates positive net-power. This lack of experimental testing was the main motivation to develop and test a prototype (see Chapter 4).

Table 2-1: Summary of the Ericsson engine literature review.

References	Application Cycle type	V_{exp},V_{cp} [cm³], volume ratio	Operating temperature, pressure ratio, speed	Power	Nature of the study
(Blank and Wu 1996)	Ericsson regenerative closed cycle		/ 2.64 /		Theoretical
(Brzeski and Kazimierski 2001)	/ Closed cycle	432.8 432.8 1	550-800°C 3.25 360-720 RPM	Self-sustain	**Experimental**
(Wojewoda and Kazimierski 2010)	/ Closed cycle	428 323 1.33	900°C 6 1000-3000 RPM	/	Theoretical
(Stouffs 2002)	Open recuperation cycle Thermolysis syngas combustion	145e3 62e3 2.3	800°C 6 500 RPM	113 kW	Theoretical
(Bell and Partridge 2003)	Open recuperation cycle, internal combustion CHP		1000°C 6-8 /	1-5 kW	Theoretical
(Allen 2008)	Open cycle, Internal combustion CHP	1250 625 2	870°C 4 /	Self-sustain	**Experimental**
(Moss, Roskilly, and Nanda 2005)	Open recuperation cycle, internal combustion CHP	4650 1770 2.6	/ 7.5 1000 RPM	5 kW	Theoretical
(Bonnet, Alaphilippe, and Stouffs 2005)	Open recuperation cycle CHP	2200 957 2.3	800°C 6 1000 RPM	10 kW	Theoretical
(Mikalsen and Roskilly 2012)	Open recuperation cycle, internal combustion CHP	773 386 2	800°C 5.9	4.5 kW	Theoretical
(Creyx et al. 2013)	Open cycle, CHP	160 / /	400-650°C 4 100-1400 RPM		Theoretical
(Lontsi et al. 2013)	Open cycle CHP	425 226 1.88	800 °C 4 480 RPM	1.6 kW	Theoretical

(Alaphilippe, Bonnet, and Stouffs 2007)	Open recuperation cycle Solar power		722 °C 3	0.73 kW	Theoretical
(Touré 2010)	Only expander /	650 cm³ / /	300-500 °C 3.5 500-950 RPM	1 kW Expander only!	**Experimental**
(Galindo, Serrano, et al. 2015)	/ WHR in vehicle				Theoretical

4. Rankine cycle

4.1. Working principle

The Rankine cycle is a power cycle using the expansion of vapor to produce power. Figure 2-13 shows the temperature-entropy (T-s) diagram of a Rankine cycle. It is shown that the fluid is first in a liquid state and is pumped from the low pressure condenser to the high pressure evaporator. In the evaporator, the pressurized fluid is heated up, evaporated and then superheated. Then, the fluid expands in the expansion device where it produces the useful power. Afterward, the fluid is condensed in the condenser and the sub-cooled liquid is pumped back to the evaporator.

In general, Rankine cycle refers to vapor cycle using water as working fluid while Organic Rankine Cycle (ORC) uses fluid such as refrigerant or hydrocarbon fluid (organic fluids) showing lower normal boiling points. Unlike water, some organic fluids are “dry”, i.e. the slope of their vapor saturation curve on the T-s diagram is positive. This property enables, as in Bratyon cycle, the use of a recuperator to recover the heat still available at the outlet of the expander to preheat the liquid before it enters the evaporator.

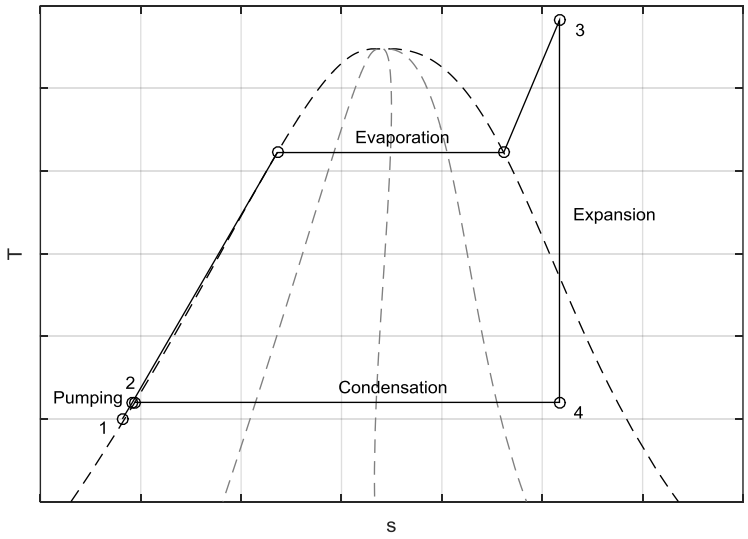

Figure 2-13: T-s diagram of a Rankine cycle

During the recent years, a particular attention has been paid on expansion machines used in small scale ORC systems. Indeed, the expander plays a key role in terms of system efficiency and other components (pump and heat exchangers) are already mature technologies. While turbines are used in large-scale Rankine systems, volumetric expanders are often preferred for low-scale applications (<25 kW), because of their low rotational speed and their ability to ingest liquid and handle high pressure ratios. Among other technologies of positive displacement machines such as scroll or screw expanders, piston expanders are more and more considered in the literature.

4.2. Previous work on the use of piston expander in (Organic) Rankine cycle

Using piston expanders in (O)RC has been recently considered in many applications. The present literature review is organized in according of these applications.

4.2.1. Steam cars

In the 70's, Rankine cycle heat engines were reconsidered for low exhaust emission passenger car propulsion, because standards became stricter. The Rankine cycle, often call "steam engine" in this field, allowed low emission of CO, HC and NOx because combustion process is continuous and can be carefully controlled (Hoagland, Demler, and Gerstmann 1974). Reciprocating expander was considered because of the better efficiency for the ranging speed and favorable torque characteristic for automotive applications compared to turbines. A car equipped with a steam engine was tested by GM (Vickers et al. 1970) and the Scientific Energy Systems Corporation (SES) (Technologie Assesment and Evaluation Branch 1974). The SES expander was 2200 cm^3 uniflow expander with two in-series cam-actuated poppet valves admission system allowing variable cut-off to control the load. The expander was fed with steam at 69 bar and 538°C and produced a maximum power of 100 kW. Maximum isentropic efficiency was about 60%.

In the context of the steam engine passenger car, Demler (1976) studied the influence of cut-off, recompression ratio, supply pressure drop, heat transfer and mechanical losses on piston expander performance. According to the author, almost all volumetric expanders for car applications were piston expanders, but differ between uniflow or counter flow and constant or variable cut-off.

4.2.2. Expansion valve in CO2 cycle

According to Huff and Radermacher (2003), since 1990, several studies had considered the use of expanders to replace the expansion valves in CO2 refrigeration cycle systems. Simulation showed that gas-wall heat transfer had no influence on the performance for this application. Comparison with scroll machines showed that, for this application where pressure difference is very large (e.g. P_{su}=85 bar and P_{ex}=41 bar), the scroll is more dependent on the leakage gap size because of the larger sealing length. The authors reported two experimental studies performed by Heyl and Quack (2000) and Maurer and Zinn (2000) for this application, where the expanders showed isentropic efficiencies of 51% and 50% respectively.

Baek and al. (Baek, Groll, and Lawless 2002) (Baek, Groll, and Lawless 2005) tested prototypes for CO2 trans-critical compression cycle. The piston expander allows the recovering of the work from expansion and the minimization of the entropy creation during the process. The expander was made off a bi-cylinder

internal combustion engine of 2 X 13.26 cm³ adapted for the application. In order to achieve precise control of valve timing, solenoid-actuated valves were used. Supply pressure varied from 60 to 72.5 bar for pressure ratios from 2.5 to 3.2. The maximal isentropic efficiency achieved was 11%, the power ranged from 24 to 36 W and the presence of the expander increases the COP of CO2 cycle by 10.5%. The main source of losses was the leakages.

Heyl and Quack (1999) and Zhang et al. (2007) experimented the use of a free expander-compressor unit composed of two double-acting pistons in replacement of the expansion valve in a CO_2 refrigeration cycle. The expander of (Zhang et al. 2007) is a 2 X 18.4 cm³ piston expander, the inlet/outlet process was achieved by a novel slider-based valves control system. Inlet pressure varied from 7.8 to 54.5 bar for pressure ratios ranging in 1.67 – 3.3. The maximum achieved isentropic efficiency was 62%.

4.2.3. WHR in vehicles

During the last decades, piston expanders have been more and more considered for WHR from ICE. The ORC system recovers the thermal energy from the exhaust gases and sometime from cooling water.

Endo et al. (2007) tested a 7-cylinder, 185cm³ swash plate piston expander in an ORC integrated into a hybrid vehicle. The expander was lubricated by an integrated gear pump and had an electrical generator directly connected to the shaft. The working fluid was water, supply temperature was 450°C, supply pressure varied from 40 bar to 60 bar and rotational speed from 500 RPM to 2000 RPM. The expander produced a maximal power of 3kW and thermal efficiency of the ORC varied from 8% to 13%.

VOLVO investigated and tested a piston expander into a RC for WHR from truck engines (Howell, Gibble, and Tun 2011).

Seher et al. (2012) tested a prototype of a single cylinder double acting piston with a total swept volume of 900 cm³ for WHR on heavy duty vehicle engine (12000 cm³). The inlet/outlet process is made by gliding valves. The valves and the piston ring are not lubricated. The mechanical power produced by the expander with water as working fluid is about 4.4% of the ICE, the maximal power was 14 kW and the mechanical efficiency at 1500 RPM was 85%. The maximal inlet pressure and temperature was 32 bar and 380°C. The authors tested also a micro-turbine and studied several fluids. They have concluded that the best technology is piston with water or ethanol or turbine with ethanol.

Daccord et al. (2013) designed and tested an oil-free single-cylinder piston expander of 443 cm³. The expander used a camshaft to actuate poppet valves, had a fly-wheel and a permanent magnet generator integrated on the crankshaft. The cam can be easily changed in order to modify the timing of the valves and an additional exhaust port at the bottom dead center can be added by drilling the cylinder. The latter feature allowed the test of the expander in three different configurations: crossflow, uniflow and multiflow. The expander was tested with superheated steam at pressure from 18 to 36 bar and with pressure ratio from 20 to 50. The machine showed a maximal isentropic efficiency of 54% for a power of about 2kW. Then, the authors developed a new prototype based on swash plate technologies (Daccord, Darmedru, and Melis 2014). The expander has 5 cylinders for a total swept volume of 183 cm³. The hot part is oil-free in order to prevent burnt lubricant to foul the evaporator. The expander was tested with water at 300°C, pressure ratio varying from 16 to 34, rotational speed from 2000 RPM to 4000 RPM and

mechanical power from 2 to 3.6 kW. The last version of expander developed by the authors is larger with a total swept volume of 300 cm³ (Daccord and Sager 2015). The prototype is a swashplate, uniflow expander with integrated oil pump. It was tested with ethanol as working fluid. During the test, the expander produced mechanical power from 5 kW to 9.5 kW, the inlet pressure ranged between 24 bar and 37 bar, outlet pressure varied from 1 bar to 1.8 bar and supply temperature was about 230°C. A maximal isentropic efficiency of 56% was achieved.

Galindo, Ruiz, et al. (2015) (Galindo, Dolz, et al. 2015) tested a 3-cylinder swash-plate piston expander integrated into an ORC using ethanol and coupled with a 2l gasoline engine. Inlet pressure varied from 14.8 bar to 24.8 bar for pressure ratio from 6.4 to 9.5 in the first study and pressure up to 28.65 bar in the second one. Shaft power ranging from 0.64 to 1.83 kW was achieved. In the first study the maximal isentropic efficiency was 38.2 % and the system can lead to an increase of 3.7% of the ICE efficiency by using the power produced by the expander. In the second study, achieved isentropic efficiency was in the range 45-48% and mechanical efficiency in the range 77-95%.

Latz, Andersson, and Munch (2013) used dimensional analysis and similarity parameters (specific speed and diameter) to select the expansion machine for ICE WHR application. They concluded that piston expanders are best suited for heavy duty vehicle. Later,(Latz et al. 2015) (Latz 2016) tested a 2-cylinder uniflow 760 cm³ piston expander in a RC system coupled to the EGR of a Volvo D13 heavy-duty diesel engine. The admission system was a classic cam actuated valve system. The expander was initially designed for WHR on EGR and exhaust gases and worked with ethanol. The expander was then tested in off-design conditions. Power ranged from 1.5 to 2.6 kW for inlet pressure of 20 to 30 bar and inlet temperature of 200 to 300 °C. By measuring the water quantity in the lubricant, the leakages were estimated at 15-20% of the total mass flow rate.

IAV developed a prototype of piston expander for WHR on truck (Dingel, Töpfer, and Seebode 2015). This prototype is a 350 cm^3 multi-flow engine with maximal inlet pressure and temperature of 50 bar and 270 °C and a targeted power of 12 kW.

4.2.4. Combined Heat and Power (CHP)

Another application of RC or ORC using reciprocating expander is small-scale CHP.

Platell (1993) studied positive displacement expanders for small scale (50 kW-1MW) cogeneration application operating according to a Ranking cycle. He considered twin-screw and reciprocating machines. He proposed an analytical model to simulate the performance of piston expander including cut-off, recompression and mechanical losses.

Badami et al. studied the use of a reciprocating steam expander in a 100 bar and 450°C Rankine cycle system. The RC was fed by the exhaust gases of an ICE (Badami et al. 2008) or by a wood boiler (Badami and Mura 2009). The expander was designed to show a displacement of 300 cm³ in order to produce 24 kW for a rotational speed about 2400 RPM. He showed that a trade-off between isentropic and mechanical efficiencies can be found when varying the cut-off ratio. Three part load strategies were considered: variable speed, variable cut-off ratio and throttling valve.

Ferrara, Manfrida, and Pescioni (2013) considered the use of a 300-cm^3 single cylinder reciprocating steam expander in a RC for domestic CHP application generating about 2.5 kWe. The supply operating conditions were 160°C and 5 bar in order to be adapted for low-enthalpy heat sources.

Wronski et al. (2012) studied an innovative double-acting two-stage expansion reciprocating expander using pentane. During the first stroke, high-pressure expansion occurs in a first small chamber while exhaust occurs in a second chamber. Then, the two chambers are connected and low-pressure expansion occurs in both the chambers. The device is used to expand saturated liquid with heat addition during expansion. Later, the authors tested a 730 cm^3 single-cylinder single-stage piston expander prototype in an ORC using n-pentane (Wronski 2015). The admission system, consisting of a rotary valve, enabled the variation of the the cut-off and two different camshafts allowed the test of two different exhaust timings. The maximal power and isentropic efficiency was 2.5 kW and 74%. Inlet pressure ranged from 10 to 15 bar for pressure ratio from 9.5 to 17 and inlet temperature of about 150°C. The torque was measured with a high speed data acquisition, allowing the oscillation to be shown during one revolution. The advantages of a variable cut-off system in cogeneration application are evaluated by simulation. The variable cut-off was used to match the ORC pressure ratio (ratio between the evaporating and condensing pressures) varying with the condenser temperature during the year.

4.2.5. ORC in general and flash cycle

Recently, piston expanders have often been compared with other volumetric expanders for the use in small power ORC systems, whatever the application.

Clemente et al. (2011) studied the possibility to use a reciprocating expander of 169 cm^3 in ORC about 2 kW using R245fa or isopentane. By comparing it with previous work performed on scroll expanders, he concluded that both technologies are good candidates for low-scale ORC applications. Since 2013, several papers comparing expansion machines for ORC applications have shown that piston expanders are candidates as good as scroll machines, screw machines and turbines (Lemort et al. 2013) (Clemente et al. 2013) (Bao and Zhao 2013)

Two advantages of piston expanders are their ability to support liquid and the possibility of a high built-in volume expansion ratio. This feature leads to the consideration of the use of reciprocating expander in a trilateral cycle with flash expansion of saturated liquid. Steffen, Löffler, and Schaber (2013) proposed to use cyclone above the expander to keep the liquid phase outside the cylinder and the temperature is kept at the injection temperature by heat injection through the wall to avoid condensation. According to the authors, up to a heat source temperature of 200°C, the flash cycle with water has 35%-70% higher exergetic efficiency than ORC. Kanno and Shikazono (2014) compared classic, supercritical and trilateral ORC cycles for several fluids and for two kinds of heat sources, a “cold” one at 80°C and a “hot” one at 400°C. The authors concluded that the trilateral cycle shows better exergetic efficiency for the colder heat source.

4.2.6. Others applications

Overman (1992) considered the use of a 7.2 cm^3, 375 W, two-cylinder piston engine with water for an individual soldier power system. The vapor cycle was compared to ICE and gas cycle. According to the

author, steam engine has the advantages of being quiet, showing great fuel flexibility and a compact size but is more expensive and heavy.

Bidini, Manuali, and Saetta (1998) considered steam power plant fired by waste wood with reciprocating expander. In their study, power varied from 85 to 520 kWe with pressure up to 29 bar and temperature of 380°C.

Champagne and Weiss (2013b) (Champagne and Weiss 2013a) performed some tests with air on MEMS (Micro-electromechanical system) free piston with bore of 3,97 mm and 4,76 mm and concluded that such a system is technically feasible.

4.2.7. Conclusion

Piston expanders have been considered for several applications. In the 70's, piston expander were considered for steam cars in RC systems. Then, in the beginning of 21st century, in the context of the phase-out of several refrigeration fluids, several studied proposed to replace expansion valve of CO2 compression cycle in order to increase the COP of such systems. Recently, piston expanders have been more and more considered to be used in ORC applications such as in micro-CHP applications and in particularly for WHR on vehicle ICE engines.

As it can be seen in Table 2-2 resuming experimental works on piston expanders, the size, the type and the operating conditions of piston expander are comprised in a large range. Swept volumes vary from 26.5 cm³ to 2200 cm³ for powers from 0.036 kW to 100 kW. Maximum values of inlet conditions range between 15 bar and 72 bar and temperatures from 30 °C to 538 °C.

Table 2-2: Piston expander experimental studies summary

References	Application	Size (cm³)	Type	Admission system actuation	Maximal operating conditions	Power / Isentropic efficiency
(Technologie Assesment and Evaluation Branch 1974)	Steam car	2200	Uniflow	Cam	69 bar 538 °C	100 kW -
(Baek, Groll, and Lawless 2002)	CO2 compression cycle	26.5	Adapted 2 cylinders ICE	Solenoid	72.5 bar 30 °C	0.036 kW 11%
(Zhang et al. 2007)	CO2 compression cycle	36.8	Free-piston, Double acting piston	Sliding valves	54.5 bar -	
(Endo et al. 2007)	Vehicle WHR, RC	185	7 cylinders Swash plate	Rotary valves	60 bar 450°C	3 kWe -
(Seher et al. 2012)	Vehicle WHR, RC	900	Double acting piston	Sliding valve	32 bar 380 °C	14 kW -

(Daccord et al. 2013)	Vehicle WHR, RC	443	1 cylinder Uniflow/ Cross-flow/ Mutliflow	Cam	36 bar -	2 kWe 54 %
(Daccord, Darmedru, and Melis 2014)	Vehicle WHR, RC	183	5 cylinders Swash plate Uniflow	Camless	29 bar 300 °C	3.6 kW
(Daccord and Sager 2015)	Vehicle WHR, ORC ethanol	300	6 cylinders Swach plate Uniflow	Cam	37 bar 230 °C	9.5 kW 56%
(Galindo, Dolz, et al. 2015)	Vehicle WHR, ORC ethanol	117	3 cylindres Swash plate Uniflow		28.7 bar 200 °C	1.83 kW 58 %
(Latz et al. 2015)	Vehicle WHR, RC	760	2 cylindres Uniflow	Cam	30 bar 300 °C	2.6 kW -
(Wronski 2015)	Micro-CHP n-penthane	730	1 cylinders	Rotary valve	15 bar 150 °C	2.5 kW 74 %

5. Conclusions

The working principle of a piston expander is well described by its indicator diagram. The sources of losses that affect the ideal expansion cycle are under- or over-expansion and compression, pressure drop, heat transfer, leakages and friction. Under- or over-expansion and compression losses are due to a mismatch between the built-in volume ratios of expansion and compression to the pressure ratio imposed to the machine. These losses can be minimized by an adequate timing of the valves. The performance of volumetric expander can be expressed in terms of filling factor for volumetric performance, isentropic efficiency for energy conversion performance and mean effective pressure for compactness. The filling factor and isentropic efficiency can be disaggregated into several factors in order to separate the effect of the different sources of losses.

The mechanical design of piston expanders can largely differ from one to another. Two main kinds of linear to rotational conversion systems exist: crank train and swash/wobble plate. Valves are also an important issue: the timing of the valves fixes built-in volume ratios and valve actuation systems are the source of friction losses.

The literature review shows that this kind of expander was the oldest expansion machine used in Brayton and Rankine cycle systems already used in the late 19th century. However, these systems have regained interest in the last few years for small-scale (<50 kW) decentralized power generation in applications such biomass combined heat and power, solar power or waste heat recovery.

6. References

Alaphilippe, M., S. Bonnet, and P. Stouffs. 2007. “Low Power Thermodynamic Solar Energy Conversion: Coupling of a Parabolic Trough Concentrator and an Ericsson Engine.” *International Journal of Thermodynamics* 10 (1): 37–45. doi:10.5541/ijot.1034000186.

Allen, R. W. 2008. “The Reciprocating Joule Cycle Engine for Micro Combined Heat and Power Applications.” PhD Thesis, University of Plymouth. https://pearl.plymouth.ac.uk//handle/10026.1/759.

Badami, M., and M. Mura. 2009. “Preliminary Design and Controlling Strategies of a Small-Scale Wood Waste Rankine Cycle (RC) with a Reciprocating Steam Engine (SE).” *Energy* 34 (9): 1315–24. doi:10.1016/j.energy.2009.04.031.

Badami, M., M. Mura, P. Campanile, and F. Anzioso. 2008. “Design and Performance Evaluation of an Innovative Small Scale Combined Cycle Cogeneration System.” *Energy* 33 (8): 1264–76. doi:10.1016/j.energy.2008.03.001.

Baek, J., E.A. Groll, and P.B. Lawless. 2005. “Piston-Cylinder Work Producing Expansion Device in a Transcritical Carbon Dioxide Cycle. Part I: Experimental Investigation.” *International Journal of Refrigeration* 28 (2): 141–51. doi:10.1016/j.ijrefrig.2004.08.006.

Baek, J., E. Groll, and P. Lawless. 2002. “Development Of A Piston-Cylinder Expansion Device For The Transcritical Carbon Dioxide Cycle.” *International Refrigeration and Air Conditioning Conference*, January. http://docs.lib.purdue.edu/iracc/584.

Bao, J., and L. Zhao. 2013. “A Review of Working Fluid and Expander Selections for Organic Rankine Cycle.” *Renewable and Sustainable Energy Reviews* 24 (August): 325–42. doi:10.1016/j.rser.2013.03.040.

Bell, M.A., and T. Partridge. 2003. “Thermodynamic Design of a Reciprocating Joule Cycle Engine.” *Proc. of the Institution of Mechanical Engineers, Part A: Journal of Power and Energy* 217 (3): 239–46. doi:10.1243/095765003322066475.

Bidini, G., A. Manuali, and S. Saetta. 1998. “Reciprocating Steam Engine Power Plants Fed by Woodwaste.” *International Journal of Energy Research* 22 (3): 237–48. doi:10.1002/(SICI)1099-114X(19980310)22:3<237::AID-ER384>3.0.CO;2-R.

Blank, D.A., and C. Wu. 1996. “Power Limit of an Endoreversible Ericsson Cycle with Regeneration.” *Energy Conversion and Management* 37 (1): 59–66. doi:10.1016/0196-8904(95)00020-E.

———. 1998. “Finite-Time Power Limit for Solar-Radiant Ericsson Engines in Space Applications.” *Applied Thermal Engineering* 18 (12): 1347–57. doi:10.1016/S1359-4311(97)00080-X.

Bonnet, S., M. Alaphilippe, and P. Stouffs. 2005. “Energy, Exergy and Cost Analysis of a Micro-Cogeneration System Based on an Ericsson Engine.” *International Journal of Thermal Sciences*, A tribute to Bernard Spinner (1940-2004), 44 (12): 1161–68. doi:10.1016/j.ijthermalsci.2005.09.005.

Brzeski, L, and Z Kazimierski. 2001. “Experimental Investigations of the Externally Heated Valve Engine Model.” *Proc. of the Institution of Mechanical Engineers, Part A: Journal of Power and Energy* 215 (4): 487–94. doi:10.1243/0957650011538749.

Champagne, C., and L. Weiss. 2013a. “Performance Analysis of a Miniature Free Piston Expander for Waste Heat Energy Harvesting.” *Energy Conversion and Management* 76: 883–92. doi:10.1016/j.enconman.2013.08.045.

———. 2013b. “DESIGN AND OPTIMIZATION OF FREE PISTON EXPANDER FOR ENERGY HARVESTING.” In *Proc. of the ASME 2013 International Mechanical Engineering Congress and Exposition*.

Clemente, S., D. Micheli, M. Reini, and R. Taccani. 2011. “Performance Analysis and Modeling of Different Volumetric Expanders for Small-Scale Organic Rankine Cycles.” In *Proc. of the ASME 2011 5th International Conference on Energy Sustainability*, 375–84. Washington DC, USA: ASME. doi:10.1115/ES2011-54302.

———. 2013. “Bottoming Organic Rankine Cycle for a Small Scale Gas Turbine: A Comparison of Different Solutions.” *Applied Energy* 106 (June): 355–64. doi:10.1016/j.apenergy.2013.02.004.

Creyx, M. 2015. “Etude théorique et expérimentale d’une unité de micro-cogénération biomasse avec moteur Ericsson.” PhD Thesis, Université de Valanciennes et du Hainaut-Cambresis.

Creyx, M., E. Delacourt, C. Morin, B. Desmet, and P. Peultier. 2013. “Energetic Optimization of the Performances of a Hot Air Engine for Micro-CHP Systems Working with a Joule or an Ericsson Cycle.” *Energy* 49 (January): 229–39. doi:10.1016/j.energy.2012.10.061.

Daccord, R., A. Darmedru, and J. Melis. 2014. “Oil-Free Axial Piston Expander for Waste Heat Recovery.” In . doi:10.4271/2014-01-0675.

Daccord, R., J. Melis, T. Kientz, A. Darmedru, R. Pieyre, N. Brisseau, and E. Fonteneau. 2013. “Exhaust Heat Recovery with Rankine Piston Expander.” In . Vol. R-2013-05-10. Société des Ingénieurs de l’Automobile. http://www.sia.fr/publications/359-exhaust-heat-recovery-with-rankine-piston-expander.

Daccord, R., and M. Sager. 2015. “A Piston Expander for Exhaust Heat Recovery on Heavy Commercial Vehicles.” presented at the AORCC 2015, Denver, Colorado.

Demler, R.L. 1976. “The Application of the Positive Displacement Reciprocating Steam Expander to the Passenger Car.” 760342. SAE Technical Paper. http://papers.sae.org/760342/.

Dingel, O., T. Töpfer, and J. Seebode. 2015. “Efficiency Potentials of HD Powertrains as a Function of Emissions Concept and Waste Heat Recovery.” presented at the AORCC 2015, Denver, Colorado.

Endo, T., S. Kawajiri, Y. Kojima, K. Takahashi, T. Baba, S. Ibaraki, T. Takahashi, and M. Shinohara. 2007. “Study on Maximizing Exergy in Automotive Engines.” In *2007 World Congress Detroit*. Detroit, Michigan. doi:10.4271/2007-01-0257.

Ferrara, G., G. Manfrida, and A. Pescioni. 2013. “Model of a Small Steam Engine for Renewable Domestic CHP (Combined Heat and Power) System.” *Energy* 58: 78–85. doi:10.1016/j.energy.2013.03.035.

Fula, A., P. Stouffs, and F. Sierra. 2013. “In-Cylinder Heat Transfer in an Ericsson Engine Prototype.” In *International Conference on Renewable Energies and Power Quality (ICREPQ’13)*. Bilbao, Spain.

Galindo, J., V. Dolz, L. Royo-Pascual, R. Haller, and J. Melis. 2015. “Study of a Volumetric Expander Suitable for Waste Heat Recovery from an Automotive IC Engine Using an ORC with Ethanol.” In *Proc. 3rd International Seminar on ORC Power Systems*. Brussels, Belgium. http://www.asme-orc2015.be/online/proceedings/display_manuscript/85.htm.

Galindo, J., S. Ruiz, V. Dolz, L. Royo-Pascual, R. Haller, B. Nicolas, and Y. Glavatskaya. 2015. “Experimental and Thermodynamic Analysis of a Bottoming Organic Rankine Cycle (ORC) of Gasoline Engine Using Swash-Plate Expander.” *Energy Conversion and Management* 103 (October): 519–32. doi:10.1016/j.enconman.2015.06.085.

Galindo, J., J. Serrano, V. Dolz, and P. Kleut. 2015. “Brayton Cycle for Internal Combustion Engine Exhaust Gas Waste Heat Recovery.” *Advances in Mechanical Engineering* 7 (6). doi:10.1177/1687814015590314.

Grip, R-L. 2009. “A Mechanical Model of an Axial Piston Machine.” Licenciate Thesis, Stockholm, Sweden: KTH Royal Institute of Technology.

Heyl, P., and H. Quack. 1999. “Free Piston Expander–compressor for CO2 – Design, Applications and Results.” In *20th International Congress of Refrigeration*. Sydney, Australia.

———. 2000. “Transcritical CO2-Cycle with Expander-Compressor.” In *Proc. of the International Refrigeration Conference at Purdue*. West Lafayette, Indiana.

Heywood, J.B. 1988. *Internal Combustion Engine Fundamentals*. McGraw-Hill Series in Mechanical Engineering. New York: McGraw-Hill.

Hoagland, L. C., R. L. Demler, and J. Gerstmann. 1974. “Design Features and Initial Performance Data on an Automotive Steam Engine Part I - Overall Powerplant Description and Performance.” In . Vol. 740295. SAE. doi:10.4271/740295.

Howell, T., J. Gibble, and C. Tun. 2011. "Development of an ORC System to Improve HD Truck Fuel Efficiency." presented at the DEER conference, Detroit, Michigan.

Huff, H-J., and R. Radermacher. 2003. "CO2 Compressor-Expander Analysis." Technical Report ARTI-21CR/611-10060-01. Arlington, Virginia: Air-Conditioning and Refrigeration Technology Institute.

Kanno, H., and N. Shikazono. 2014. "Thermodynamic Simulations of Rankine, Trilateral and Supercritical Cycles for Hot Water and Exhaust Gas Heat Recovery." *Mechanical Engineering Journal*, October, TEP0046. doi:10.1299/mej.2014tep0046.

Latz, G. 2016. "Waste Heat Recovery from Combustion Engines Based on the Rankine Cycle." PhD Thèsis, Gothenburg, Sweden: Chalmer University of Technology.

Latz, G., S. Andersson, and K. Munch. 2013. "Selecting an Expansion Machine for Vehicle Waste-Heat Recovery Systems Based on the Rankine Cycle." In . SAE International. doi:10.4271/2013-01-0552.

Latz, G., O. Erlandsson, T. Skare, and A. Contet. 2015. "Water-Based Rankine-Cycle Waste Heazt Recovery Systems for Engines: Challanges and Opportunities." In *Proc. 3rd International Seminar on ORC Power Systems*. Brussels, Belgium: ASME.

Lemort, V., L. Guillaume, A. Legros, S. Declaye, and S. Quoilin. 2013. "A Comparison of Piston, Screw and Scroll Expanders for Small Scale Rankine Cycle Systems." In *Proc. of the 3rd International Conference on Microgeneration and Related Technologies*. Napoli, Italy. http://hdl.handle.net/2268/147369.

Lontsi, F., O. Hamandjoda, K. Fozao, P. Stouffs, and J. Nganhou. 2013. "Dynamic Simulation of a Small Modified Joule Cycle Reciprocating Ericsson Engine for Micro-Cogeneration Systems." *Energy* 63: 309–16. doi:10.1016/j.energy.2013.10.061.

Maurer, T., and T. Zinn. 2000. "Experimentelle Untersuchung von Entspannungsmaschinen Mit Mechanischer Leistungsauskopploung Fuer Die Transkritische CO2- Kaeltemaschine." In *Proc. of DKV Tagungsbericht Berlin, v26 nII.1*, 304–18. Berglin, Germany.

Mikalsen, R., and A.P. Roskilly. 2012. "The Free-Piston Reciprocating Joule Cycle Engine: A New Approach to Efficient Domestic CHP Generation." In *Proc. of ICAE2012 Conference*. Suzhou, China. http://www.mikalsen.eu/papers/FreeCHP.pdf.

Moss, R. W., A. P. Roskilly, and S. K. Nanda. 2005. "Reciprocating Joule-Cycle Engine for Domestic CHP Systems." *Applied Energy* 80 (2): 169–85. doi:10.1016/j.apenergy.2004.03.007.

Overman, D. 1992. "External Combustion Engine Technology (Vapor and Liquid Cycles) for PE: P62120 Individual Soldier Power Systems." HDL-TR-2212. Adelphi, Maryland: U.S. Army Laboratory Command.

Platell, P. 1993. "Displacement Expanders for Small Scale Cogeneration." Licenciate Thesis, Stockholm, Sweden: KTH Royal Institute of Technology.

Seher, D., T. Lengenfelder, J. Gerhardt, N. Eisenmenger, M. Hackner, and I. Krinn. 2012. "Waste Heat Recovery for Commercial Vehicles with a Rankine Process." In *21st Aachen Colloquium Automobile and Engine Technology 2012*. Aachen.

Steffen, M., M. Löffler, and K. Schaber. 2013. "Efficiency of a New Triangle Cycle with Flash Evaporation in a Piston Engine." *Energy* 57 (August): 295–307. doi:10.1016/j.energy.2012.11.054.

Stouffs, P. 2002. "Le Moteur d'Ericsson, Un Moyen de Valorisaton Du L'énergie Thermique À Réhabitliter?" *TERMOTEHNICA* 2: 37–42.

Technologie Assesment and Evaluation Branch. 1974. "Exhaust Emission Test of the Carter Steam Car."

Touré, A. 2010. "Etude Théorique et Expérimentale D'un Moteur Ericsson À Cycle de Joule Pour Conversion Thermodynamique D'énergie Solaire Ou Pour Micro-Cogénération." PhD Thesis, Université de Pau et des Pays de l'Adour.

Vickers, P. T., J. R. Mondt, W. H. Haverdink, and W. R. Wade. 1970. "General Motors' Steam-Powered Passenger Cars - Emissions, Fuel Economy and Performance." In . SAE International. doi:10.4271/700670.

Wojewoda, J., and Z. Kazimierski. 2010. “Numerical Model and Investigations of the Externally Heated Valve Joule Engine.” *Energy* 35 (5): 2099–2108. doi:10.1016/j.energy.2010.01.028.

Wronski, J. 2015. “Design and Modelling of Small Scale Low Temperature Power Cycles.” PhD Thesis, Kongens Lyngby, Danmark: DTU Mechanical Engineering.

Wronski, J., M-J. Skovrup, B. Elmegaard, H-N. Rislå, and F. Haglind. 2012. “Design and Modelling of a Novel Compact Power Cycle for Low Temperature Heat Sources.” Edited by E. Sciubba. *Proc. of ECOS 2012*.

Zhang, B., X. Peng, Z. He, Z. Xing, and P. Shu. 2007. “Development of a Double Acting Free Piston Expander for Power Recovery in Transcritical CO2 Cycle.” *Applied Thermal Engineering* 27 (8–9): 1629–36. doi:10.1016/j.applthermaleng.2006.05.034.

Chapter 3: Modeling piston expanders

Contents

1. Introduction

Several papers can be found in the literature about the modeling of piston expander's performances and losses. Almost all proposed model have its own specificities and can be distinguished in two kinds: models based on theoretical indicator diagram and models based on the evolution, in terms of crank angle, of the state of the fluid inside the control volume defined by the cylinder and the piston.

Platell (1993) have proposed a model based on theoretical PV diagram considering perfect gases and where mechanical losses are modeled with a dedicated model (see section 4). Demler (1976) also used theoretical PV diagram and defined ratios to take into account the main sources of losses: over- or under-expansion and compression, pressure drop and heat transfer. Mechanical losses were modeled with a correlation. Badami et al. (2008) considered heat losses of 5% and a mechanical efficiency of 94%. Daccord, Darmedru, and Melis (2014) have modeled leakages considering a fictive isentropic nozzle and mechanical losses with a polynomial law.

Several authors have proposed models based on conservation of energy and mass in the control volume defined by the cylinder wall and the piston. These models differ mainly by the fluid state equation and by the way to model the sources of losses. A literature review of losses modeling is summarized in Table 3-1. It appears that supply and exhaust mass flows are modeled in two ways; assuming incompressible flow or assuming compressible flow through isentropic nozzle. The leakage flow is either neglected or modeled as mass flow or assumed to be a percentage of the total flow. Heat transfer coefficients are principally estimated with the help of correlations established for ICE engines ((Morel and Keribar 1985) and (Annand 1963)) or from reciprocating compressors (Adair, Qvale, and Pearson 1972). Finally, mechanical losses are taken into account with either constant mechanical efficiency, correlations or a dedicated detailed model (see section 4).

Table 3-1: Literature review about losses modelling

Reference	State equation	Mass flow rate	Leakages	Heat transfer	Mechanical losses
(Huff and Radermacher 2003)	Not specified	Incompressible flow	Incompressible flow	Adair correlation	None
(Baek, Groll, and Lawless 2005)	(Span and Wagner 1996)	Incompressible flow	30-40 % of the mass in the cylinder	None	Dedicated model
(Clemente et al. 2011)	(Lemmon and Span 2006)	Isentropic nozzle	2% of the flow	12% of the work	η_m=88 %
(Mckenna, Mccullough, and Douglas 2012)	Perfect gases	Isentropic nozzle	None	Annand correlation	Correlation (see section 4)

(Ferrara, Manfrida, and Pescioni 2013)	Perfect gases	Isentropic nozzle	None	$h_c = cst$ during expansion, otherwise $hc = 0$	None
(Wronski 2015)	CoolProp (Bell et al. 2014)	Incompressible flow	Incompressible flow	Adair correlation	Correlation (see section 4)
(Latz 2016)	Not specified	Not specified	Not specified	Morel & Keribar	Correlation (see section 4)

In this chapter, a detailed and a semi-empirical model of expander are proposed. The former is a control volume-based model and the latter is an indicator diagram-based model. It should be noted that the detailed model is also able to describe reciprocating compressor and will be used to model the compressor of the Ericsson engine. Both models allow to compute the indicated power and the friction model used to compute the shaft power is the same for both modeling approaches. The detailed model is used for the pre-design (see chapter 4) of the Ericsson engine. Both models are validated based on experimental results collected on the Ericsson engine and on the expander integrated in an ORC system. Then, the validated detailed model is used to analyze the sources of losses and the semi-empirical model is used to simulate the Ericsson and the ORC expander in CHP systems.

2. Detailed model

The proposed detailed model of piston engine is based on conservation of energy and mass in the control volume defined by the cylinder wall and the piston (see Figure 3-1). The goal of the model is to compute the state of the fluid in terms of shaft angle evolution. In the proposed model, two assumptions are made:

- The state of the fluid is homogeneous inside the cylinder
- The temperature of the cylinder walls is uniform

In order to compute the state of the fluid, a geometrical model is needed to define the volume of the open system defined by the control volume boundaries and the cross section area of the inlet and exhaust ports. A heat transfer model is proposed to compute heat flux rejected by the gases to the wall. Then, the supply and exhaust flows have to be computed as a function of the upstream and downstream pressures. Finally, conservation of energy and mass, coupled with fluid state model allow to compute the state of the fluid inside the cylinder. Once the in-cylinder fluid state is known, the volume and the mass flows can be determined according to the shaft angle. Also, values as indicated power and exhaust temperature averaged over one revolution can be computed.

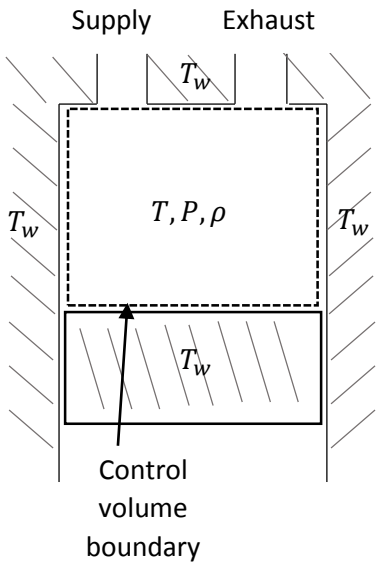

Figure 3-1: Control volume of detailed model

2.1.Geometric model

2.1.1. Cylinder volume

The goal of the geometric model is to express the cylinder volume in terms of the shaft angle θ (Figure 3-2). This volume can be expressed as:

$$V = V_0 + \pi . \frac{D^2}{4} . x \qquad (3\text{-}1)$$

where V_0 is the clearance volume, D is the bore diameter and x is the distance between the TDC and the piston head. The expression of this last value depends on the linear to rotation motion conversion system. For crankshaft system, equation (3-2) can be used and for swash or wobble plate, this distance is given by equation (3-3).

$$x = B + \frac{L}{2} . (1 - \cos(\theta)\,) - \sqrt{B^2 - \left(\frac{L}{2}\right)^2 . \sin^2(\theta)} \qquad (3\text{-}2)$$

$$x = \frac{L}{2} . (1 - \cos(\theta)) \qquad (3\text{-}3)$$

where B is the length of the connecting rod, R is the crank radius and L the piston stroke (see Figure 3-2).

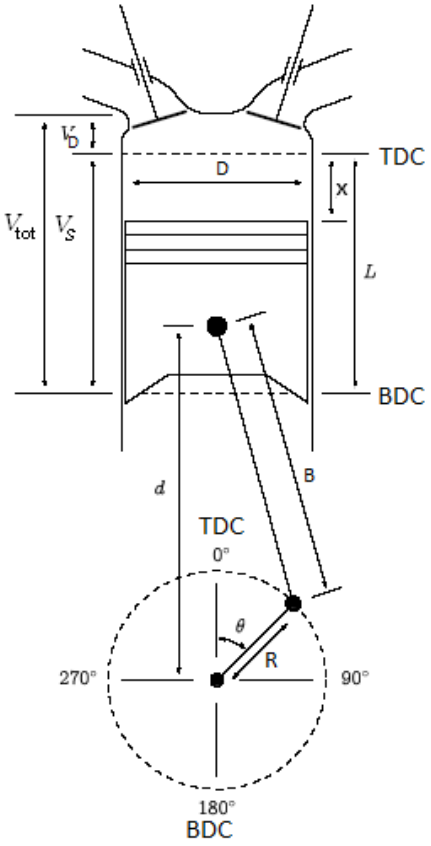

Figure 3-2: Sketch of the set cylinder, piston, connecting rod and crankshaft

2.1.2. Supply and exhaust port cross section area

The calculation of a port cross section area depends on the valve type (poppet valve, sliding valve, etc.) and dimensions. For each machine, valves dimensions and motion have to be defined. However, poppet valves with cam actuation are a widespread system and generic equation for valve lift and cross section can be found in the literature.

For poppet valves (see Figure 3-3), the cross section area depends on the dimension of the valve head, seat and stem and go through three different stages when lift increases (Heywood 1988):

For $0 < L_v < \frac{w}{\sin\beta.\cos\beta}$

$$A_v = \pi . L_v . cos\beta . (D_v - 2.w + \frac{L_v}{2} . \sin 2\beta)$$

For $\frac{w}{\sin\beta.\cos\beta} < L_v < \left[\left(\frac{{D_{vi}}^2 - D_S^2}{4.D_m}\right) - w^2\right]^{\frac{1}{2}} + w.\tan\beta$

$$A_v = \pi . D_m . [(L_v - w.\tan\beta)^2 + w^2]^{\frac{1}{2}} \quad (3\text{-}4)$$

For $\left[\left(\frac{{D_{vi}}^2 - D_S^2}{4.D_m}\right) - w^2\right]^{\frac{1}{2}} + w.\tan\beta < L_v$

$$A_v = \frac{\pi}{4} . ({D_{vi}}^2 - D_s^2)$$

where L_v is the lift, w the seat width, β the seat angle, A_v the cross section area, D_v the valve head diameter, D_{vi} the inner seat diameter and $D_m = (D_v - w)$ the mean diameter (see Figure 3-3).

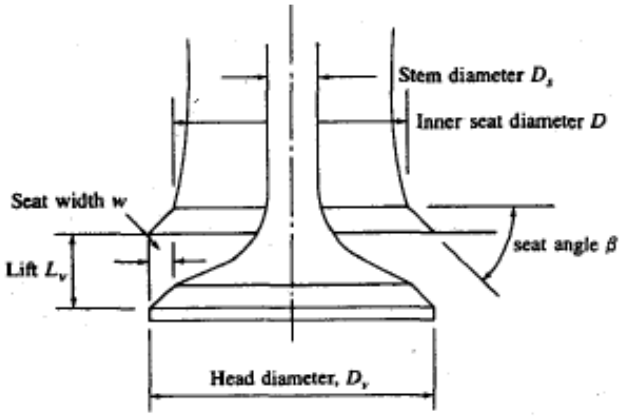

Figure 3-3: Poppet valve dimensions (Heywood 1988)

The valve lift depends on the cam profile and on the dynamic behavior of the valve train. Indeed, some deformations, rebound, etc. can appear when the valve train is in motion, making the dynamic lift different from the kinematic lift. (Blair 1999) proposed a general description of cam-actuated valve lift. The lift is composed of five parts: ramp up, main lift up, dwell, main lift down and ramp down.

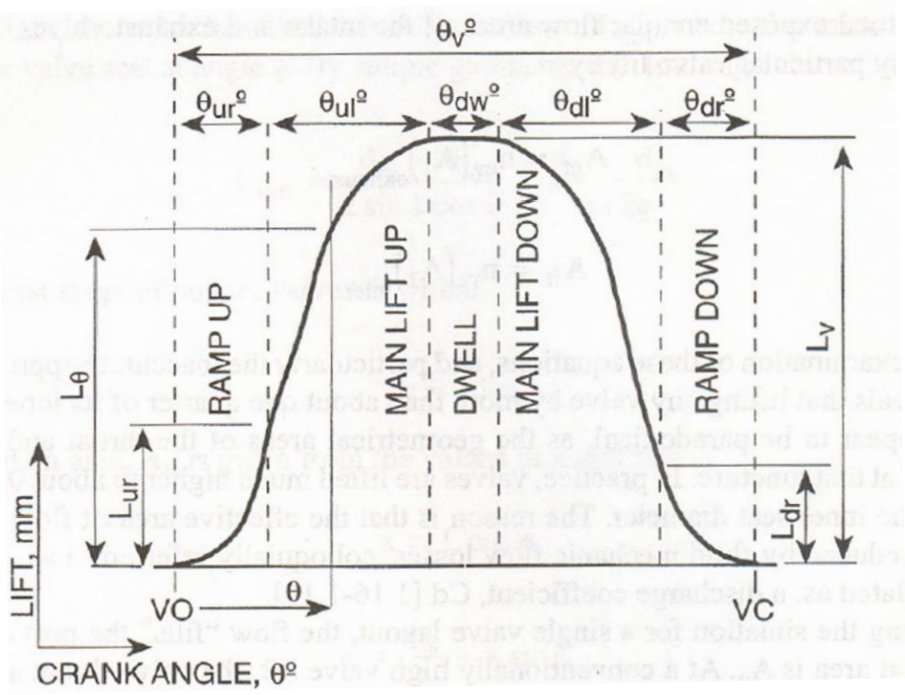

Figure 3-4: Valve lift description (Blair 1999).

2.2.Heat transfers

The gas inside the cylinder is at a different temperature from the one of the cylinder wall, and piston head and then exchanges heat with it. Considering a uniform temperature of the gas and of the wall, the heat flux rejected by the gas can be expressed as:

$$\dot{Q}_w = h_c . S_w . (T - T_w) \qquad (3\text{-}5)$$

where h_c is the convection heat transfer coefficient, S_w the area of the cylinder wall and piston head and T_w the uniform temperature of this wall.

The convective heat transfer coefficient h_c can be estimated through several correlations that give the Nusselt number. As seen in section 1, different correlations can been found in the literature for piston machine such as ICE or reciprocating compressors. These correlations allowing the computation of the Nusselt number are most often in the form of equation (3-6).

$$Nu = a . Re^b . Pr^c \qquad (3\text{-}6)$$

where Re and Pr are respectively the Reynolds and the Prandtl number. The correlations differ by the values of the constants a, b and c and by the choice of characteristic the lengths L_c and the fluid speed C used to compute the Reynolds number. These values are presented in Table 3-2 for three correlations.

Table 3-2: Heat transfers correlation parameters values

Authors	Parameters values		Original application
(Woschni 1967)	$a = 0.035$ $b = 0.8$ $c = 0$	$L_c = D$ $C_p = 6.18(2.\mathrm{L}.\frac{\omega}{2\pi})$ gas exchange $C_p = 2.28(2.\mathrm{L}.\frac{\omega}{2\pi})$ expansion and compression	ICE
(Annand 1963)	$a = 0.35$ $b = 0.7$ $c = 0$	$L_c = D$ $C_p = 2.\mathrm{L}.\frac{\omega}{2\pi}$	ICE
(Adair, Qvale, and Pearson 1972)	$a = 0.053$ $b = 0.8$ $c = 0.6$	$L_c = D$ $C_p = 2.\mathrm{L}.\frac{\omega}{2\pi}$	Reciprocating compressor

2.3.Mass flow rates

In order to solve the mass and energy conservations, the mass flows entering and leaving the control volume have to be known. In the proposed model, the different orifices are treated as convergent nozzles and flows are assumed to be isentropic. Then, the mass flow rates are computed by the following equation:

$$\dot{m} = C_d.A_v.\rho_{thr}\sqrt[2]{2.(h_{up} - h_{thr})} \quad (3\text{-}7)$$

where A_v is the cross flow area, h_{up} is the enthalpy of the upstream fluid and h_{thr} and ρ_{thr} are the enthalpy and the density at the throat of the nozzle. The state of the fluid at the throat of the nozzle is computed assuming isentropic flow, therefore with the entropy of the upstream fluid. Considering that the flow can be choked, the pressure at the nozzle throat is:

$$\begin{aligned} &\text{If } P_{down} > P_{crit} : P_{thr} = P_{down} \\ &\text{If } P_{down} < P_{crit} : P_{thr} = P_{crit} \end{aligned} \quad (3\text{-}8)$$

where P_{down} is the downstream pressure and P_{crit} is the critical value of the downstream pressure at which the flow becomes choked. Assuming a perfect gas, this critical value is:

$$P_{crit} = P_{up}.\left(\frac{2}{\gamma+1}\right)^{\frac{\gamma}{\gamma-1}} \quad (3\text{-}9)$$

where $\gamma = c_p/c_v$ is the isentropic coefficient.

Leakage mass flow rates are computed in the same way, with a fictional lumped cross section area by-passing the cylinder.

2.4. Conservation equations and derivation of differential equations governing the process

The boundaries of the volume defined above (Figure 3-1) forms an open thermodynamic system. The conservation of energy of a control volume is:

$$\frac{dE}{dt} = \dot{Q} + \dot{W} + \sum \dot{m}_{su}.\left(h + \frac{C^2}{2} + g.z\right)_{su} - \sum \dot{m}_{ex}.\left(h + \frac{C^2}{2} + g.z\right)_{ex} \quad (3\text{-}10)$$

where E is the total energy of the sytem, $\dot{Q}$ is the heat transfer, $\dot{W}$ is the power, $\dot{m}_{su}$ and $\dot{m}_{ex}$ are the mass flow rates entering and leaving the system, and $\left(h + \frac{C^2}{2} + g.z\right)$ is the total enthalpy.

And the mass balance of a control volume is:

$$\frac{dm}{dt} = \sum \dot{m}_{su} - \sum \dot{m}_{ex} \quad (3\text{-}11)$$

By neglecting the kinetic and potential energies, the total energy of the system is the internal energy of the fluid U and the left hand side of equation (3-10) can be written as:

$$\frac{dE}{dt} = \frac{dU}{dt} = m.\frac{du}{dt} + u.\frac{dm}{dt} \quad (3\text{-}12)$$

The goal of the following development is to express the derivative of the temperature. Indeed, the derivatives of the temperature and of the mass allow, knowing the volume by equation (3-1), to compute the temperature and the specific volume of the fluid inside the cylinder. Since the development is different if the fluid is superheated or saturated, the two cases are considered, allowing the model to simulate a potential condensation of the fluid inside the cylinder.

2.4.1. Single-phase case

Combining equations (3-11) and (3-12) and considering that:

- The change of specific internal energy of an open control volume is:

$$du = c_v.dT + \left[T\left(\frac{\partial P}{\partial T}\right)_v - P\right].dv \quad (3\text{-}13)$$

- The specific internal energy can be expressed as:

$$u = h - P.v \quad (3\text{-}14)$$

- Assuming uniform pressure inside the control volume, the power is:

$$\dot{W} = -P.\frac{dV}{dt} \quad (3\text{-}15)$$

equation (3-10) can be rewritten as:

$$m.c_v.\frac{dT}{dt} + T.\left(\frac{dP}{dT}\right)_v.\left[\frac{dV}{dt} - \frac{1}{\rho}.\frac{dm}{dt}\right] + h.\frac{dm}{dt} = \dot{Q} + \sum \dot{m}_{su}.h_{su} - \sum \dot{m}_{ex}.h_{ex} \quad (3\text{-}16)$$

And finally, as $h_{ex} = h$ and applying the variable change $d\theta = \omega . dt$, the derivative of the temperature with respect to shaft angle can be expressed as:

$$\frac{dT}{d\theta} = \frac{1}{m.c_v} . \left[-T . \left(\frac{\partial P}{\partial T} \right)_v . \left(\frac{dV}{d\theta} - v . \frac{dm}{d\theta} \right) + \frac{\dot{Q}}{\omega} + \sum \frac{\dot{m}_{su}}{\omega} . (h_{su} - h) \right] \quad (3\text{-}17)$$

In this equation, the heat transfer is the heat brought to the fluid, then $\dot{Q} = -\dot{Q}_w$ (see equation (3-5)), and the different mass flow rates are computed with equation (3-7).

2.4.2. Two-phase case

A similar type of development can be made if the fluid is saturated. (Liu and Soedel 1995) have shown that the derivative of the temperature can be expressed as:

$$\frac{dT}{d\theta} = \frac{1}{a} . \left[\frac{\dot{Q}}{\omega} - \frac{h_g - h_l}{v_g - v_l} . \frac{dV}{d\theta} + v . \frac{h_g - h_l}{v_g - v_l} . \frac{dm}{d\theta} + \sum \frac{\dot{m}_{su}}{\omega} . (h_{su} - h) \right] \quad (3\text{-}18)$$

where

$$a = m . \left[x . \left(\frac{dh_g}{dT} - \frac{h_g - h_l}{v_g - v_l} . \frac{dv_g}{dT} \right) + (1 - x) \left(\frac{dh_l}{dT} - \frac{h_g - h_l}{v_g - v_l} . \frac{dv_l}{dT} \right) - v . \frac{dP}{dT} \right] \quad (3\text{-}19)$$

2.5. Gas state equation

As mentioned hereunder, by solving the differential equations (3-17) or (3-18) and (3-11), the specific volume and the temperature of the fluid in the cylinder can be computed as a function of the crank angle. In order to compute the pressure, an equation of state is needed (equation (3-20)). For this purpose, the CoolProp library (Bell et al. 2014) is used (CoolProp is C++ library that implements equations of state of a wide range of fluids).

$$P = P(T, v) \quad (3\text{-}20)$$

2.6. Average values

When the shaft angle evolutions of the variables of interest are known, an average can be computed on one revolution. Considering a variable $y(\theta)$, its average value on one revolution is given by:

$$\bar{x} = \frac{1}{2.\pi} \int_{\theta=0}^{\theta=2.\pi} y(\theta) . d\theta \quad (3\text{-}21)$$

Using this equation, averages of the mass flow rate, indicated power delivered by the fluid and thermal power rejected to the cylinder wall can be computed.

In order to compute the average exhaust temperature, the specific average exhaust enthalpy is computed by:

$$\overline{h_{ex}} = \frac{\int_{\theta=0}^{\theta=2.\pi} \dot{M}_{ex}(\theta).h_{ex}(\theta).d\theta}{\int_{\theta=0}^{\theta=2.\pi} \dot{M}_{ex}(\theta).d\theta} \quad (3\text{-}22)$$

The average exhaust temperature can be calculated considering the average exhaust enthalpy and the exhaust pressure.

2.7. Average energy balance

In steady-state regime, the following energy balance can be written about the cylinder wall:

$$\dot{Q}_w + \dot{W}_{loss} = \dot{Q}_{amb} + \dot{Q}_{cooling} \quad (3\text{-}23)$$

where $\dot{W}_{loss}$ is the mechanical friction losses dissipated as heat (see section 4), $\dot{Q}_{cooling}$ is the heat removed by a possible cooling system (e.g. water cooled engine) and $\dot{Q}_{amb}$ is the ambient heat loss:

$$\dot{Q}_{amb} = AU_{amb}.(T_w - T_{amb}) \quad (3\text{-}24)$$

In order to solve equations (3-23) and (3-24), either AU_{amb} is imposed and T_w is computed or inversely.

2.8. Numerical solution

The model described above has been implemented in Matlab. Figure 3-5 shows the flow chart of the implemented program. First the inputs are defined, the geometrical variables are computed, the wall temperature is either guessed or set and an assumption on initial state of the fluid is made. Then the expansion process consists in solving the governing differential equations. The Euler forward method is used to solve these equations. Once the evolution of the fluid state during one revolution is known, the guessed initial values are compared to final value. If convergence is not reached (equation (3-25)), the initial value are set to the final value until the convergence is achieved.

$$\rho(0) - \rho(2.\pi) < \epsilon \quad (3\text{-}25)$$

Then, if the wall temperature is not fixed, the wall energy balance is checked and if the convergence is not reached (equation (3-26)), T_w is adjusted by the bisection method until it converges.

$$\dot{Q}_w + \dot{W}_{loss} - \dot{Q}_{amb} - \dot{Q}_{cooling} < \epsilon \quad (3\text{-}26)$$

Finally, average values are computed.

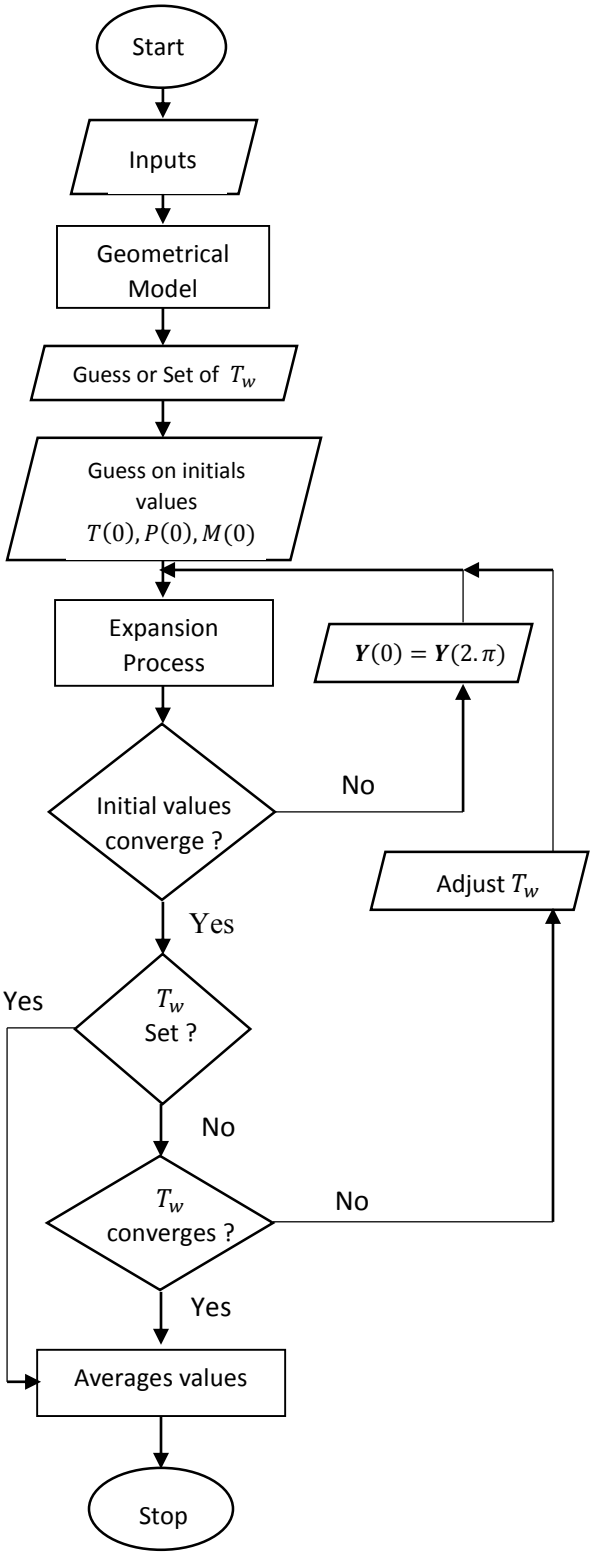

Figure 3-5: Control volume-based model numerical resolution flow chart

3. Semi empirical model

The semi-empirical model of a scroll-expander proposed by (Lemort et al. 2009), has been adapted to piston expander. The major difference between the modeling of a scroll and a piston expander lies in the presence of a clearance volume in the latter machine, which is responsible for the recompression of a part of the fluid after the exhaust process. This difference has led to a modification of the scroll expander model in order to take into account the recompression process.

3.1. Losses model

As shown in Figure 3-6, the evolution of the fluid through the expander is decomposed into seven steps representing the main physical features:

- Adiabatic supply pressure drop, modeled assuming isentropic flow through a convergent nozzle of throat cross section area A_{su}. (Equation (3-7) can be used to compute the pressure drop as a function of the supply mass flow rate.)
- Supply heat transfer between the fluid and the uniform temperature wall characterized by overall heat transfer coefficient AU_{su}.
- Split between internal mass flow rate and leakage mass flow rate. The leakage mass flow rate is also modeled by an isentropic flow through a convergent nozzle, with a throat cross section area A_{leak}.
- Expansion process, described in the next section.
- Adiabatic mixing of internal mass flow and leakage mass flow.
- Exhaust heat transfer area between the fluid and the uniform temperature wall characterized by overall heat transfer coefficient AU_{ex}.
- Adiabatic exhaust pressure drop, again computed as an isentropic flow through a convergent nozzle. The throat cross section area is A_{ex}.

As for the detailed model, the energy balance applied to the wall allows the computation of the uniform wall temperature:

$$\dot{Q}_{su} + \dot{Q}_{ex} + \dot{W}_{loss} = AU_{amb}.(T_w - T_{amb}) \quad (3\text{-}27)$$

and mass conservation gives:

$$\dot{M} = \dot{M}_{in} + \dot{M}_{leak} \quad (3\text{-}28)$$

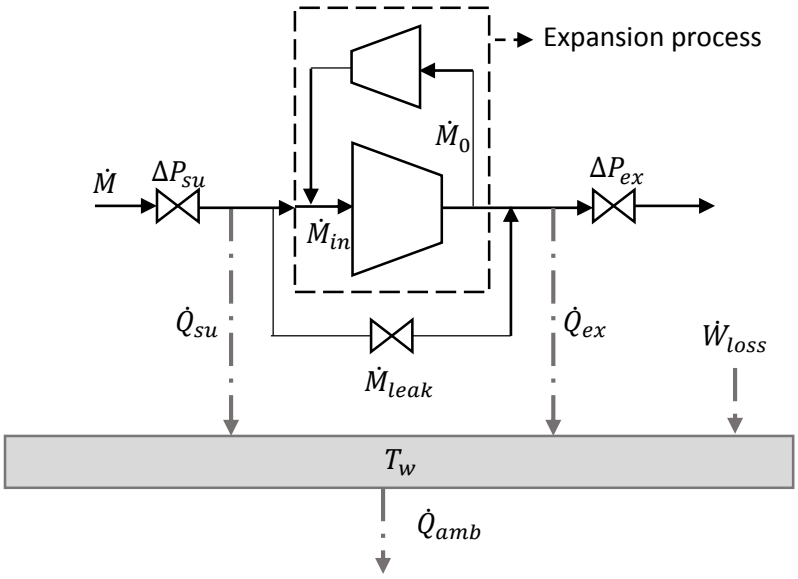

Figure 3-6: Semi-empirical model scheme

3.2. Theoretical indicator diagram-based expansion process

The theoretical indicator diagram is shown in Figure 3-7. This diagram is composed of six evolutions of the fluid:

- 1-2: isobaric intake
- 2-3: isentropic expansion
- 3-4: constant machine volume expansion
- 4-5: isobaric exhaust
- 5-6: isentropic compression
- 6-1: constant machine volume compression

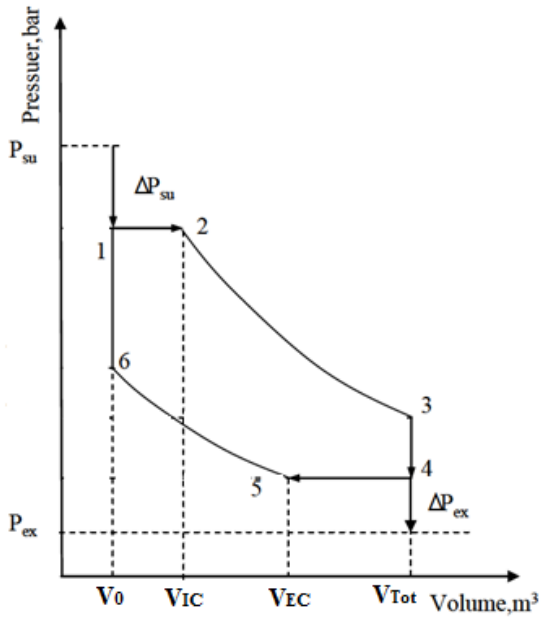

Figure 3-7 : Theoretical indicator diagram based expansion process

The state of the fluid in point 2 can be computed by the energy balance between points 6 and 2:

$$m_2.u_2 = m_6.u_6 + (m_2 - m_6).h_{su} - P_2.(V_2 - V_1) \quad (3\text{-}29)$$

Considering isentropic expansion, the state of the fluid at point 3 is deduced from point 2.

As during the constant machine volume expansion the state of the fluid leaving the expander varies, the energy balance during the step 3-4 is not straightforward and would necessitate an integration. In order to avoid such a calculation, it is assumed that the enthalpy of the fluid leaving the expander is the average enthalpy of points 3 and 4.

$$m_4.u_4 = m_3.u_3 - (m_3 - m_4).\frac{h_3+h_4}{2} \quad (3\text{-}30)$$

The state of the fluid at point 5 is the same as at point 4. Finally, the state of the fluid at point 6 is computed considering an isentropic compression during the step 5-6.

The indicated work of the expansion cycle is composed of four works expressed in equation (3-31) : isobaric admission, expansion, isobaric exhaust and compression works.

$$W_{in} = P_1.(V_2 - V_0) + \frac{V_2}{v_2}.(u_2 - u_3) - P_4.(V_{Tot} - V_5) - \frac{V_5}{v_5}.(u_6 - u_5) \quad (3\text{-}31)$$

where $V_2 = V_{IC}$ is the intake closing volume and $V_5 = V_{EC}$ the exhaust closing volume, V_0 the clearance volume and v stands for specific volume. As in chapter 2, V_{IC} is defined with the cut-off ratio or built-in expansion ratio and V_{EC} with the built-in compression ratio:

$$CO = \frac{V_{IC}}{V_{tot}} = \frac{1}{r_{v,inexp}} \quad \text{and} \quad r_{v,in,cp} = \frac{V_{EC}}{V_0} \qquad (3\text{-}32)$$

The average enthalpy leaving the expander between points 3 and 5 is computed by the energy balance over the expansion process:

$$\dot{W}_{in} = \dot{M}_{in}.(h_{\mathrm{su}} - h_{\mathrm{ex}}) \qquad (3\text{-}33)$$

The internal mass flow rate depends on geometric parameters and operating conditions:

$$\dot{M}_{in} = N.\left(\frac{V_{IC}}{v_2} - \frac{V_{EC}}{v_5}\right) \qquad (3\text{-}34)$$

4. Friction model

In order to precisely model friction losses in all the components of a piston engine, complex typological models have to be built. However, friction losses are more often modeled with the help of correlations taking into the account main influential parameters. These parameters are principally the rotational speed and the peak pressure (in order to take into account the load). These correlations are based on friction power measurements. For piston expander, the two most common measurement methods consist in: 1) measuring the indicated and shaft power to compute the friction power or 2) to motor the engine and to measure the required power to overcome the friction forces. The second method is less precise because the expander or the engine does not run in representative operating conditions (temperature, in-cylinder pressure, etc.).

This section presents some friction correlations and models found in the literature for ICEs and piston expanders and the correlation used in this work.

4.1. Frictions correlation in ICE application

Several authors proposed correlation for friction in ICE based on measurement. Some of these correlations are listed in Table 3-3. The Gish correlation is a bit limited because done on a four cylinder SI engine at a constant speed of 1600 RPM but shows the influence of the peak pressure. The correlation of Chen and Flyn, Barness and Mosts Millington are more general because the authors motored several engine and aggregated the data in one correlation.

It can be seen that these correlation depend on the rotational or mean piston speed, the peak pressure and the “total work” for (Taylor 1961). The total work is the sum of the work produced during the expansion and the work consumed during the compression. In these correlations, the constant term and the one proportional to the peak pressure or the total work represent boundary regime frictions. The term proportional to the speed represents friction in hydrodynamic regime. Finally, the term proportional to the square of the speed represents the pumping losses. Actually, the pumping losses are not friction losses but represent the indicated work lost during admission and exhaust process of a four stroke engine. Therefore, this squared term should not appear in a piston expander mechanical friction model.

Table 3-3: ICE $fmep$ correlations ($fmep$ [bar], N [RPM], $\overline{C}_p$ [m/s], P_{peak} [bar])

Authors	Correlations	Measurement method
(Gish et al. 1958)	$fmep = 1 + 0.0125.P_{peak}$	$Imep$ measurement
(Chen and Flynn 1965)	$fmep = 0.138 + 0.005.P_{peak} + 0.164.\bar{C}_p$	Direct motoring
(Barnes-Moss 1975)	$fmep = 0.97 + 0.15.\left(\frac{N}{1000}\right) + 0.05.\left(\frac{N}{1000}\right)^2$	Direct motoring
(Winterbone and Tennant 1981)	$fmep = 0.061 + 0.294.\frac{N}{1000} + 0.016.P_{peak}$	Direct motoring
(Millington and Hartles 1968)	$fmep = 1.1 + 0.48.\left(\frac{N}{1000}\right) + 0.004.\bar{C}_p^2$	Direct motoring
(Taylor 1961)	$fmep = 0.34 + 0.068.\bar{C}_p + 2.9\ 10^{-4} imep_{tot}.\bar{C}_p$	Direct motoring

Figure 3-8 shows the evolution of these different correlations in terms of rotational speed. The squared term are not taken into account since pumping losses are not present in piston expander. If peak pressure was needed, it has been set to 15 bar. In Chen correlation, the mean piston speed was computed with two different strokes: 0.05 m and 0.1 m. The differences between the correlations come from the differences between the measurement processes, the type of engine (Diesel, Spark Ignition, number of cylinder,…), Moreover, some correlations include the auxiliaries consumption (e.g. Gish and Millington) while others correlations represent only friction losses (e.g. Chen).

4.2.Friction modeling in piston expander application

As shown in Table 3-1, different complexities of mechanical losses model can be found in the literature. Platell (1993) has given expressions to compute the normal force acting on: piston ring oil film, piston-sleeve transvers force and conrod bearing. The friction forces are then the normal forces multiplied by the friction coefficients. However, the author does not give friction coefficients, which strongly depends on the regime of lubrication. Baek, Groll, and Lawless (2005) resolved a Reynold equation (partial differential equation derived from Navier-Stokes equation) proposed in (Heywood 1988) in order to compute the oil film thickness and pressure distribution between piston ring and cylinder wall. He has concluded that the friction between these two surfaces is in boundary lubrication regime, which is explained by the low rotational speed (120-600 RPM). Latz (2016) and Demler (1976) used correlation from ICE applications ((Chen and Flynn 1965) and (Taylor 1961) respectively). Finally, both Creyx (2015) and Touré (2010) measured friction in expanders considered for an Ericsson engine application. Creyx (2015) used a modified mono-cylinder four-stroke engine of 160 cm³ while Touré (2010) tested a prototype of piston expander with one cylinder of 650 cm³. Both gave a correlation of friction torque Tm_f in terms of rotational speed. The Table 3-4 gives the corresponding $fmep$ considering that:

$$fmep = \frac{T_{mf}.2.\pi}{V_{tot}} \quad (3\text{-}35)$$

Table 3-4: Piston expander $fmep$ correlations (T_f $[Nm]$, $fmep$ [bar], N [RPM])

Authors	Correlations
(Creyx 2015)	$T_{mf} = 0.52 + 0.00025N$ $fmep = 0.204 + 9.8\ 10^{-5}N$
(Touré 2010)	$T_{mf} = 3.2 + 0.00079.N$ $fmep = 0.31 + 7.6\ 10^{-5}\ N$
(Wronski 2015)	$T_{mf} = 2.5.\left(\frac{N}{1000}\right)$ $fmep = 0.21.\left(\frac{N}{1000}\right)$

These correlations give $fmep$ lower than for ICE (see Figure 3-8) and the five correlations predict similar results. The lower value can be explained by the absence of auxiliaries and, for (Touré 2010), the different design as it is a prototype.

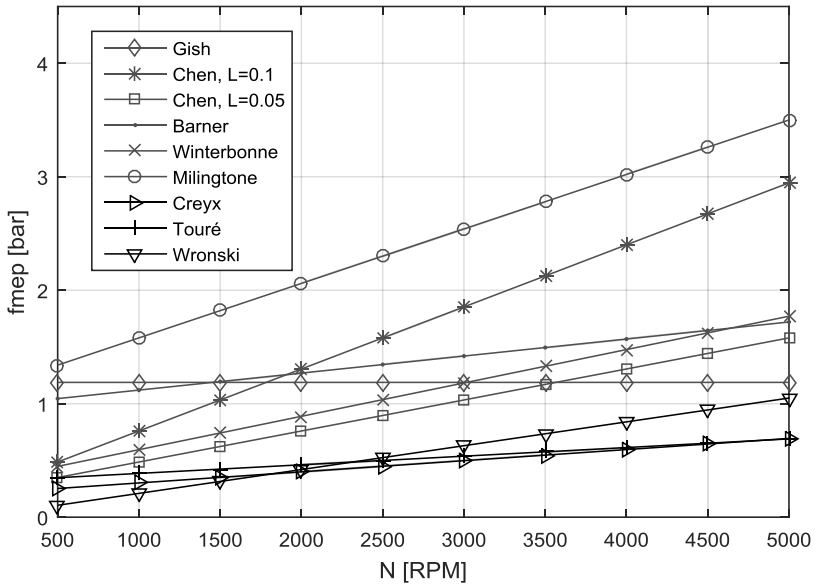

Figure 3-8: Comparison of different $fmep$ correlations (Peak pressure is set to 15 bar and, in Chen correlation, stroke is set to 0.05 m and 0.1 m)

In the present work, it was decided to derive a correlation from $imep$ and shaft power measurement (see Chapters 4 and 5). The correlation has a constant term, a term proportional to the supply pressure to take into account the load, and a term proportional to the rotational speed:

$$fmep = A + B.P_{su} + C.N \qquad (3\text{-}36)$$

5. Conclusions

Literature review shows that two types of models are often used to simulate piston machines. These two types of models differ by the way they describe the expansion process. Indeed, the simplest models are based on the theoretical indicator diagram. The more detailed models are based on the resolution of the differential equation governing the evolution of the state of the fluid in an open control volume described by the cylinder. These differential equations describe the conservation of energy and mass over the system in terms of time or shaft angle. In these two categories of model, the different sources of losses can be modeled in different manners.

Both types of models have been developed in this work and are presented in this chapter. For both models, mass flow rates are described by an isentropic flow through a convergent nozzle and heat transfer is computed considering a uniform wall temperature. In the detailed model, the evolution of mass flow rates and heat transfer are computed over one revolution while in the semi empirical model, average mass flow rate and heat flux are directly computed.

The detailed model will be used in the next chapter to pre-design an Ericsson engine. It is then validated on measurements collected from a prototype of Ericsson engine as well as from a piston expander integrated into an ORC. Finally, this model is used to perform losses analysis. The semi-empirical model is combined with other components models in order to simulate CHP systems based on an Ericsson engine and on an ORC system (chapter 6).

6. References

Adair, R.P., E.B. Qvale, and J.T. Pearson. 1972. “Intantaneous Heat Transfer to the Cylinder Wall in Recipr Ocating Compressors.” In *Proc. of Internationl Compressor Engineering Conference*. Purdue, USA.

Annand, W.J.D. 1963. “Heat Transfer in the Cylinders of Reciprocating Internal Combustion Engines.” In *Proc. Instn Mech. Engrs*, 117:973–90.

Badami, M., M. Mura, P. Campanile, and F. Anzioso. 2008. “Design and Performance Evaluation of an Innovative Small Scale Combined Cycle Cogeneration System.” *Energy* 33 (8): 1264–76. doi:10.1016/j.energy.2008.03.001.

Baek, J.S., E.A. Groll, and P.B. Lawless. 2005. “Piston-Cylinder Work Producing Expansion Device in a Transcritical Carbon Dioxide Cycle. Part II: Theoretical Model.” *International Journal of Refrigeration* 28 (2): 152–64. doi:10.1016/j.ijrefrig.2004.08.007.

Barnes-Moss, H.W. 1975. “A Designer’s Viewpoint in Passenger Car Engines.” In , 133–47. London: Institution of Mechanical Engines.

Bell, I., J. Wronski, S. Quoilin, and V. Lemort. 2014. “Pure and Pseudo-Pure Fluid Thermophysical Property Evaluation and the Open-Source Thermophysical Property Library CoolProp.” *Industrial & Engineering Chemistry Research* 53 (6): 2498–2508. doi:10.1021/ie4033999.

Blair, G. 1999. *Design and Simulation of Four-Stroke Engines*. Warrendale, PA: Society of Automotive Engineers.

Chen, S., and P. Flynn. 1965. “Development of a Single Cylinder Compression Ignition Research Engine.” In . SAE International. doi:10.4271/650733.

Clemente, S., D. Micheli, M. Reini, and R. Taccani. 2011. “Performance Analysis and Modeling of Different Volumetric Expanders for Small-Scale Organic Rankine Cycles.” In *Proc. of the ASME 2011 5th International Conference on Energy Sustainability*, 375–84. Washington DC, USA: ASME. doi:10.1115/ES2011-54302.

Creyx, M. 2015. “Etude théorique et expérimentale d’une unité de micro-cogénération biomasse avec moteur Ericsson.” PhD Thesis, Université de Valanciennes et du Hainaut-Cambresis.

Daccord, R., A. Darmedru, and J. Melis. 2014. “Oil-Free Axial Piston Expander for Waste Heat Recovery.” In . doi:10.4271/2014-01-0675.

Demler, R.L. 1976. “The Application of the Positive Displacement Reciprocating Steam Expander to the Passenger Car.” 760342. SAE Technical Paper. http://papers.sae.org/760342/.

Ferrara, G., G. Manfrida, and A. Pescioni. 2013. “Model of a Small Steam Engine for Renewable Domestic CHP (Combined Heat and Power) System.” *Energy* 58: 78–85. doi:10.1016/j.energy.2013.03.035.

Gish, R. E., J. D. Mccullough, J. B. Retzloff, and H. T. Mueller. 1958. “DETERMINATION OF TRUE ENGINE FRICTION.” 580063. Warrendale, PA: SAE International. http://www.sae.org/technical/papers/580063.

Heywood, J.B. 1988. *Internal Combustion Engine Fundamentals*. McGraw-Hill Series in Mechanical Engineering. New York: McGraw-Hill.

Huff, H-J., and R. Radermacher. 2003. "CO2 Compressor-Expander Analysis." Technical Report ARTI-21CR/611-10060-01. Arlington, Virginia: Air-Conditioning and Refrigeration Technology Institute.

Latz, G. 2016. "Waste Heat Recovery from Combustion Engines Based on the Rankine Cycle." PhD Thèsis, Gothenburg, Sweden: Chalmer University of Technology.

Lemmon, E., and R. Span. 2006. "Short Fundamental Equation of State for 20 Industrial Fluids." *Journal of Chemical and Engineering Data* 51: 785–850.

Lemort, V., S. Quoilin, C. Cuevas, and J. Lebrun. 2009. "Testing and Modeling a Scroll Expander Integrated into an Organic Rankine Cycle." *Applied Thermal Engineering* 29 (14–15): 3094–3102. doi:10.1016/j.applthermaleng.2009.04.013.

Liu, Z., and W. Soedel. 1995. "A Mathematical Model for Simulating Liquid and Vapor Two-Phase Compression Processes and Investigating Slugging Problems in Compressors." *HVAC&R Research* 1 (2): 99–109. doi:10.1080/10789669.1995.10391312.

Mckenna, S., G. Mccullough, and R. Douglas. 2012. "Thermodynamic Modelling of a Reciprocating Expander in an Organic Rankine Cycle." In *Proc. of 5th International Conference on Sustainable Energy & Environmental Protection*, 357–62. Dublin, Ireland.

Millington, B., and E. Hartles. 1968. "Frictional Losses in Diesel Engines." In . SAE Technical Paper 680590. doi:10.4271/680590.

Morel, T., and R. Keribar. 1985. "A Model for Predicting Spatially and Time Resolved Convective Heat Transfer in Bowl-in-Piston Combustion Chambers." In . SAE International. doi:10.4271/850204.

Platell, P. 1993. "Displacement Expanders for Small Scale Cogeneration." Licenciate Thesis, Stockholm, Sweden: KTH Royal Institute of Technology.

Span, R., and W. Wagner. 1996. "A New Equation of State for Carbon Dioxide Covering the Fluid Region from the Triple-Point Temperature to 1100 K at Pressures up to 800 MPa." *Journal of Physical and Chemical Reference Data* 25 (6): 1509. doi:10.1063/1.555991.

Taylor, C.F. 1961. *Internal Combustion Engine in Theory and Practice*. International Texbook Company. Scranton Pensylvania.

Touré, A. 2010. "Etude Théorique et Expérimentale D'un Moteur Ericsson À Cycle de Joule Pour Conversion Thermodynamique D'énergie Solaire Ou Pour Micro-Cogénération." PhD Thesis, Université de Pau et des Pays de l'Adour.

Winterbone, D. E., and D. W. H. Tennant. 1981. "The Variation of Friction and Combustion Rates During Diesel Engine Transients." In . doi:10.4271/810339.

Woschni, G. 1967. "A Universally Applicable Equation for the Instantaneous Heat Transfer Coefficient in the Internal Combustion Engine." In . SAE International. doi:10.4271/670931.

Wronski, J. 2015. “Design and Modelling of Small Scale Low Temperature Power Cycles.” PhD Thesis, Kongens Lyngby, Danmark: DTU Mechanical Engineering.

Chapter 4: Development of an Ericsson engine

Contents

1. Introduction

This chapter presents the experimental work and the result exploitations done by the author in the context of a collaboration project. This project aimed to develop an Ericsson engine with the goal of operating as a cogeneration plant producing about 30 kWe and using biomass fuel. One of the main features of this project was to build a hot air engine by modifying an existing internal combustion engine (ICE), which allows the reduction of the development effort and production cost.

The purpose of the work presented in this chapter is to build a demonstrator of such an Ericsson engine, to verify its technical feasibility and to get experimental data for model calibration and validation.

The chapter is organized as follows. First, the detailed model presented in Chapter 3 is used to assess the potential performances of the engine and to design the main features. Then, the modifications made on the ICE are presented as well as the test facility. After that, some experimental results are presented and analysed. The last section of the chapter presents the perspectives and conclusions.

2. Preliminary design of an Ericsson engine

In this section, the detailed model presented in Chapter 3 is used to assess the performance of an Ericsson engine and to predefine some geometrical parameters. First, some primary assumptions based on state of the art are made in order to set inputs of the model. Then, the compressor and the expander are simulated separately in order to show the effect of their losses on the heat engine performance. Finally, the whole Ericsson engine is studied and some guidelines for the next section are drawn.

2.1. Preliminary selection of geometrical parameters and operating conditions

The goal of this section is to predesign operating conditions and some geometrical parameters, however some operating parameters can be set by simply considering that, as explained above, the Ericsson engine can be described by the Brayton cycle. Indeed, it is possible to demonstrate that (Lebrun 1998)

- For the ideal cycle (isentropic efficiencies of components equal to one), the efficiency of the cycle increases with the pressure ratio and is independent of the temperature ratio.
- For the real cycle (isentropic efficiencies of components <1), efficiency (with and without regenerator) and power increase with temperature ratio and there is an optimum pressure ratio that maximizes these values.
- The optimum pressure ratio is smaller and the efficiency is higher for cycle with regeneration (see chapter 2).

Considering this, the temperature ratio needs to be higher but it is limited by material constraints. It is set to $r_T = 3.6$, which corresponds to an expander supply temperature of $T_{su,E} = 800\,°C$ for a compressor supply temperature of $T_{su,C} = 25\,°C$. Concerning the pressure ratio, it will be shown that this operating parameter depends on geometrical parameters and will be optimised thereafter. Even so, the pressure ratio is set to 6 for simulation on separate compressor and expander.

For geometrical parameters, it was decided, in first place, to consider common dimension of ICE. In particular, square cylinders with bores of 90 mm are considered. Valve dimensions (see Figure 4-1) are

proportional to the bore of the cylinder in order to keep generality despite the fixed bore, and according to (Heywood 1988). These geometrical parameters are summarized in Table 4-1. The flow cross sectional area depends on the lift and is computed according to (Heywood 1988). The lift depends on the shaft angle and the maximal lift and is calculated according to (Blair 1999). For kinematics (cam profile) and dynamics (acceleration of the valve and thus stress in valve train) considerations, the maximal lift will be assumed proportional to the duration of the cam θ_v(see equation (4-1) and Figure 4-1). This cam duration fixes the timing of the valve and therefore, as explained in chapter 2, the cut-off. In order to avoid under- or over-expansion losses, the cam duration is adapted to the pressure ratio.

$$L_{v,max} = \frac{L_{v,max,ref}}{\theta_{v,ref}} . \theta_v \qquad (4\text{-}1)$$

Table 4-1: Preliminary selected geometric parameters of the Ericsson engine

Cylinder		**Valves**	
$\boldsymbol{D}$	90 mm	D_v	$0.4D$
$\boldsymbol{L}$	90 mm	D_{vi}	$D_v/1.11$
$\boldsymbol{B}$	150 mm	D_{vs}	$0.221D_{vi}$
$\boldsymbol{CF}$	0.05 [-]	$L_{v,max,ref}$	$D_v/4$

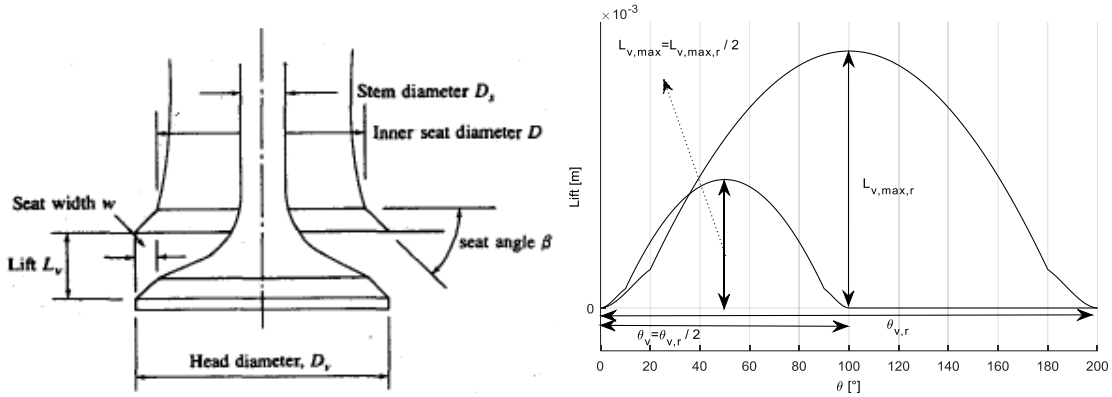

Figure 4-1: Valves dimensions (Heywood 1988) on the left and lift on the right

Finally, a 1500 RPM rotational speed is assumed in order to keep low mechanical friction and the wall temperature is set to 100 °C considering that cylinders are water cooled (Dubouil 2012).

2.2.Simulation of compressor and expander separately

Two sources of losses are modelled: the pressure drops and the heat transfer. In order to evaluate the influence of these sources of losses, three simulations are performed and compared: one without loss (WL) which corresponds to an isentropic process, one with the pressure drops (PD) and one with the pressure drops and the heat transfer (PD + HT). Finally, the influence of the valve timing is also evaluated.

2.2.1. Loss influences

Figure 4-2, Figure 4-3 and Figure 4-4 show respectively the crank angle evolution of the cylinder pressure, the crank angle evolution of the in-cylinder temperature and the indicator diagrams for both the compressor and the expander. The pressure profiles show that the pressure drops on high-pressure side are more important for the compressor. This is explained by the fact that the compressor admits a higher mass flow (more than the double, see Table 4-2) rate through the same flow area. The heat transfer does not induce significant changes on the pressure but does on the temperature, especially for the expander. This induces change in the mass flow rate and the exhaust temperature. Indeed, for the expander, the mass flow rate rises from 6.2 g/s to 6.6 g/s (because of supply cooling down) and the exhaust temperature rises from 420 °C to 350 °C when the heat transfers are taken into account.

Finally the isentropic efficiency of the compressor is 0.8 and the one of the expander is 0.91. Heat transfers are more important for the expander (because gas temperature is higher) and then, affect more the performances. The mass flow rate of the compressor decreases with the losses while the one of the expander increases because of the cooling down of the fluid entering the cylinder. The exhaust temperature of the compressor increases while the one of the expander decreases.

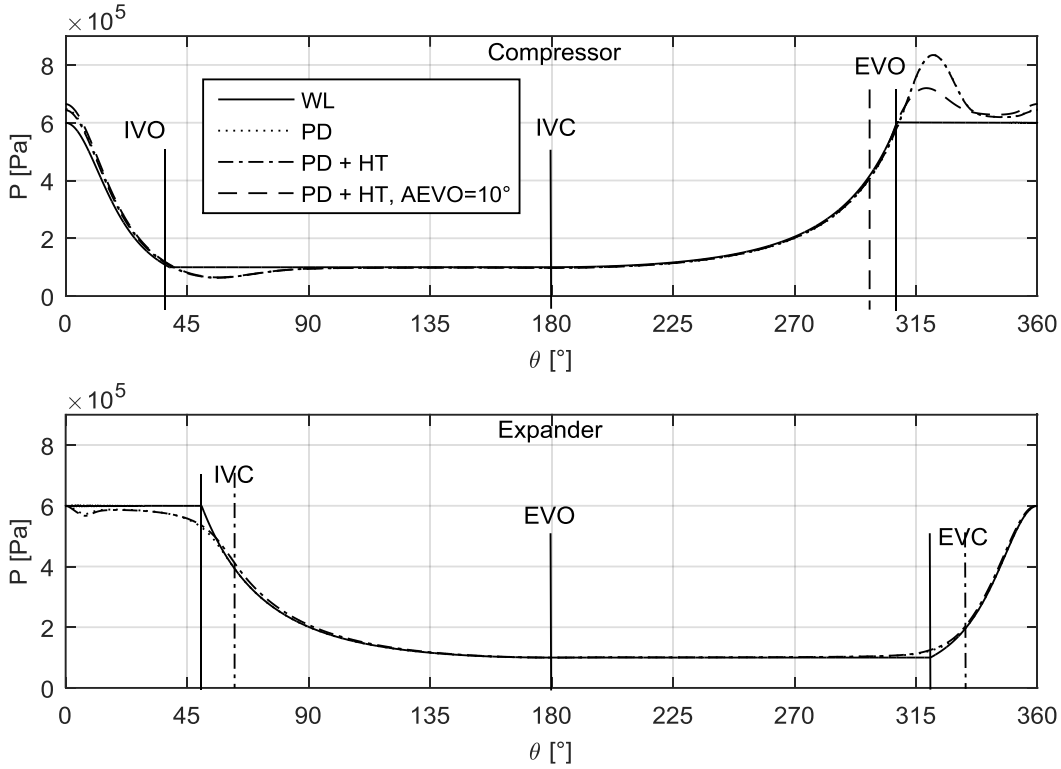

Figure 4-2: Crank angle evolution of the pressure inside the cylinders

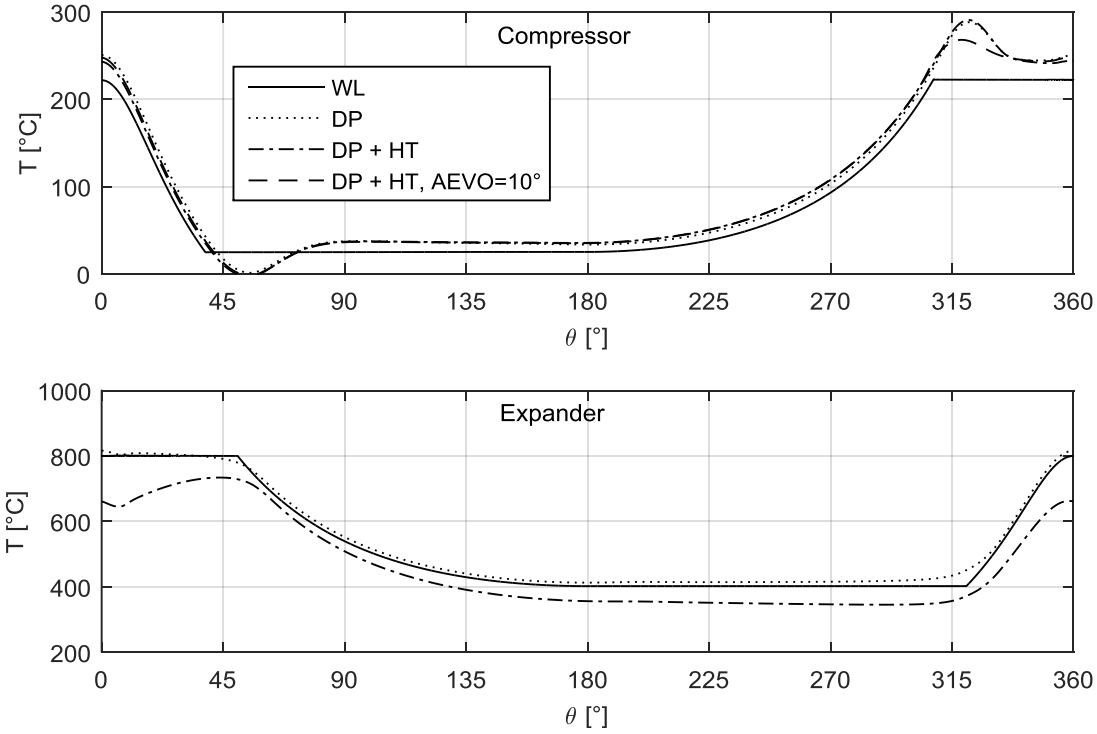

Figure 4-3: Crank angle evolution of the temperature inside the cylinders

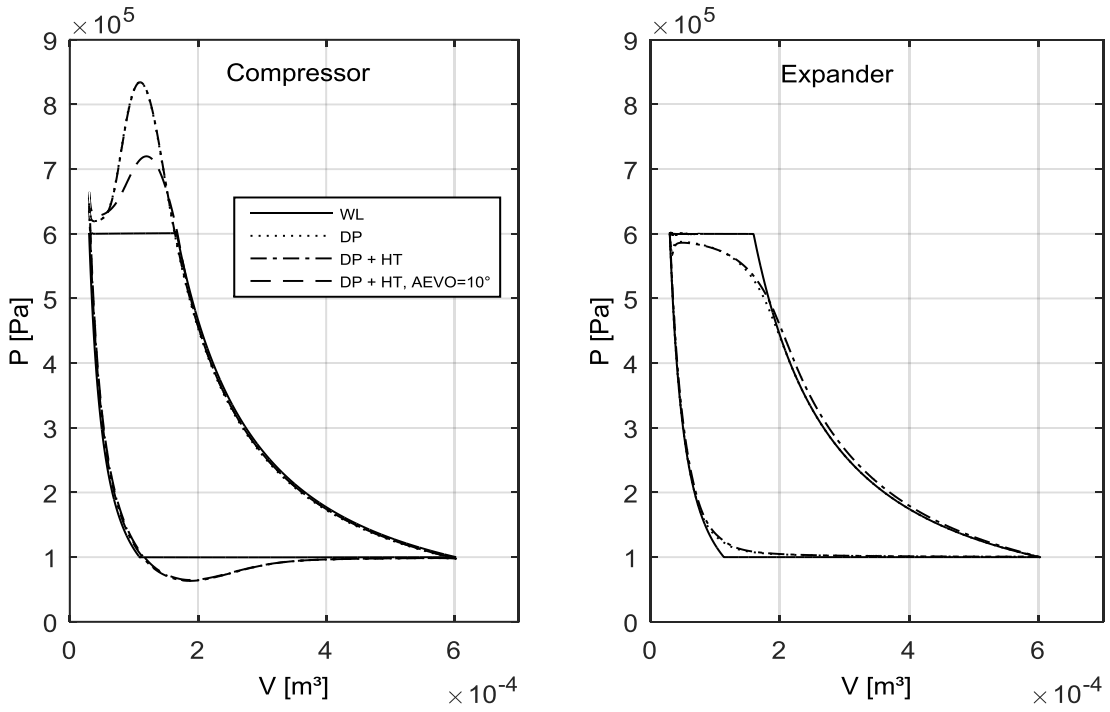

Figure 4-4: Indicator diagrams.

Table 4-2: Results for separates compressor and expander

	Compressor			Expander		
	WL	**PD**	**PD + HT**	**WL**	**PD**	**PD + HT**
$\dot{W}$ $[W]$	2890	3318	3347	2792	2626	2690
$\dot{M}$ $[g/s]$	14.43	13.44	13.35	6.3	6.2	6.6
w **[kJ/kg]**	200	246	250	443	423	404
T_{ex} $[°C]$	222	267	268	402	420	350
$\dot{Q}_w$ $[W]$	0	0	38	0	0	622
ϵ_s $[-]$	1	0.81	0.8	1	0.96	0.91

2.2.2. Adjustment of valve timings

To match the two criteria that condition the timing of the valves of the expander, i.e. that the pressure in the cylinder has reached the outlet pressure at the end of the down-stroke and the inlet pressure at the end of the upstroke, θ_{IVC} and θ_{EVC} had to be adjusted. This adjustment can be seen in Figure 4-2.

For the compressor, no adjustment has to be made. However, it was found that anticipating slightly the EVO allows a decrease in the pressure drop and an increase in the isentropic efficiency. The diminution of the pressure drop at the exhaust can be seen in Figure 4-2 and Figure 4-4 where the opening of the exhaust valve is anticipated of 10° (AEVO=10°). The isentropic efficiency increases from 0.8 to 0.84 and the mass flow rate decreases from 13.35 g/s to 13.29 g/s.

The same opening anticipation can be made on the intake of the expander. But it was found that the increase of the power is offset by the increase of the mass flow rate. This leads to the same specific work and then to no increase of the efficiency.

2.3.Simulation of the whole Ericsson engine

In this section, the simulation models of the compressor and the expander are combined to describe the whole Ericsson engine. By doing so, one degree of freedom is removed as the compressor mass flow rate is now equal to the one of the expander. Therefore, for a given temperature ratio, the pressure ratio depends on the swept volume of the expander. This swept volume can be described relatively to the swept volume of the compressor by defining the volume ratio:

$$\phi = \frac{V_E}{V_C} \qquad (4\text{-}2)$$

where V_E and V_C are the total swept volumes of the expander and of the compressor respectively.

The inputs are the same as the above, except that:

- The pressure ratio becomes an output that depends on the volume ratio.
- The volume ratio is optimized hereafter.
- The heat exchangers efficiencies are set to $\epsilon = 0.8$.

2.3.1. Optimisation of the volume ratio

As explained just above, for a given temperature ratio, the pressure ratio depends only on the geometry. Figure 4-5 shows the evolution of the volume ratio in terms of pressure ratio. It shows that the pressure ratio increases as the volume ratio decreases and that the pressure ratio without loss is higher than the one with losses. This is explained by the fact that, with losses, the mass flow rate of the compressor decreases and the one of the expander increases.

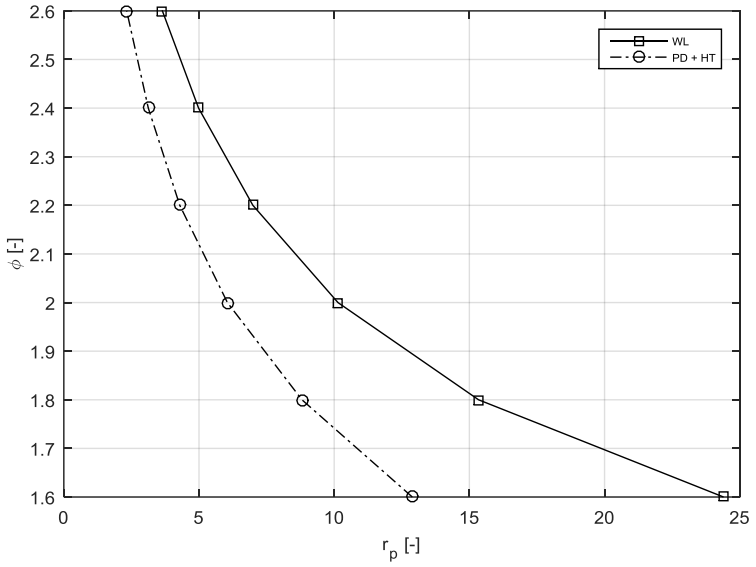

Figure 4-5: Volume ratio in term of pressure ratio.

This variation of the pressure ratio leads to a variation of the efficiency and of the power. Figure 4-6 shows the evolution of the efficiency with and without regenerator for the case without loss, with losses and with an anticipation of the EVO of the compressor. This graph shows that the losses (pressure drop and heat transfer) affect significantly the efficiency of the Ericsson engine, that the anticipation of the EVO of the compressor induces a slight increase in the efficiency and that there is an optimum around $r_p = 4.4$ which corresponds to a volume ratio of $\phi = 2.2$. As the prototype of the Ericsson engine will be made of an existing ICE, the actual ratio will depend on the number of cylinders in the ICE.

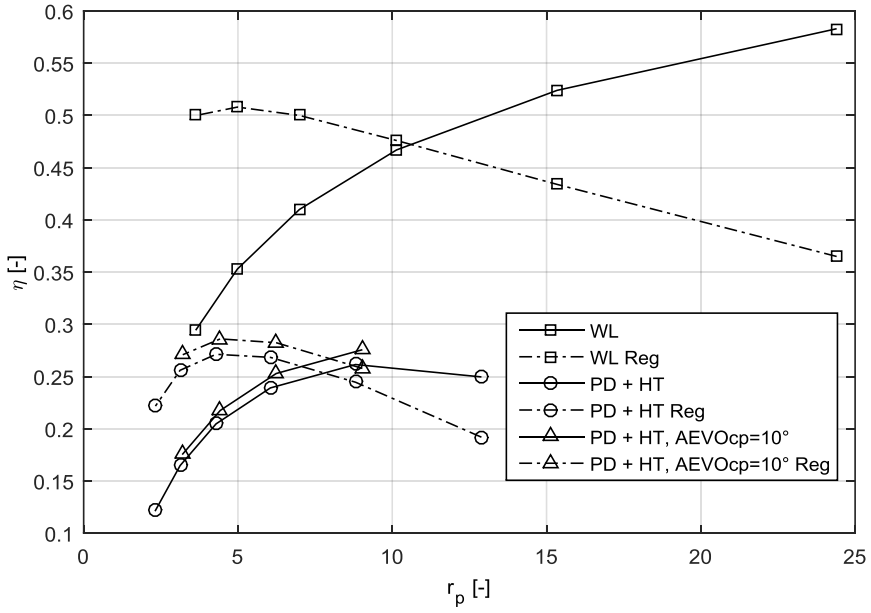

Figure 4-6: Influence of the volume ratio on the Ericsson engine efficiency

2.3.2. Potential performances

The results presented hereunder correspond to the optimum volume ratio, i.e. $\phi = 2.2$, and a mechanical efficiency of 85% (on net power) is assumed. Figure 4-7 shows the temperatures at different points of the engine. Other results are presented in Table 4-3. The efficiency of the engine is 24.3% and it produces 1.6 kW of mechanical power.

The isentropic efficiency of the compressor and of the expander are high (see Table 4-3), due to the fact that mechanical losses are not taken into account.

Table 4-3: Preliminary design simulation results

$\dot{W}_{net}$	1623 W	η	24.3 %
$\dot{M}$	14 g/s	$\epsilon_{s,exp}$	89 %
r_p	4.4 [-]	$\epsilon_{s,cp}$	77 %

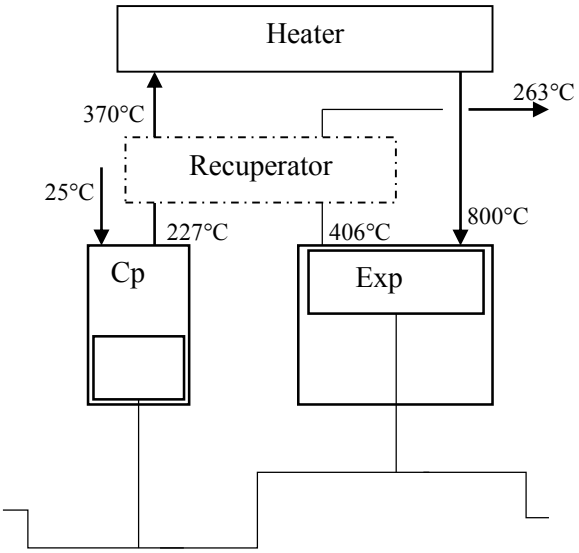

Figure 4-7: Schematic representation of an Ericsson engine with computed temperatures

2.4. Conclusions

Simulation of separate compressor and expander was conducted to show the influence of the two modelled sources of losses. One of the main conclusions is that, when losses are taken into account, the mass flow rate of the expander increases due to the cooling down of the admitted fluid while the one of the compressor decreases due to pressure drop and heating up of the admitted fluid. This leads to a lower pressure ratio when both machines are coupled to form an Ericsson engine. The other conclusion is that for the expander, the heat losses are consistent and need to be taken into account. Indeed, the heat losses induce a decrease of the temperature at the exhaust of the expander and then a decrease of the efficiency with a regenerator.

Then the model was used to study an Ericsson engine. First, the influence of the ratio between the swept volume of the expander and that of the compressor was shown. The result is that there is a volume ratio that maximizes the efficiency of the engine. This optimum volume ratio is $\phi = 2.2$. For this geometry, the Ericsson engine has a thermal efficiency of 24%. The generated power, for a 1.7 l engine (3 cylinders of 0.57 l), is 1.6 kW. However, the model needs to be validated and no leakages are considered.

3. Prototype development and test bench

The Ericsson engine prototype investigated in this thesis has been built by modifying an available internal combustion engine. Indeed, all the engine block is similar for both engines and can be used as hot air engine with few modifications detailed thereafter. The selected ICE is a 12 l six cylinders inline engine. This engine is a stationary ICE using natural gas and used for cogeneration application. Main characteristics of the engine are listed in Table 4-4. As the engine has 6 cylinders and that the optimal volume ratio is $\phi = 2.2$, two cylinders will be used in compression and four in expansion giving $\phi = 2$.

Table 4-4: ICE engine characteristics

Nominal power	76 kW
Nominal speed	1500 RPM
Number of cylinders	6
Bore	130 mm
Stroke	150 mm
Connecting rod	250 mm
Clearance volume	9 %
Maximal lift	12 mm
Valves diameter	50 mm

In order to turn the ICE engine into a hot air engine two main modifications, among others, are needed:

- Valve train adaptation: The valve timing of the Ericsson engine has been shown in the pre-study. This timing is totally different from the one of the ICE engine. The ICE engine is a four stroke engine and admission and exhaust occur both on a full stroke of the piston. The Ericsson engine is a two stroke engine and gas exchange process occurs only during a fraction of a piston stroke. Moreover, pressure forces acting on the valves are totally different.
- Change of the manifolds: The internal combustion engine has an intake and an exhausts manifold connected to the ports of each cylinder. For the Ericsson engine, four manifolds are needed; an intake and an exhaust manifold for both compressor and expander parts.

These modifications are described below just as the modifications allowing the reduction of the clearance volume. Finally, in order to test this Ericsson engine prototype, some auxiliary systems and measurement devices were used and are also detailed in the next sections.

3.1. Valve timing and camshaft design

In order to design the camshaft of the Ericsson engine, the valve timings of both compressor and expander have to be computed. The detailed model was used to simulate the system with the ICE engine geometric parameters (see Table 4-4) and iteration was made with mechanical designer in order to adjust the cam lifts. Figure 4-8 shows valve lifts in terms of crank-angle. The 1st simulation curves correspond to ICE geometrical parameters and lift computed according to (Blair 1999) as in section 2. The final cam lifts represent the lifts obtained with actual designed camshaft, taking into account the mechanical dynamic behaviour of the valve train. The asymmetric profiles and differences between compressor and expander comes from the deformations occurring in the valve train. It can be seen that, compared to the first assumption, higher lifts are achieved for the short duration cams and higher duration has been chosen in order to reduce the pressure drops. The resulting pressure evolutions in the cylinder of the compressor and of the expander are represented in Figure 4-9.

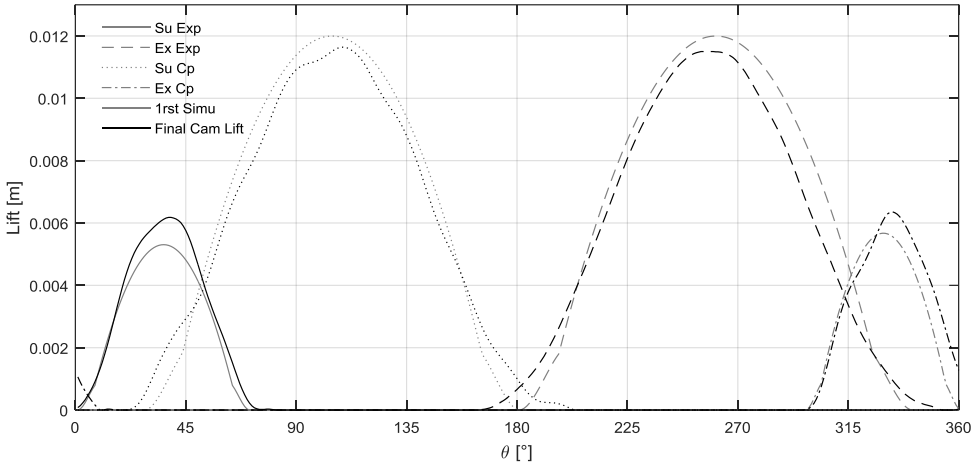

Figure 4-8: Crank-angle evolution of the valve lifts. Two sets of lifts are represented. The first one comes from a 1st simulation and lifts as proposed in (Blair 1999). The second one comes from the final camshaft design

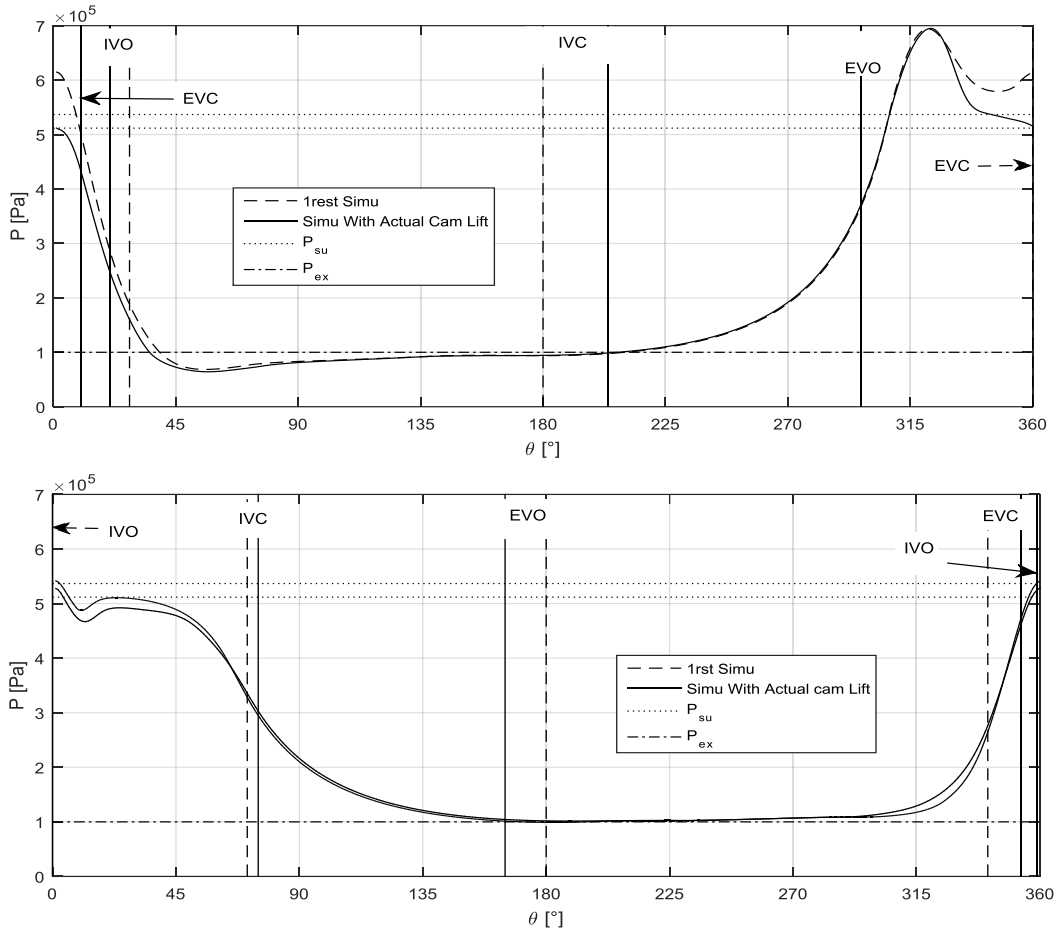

Figure 4-9: Crank-angle evolution of the pressure in the compressor (upper) and the expander (lower). One curve corresponds to the 1st simulation and the other to the final camshaft design

3.2. Valve train change

First, the gear set that trains the camshaft had to be modified to change the rotational speed of the camshaft. Indeed, as the ICE is a four stroke engine, the camshaft originally rotates two times slower than the crank shaft. It would have been possible to keep this configuration but the cam duration would have been two times smaller, considering 80° of opening of supply expander valve, as designed in section 3.1, cam duration would have been 40° leading to too small lift. Then, the gears set was modified to allow the camshaft to rotate at the same speed as the crank shaft speed. First, the gear set was replaced by a chain set (see Figure 4-10), but too important constraints lead to several issues such as a very fast wear of the cam shaft cog. It was then decided to add an intermediary gear instead of the chain, which led to a more robust mechanism.

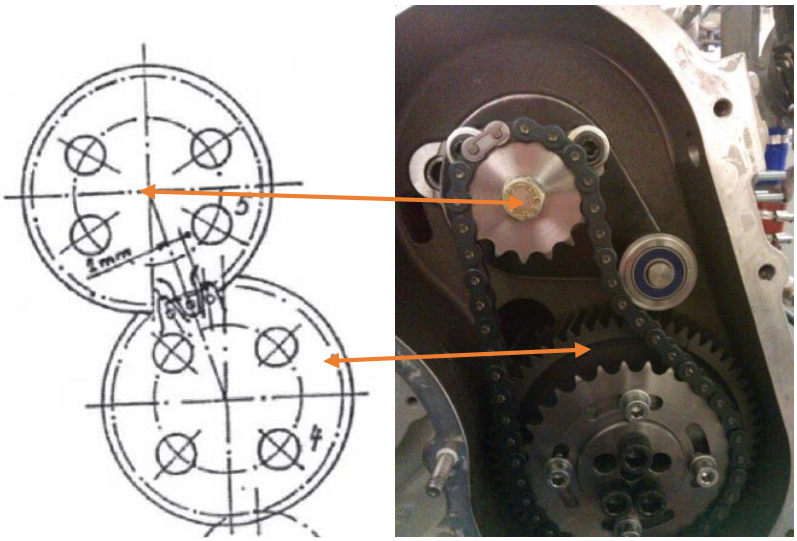

Figure 4-10: Valve train gear set modification: initial gear set scheme on the left and modified chain set on the right

Then, some valve springs have to be changed. Indeed, for compressor exhaust and expander inlet valves, the high pressure tends to pull down the valves (see Figure 4-11) while in the ICE engine, no pressure acts on this side of the valve. In order to resist to the pressure induced force, the spring rate has to be increased. If a classic coil spring was used, the force of the rocker arm acting on the valve would have increased while the lift increased, leading to very high stresses at the maximal lift. Then, it was decided to use pneumatic springs connected to a buffer tank. This system allows to have constant force with lift and a reduction of the mechanical stress in the valve train.

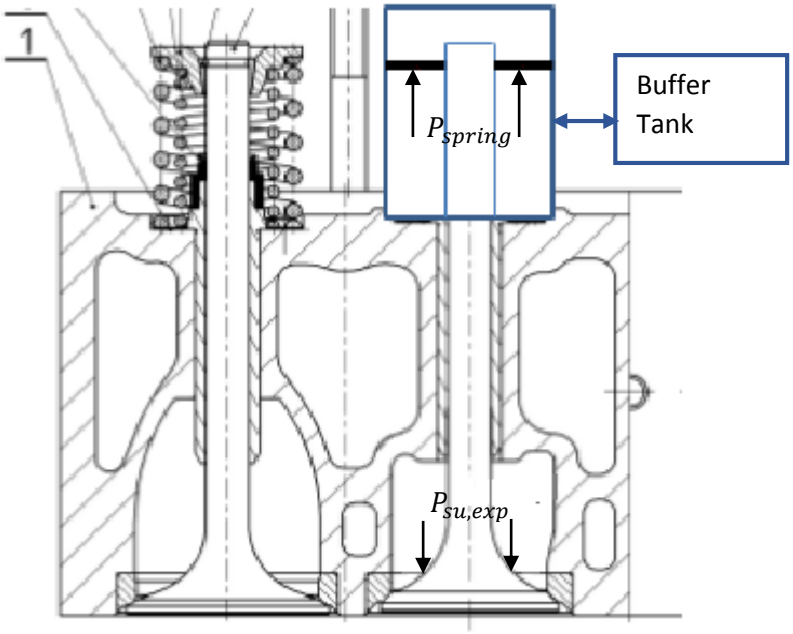

Figure 4-11: Valve spring change

3.3.Manifolds

Four manifolds have to be built. It was decided to connect exhaust ports of the original engine to the hot part of the Ericsson engine. As explained above, two cylinders will be used as compressor and four cylinders as expander. Then, the compressor intake manifolds connect the two supply ports of the two first cylinders and the exhaust manifolds connect the two exhaust ports. Inversely, the intake manifold of the expander connect the ICE exhaust ports of the four cylinders used as expander and finally the expander exhaust manifold connect the ICE supply port. Special attention had to be paid on the expander supply manifold as it has to resist to a pressure of 5 bar (see section 3.1) and a temperature of 800°C. Then, this manifold was built in stainless steel AISI 316 which is more resistant at high temperature. In order to absorb the heat induced expansion of the two hot manifolds, expansion joints are placed before the fixed bridles that connect the manifolds to the furnace and between the two fixed parts of the expander inlet manifold.

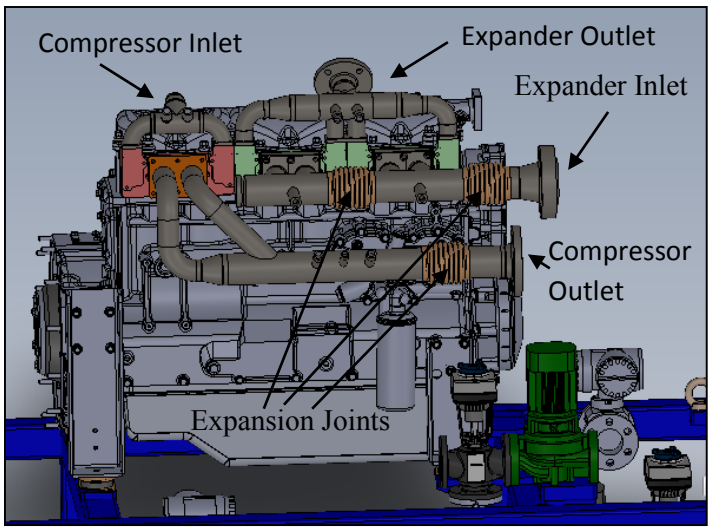

Figure 4-12: Manifolds of the Ericsson engine

3.4. Clearance volume reduction

In addition to the main required modifications explained above, some other modifications were made in order to improve the operation of the Ericsson engine. An important one is the replacement of the pistons. Indeed, the original pistons were bowl-in-pistons (see Figure 4-13). In order to reduce the clearance volume, and then to improve the efficiency of both the compressor and the expander, new flat top pistons with two valve reliefs were machined (see Figure 4-13). With these pistons, the new clearance volume is 1.6% rather than 9% on the initial ICE.

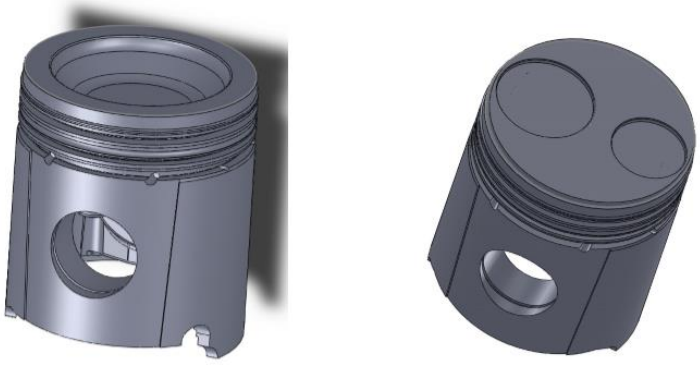

Figure 4-13: Initial bowl-in piston on the left and new flat top piston with two valve reliefs on the right

3.5. Auxiliary systems

In order to convert the mechanical power, the Ericsson engine is connected to an electrical generator. The generator is an asynchronous machine controlled with a four-quadrant variable frequency drive. This configuration allows the control of the speed and the start of the engine. Indeed, to start the engine, it is driven by the electrical motor until the pressure and the temperature are sufficient for the Ericsson engine to produce power.

The heat is supplied by an electrical heater that allows the control of the expander supply temperature.

The engine is cooled down with water as the original ICE is. This primary water loop is cooled down by a plate heat exchanger connected to a secondary water loop. The heat of the secondary water loop is rejected by an air-cooled heat exchanger located outside the building. A by-pass line controlled by a three-way valve allows the control of the supply temperature of the plate heat exchanger and then, the water temperatures of the primary loop.

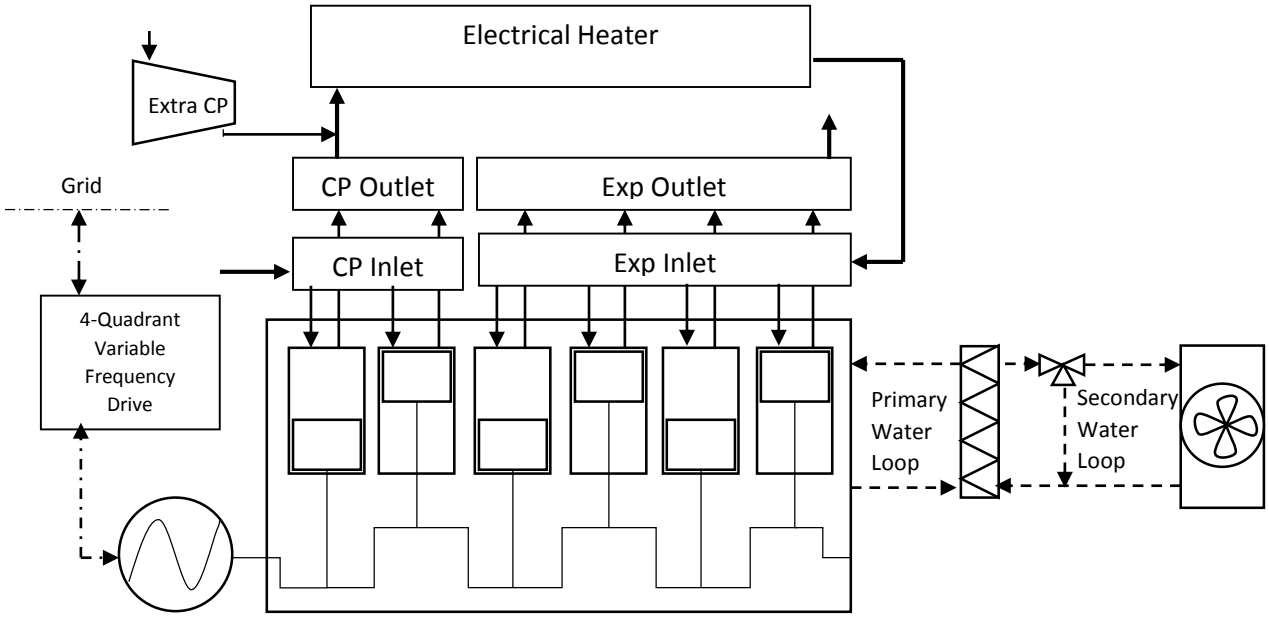

Figure 4-14: Schematic representation of the test bench

After the first experimental results, it was decided to use an extra compressor to feed the expander with a larger mass flow rate. This extra compressor injects air before the electrical heater and allows overcoming the limitation of the electrical heater and of the built-in compressor (see section 5).

3.6.Measurement system

In order to monitor the operation and to assess the performance of the engine, several sensors are placed all over the test facility. Pressure and temperature of the air and of the cooling water are measured at each point of the heat engine. These measurements are achieved with piezoresistive pressure sensors and PT100 temperature sensors or K-type thermocouples for high temperature. A hot wire mass flow rate sensor is placed at the admission of the compressor in order to measure the entering mass flow rate. As for most of the tests, additional mass flow rate has to be injected in the expander by the extra compressor, an orifice plate is placed at the exhaust of the expander in order to measure the total mass flow rate according to standard ISO 5167 (ISO/TC 30 2003) with a differential pressure sensor. The electrical power (consumed or produced) and the rotational speed are given by the variable frequency drive.

In addition to these measurements, piezoelectric pressure sensors are placed instead of spark plugs in some cylinders in order to measure the evolution of the pressure inside these cylinders. One sensor is

placed in a compressor cylinder and three in expander cylinders. These sensors, coupled with a rotary encoder giving the angular position of the crank shaft, allow to draw indicator diagram and then, to compute indicated works.

Table 4-5: Sensors features

Type	Range	Error
Class B PT100	0 to 200°C 0 to 400°C	0.3+0.005.T°C *
Class 2 K type thermocouple	-40 to 1200°C	[-40 to 333]:+-2.5°C; [333 to 1200°C]: +-0.75 % **
Piezoresistive pressure sensor	0 to 16 bar	0.5 %
Piezoelectric pressure sensor	0 to 344 bar	1%
Piezoelectric pressure sensor	0 to 200 bar	0.3 % FS
Hot wire mass flow rate	38-3750 kg/h	1.5 %
Strength gauge differential pressure sensors	0-150 mbar	0.25 % FS

* EN60751 (Technical Committee 65 2008)

** EN60584 (Subcommittee 65B : Measurement and control devices 2013)

4. First experimental results

The Ericsson engine prototype described above was tested several times before some modifications have been made. During these first tests, the rotational speed varied from 300 RPM to 1200 RPM and the expander supply temperature reaches 360°C. This low temperature, compared to the 800°C target, did not allow the pressure to rise enough. Indeed, for this temperature, the pressure was 2.47 bar, 3.15 bar and 4 bar for respectively 300 RPM, 660 RPM and 1200 RPM instead of 5 bar as simulated in section 3.1. In these conditions, the engine consumed power and was always driven by the electrical generator.

4.1. Indicator diagrams

During the test, pressure in one of the cylinders of the expander was measured. Figure 4-15 shows the indicator diagram based on this measurement for 300 RPM, 660 RPM and 1200 RPM. It can be seen that supply and exhaust pressure drops significantly affect indicator diagrams and then the available power, especially for high rotational speeds. Moreover, at 1200 RPM, the recompression of the fluid at the end of the exhaust stroke lead to over-compression as the pressure rose up to 9 bar at TDC for a supply pressure of 4 bar.

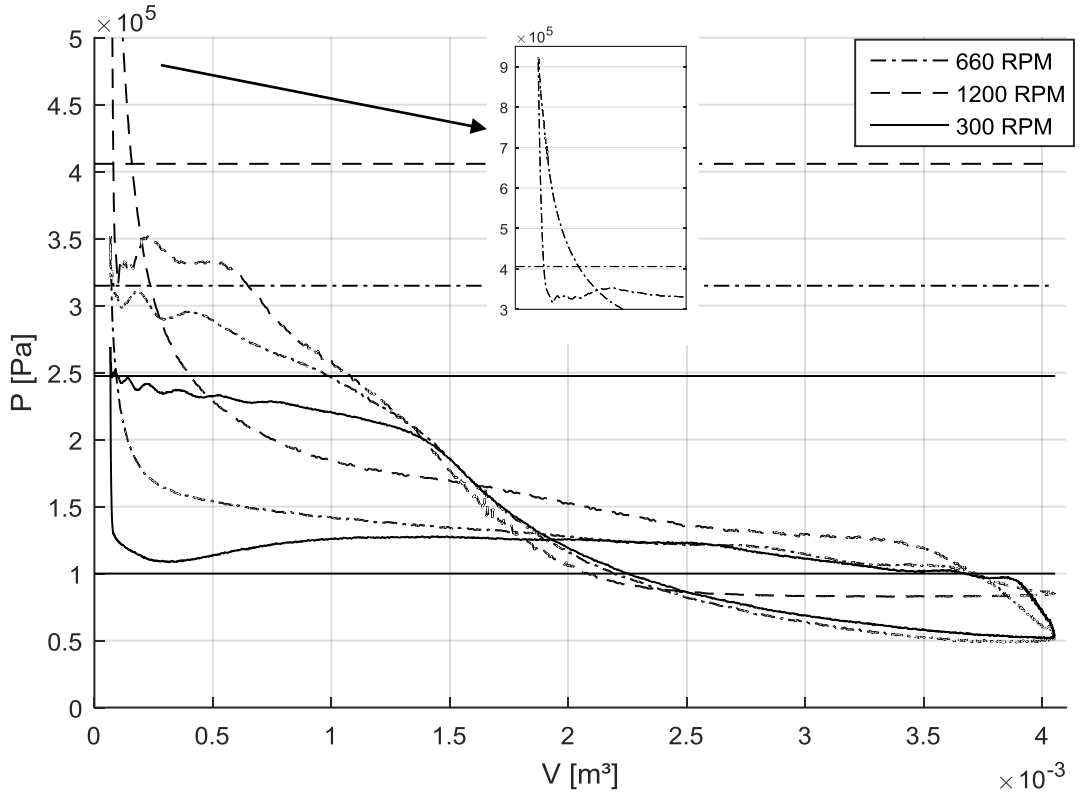

Figure 4-15: Expander indicator diagrams (first tests)

4.2.Modifications

The indicator diagrams analyses have shown that too high pressure drops occurred during the admission and exhaust processes. In addition, the fluid was recompressed at pressure more than two times the inlet pressure for 1200 RPM, showing that the valve timing was not well suited. Then, the camshaft has been redesigned with higher valve opening durations. Figure 4-16 shows the new camshaft lifts. With this camshaft, expander supply and compressor exhaust valves open during 95° with a maximal lift of 9 mm instead of 80° and 6 mm with the former camshaft. Expander exhaust and compressor supply valves open during 200° instead of 190° with similar maximal lift. In order to reduce the expander supply pressure drop, the opening of the supply valves is anticipated of 5° while the exhaust vales closes 10° after TDC in order to reduce recompression.

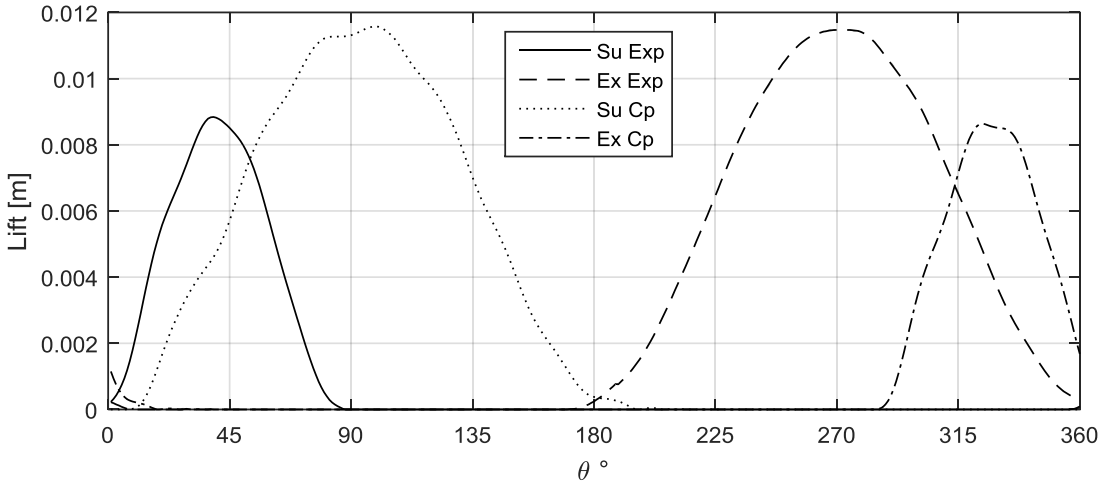

Figure 4-16: Second camshaft design lifts

Moreover, as explained above, some mechanical issues were encountered with the valve train. Indeed, after several running hours, the camshaft cogwheel was abnormally worn out. It was then decided to replace the chain set by a more robust gear set.

5. Second set of experimental results

The engine equipped with the new camshaft described in the previous section was tested with an extra compressor (see Figure 4-14). Indeed, the pressure did not rise to a sufficient level with only the built-in compressor. Maximal pressure reached was 1.8 bar instead of 5 bar as expected. Then, in order to test and characterize the expander for different supply pressures, additional air mass flow was injected before the electrical heater which allows the increase of the pressure up to 7 bar. A total of 54 steady state points were measured with rotational speed varying from 300 to 900 RPM. For all the points, the expander supply temperature was comprised between 420°C and 480°C. Unfortunately, the electrical heater did not manage to reach 800°C as desired.

However, analyses of the measurements are performed in this section in order to assess the different sources of losses that affect the expander. This analysis, combined with model calibration performed in next section, will help to understand why the engine did not run as expected in the design phase and to evaluate some perspectives in the next chapter.

5.1. Quality of the results

5.1.1. Outliers detection

A machine learning method based on Gaussian Processes regressions and implemented into the open-source GPExp library was applied to detect outliers (Quoilin and Schrouff 2016).This method consists in building a Bayesian, non-parametric model of an output in terms of a selected set of inputs. The regression provides the most likely response surface of the process together with a normally-distributed probability density function. Interestingly, the standard deviation of this function varies within the inputs

space: it is low where data scattering is low, and increases if the data density decreases or if the noise increases. It can therefore be viewed as a statistically-derived confidence interval. The Mean Average Relative Error (MARE) between the response surface and each data sample is then computed and compared to the standard deviation at this point. This provides a robust indicator of the correlation between each data point and the selected inputs, finally allowing to detect potential outliers.

This method was applied on supply and exhaust mass flow rates, compressor and expander indicated work, electrical power, expander indicated isentropic efficiency and filling factor. Results are summarized in Table 4-6. For the five outputs, the best relevant inputs are the rotational speed and the high pressure (compressor exhaust pressure or expander supply pressure), except for indicated isentropic efficiency for which the pressure ratio gives better correlation. These inputs give very low MARE (<1%) for indicated works and electrical power, a MARE of 1.83 % for exhaust mass flow rate and a high MARE of 10.64 % for supply mass flow rate. This last result shows that the quality of the supply mass flow rate measurement is poor. This poor quality can be explained by the pulsating characteristic of the flow.

Table 4-6: Results of the Gaussian regression process

	$\dot{M}_{cp}$	$\dot{M}_{exp}$	$W_{in,cp}$	$W_{in,exp}$	$\dot{W}_{el}$	FF_{exp}	$\epsilon_{s,in,exp}$
Inputs	$RPM, P_{ex,cp}$	$RPM, P_{su,exp}$	$RPM, P_{ex,cp}$	$RPM, P_{su,exp}$	$RPM, P_{su,exp}$	$RPM, P_{su,exp}$	$RPM, R_{p,exp}$
MARE [%]	10.64	1.83	0.83	0.66	0.61	4.54	4.95
Outliers (RPM/P)	600/3.4 600/6.4	600/4 750/4.1	450/6.5	600/7.5	600/6.4 750/6.3	300/1.7 450/1.8	300/4.5 750/4.1
Error/σ	1.97 2.37	1.96 2.97	2.68	2.1	1.9 2.67	2.36 2.97	2.09 3.8

5.1.2. Uncertainties

Calculated values (Y) based on measurements (X_i) have, from the sensors error (E_{x_i}), uncertainties (E_y). These uncertainties are calculated by the propagation method:

$$E_y = \sqrt{\sum_i \left(\frac{\partial Y}{\partial X_i}\right)^2 . E_{x_i}^2} \qquad (4\text{-}3)$$

This formula is not applicable to compute uncertainty on indicated work and power. Indeed, as explained earlier, indicated work and power are computed with an integral and depend on the uncertainty of the in-cylinder pressure and on the uncertainty of the angular position of the PMH (θ_{PMH}). The uncertainty of the in-cylinder pressure is the uncertainty of the piezoelectric sensor and the uncertainty of angular position is estimated to be +-0.5°. The proposed method to compute uncertainty due to these values consists in applying Monte-Carlo method (Cordero et al. 2008) on the pressure for $\theta_{PMH} - 0.5°$,θ_{PMH} and $\theta_{PMH} + 0.5°$.

Finally, the uncertainty on the mass flow rate measured with the help of an orifice plate and a differential pressure sensor is computed according to the standard ISO 5167 (ISO/TC 30 2003).

The minimal, maximal and average computed relative uncertainties on expander mass flow rate, compressor and expander indicated works, expander filling factor and expander indicated isentropic efficiency are listed in Table 4-7. The average relative uncertainties are under 2% for all variables showing that these variables are computed with a good confidence.

Table 4-7: Minimal, maximal and average computed relative uncertainties

	$\dot{M}_{exp}$	$W_{in,cp}$	$W_{in,exp}$	FF_{exp}	$\epsilon_{s,in,exp}$
Min	1.1 %	0.2%	0.3%	1.2%	1.3%
Max	1.6 %	1.6%	9%	1.7%	9.9%
Average	1.2 %	0.9%	1.3%	1.3%	2%

5.2. Electromechanical losses

5.2.1. Ericsson engine electromechanical losses

As both compressor and expander indicated powers are known, the net indicated power transmitted to the shaft can be computed. This net indicated power is lowered by the mechanical losses of the engine and the efficiency of the electrical generator. These electromechanical losses can be computed with the measurement of the electrical power, but the mechanical losses of the engine have to be computed with the generator efficiency.

As, during the test, the electrical power was always lower than 25 % of the rated power (rated power is 50 kW), electrical losses of the generator influence greatly the electromechanical losses. Indeed, it is well known that electrical generator efficiency decreases when power is below 25 % of the rated power (U.S. Departement of Energy 1997). This is illustrated in Figure 4-17 where electromechanical efficiency of the engine and electrical generator efficiency are plotted in terms of electrical power. The deduced mechanical efficiency is also plotted in Figure 4-17 and varies between 40 % and 85 %.

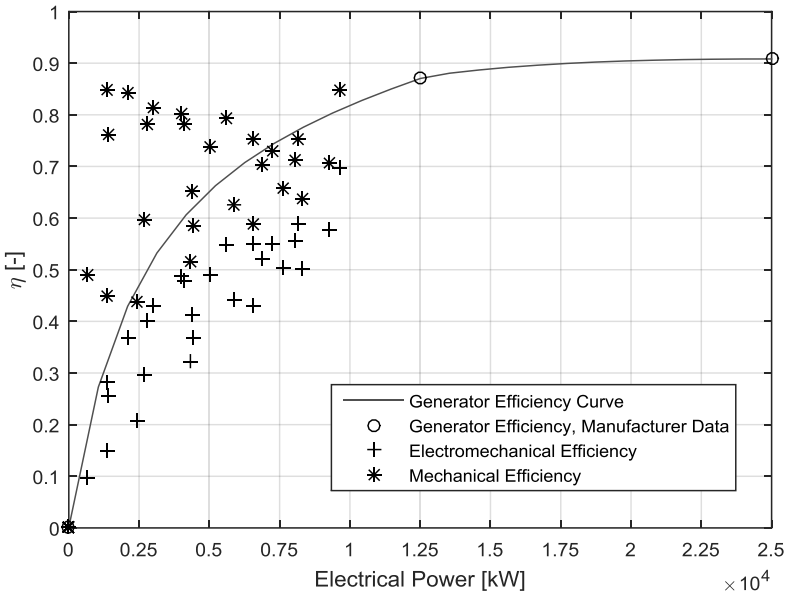

Figure 4-17: Generator electrical, engine-generator electromechanical and engine mechanical efficiency in terms of electrical power

Figure 4-18 shows that the mechanical friction work is well correlated for rotational speed higher than 450 RPM while it is scattered for low rotational speed. Moreover, mechanical losses can be higher for low rotational speed. This phenomenon can be explained by the regime of lubrication. Indeed, at low rotational speed, piston assembly and bearing friction can be in boundary lubrication regime, leading to higher friction forces. Therefore, the linear correlation given in Equation (4-4) is determined with a coefficient of determination of only 15% but seems to fit for high rotational speeds.

$$W_{mf}[J] = 257.48 + 10.9\ N \qquad (4\text{-}4)$$

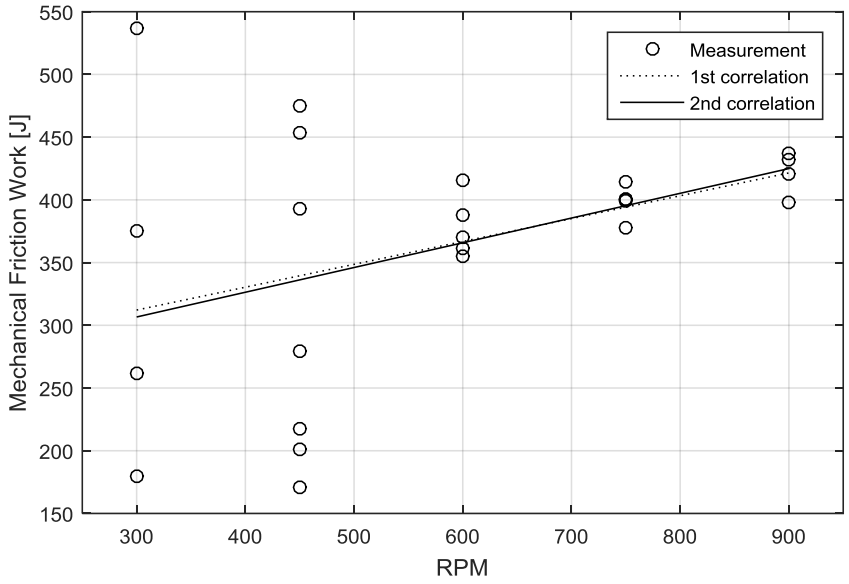

Figure 4-18: Mechanical friction work in terms of rotational speed

Figure 4-19 shows the evolution of mechanical friction work in terms of the expander supply pressure with distinction between low rotational speed (RPM < 600) and high rotational speed (RPM > 450). For low rotational speeds, the mechanical friction work is well correlated with the supply pressure while for high rotational speeds, it seems pretty constant. This observation confirms that, at low rotational speed, boundary lubrication regime is encountered, as the friction force for this regime is dependent on the load and independent of the speed.

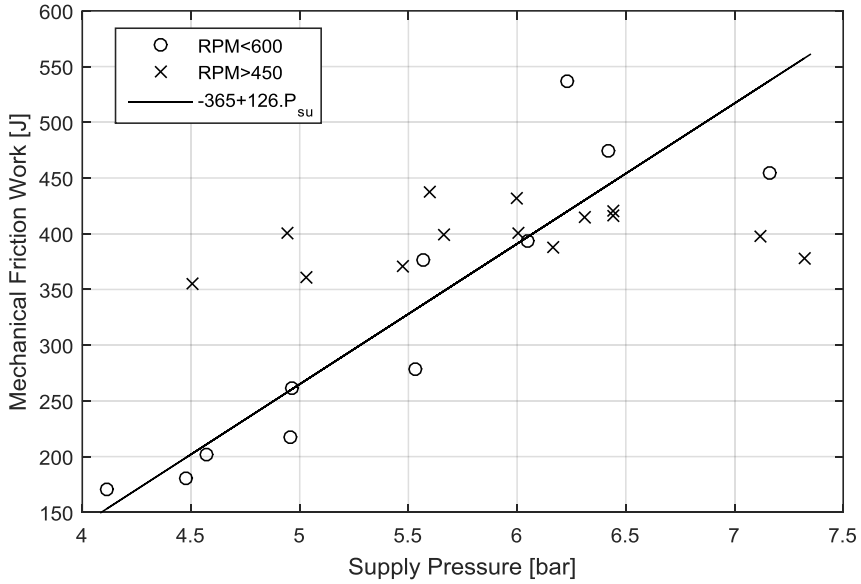

Figure 4-19: Mechanical friction work in terms of supply pressure

In the same way, Figure 4-20 shows the evolution of the mechanical friction power in terms of rotational speed. It can be seen that the loss power seems better correlated to the rotational speed than the corresponding loss work. This is confirmed by the coefficient of determination of 89% obtained with the equation (4-5) (nearly equivalent of equation (4-4)) . This can be explained by the fact that the error made on the power is the error made on the work multiplied by the speed, and that the error on the work is greater for low rotational speed. It should be noted that adding a term including the supply pressure does not lead to a significant improvement (coefficient of determination of 90% instead of 89%).

$$\dot{W}_{mf}\,[W] = 247.47\,N + 11.8\,N^2 \qquad (4\text{-}5)$$

The corresponding $fmep$ is obtained by dividing the work by the swept volume of the engine (12 l):

$$fmep = 0.205 + 0.00016.RPM \qquad (4\text{-}6)$$

with $fmep$ in bar.

This last correlation is in the same order of magnitude that those given by (Touré 2010) and (Creyx 2015) and presented in chapter 3.

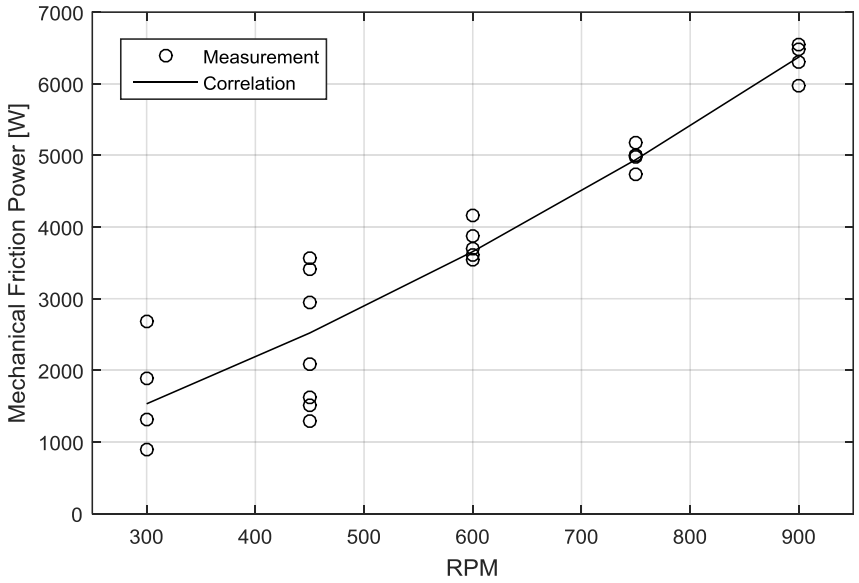

Figure 4-20: Mechanical friction power in terms of rotational speed

In conclusion, a correlation for mechanical friction work is difficult to establish because of the different lubrication regimes encountered when the rotational speed varies. Nevertheless, the mechanical friction power is less subject to the error made at low rotational speed and can therefore be well correlated with the speed.

5.2.2. Expander mechanical efficiency

As the compressor and the expander are mounted on the same shaft, the mechanical efficiency of the expander alone cannot be directly computed. However, if the whole six cylinders (instead of 4 cylinders) have been used in expander mode, the mechanical losses would have been the same that the one measured on the Ericsson engine. On the other hand, the indicated power would have been 6/4 times greater, leading to a better mechanical efficiency. Expander mechanical efficiency computed by this ways is plotted in Figure 4-21. It can be seen that mechanical efficiency increases with the pressure ratio. Indeed, when pressure ratio increases, indicated power increases relatively more than mechanical losses, which are more dependent on the speed, especially at high speed. This expander mechanical efficiency is used to compute shaft power and shaft isentropic efficiency in the next sections.

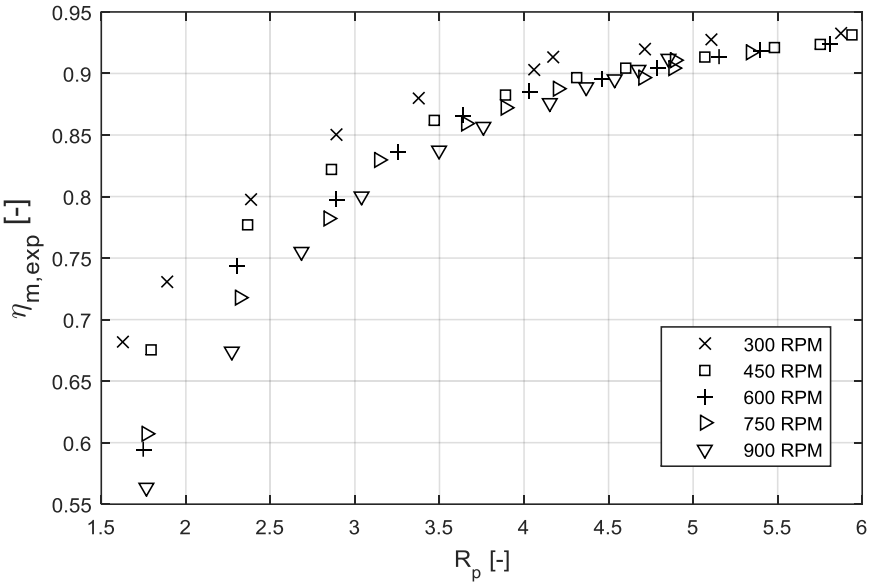

Figure 4-21: Evolution of the expander mechanical efficiency in terms of pressure ratio (measured mechanical losses but assuming that the whole 6 cylinder are working in expander mode)

5.3. Performance maps

Figure 4-22 shows shaft power and isentropic efficiency map in terms of pressure ratio and rotational speed. It should be noted that these values are not directly measured but are computed as explained in section 5.2.2. The shaft power varies from 0.5 to 3.5 kW and the isentropic efficiency from 0.1 to 0.59. The isentropic efficiency first rises with pressure ratio until reaching an optimum at $R_p = 4.5$ and then slightly decreases. It can also be seen that there is a slight optimum in terms of rotational speed at 600 RPM (this optimum is better illustrated in Figure 4-24). The mechanical power increases with the pressure ratio and the speed and does not present any optimum, maximal power being at maximal pressure ratio and rotational speed.

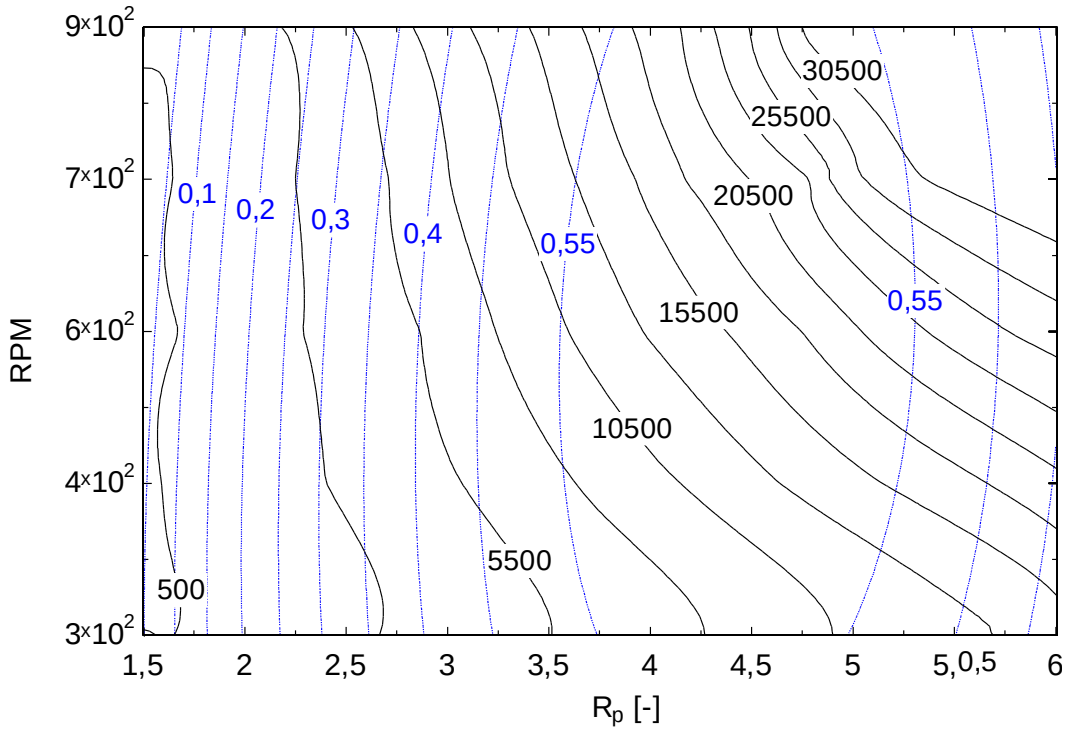

Figure 4-22: Shaft power [W] and isentropic efficiency [-] map (values computed as explained in section 5.2.2)

5.4. Measurement-based expander losses analysis

As shown in Chapter 2, different kinds of losses affect the isentropic efficiency of an expander and it is possible to split the latter in order to disaggregate the effect of each loss. As, in the tested Ericsson engine, the expander and the compressor are mounted on the same shaft, the effect mechanical losses are taken into account according to the expander mechanical efficiency computed in previous section. This disaggregation is illustrated in the next figures.

Figure 4-23 shows the evolution of the theoretical isentropic efficiency. The theoretical isentropic efficiency shows the effect of over/under expansion and compression losses. It can be seen that the maximal theoretical efficiency is close to one for pressure ratios around 2. Indeed, the built-in expansion volume ratio is adapted to this pressure ratio and the clearance volume is very small (1.6%) and thus has a very small impact on efficiency. When the pressure ratio is below 2, efficiency drops because of over-expansion. Efficiency decreases for pressure ratios above 2 and reaches 85% for a pressure ratio of 6.

The effect of pressure drops and heat transfer on the indicated work is shown in Figure 4-25 with the evolution of the diagram factor in terms of pressure ratio. It can be seen that the diagram factor is comprised between 0.2 and 0.82, increases with the pressure ratio and decreases with the rotational speed. Indeed, relative (in respect to the supply pressure) pressure drop increases with the speed and decreases with pressure ratio, as shown in PV diagrams in next section.

The evolution of the filling factor is shown in Figure 4-26. It is comprised between 0.8 and 1.4 and it is always higher than one for 300 RPM, showing the importance of the leakages. As pressure drop

increases with the speed and as leakages have less impact at higher speed, the filling factor decreases with the speed.

As the diagram factor and the filling factor decrease with the speed, and that this two loss factors have opposite effect on the indicated isentropic efficiency shows a slight optimum with respect to the speed. Indeed, a reduction of the filling factor leads to an increase in the isentropic efficiency by decreasing the reference mass flow rate.

Finally, shaft isentropic efficiency is obtained by considering mechanical losses. Figure 4-23 and Figure 4-24 show the evolution of shaft isentropic efficiency in terms of pressure and rotational speed respectively. It can be seen that the optimal rotational speed is 600 RPM and a maximal value of 61% was obtained. At low pressure ratios, both indicated and shaft isentropic efficiencies drop because filling factor increases and diagram factor and mechanical efficiency decrease.

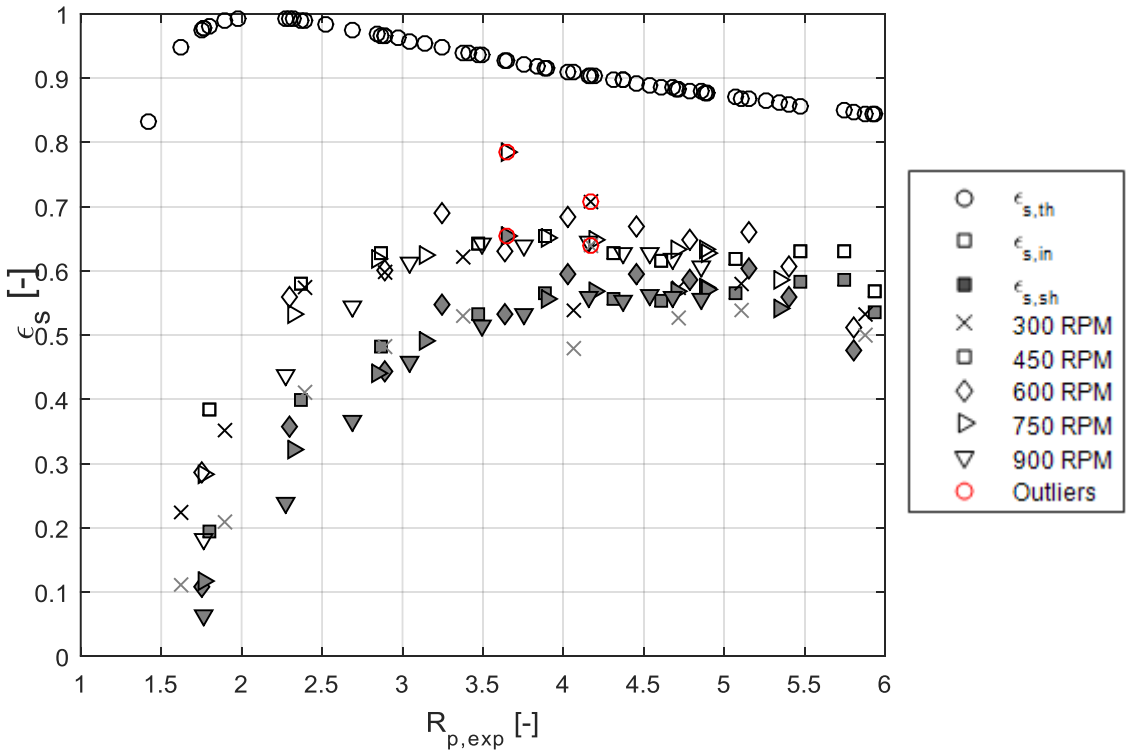

Figure 4-23: Expander indicated isentropic efficiency in terms of pressure ratio

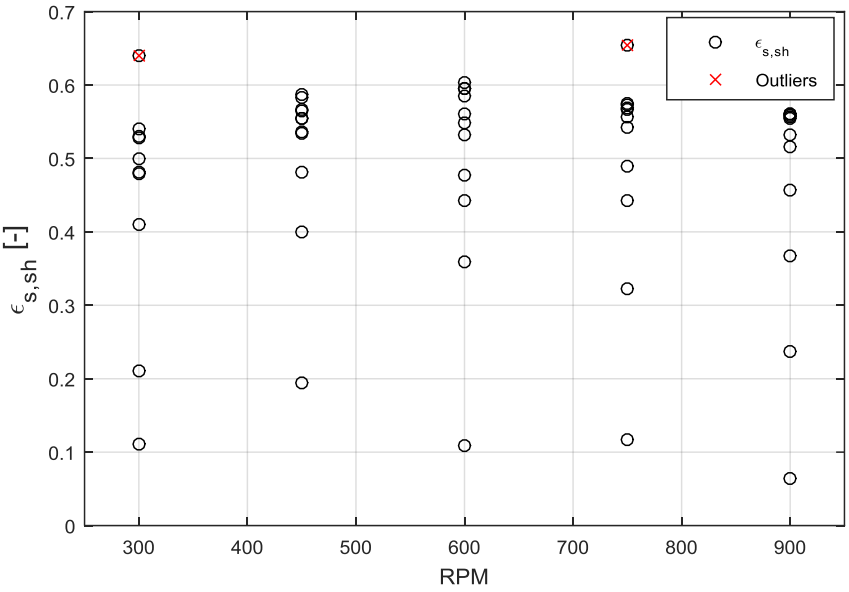

Figure 4-24: Expander shaft isentropic efficiency in terms of rotational speed

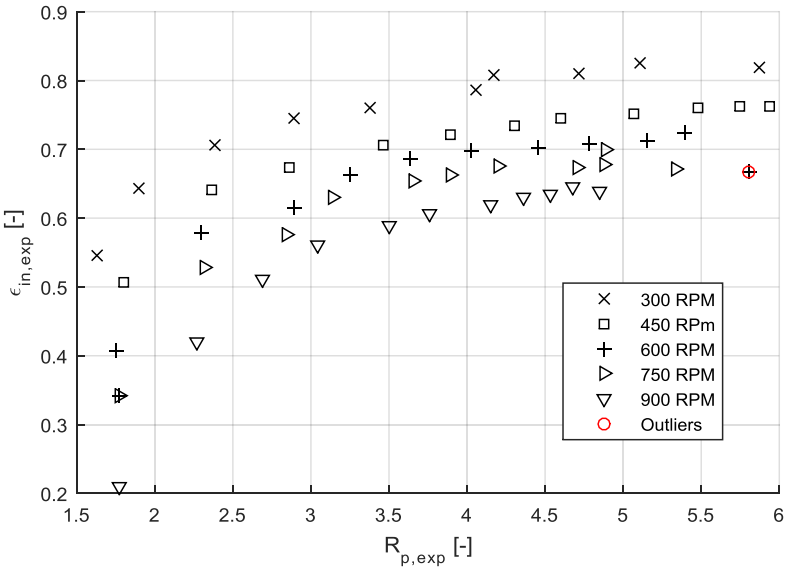

Figure 4-25: Expander diagram factor in terms of pressure ratio

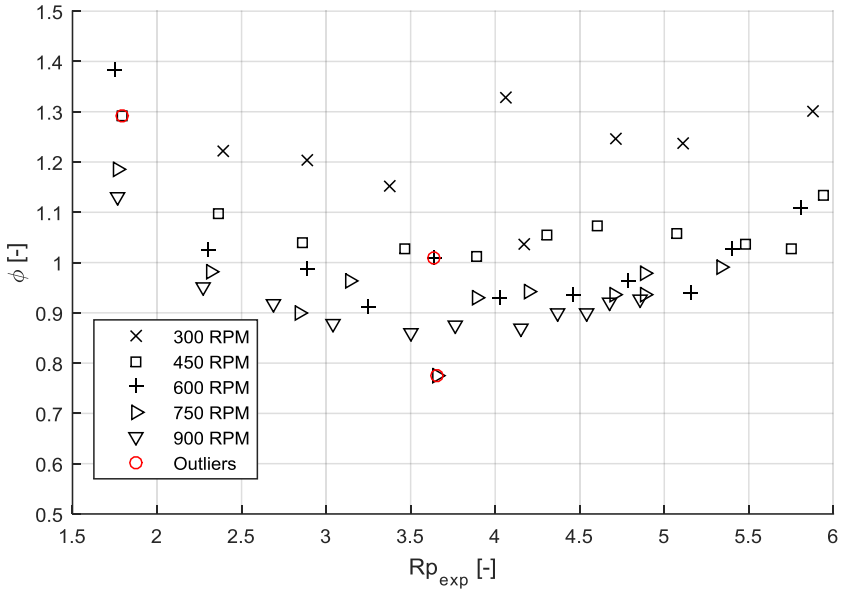

Figure 4-26: Expander filling factor in terms of pressure ratio

5.5. Expander indicator diagrams

As explained in section 3.6, in-cylinder pressure sensors are placed instead of spark-plugs in order to measure in-cylinder pressure. These measurements allow to draw indicator diagrams and to compute indicated works (used in the previous section to compute indicated isentropic efficiency).

Figure 4-27 shows indicator diagrams of the three cylinders equipped with a pressure sensor (cylinders n°1, 2 and 4). It can be observed that the three diagrams differ. The pressure during the admission process is lower for cylinder n°4 and drops faster in cylinder n°2 than in cylinder n°1. This phenomenon was observed for each measured point and can be explained by the pressure pulsations, which occurred in the high-pressure parts of the engine. Indeed, by looking to the compressor exhaust and the expander supply valves timing diagram (Figure 4-28), it can be seen that supply valves of cylinders n°3 and n°4 open at the same time, leading to a high pressure decrease in the expander supply manifold. It can also be seen that the cylinder n°1 supply valve opening overlaps with the two compressor exhaust valve openings, which could explain the lower pressure drop at the end of the admission process in cylinder n°1. As the indicator diagrams are different for each cylinder, the indicated work was computed with the average of the four cylinders considering that cylinder n°3 is similar to cylinder n°4.

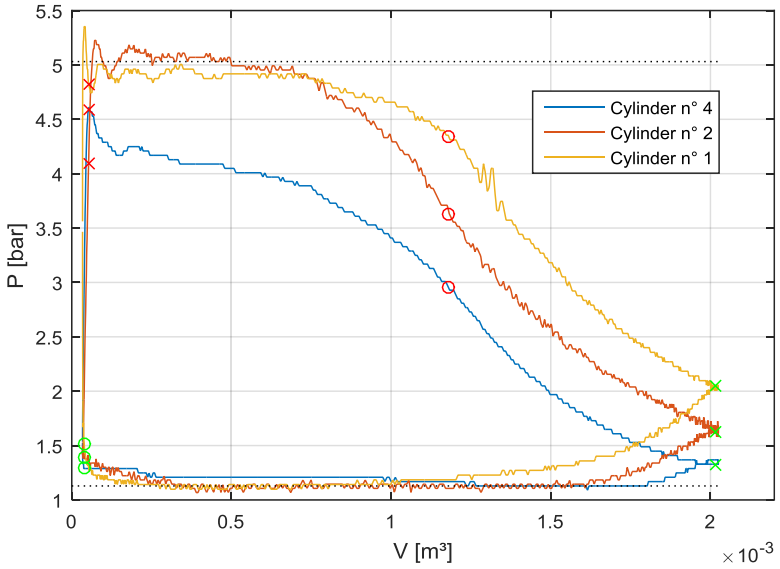

Figure 4-27: Expander indicator diagrams for Psu=5 bar and 600 RPM in three different cylinders (opening and closing volume are respectively represented by green and red markers)

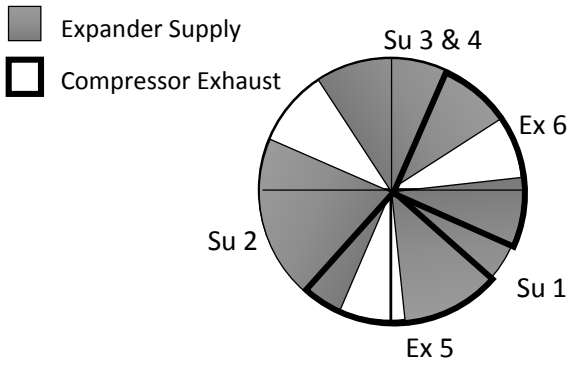

Figure 4-28: Compressor exhaust and expander supply valves timing diagram (cylinders n° 5 and 6 are used as compressor and cylinders n° 1, 2, 3 and 4 are use as expander)

Figure 4-29 shows the effect of rotational speed on the indicator diagram (cylinder n°2) for a supply pressure of 5 bar. This figure shows that, as expected, supply pressure drop increases with the rotational speed. The in-cylinder pressure at the inlet closing volume passes from 4.35 bar to 2.96 bar for rotational speed increasing from 300 RPM to 900 RPM. The exhaust pressure drops are less significant. This increase in pressure drop leads to a decrease in the diagram factor, which goes down from to 81 % to 62 % (see Figure 4-25).

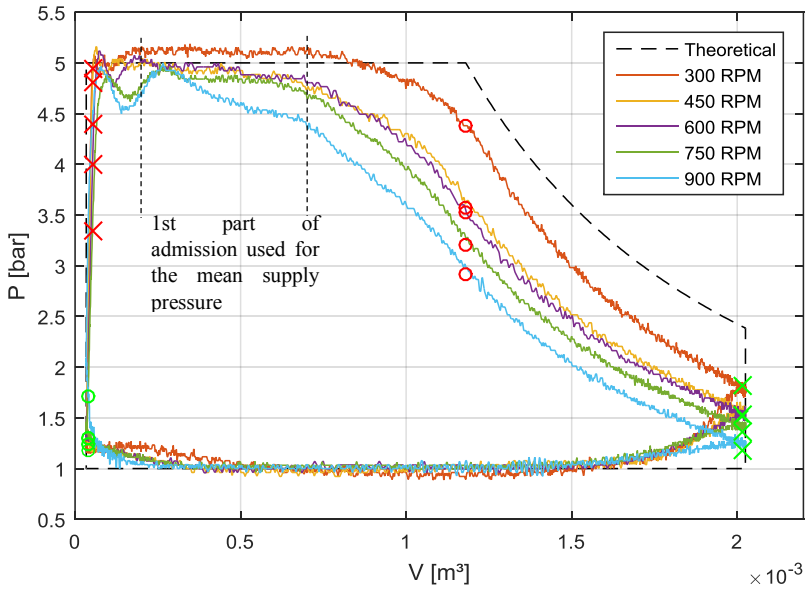

Figure 4-29: Cylinder n°2 indicator diagram for Psu=5 bar and different rotational speeds (opening and closing volumes are respectively represented by green and red markers)

Indicator diagrams for 600 RPM and different supply pressures are shown in Figure 4-30. First, it can be seen that supply pressure drop induces higher under expansion than theoretically for 1.8 bar and 3 bar of supply pressure. Second, the absolute supply pressure drop (the difference between supply pressure and in-cylinder pressure at inlet closing volume) increases with the supply pressure, but the relative supply pressure drop (the ratio between in-cylinder pressure at inlet closing volume and supply pressure) decreases. This explains why the diagram factor increases with the pressure ratio (see Figure 4-25).

On all these PV diagrams, a small decrease in the in-cylinder pressure occurs at the very beginning of the admission process. This in-cylinder pressure drop occurs because the volume increases but the supply port cross section area is still small. Another, larger, in-cylinder pressure decrease occurs in the last part of the expansion process. Indeed, at this moment, the supply port cross section area decreases while the cylinder volume continues to rise. This last phenomenon is called pre-expansion. These two in-cylinder pressure drops can also been observed in twin-screw expander (Papes, Degroote, and Vierendeels 2015).

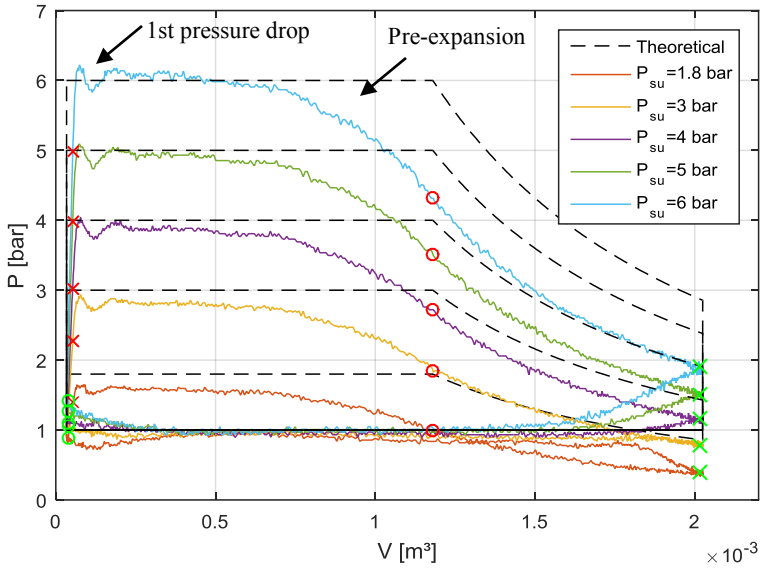

Figure 4-30: Cylinder n°2 indicator diagram for 600 RPM and different supply pressures (opening and closing volumes are respectively represented in green and red)

6. Detailed model validation and analysis

6.1. Geometrical parameters

The evolutions, in terms of shaft angle, of geometrical parameters that have to be defined are:

- the in-cylinder volume
- the heat transfer surface area
- the cross sectional areas of the supply and exhaust ports

Evolution of the volume and of the heat transfer surface area are calculated by equations (3-1) and (3-4) given in chapter 3. All geometrical data needed is given in Table 4-4, except that clearance volume is 1.6 % of the total volume instead of 9% as explained in section 3.4.

Cross sectional areas of supply and exhaust ports can be deduced from geometrical dimensions of the valves and from the valve lifts. The dimensions of the valves are given in Table 4-8 and the lifts are given in Figure 4-16.

Table 4-8: Valves dimensions

Exhaust expander and supply compressor valves		Supply expander and exhaust compressor calves	
D_v	57 mm	D_v	50 mm
D_{vi}	51.3 mm	D_{vi}	42 mm
D_{vs}	12 mm	D_{vs}	12 mm

6.2. Calibration process

First, the P-V diagrams computed by the model without calibration are compared to the measured ones. This comparison is made for cylinder n°2 as it seems to be less affected by the pressure pulsations in the supply manifold. Figure 4-31 and Figure 4-32 show that, without calibration, the model underestimates pressure drops. In order to correct this disparity, flow coefficients are set to 0.75 and 0.6 for supply and exhaust ports respectively. With these values of the flow coefficients, a better agreement between simulated and measured data is obtained. However, it can be seen that a trade-off has to be found because, for some points (e.g. 6 bar/ 600 RPM), supply pressure drop is a bit overestimated while for others (e.g. 5 bar / 900 RPM), supply pressure drop is still a bit underestimated.

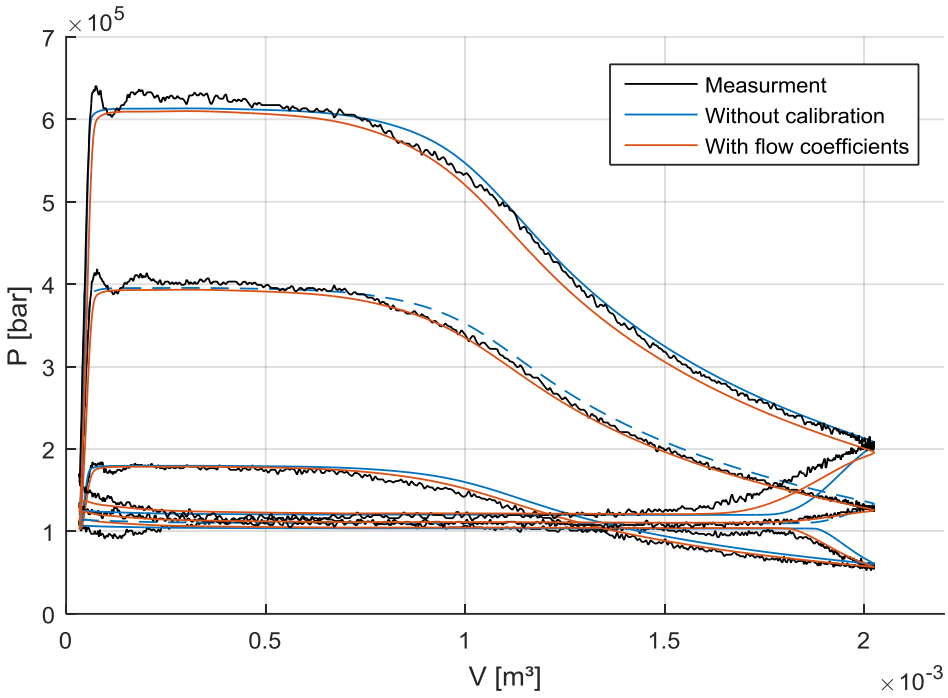

Figure 4-31: Comparison between measured (cylinder n° 2) and simulated indicator diagrams for RPM=600 and Psu=1.8, 4 and 6 bar

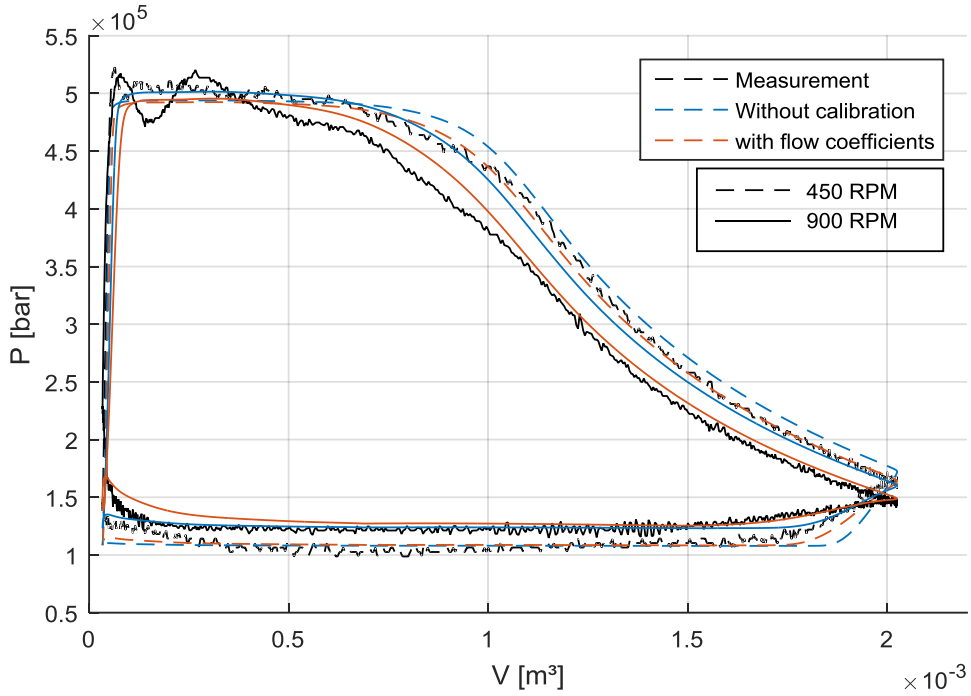

Figure 4-32: Comparison between measured (cylinder n° 2) and simulated indicator diagrams for Psu=5 bar and RPM=450 and 900

According to (Heywood 1988), despite of its pulsating characteristic, many aspects of the gas exchange process can be treated on a quasi-steady basis with time average pressure. The average value of the supply manifold pressure is assumed to be a fraction of the supply pressure measured upstream to the manifold. The supply pressure is multiplied by 0.94. This number is the mean ratio between the in-cylinder supply pressure during the first part of the admission process (see Figure 4-29) and the pressure measured upstream of the supply manifold for 300 RPM points. Indeed, for these points, supply pressure drops are negligible. With this average supply pressure and values of flow coefficient given just above, the model is able to predict indicated work with a good agreement in respect to the measurements, as shown in Figure 4-33.

However, Figure 4-34 and Figure 4-35 show that mass flow rate and exhaust temperature are respectively under and over-estimated. To obtain a better agreement, leakages have to be added by introducing lumped leak flow cross section area. Finally, in order to decrease the simulated exhaust temperature, the in-cylinder heat transfer coefficient (Annand correlation, see chapter 3) is multiplied by a correction factor given in Table 4-9. With this correction factor, exhaust temperature is still overestimated for some points.

Table 4-9: Detailed model calibrated parameters

$C_{d,su}$ [-]	$C_{d,ex}$ [-]	A_{leak} $[mm^2]$	*Heat transfer correction factor*
0.75	0.6	8.5	4

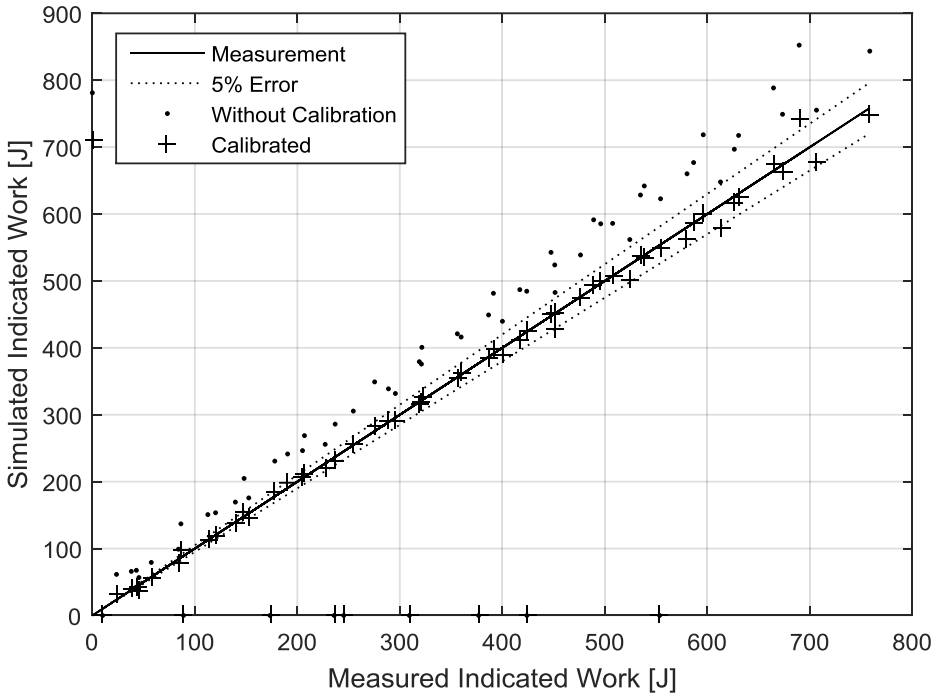

Figure 4-33: Comparison between measured and simulated indicated works

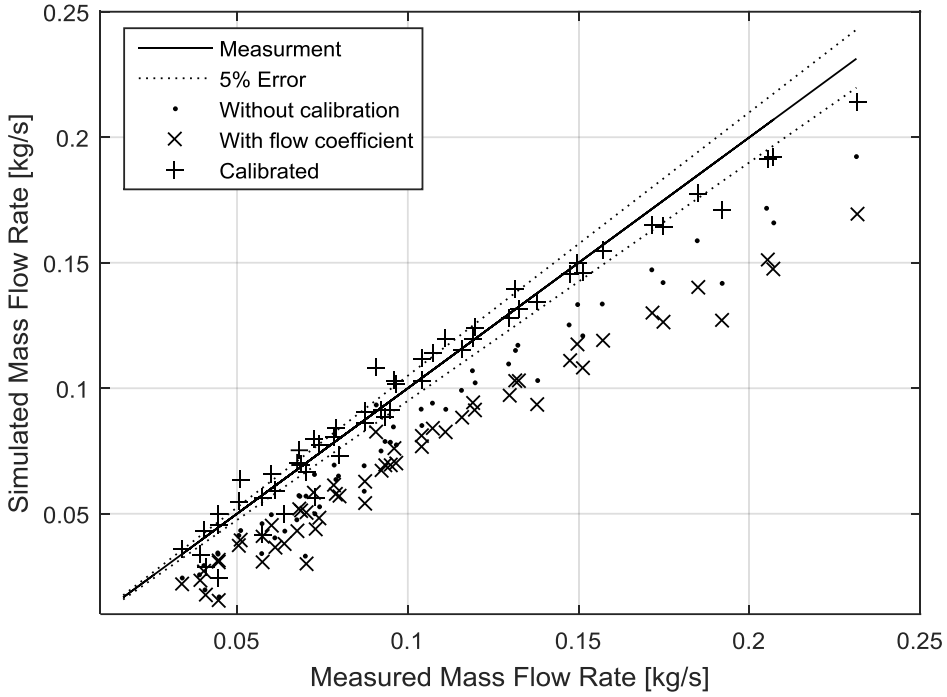

Figure 4-34: Comparison between measured and simulated mass flow rates

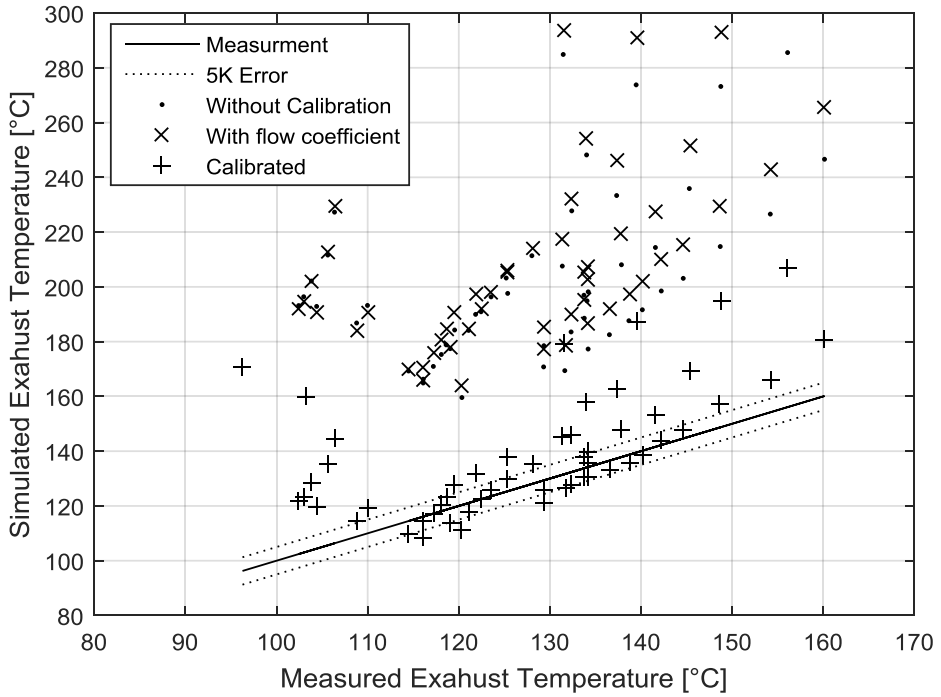

Figure 4-35: Comparison between measured and exhaust temperatures

6.3.Model-based losses analysis

The model allows distinguishing the effects of pressure drops, heat transfer and leakages and conducting the filling factor disaggregation presented in chapter 2. Figure 4-36 shows the internal filling factor without and with heat transfer as well as leakage and global filling factors. It can be seen that, as expected, pressure drop decreases filling factor. Heat transfer slightly increases it (as shown in section 2.2) but internal filling factor stays below one. Conversely, leakage filling factor is greater than one and is comprised between 1.6 and 1.2, showing that performance of the expander is greatly affected by the leakages. Indeed, these values lead to a decrease of 37.5 % and 16 % respectively of the isentropic efficiency.

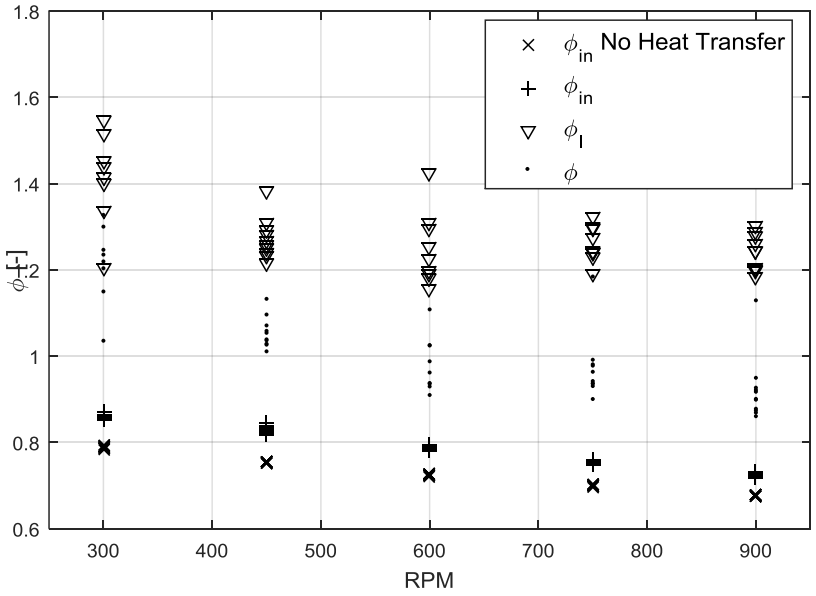

Figure 4-36: Filling factor disaggregation in terms of rotational speed

In chapter 2, the specific diagram factor has been defined as the ratio between diagram factor and internal filling factor in order to quantify the influence of pressure drop and heat transfer on isentropic efficiency. The evolution of specific diagram factor in terms of rotational speed is shown in Figure 4-37 and is compared to the diagram factor. This plot shows that, as pressure drops decrease the mass flow rate, the specific diagram factor is higher than the diagram factor. Then, the effect of pressure drop is less significant on the isentropic efficiency than on the compactness. Indeed, the compactness is directly affected by the diagram factor.

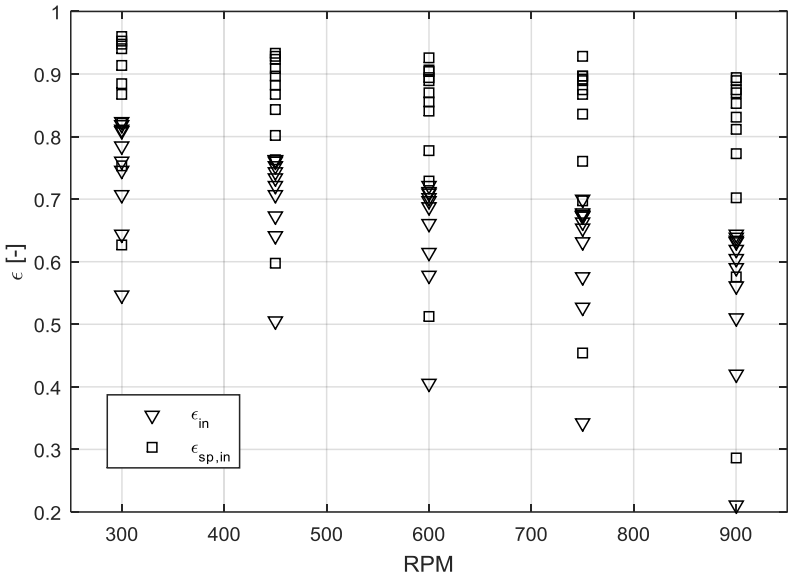

Figure 4-37: Diagram and specific diagram factors in term of rotational speed

7. Comparison between design and post-validation simulations

This section aims at understanding why the Ericsson engine did not operate as expected in the pre-design and design simulations (section 2.3 and 3.1) by simulating and comparing several cases. The first case is the design case presented in section 3.1 with the first camshaft design and an expander supply temperature of 800°C. The second case considers the second camshaft design presented in section 4.2, which increases the cut-off ratio and then the mass flow rate of the expander, again with 800°C as expander supply temperature. Then, the influence of the expander supply temperature is shown in the third case by considering an expander supply temperature of 450°C as during the test. The fourth case takes into account the leakages that occur in the compressor and the expander and represents the simulation of the actual prototype. Finally, the fifth case shows what could have been obtained if the electrical heater would have delivered an air temperature of 800°C.

Figure 4-38 shows simulated mass flow rates in terms of rotational speed for the different cases. The mass flow rates increase with the rotational speed and are the same for cases without leaks and decrease when leaks are added. Then, Figure 4-39 shows comparison between simulated and measured compressor mass flow rates. As shown in section 5.1.1, the quality of the measures of compressor mass flow rate is poor and measured values are scattered. However, simulated mass flow rates with leakages seem to give a good estimation of the measured ones.

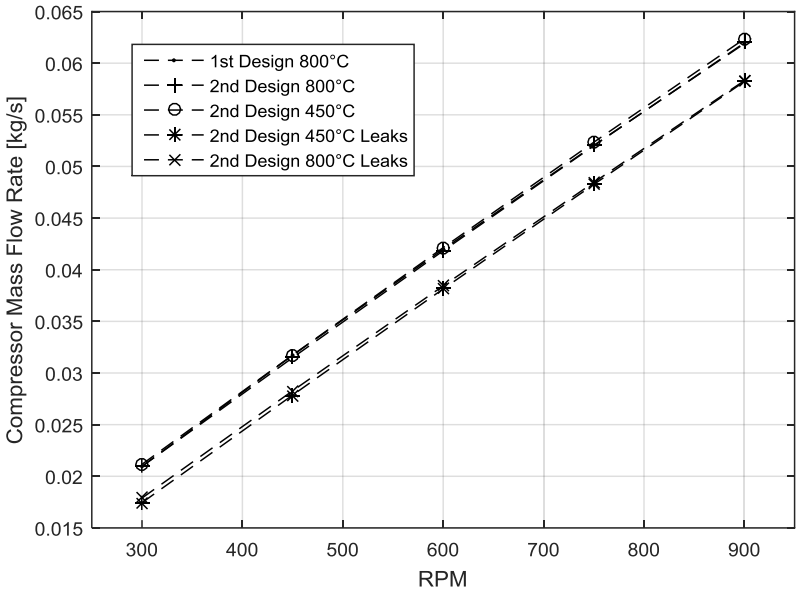

Figure 4-38: Simulated mass flow rate in terms of rotational speed

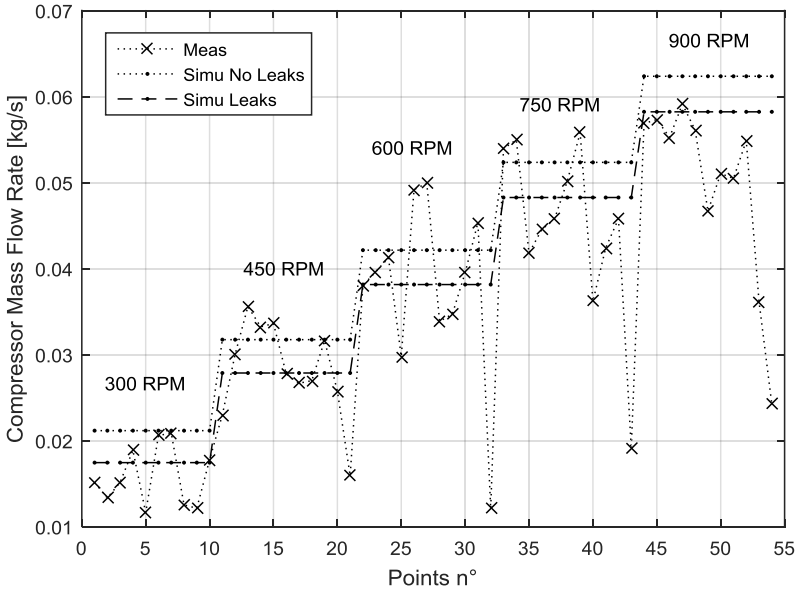

Figure 4-39: Comparison between measured and simulated compressor mass flow rates

Figure 4-40 shows simulated expander supply pressure in terms of rotational speed for the different cases. It can be seen that the increase in the cut-off ratio induced by the second camshaft design leads to a decrease in the pressure. Indeed, when the cut-off increases, the expander volumetric mass flow rate increases too and then the expander supply pressure decreases. Same effect is observed when decreasing the supply expander temperature to 450°C and when the leakages are added.

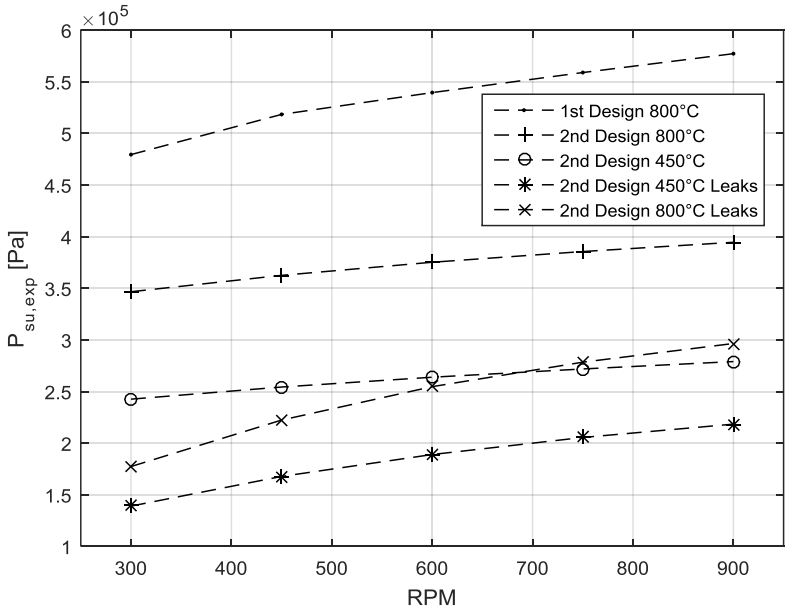

Figure 4-40: Expander supply pressure in terms of rotational speed

Finally, Figure 4-41 shows Ericsson engine efficiency without mechanical losses in terms of rotational speed. It can be seen that, with the actual prototype, the efficiency is negative with the 450°C expander supply temperature and, if the temperature would have been 800°C, the efficiency would be equal to about 1%.

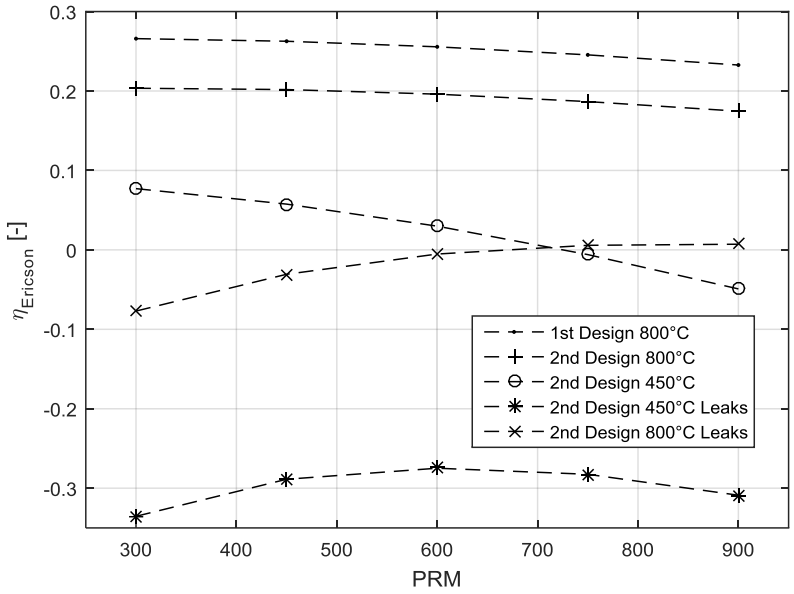

Figure 4-41: Ericsson cycle efficiency (no mechanical losses) in terms of rotational speed

In conclusion, this analysis shows that the second cam-shaft design induces lower pressure and efficiency than with the first design by increasing the cut-off. However, it is the too large leakages (and the too low expander supply temperature) that prevent the prototype to work properly.

8. Semi empirical model validation

The same process of validation is applied to calibrate the semi-empirical model:

- Increase pressure drops (decrease supply and exhaust fictive nozzles areas A_{su} and A_{ex}) until indicated work is well predicted.
- Add leakages (increase leakage fictive nozzle area A_{leak}) in order to increase the mass flow rate until agreement with the measurements is found.
- Add heat transfers (increase the supply and exhaust overall heat transfer coefficients AU_{su} and AU_{ex}) until simulated exhaust temperature match the measurements.

The parameters found with this calibration process are listed in Table 4-10 and the results are shown in Figure 4-42, Figure 4-43 and Figure 4-44. These results show that the semi empirical model is able to predict indicated work and mass flow rate as well as the detailed model is. As in the detailed model, the exhaust temperature is less well predicted.

Table 4-10: Calibrated parameters of the semi empirical model

A_{su} $[mm^2]$	A_{ex} $[mm^2]$	$A_{leak}[mm^2]$	AU_{su} $[W/K]$	AU_{ex} $[W/K]$
63	314	8	10	40

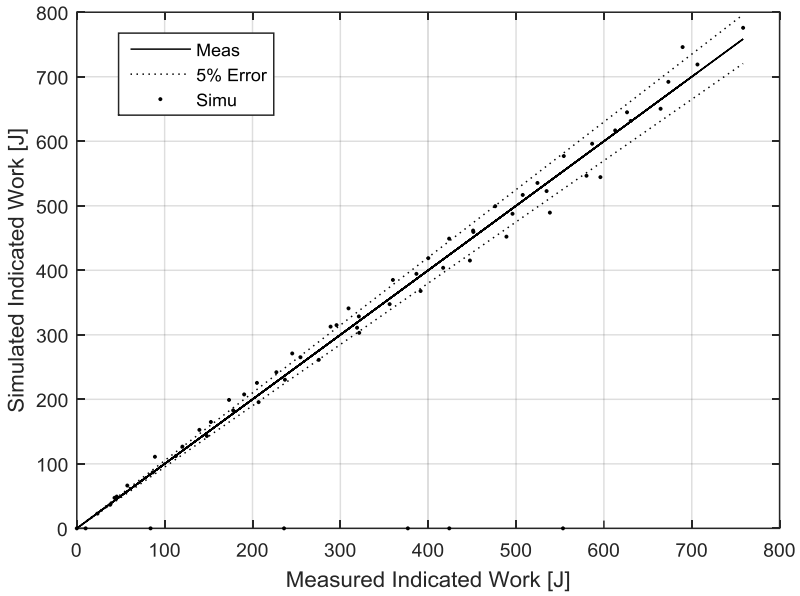

Figure 4-42: Comparison between measured and simulated indicated works

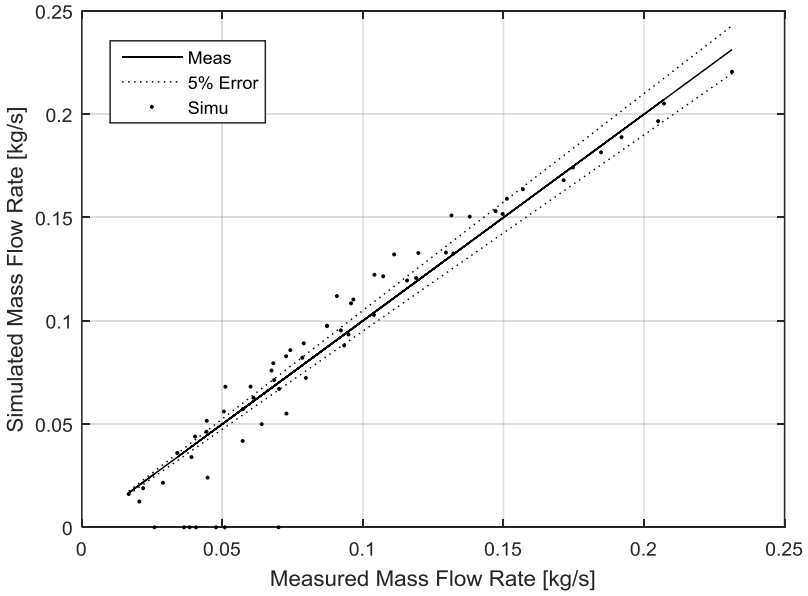

Figure 4-43: Comparison between simulated and measured mass flow rates

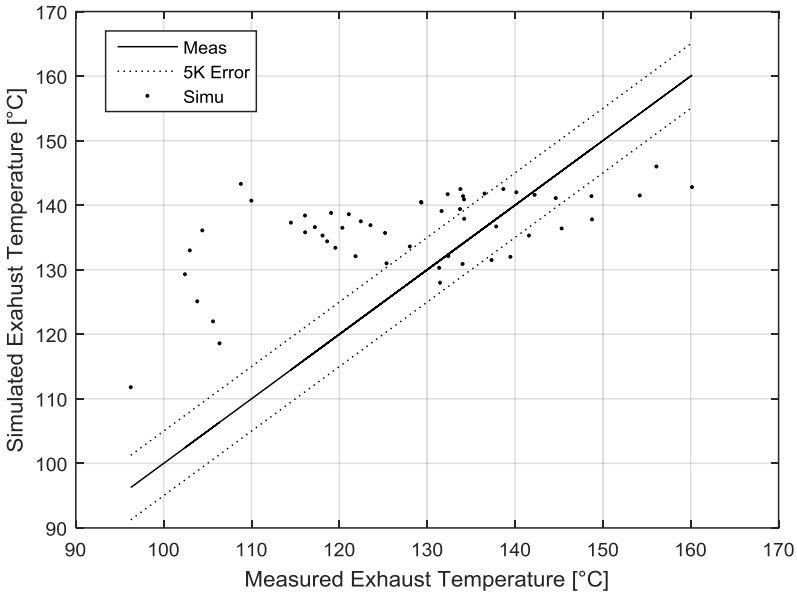

Figure 4-44: Comparison between measured and simulated exhaust temperatures

9. Conclusions

The detailed model described in chapter 3 was used to simulate an Ericsson engine and to optimize the volume ratio and the valve timings. These simulations led to a volume ratio of 2 in order to maximize the efficiency of the Ericsson engine.

Then the main modifications made to turn the ICE into an Ericsson engine were presented. These modifications concerned principally the valve train. Indeed, a special camshaft had to be designed with the valve timings found with the simulations. Also, in order to reduce mechanical constraints, the gear set was changed to decrease the rotational speed of the camshaft by two and special pneumatic springs were designed for high pressure valves. Other modifications are the change of the manifolds as the Ericsson engine needs four manifolds while ICE have two. Finally, the bowl-in pistons were replaced with pistons with just two valve reliefs in order to minimize the clearance volume.

Unfortunately, this prototype did not operate as expected, since the pressure did not rise to a sufficient level to produce power. Nevertheless, the engine was fed with an extra compressor in order to characterize the expander part of the engine. These tests have allowed the evaluation of indicated and shaft isentropic efficiencies, filling factor and mechanical losses. The in-cylinder pressure measurements have shown that pressure pulsations occur at the supply of the expander, reducing the mean supply pressure.

To extend the analysis of the expander performance, the detailed model was calibrated and used to desegregate the effect of leakages, heat transfer and pressure drops on performance indicators. This analysis has shown that it is mainly the leakages that affect the indicated isentropic efficiency of the expander. Table 4-11 lists values of the factors that affect the shaft isentropic efficiency for three rotational speeds and a supply pressure of 5 bar (optimal). It can be seen that the importance of each

source of losses depends on the rotational speed. Indeed, the effects of pressure drop and mechanical losses increase with the speed while effect of leakages decreases with the speed. For the optimal rotational speed of 600 RPM, the more detrimental one is the leakages followed by, respectively, the mechanical losses, the pressure drop and under expansion and compression.

Table 4-11: Summarize of losses analysis

Rotational speed	$\epsilon_{s,th}$ [-]	ϵ_{in} [-]	$\frac{1}{\phi_{in}}[-]$	$\frac{\epsilon_{in}}{\phi_{in}} = \epsilon_{sp,in}$ [-]	$\frac{1}{\phi_{l}}[-]$	$\epsilon_{s,in}$[-]	η_m [-]	$\epsilon_{s,sh}$ [-]
300 RPM	0.88	0.81	1.16	0.94	0.7	0.58	0.91	0.53
600 PRM	0.89	0.70	1.27	0.89	0.84	0.67	0.88	0.59
900 RPM	0.9	0.62	1.37	0.85	0.83	0.64	0.86	0.55

Then the calibrated model was used to perform simulations in order to understand why the engine prototype did not work properly. The first reason is that the expander supply temperature was only 450°C instead of 800°C due to limitation of the electrical heater. But, even if the temperature was 800°C, the engine would have just self-sustained with an efficiency around 1%. The main reason of the dysfunction is the too large leakages leading to too high mass flow rate and then low pressure. Another factor that accentuates this phenomenon is the cut-off that was higher than with the first design.

This analysis shows that some improvements are possible in order to obtain betters results. These possible improvements are:

- Decrease the leakages by using more suited valves. Indeed, as the ICE cylinders heads and valves were kept unchanged, the pressure gradient of the high-pressure valves was in the wrong direction (see Figure 4-11).
- Redesign the camshaft to decrease the cut-off.
- Attenuate supply pressure pulsations with, for example, a larger manifold.

These perspectives are considered in Chapter 6 where performances of an Ericsson engine-based CHP unit are evaluated.

10.References

Blair, G. 1999. *Design and Simulation of Four-Stroke Engines*. Warrendale, PA: Society of Automotive Engineers.

Cordero, R., G. Seckmeyer, D. Pissulla, and F. Labbe. 2008. "Uncertainty of Experimental Integrals: Application to the UV Index Calculation." *Metrologia* 45 (1): 1–10. doi:10.1088/0026-1394/45/1/001.

Creyx, M. 2015. "Etude théorique et expérimentale d'une unité de micro-cogénération biomasse avec moteur Ericsson." PhD Thesis, Université de Valanciennes et du Hainaut-Cambresis.

Dubouil, R. 2012. "Etude Par Simulation Des Transferts Hermiques Dans Un Groupe Otopropulseur Hybride Électrique Automobile." PhD Thesis, Ecole Centrale de Nantes.

Heywood, J.B. 1988. *Internal Combustion Engine Fundamentals*. McGraw-Hill Series in Mechanical Engineering. New York: McGraw-Hill.

ISO/TC 30. 2003. "ISO 5167: Mesure de Débit Des Fluides Au Moyen D'appareils Déprimogènes Insérés Dans Des Conduites En Charge de Section Circulaire."

Lebrun, J. 1998. *Thermodynamique Appliquée et Introduction Aux Machines Thermiques*. Liège Belgium: University of Liège.

Papes, I., J. Degroote, and J. Vierendeels. 2015. "New Insights in Twin Screw Expander Performance for Small Scale ORC Systems from 3D CFD Analysis." *Applied Thermal Engineering* 91 (December): 535–46. doi:10.1016/j.applthermaleng.2015.08.034.

Quoilin, S., and J. Schrouff. 2016. "Assessing Steady-State, Multivariate Experimental Data Using Gaussian Processes: The GPExp Open-Source Library." *Energies* 9 (6). doi:10.3390/en9060423.

Subcommittee 65B : Measurement and control devices. 2013. *Thermocouples. Part 1, Part 1,*. International Electrotechnical Commission.

Technical Committee 65. 2008. *Industrial Platinum Resistance Thermometers and Platinum Temperature Sensors = Thermomètres À Résistance de Platine Industriels et Capteurs Thermométriques En Platine.* International Electrotechnical Commission. Geneva: International Electrotechnical Commission.

Touré, A. 2010. "Etude Théorique et Expérimentale D'un Moteur Ericsson À Cycle de Joule Pour Conversion Thermodynamique D'énergie Solaire Ou Pour Micro-Cogénération." PhD Thesis, Université de Pau et des Pays de l'Adour.

U.S. Departement of Energy. 1997. "Determining Electric Motor Load and Efficiency." DOE/GO-10097-517.

11.Annexes

11.1. Gaussian regression results

Three plots are presented for each studied variable:

- The first one shows the results of the regression model and the measurements in terms of the two independent variables.
- The second one shows the values predicted by the regression model in terms of the measured values. Red points (train) represents the results of the model based on all the data set. The blues points (cross validation) represents the results of a model based on all the data set except the predicted values. The MARE, given in section 5.1.1, is related to the "cross validation" model.
- The third plot shows the discrepancy between the measured and predicted values on a normalized Gauss curve.

11.1.1. Electrical power

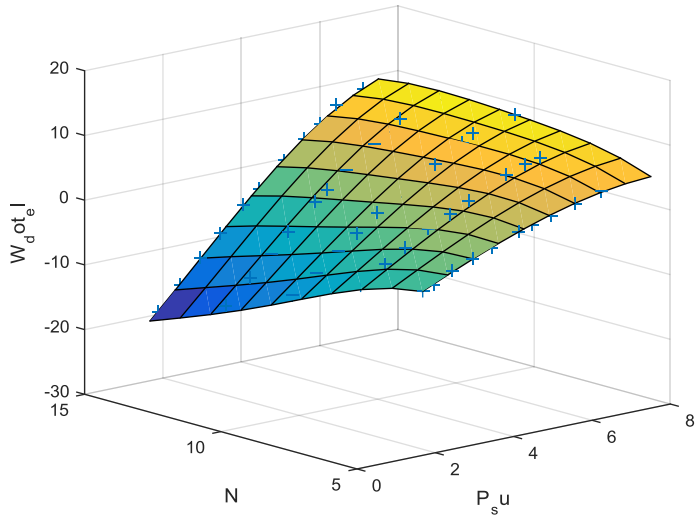

Figure 4-45: Electrical power regression model

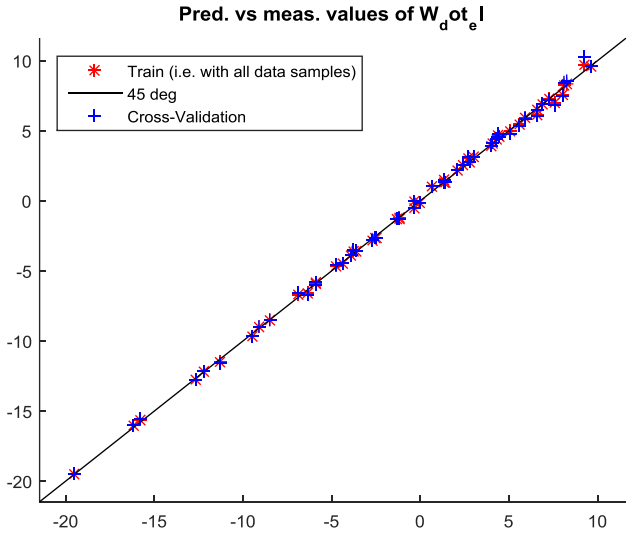

Figure 4-46: Electrical power cross validation

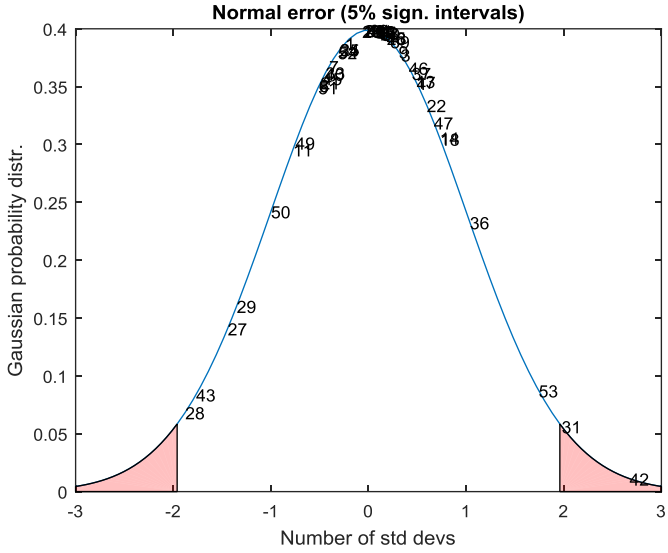

Figure 4-47: Electrical power error normal distribution

11.1.2. Compressor indicated work

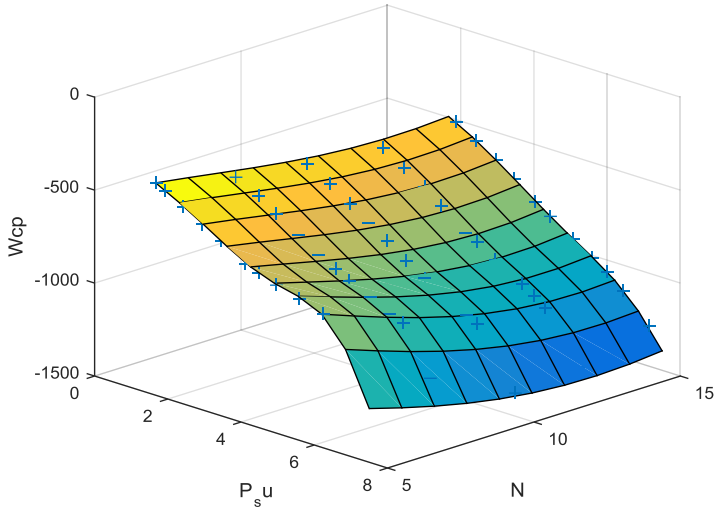

Figure 4-48: Compressor indicated work regression model

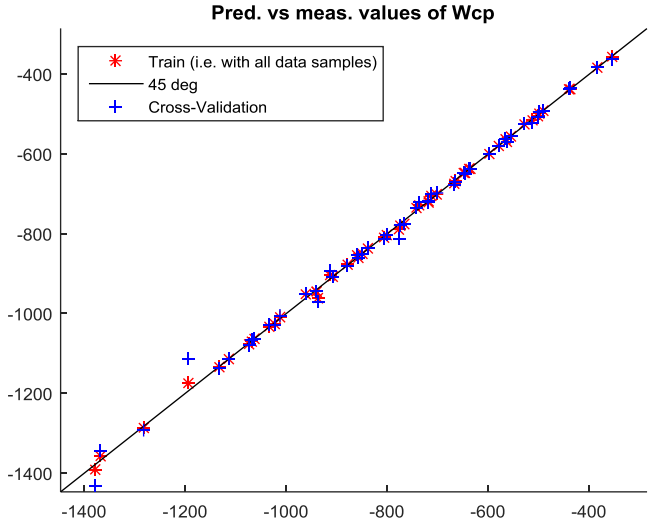

Figure 4-49: Compressor indicated work cross validation

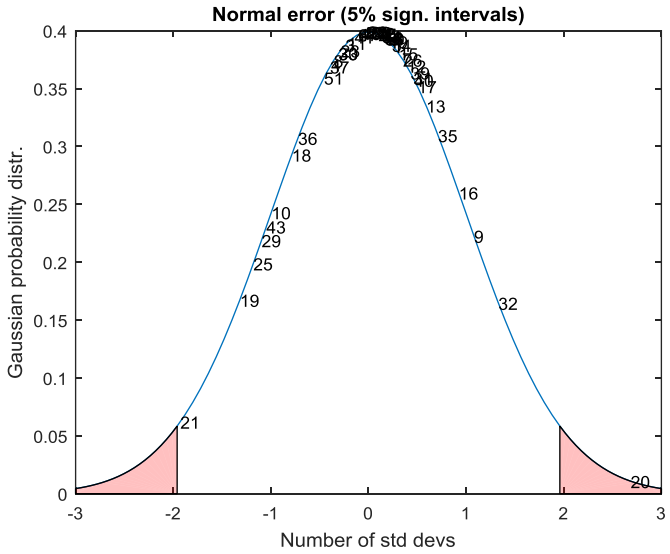

Figure 4-50: Compressor indicated work error normal distribution

11.1.3. Expander indicated work

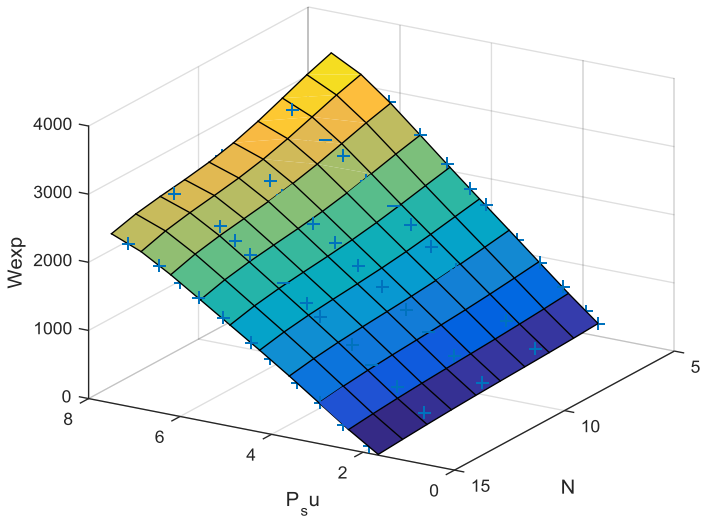

Figure 4-51: Expander indicated work regression model

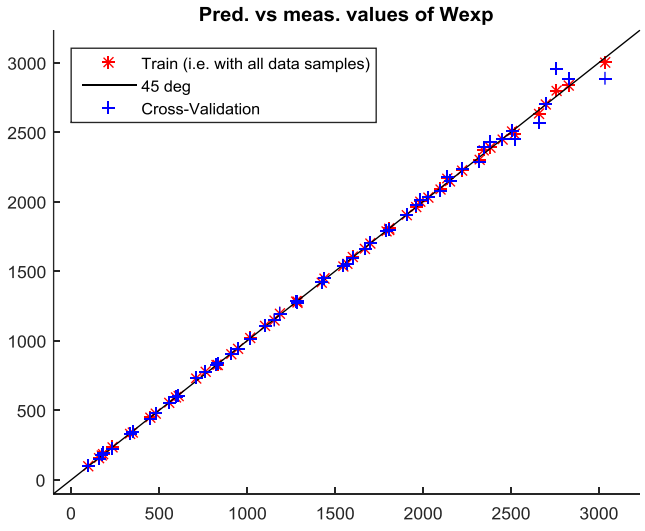

Figure 4-52: Expander indicated work cross validation

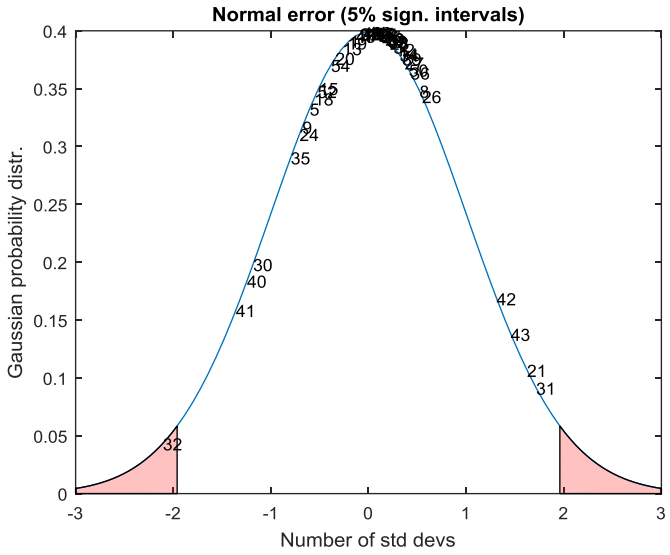

Figure 4-53: Expander indicated work error normal distribution

11.1.4. Exhaust mass flow rate

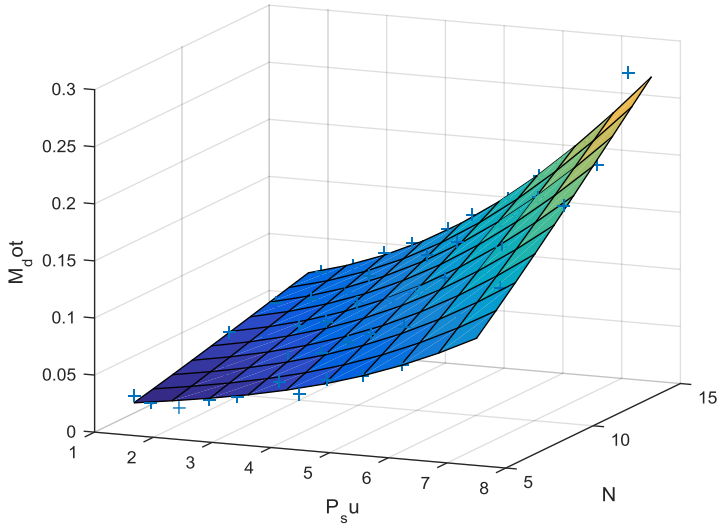

Figure 4-54: Exhaust mass flow rate regression model

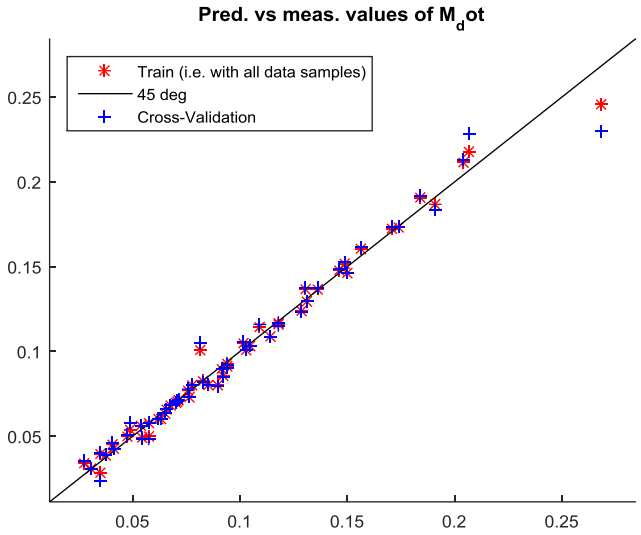

Figure 4-55: Exhaust mass flow rate cross validation

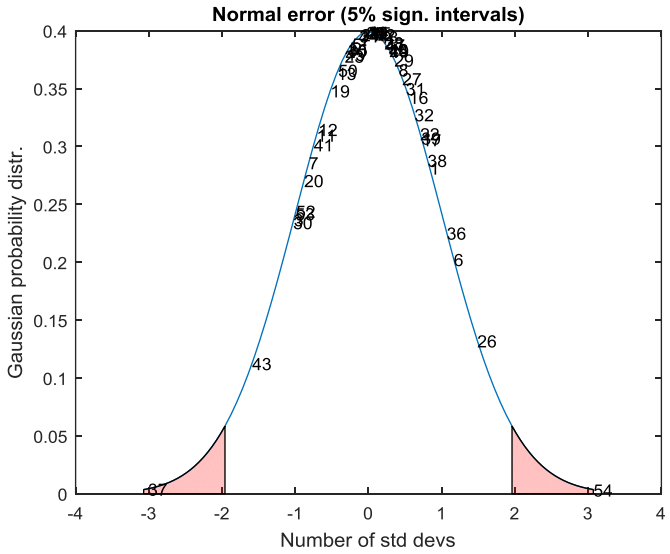

Figure 4-56: Exhaust mass flow rate error normal distribution

11.1.5. Supply mass flow rate

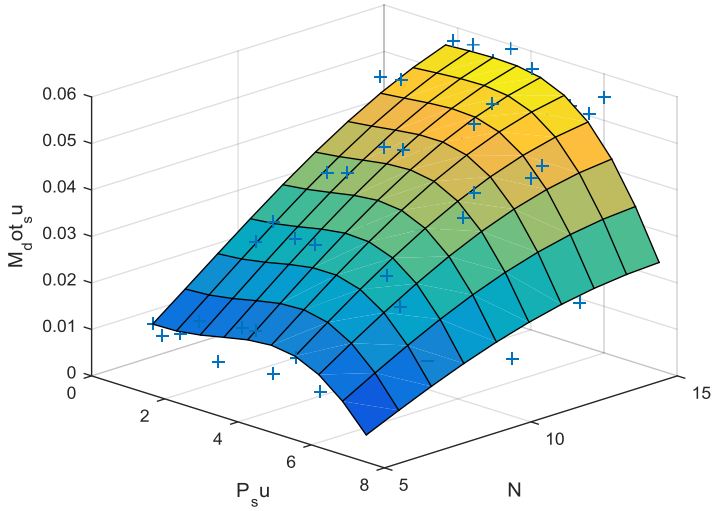

Figure 4-57: Supply mass flow rate regression model

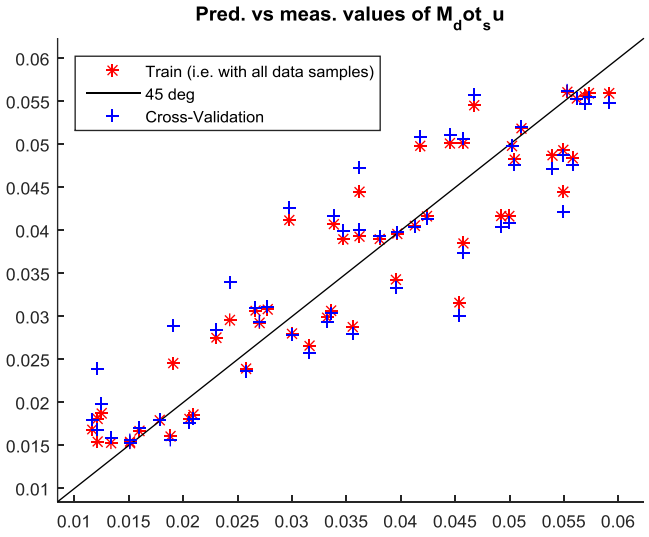

Figure 4-58: Supply mass flow rate cross validation

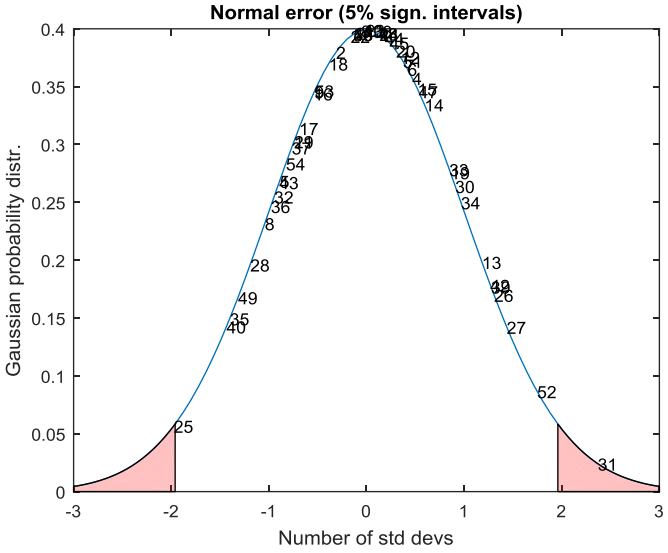

Figure 4-59: Supply mass flow rate error normal distribution

11.2. Static leakage test

In order to evaluate the sealing of the high-pressure valves, a static leakage test was performed. This test consisted in injecting air with the help of a compressor inside the high-pressure volume and keeping high-pressure valves closed with pneumatics valve springs (see 3.2). The operation was repeated for three different pneumatic spring pressures.

During this test, the pressure in the high-pressure volume increases until stabilization occurs at a certain pressure level. As shown in Figure 4-60, the level of stabilized pressure increases with the pressure in the pneumatic valves springs. When the injection of mass flow rate was stopped, the pressure decreases and seems to stabilize, also at a higher level for higher pneumatic spring pressure. These observations show that sealing performance increases with the resulting force closing the valve. Indeed, this resulting force increases when pressure differences between pneumatic spring and high-pressure volume rises.

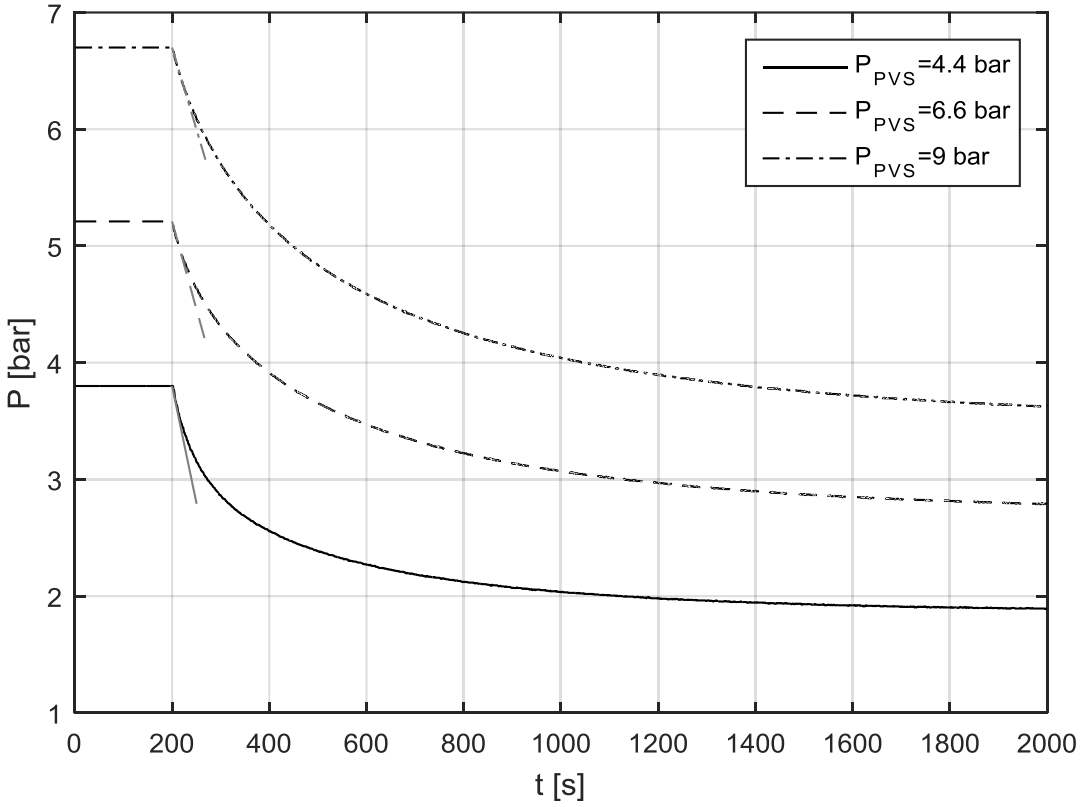

Figure 4-60: Time evolution of the pressure in the high-pressure volume during static leakage test

Chapter 5: Experimental investigation of a piston expander integrated into an ORC cycle

Contents

1. Introduction

The present chapter describes an experimental investigation conducted on a swash-plate piston expander, characterized by a total capacity of 195 cm³. The lubrication is ensured by an external oil loop with injection of oil at main friction points. This expander was tested over a wide range of operating conditions with R245fa as working fluid. First, the expander and the test bench are described and the ORC control strategy. Then, quality and validity of the measurements are assessed with the help of a statistical method and by checking energy balance over the expander. Afterwards, these measures are used to establish performance maps of the expander and to analyse the different sources of losses. Finally, the detailed model proposed in Chapter 3 is calibrated and used to disaggregate the influence of leakages and pressure drops on the efficiency.

2. Description of the test bench

2.1. Piston expander

The expander tested in this study is a prototype of swash-plate piston expander with five cylinders and characterized by a total swept volume of 195 cm³. The admission and exhaust processes are achieved by cam-less systems. The exhaust ports are located in the lower part of the cylinders and are piston-controlled (the piston cover and uncover the port). The supply port is located in the head of the cylinders and is actuated with a camless system (see Figure 5-1). These two systems induce symmetrical opening and closing compared to TDC and BDC. As the inlet port is on the head of the cylinder and exhaust port in the lower part, the expander is characterised as “uniflow”. Table 5-1 lists principles geometrical parameters values.

The lubrication of the expander is ensured by an external oil loop with injection of oil at mains frictions points (see Figure 5-1). The oil loop is composed of a tank, pump, and an oil cooler. This system allows for the lubricant to be cooled.

Finally, in order to dissipate the produced power, the shaft of the expander is connected, via a torque meter and tow elastics couplings, to an asynchronous generator. This generator is controlled by a four-quadrant variable frequency drive.

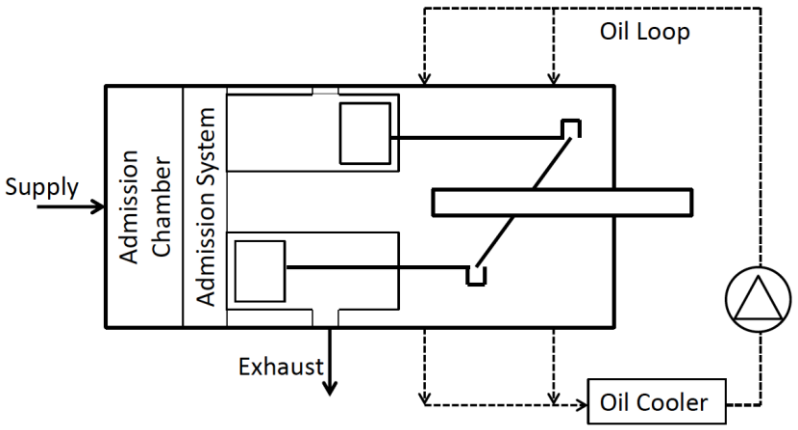

Figure 5-1: Schematic representation of the swash-plate piston expander

Table 5-1: Geometrical parameters of the piston expanders

Number of cylinders	5
Bore	40 [mm]
Stroke	31 [mm]

2.2. ORC set up

The piston expander is integrated into an ORC cycle test bench using R245fa described by Dickes et al. (2014). Figure 5-2 represents this ORC composed of a pump, a recuperator, a boiler, a condenser and a liquid tank. The boiler is fed with thermal oil heated by electrical resistances and the condenser is water-cooled. A by-pass line allows the evaporator to be heated and pressurized by bypassing the expander and the start of the expander by closing the line and opening the inlet of the expander.

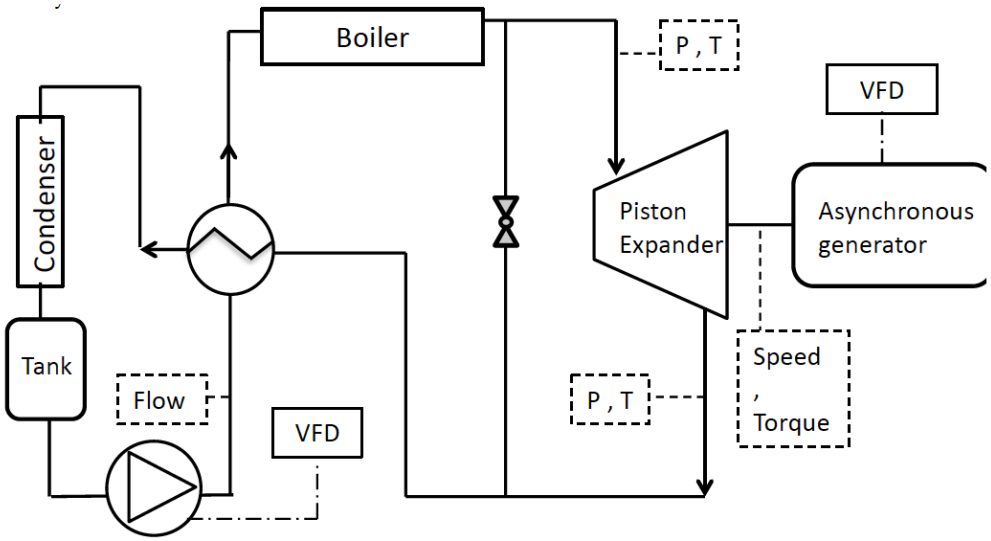

Figure 5-2: Schematic diagram of the ORC test bench

2.3. Measurement system

Several sensors are placed all over the ORC cycle and the expander set-up in order to measure the performance of the expander. The working fluid flow rate is measured at the pump outlet by a Coriolis-effect mass flow meter. The temperature and the pressure of the working fluid at the inlet and the outlet of each components of the ORC are measured with piezoresistive pressure sensors and thermocouples. Same types of sensors are also placed on the oil loop and water loop just as flow meters in order to compute heat power rejected by the lubricant. A torque measured by a torque sensor placed between the expander and the generator and the rotational speed given by the drive allow for the computation of the mechanical power. In addition of these measurements, the pressure in one of the cylinder is measured with the help of piezoelectric pressure sensor and the angular position of the shaft with a rotary encoder. This measurement system allows the indicator diagrams to be draw and therefore the computation of the indicated power and the mechanical efficiency. Finally, three contact thermocouples have been placed on the external surface of the expander in order to

assess the surface temperature (see Figure 5-3). Table 5-2 lists sensors locations, types, ranges and uncertainties.

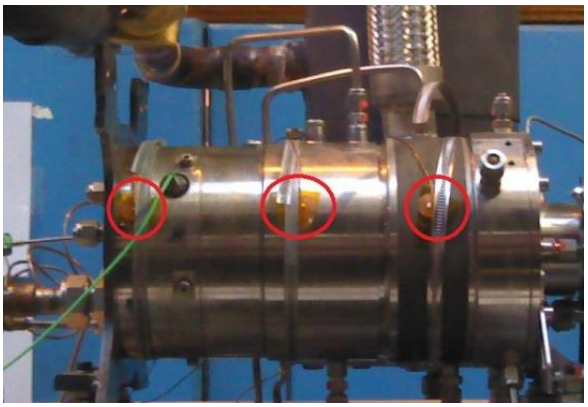

Figure 5-3: Contact thermocouples

Table 5-2: Sensors characteristics and location

Type	Range	Error
Class 2 K type thermocouple	-40 to 1200°C	[-40 to 333]:+-2.5°C; [333 to 1200 °C]: +-0.75 % *
Class 2 T type thermocouple	-40 to 350°C	[-40 to 133]:+-1°C; [133 to 350°C]: +-0.75 % *
Piezoresistive pressure sensor	0 to 16 bar	0.5 %
Piezoelectric pressure sensor	0 to 344 bar	1%
Strain gage torque meter	-20 to 20 Nm	1% FS
Coriolis flow working fluid flow meter	0 to 155 g/s	0.1 %
Epicycloid wheel oil flow meter	0.06 to 16 l/m	1.25%
Wheel counter water flow meter	/	2%

* EN60584 (Subcommittee 65B : Measurement and control devices 2013)

2.4. Control of the operating parameters

On the working fluid side, the system has four degrees of freedom:

- Rotational speed of the expander, controlled by the variable frequency drive of the asynchronous generator
- The mass flow rate of the working fluid and then of the supply pressure, controlled by the rotational speed of the pump
- The supply temperature and then the superheating, controlled by the electric oil boiler
- The exhaust pressure, controlled by throttling with a valve on the exhaust line

No particular problem was encountered with this control method to control the ORC system. The superheating was kept between 6 K and 15 K, the supply pressure between -1.2 % and +1.6 % of the set value and exhaust pressure between -2.1 % and +2.9 %.

3. Experimental results

The piston expander was tested in a wide range of operating conditions. Indeed, supply pressure varied from 18 to 30 bar, exhaust pressure varied from 2 to 3 bar and rotational speed from 1000 to 4000 RPM. A total of 65 steady-states points have been measured in these ranges. Figure 5-4 shows exhaust pressure in terms of supply pressure and pressure ratio in terms of rotational speed to illustrate the operating conditions.

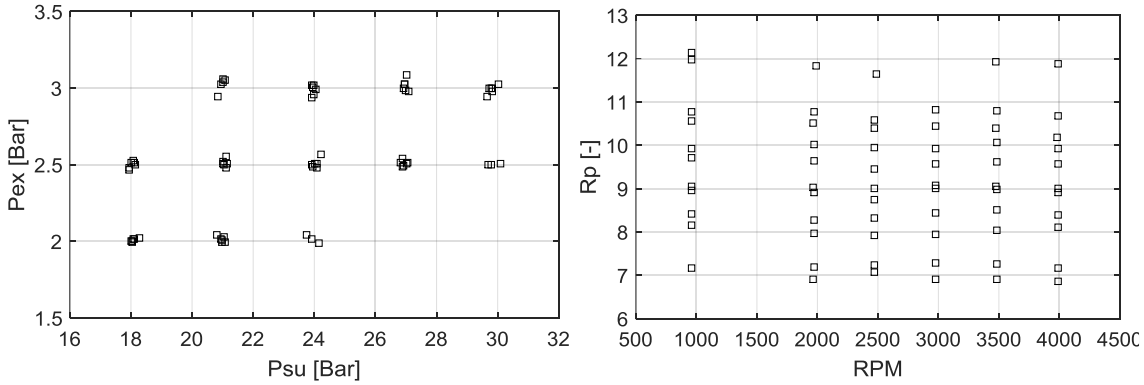

Figure 5-4: Range of operating conditions of the experimental campaign

3.1. Validity and quality of the results

In order to check the quality and validity of the results, two verifications are made. The first one is based on a Gaussian regression process allowing to check correlation between a dependent and some independents variables and the dispersion of the dependent variable. The second method consists in verifying if the measurements respect the energy balance over the expander.

3.1.1. Outliers detection

Same Gaussian regression process based method as used in Chapter 4 has been applied on indicated power, mechanical power, mass flow rate and isentropic efficiency. The results are summarized in Table 5-3. For the four outputs, the more relevant inputs are supply pressure, pressure ratio and rotational speed. These three inputs give low MARE showing the good correlation between inputs and outputs. An outlier is detected for indicated and mechanical power. Indeed, for this point the error is more than 1.96 time the standard deviation. Full results are presented in annex 8.1.

Table 5-3: Results of the Gaussian regression process

	$\dot{W}_{in}$	$\dot{W}_{m}$	$\dot{M}$	$\epsilon_{s,sh}$	FF
Inputs	P_{su}, R_p, RPM	P_{su}, R_p, RPM	P_{su}, R_p, RPM	P_{su}, R_p, RPM	P_{su}, R_p, RPM
MARE [%]	1.4534	1.0945	0.8383	3.5386	0.76
Outliers (P_{su}/ P_{ex}/RPM)	24/2.5/300	24/2.5/3000	/	/	/
Error/σ	3.059	2.0547	/	/	/

3.1.2. Uncertainties

As in Chapter 4, uncertainties on variables computed with measured values can be computed either with the propagation formula (equation (4-3)) or with the Monte-Carlo method (see section 5.1.2 of Chapter 4).

Table 5-4 lists the minimums, maximums and averages computed relative uncertainties on indicated and shaft power, shaft isentropic efficiency and filling factor. Average uncertainties for the four variables are under 3%.

Table 5-4: Minimum, maximum and average computed relative uncertainties

	$\dot{W}_{in}$	$\dot{W}_{m}$	$\epsilon_{s,sh}$	FF
Min	1.5%	0.1%	1%	1.6%
Max	5.3%	1.1%	1.6%	2.7%
Average	3%	0.4%	1.1%	2.2%

3.1.3. Energy balance

In steady-state regime, the energy balance over the system made up of the expander and the oil cooler expresses that the net enthalpy flow rate entering the system is equal to the total energy leaving the system:

$$\dot{H}_{in} = \dot{E}_{out} \quad (5\text{-}1)$$

$$\dot{M}_{wf}.\left(h_{su,exp} - h_{ex,exp}\right) = \dot{W}_m + \dot{Q}_{oil} + \dot{Q}_{amb} \quad (5\text{-}2)$$

where $\dot{Q}_{oil}$ is the thermal power evacuated by the lubricant oil and $\dot{Q}_{amb}$ the ambiance thermal losses. The thermal power evacuated by the oil can be computed with the oil volume flow rate and the difference between the temperature of the oil injected and temperature in the oil tank. For the ambient losses, the contact temperature can be exploited as in equation (5-4).

$$\dot{Q}_{oil} = \dot{V}_{oil}.\rho_{oil}.c_{p,oil}\left(T_{oil,inj} - T_{oil,tank}\right) \quad (5\text{-}3)$$

$$\dot{Q}_{amb} = AU_{amb}.\left(\frac{T_{c1}+T_{c2}+T_{c3}}{3} - T_{amb}\right) \quad (5\text{-}4)$$

The ambient heat transfer coefficient can be estimated with Nusselt number given by the Mc Adam correlation for a horizontal cylinder (Padet 2016):

$$Nu = 0.53.Ra^{0.25} \quad (5\text{-}5)$$

where Ra is the Rayleigh number. Thus, the AU_{amb} depends on the expander surface temperature. The average value is 0.9 W/K.

Figure 5-5 shows the discrepancy between the total outlet energy ($\dot{E}_{tot}$) and the net enthalpy flow rate ($\dot{H}_{in}$) with their respective uncertainties bars. The eight points represented by red square markers

indicate measurements for which the oil system was not in a steady state regime. It can been seen that, unless for the eight unsteady state measurement points, the energy balance is always in the uncertainty range confirming the consistency of the measurements.

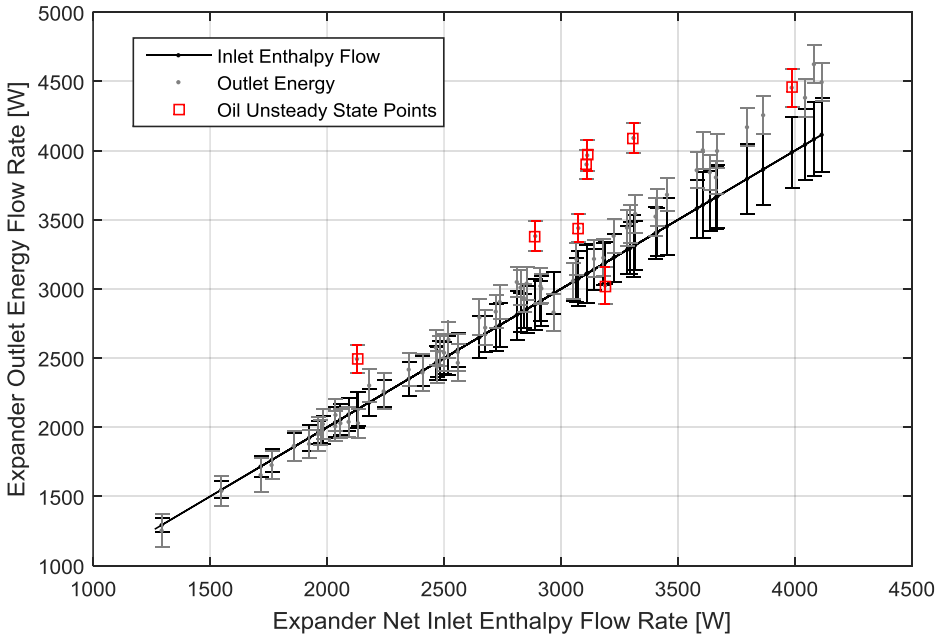

Figure 5-5: Expander energy balance: total outlet energy flow rate (sum of mechanical power, ambient heat losses and oil heat power) in terms of net inlet enthalpy flow rate with uncertainties bars (see equation (5-2))

In order to close the energy balance, the reconciliation method can be applied. This method consists in minimising, under some constraints, the weighted correction applied on the measurement. In order to perform the minimisation under constraint, the method of Lagrange multiplier is used. This leads to minimise the Lagrangian, sum of the weighted corrections and of the constraints equations multiplied by a Lagrange multipliers:

$$\alpha = \sum_{i=1}^{n} \frac{(u_i - c_i)^2}{\sigma_i^2} + \sum_{j=1}^{n} \lambda_j \psi_j \qquad (5\text{-}6)$$

where i is the points number, u_i are the measured values, c_i the corrected values, σ_i is the standard deviation of the measure i.e the error of the corresponding sensor, λ_j are the Lagrange multipliers and $\psi_j = 0$ are the constraints. In order to check the confidences of the corrected values, the weigh is evaluated:

$$w_i = \frac{|u_i - c_i|}{\sigma_i} \qquad (5\text{-}7)$$

Here, the two available constraints are the energy balances over the expander (equation (**5-2**)) and over the oil cooler. By neglecting the ambient heat loss of the oil cooler, the energy balance over the exchange can be written as follow:

$$\dot{V}_{oil} \cdot \rho_{oil} \cdot cp_{oil}\left(T_{oil,inj} - T_{oil,tank}\right) = \dot{M}_w \cdot cp_w (T_{w,ex} - T_{w,su}) \qquad (5\text{-}8)$$

Figure 5-6 shows the weight of each corrected variables. On this figure, the eight points for which the oil system was not in steady state mode are not plotted. It can be observed that the temperatures of the working fluid, oil and water are the ones the most affected by corrections. However, these corrections of the temperatures are below 1.5K which is pretty low.

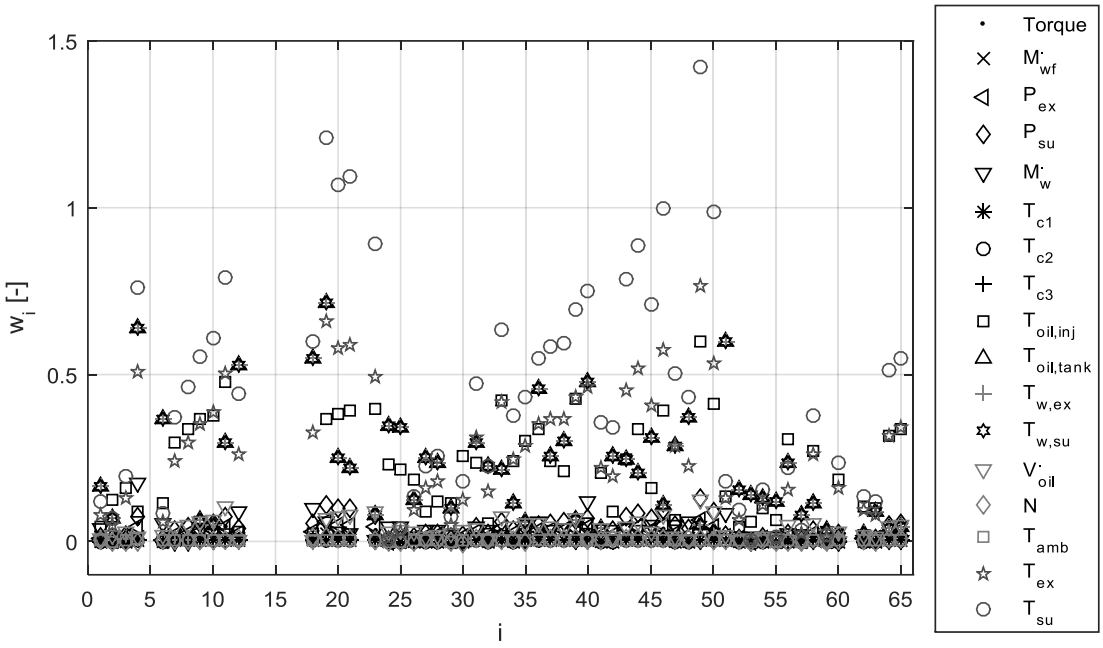

Figure 5-6: Weights of corrected variable for the 65 points

Figure 5-7 shows the discrepancy between the corrected and measured values of isentropic efficiency, filling factor and mechanical power. The discrepancy is very low, showing that correction of energy balance does not affect these performances parameters.

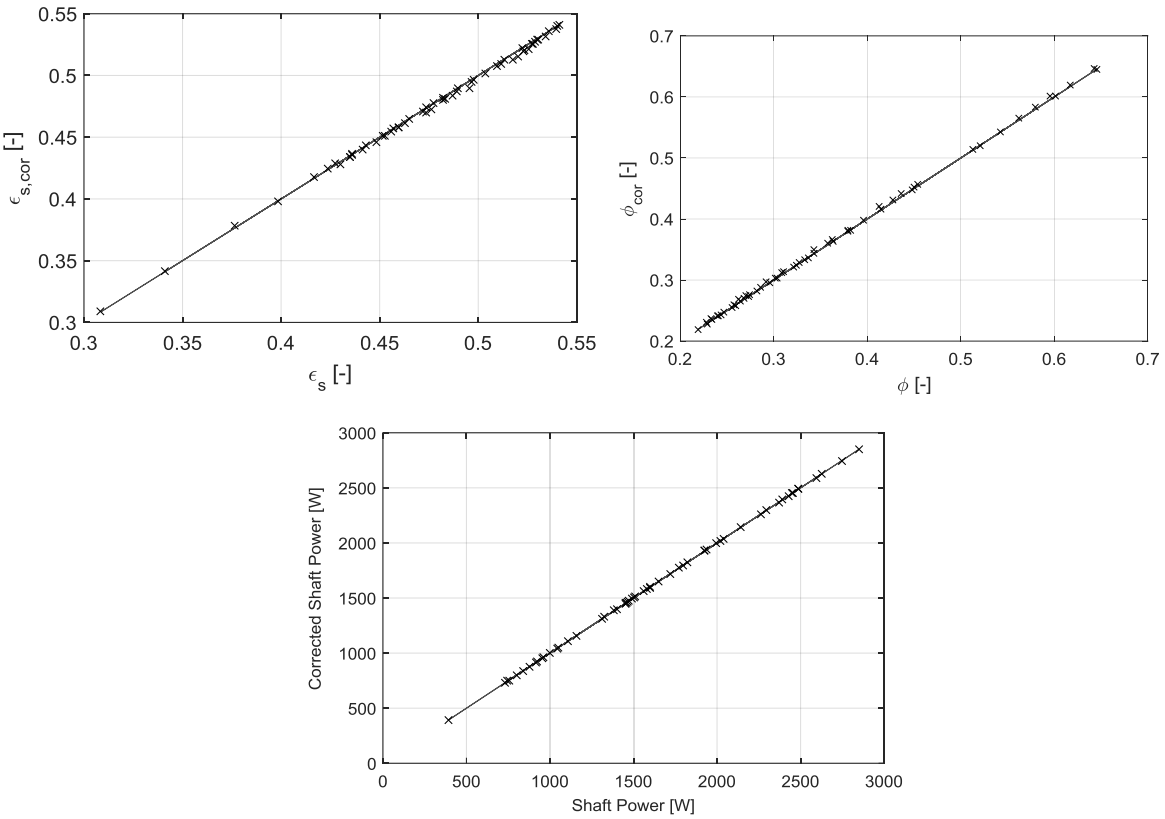

Figure 5-7: Corrected isentropic efficiency, filling factor and shaft power

In conclusion, the energy balance over the expander is correct considering sensors uncertainties. The reconciliation method allows to close the energy balance by correcting the variables that influence the most this balance, i.e. the temperatures of the working fluid, of the oil and of the water. However these corrections do not affect results linked to the performance of the expander.

3.2. Performance maps

The three next figures show maps of mechanical power and isentropic efficiency. On these map, the hatched area represent the operating conditions which had not been investigated.

It can be observed that mechanical power increases with the pressure ratio and that there is an optimal value of rotational speed around 3000 RPM that maximizes the mechanical power. This optimum is explained by the increase in the mechanical losses at high rotational speed. The comparison of the three maps shows that, for a same pressure ratio, the mechanical power is higher for higher levels of pressures. Over the 65 points, the power varies between 392 W (for $P_{su} = 18$ bar, $P_{ex} = 2.5$ bar and RPM=1000) and 2847 W (for $P_{su} = 30$ bar, $P_{ex} = 2.5$ bar and RPM=2000).

The isentropic efficiency increases until a pressure ratio around 9 and then seems to stabilize at a value between 52% and 54% depending of exhaust pressure. As for mechanical power, there is an optimal rotational speed that maximizes the isentropic efficiency. This optimal rotational speed is between 2000 RPM and 2500 RPM. Over the 65 points, the isentropic efficiency varies from 30.85 % (for $P_{su} = 18$ bar, $P_{ex} = 2.5$ bar and RPM=4000) to 54.12 % (for $P_{su} = 18$ bar, $P_{ex} = 2$ bar and RPM=2000).

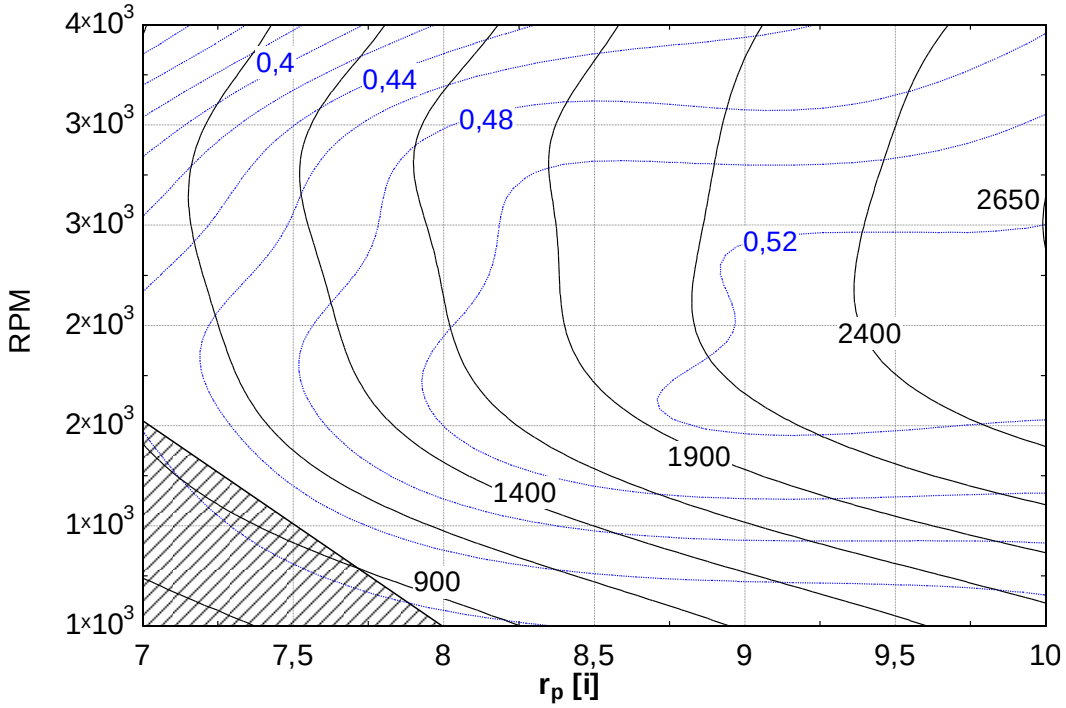

Figure 5-8: Mechanical power and isentropic efficiency map for Pex=3 bar (power in [W])

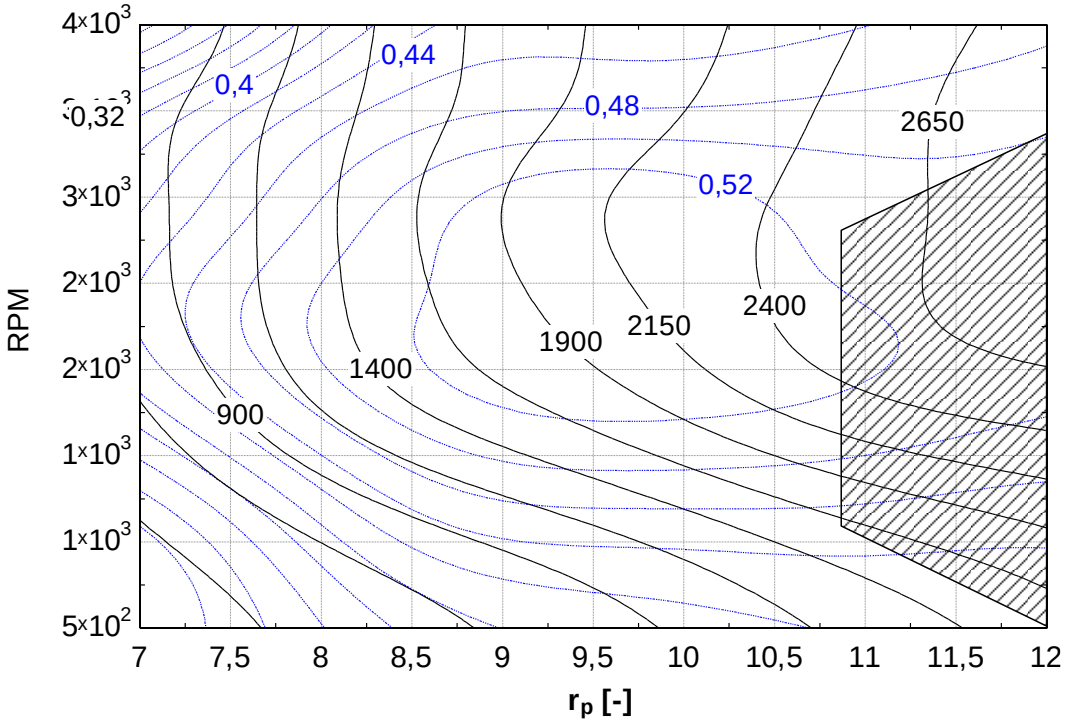

Figure 5-9 Mechanical power and isentropic efficiency map for Pex=2.5 bar (power in [W])

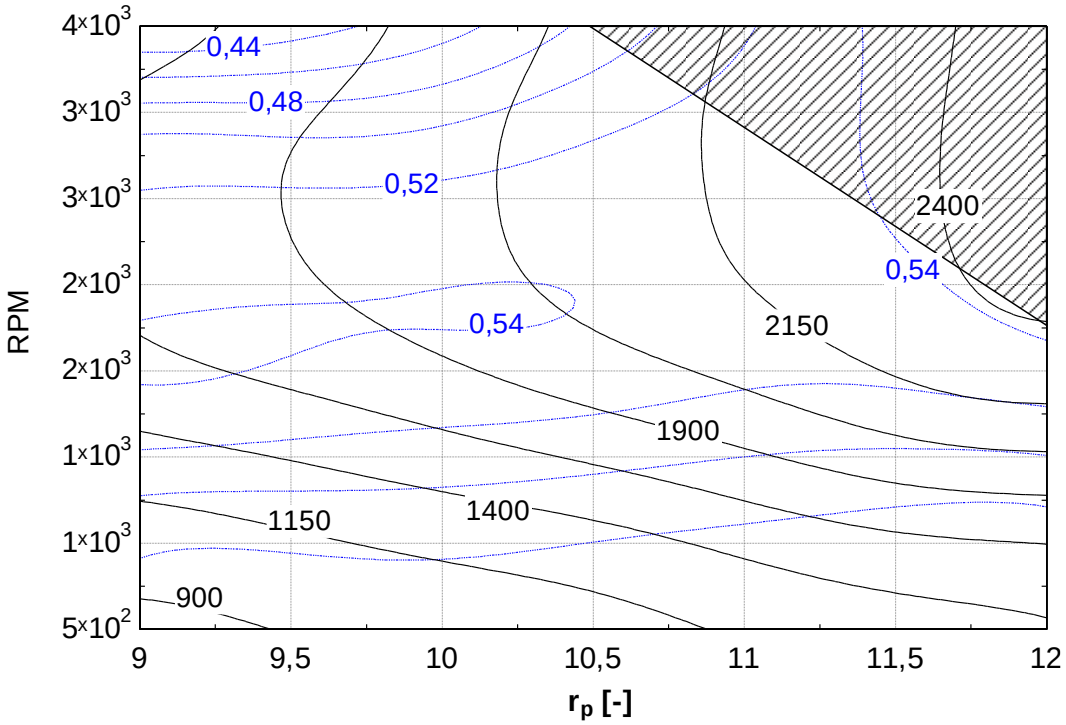

Figure 5-10: Mechanical power and isentropic efficiency map for Pex=2 bar (power in [W])

3.3. Measurements-based losses analysis

As shown in Chapter 2, different kinds of losses affect the isentropic efficiency and it is possible to split the latter in order to disaggregate the effect of each of the losses. Figure 5-11, Figure 5-12, Figure 5-13 and Figure 5-14 illustrate the disaggregation of the isentropic efficiency of the tested expander.

Starting with a full isentropic process, under-expansion and compression affect the isentropic efficiency of the theoretical cycle. It can be seen on Figure 5-11 that under-expansion and compression losses limit the isentropic efficiency at values between 70% and 90% and, as expected, increase with pressure ratio.

Then, pressure drops and heat transfer tend to decrease the indicated power compared to the theoretical power. The ratio between the actual and the theoretical indicated power (diagram factor) is shown in Figure 5-12. This ratio varies from 0.35 to 0.8 and decreases with the rotational speed because of the increase in the pressure drops with the speed. Effect of speed and pressure ratio on pressure drop and then on indicator diagram is well illustrated in next section (Figure 5-17 and Figure 5-18).

Figure 5-13 shows the evolution of the filling factor with the pressure ratio. It can be seen that the filling factor decreases with the speed. This decrease is due to the increases of the pressure drop and the decreases of the impact of the leakages. Indeed the leakages flow rates stay quite constant with the speed and then have more impact at low rotational speed as the mass flow rate displaced by the expander is lower to. As already mentioned in Chapter 2, a reduction of the filling factor leads to an increase in the isentropic efficiency by decreasing the reference mass flow rate. This is why indicated isentropic efficiency rises with the speed despite of the decrease of the diagram factor. Filling factor also decreases with pressure ratio, increasing the indicated isentropic efficiency for low pressure ratio. Indeed, Figure 5-11 shows that difference between theoretical and indicated isentropic efficiency is

larger at low pressure ratio. As explained in Chapter 2, filling factor depends on two antagonist effects: pressure drops and leakages tend to respectively decrease and increase the filling factor. These effects cannot be analysed with the measurement but will be analysed with the model.

Finally, mechanical losses affect the shaft power. It can be seen that mechanical efficiency decreases with the rotational speed (see Figure 5-14), counterbalancing the effect of the leakages. These two opposite effects on the isentropic efficiency lead the optimal rotational speed around 2000-2500 RPM observed in the previous section(see Figure 5-8, Figure 5-9 and Figure 5-10). It can be seen in Figure 5-11 that isentropic efficiency decreases for low pressure ratio. Indeed, when pressure ratio decreases, indicated power also decreases but constant mechanical losses remain present, leading to a decrease of the mechanical efficiency (see Figure 5-14). As shown in Figure 5-14, mechanical efficiency varies from 40 % to 90 %.

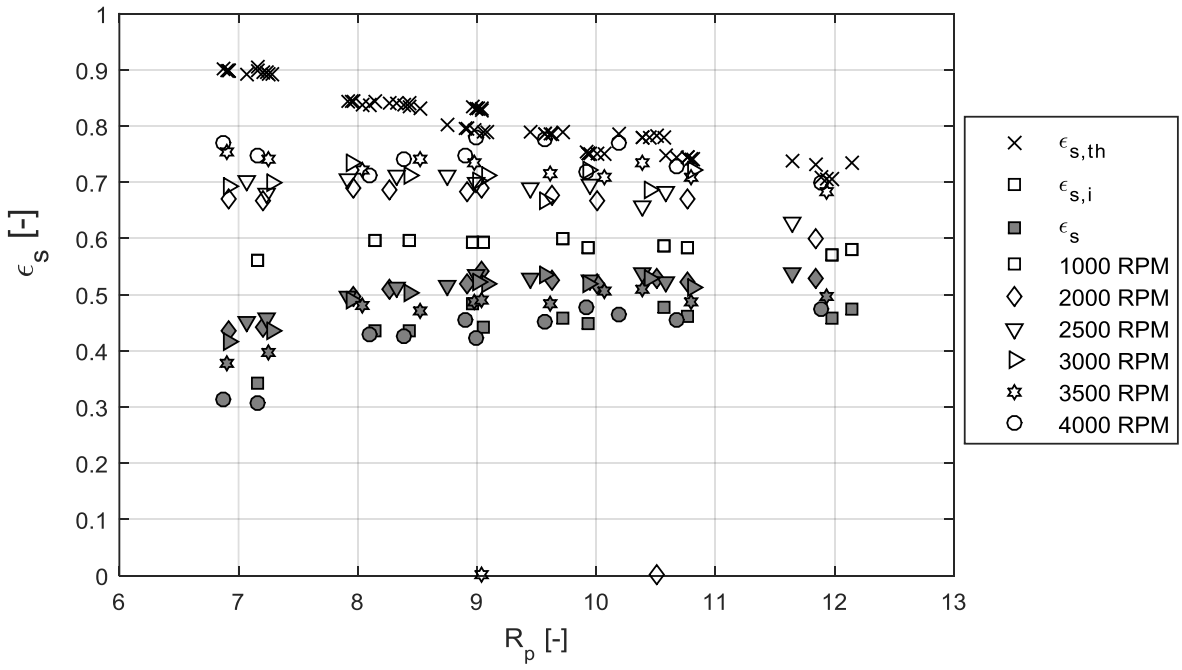

Figure 5-11: Isentropic efficiency disaggregation in term of pressure ratio

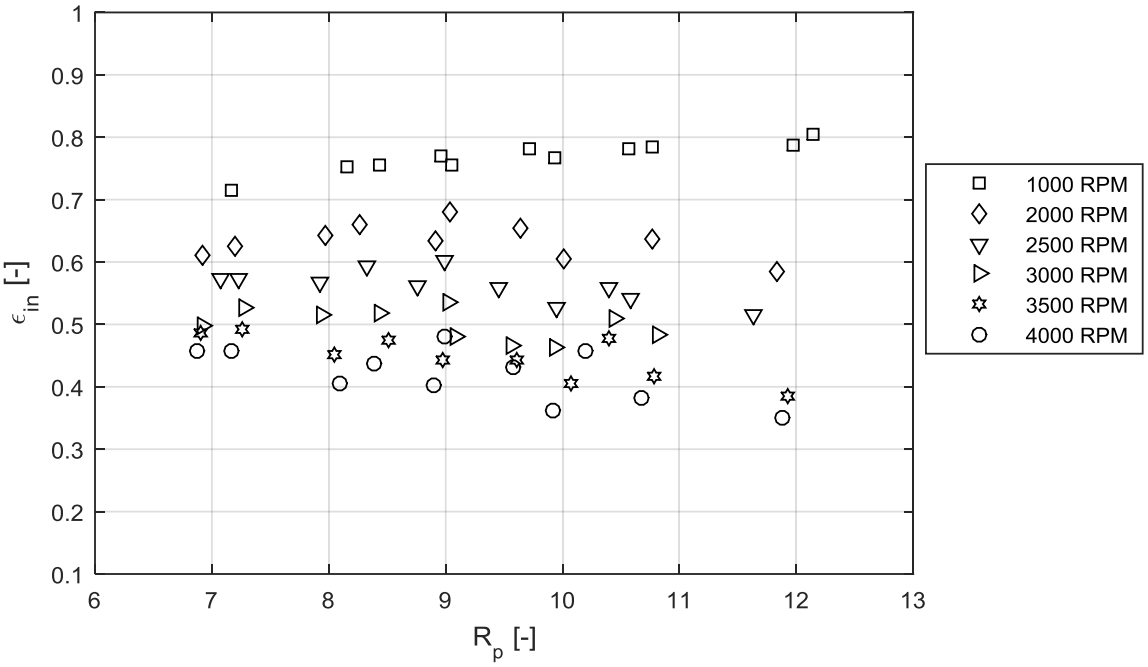

Figure 5-12: Diagram factor in term of pressure ratio

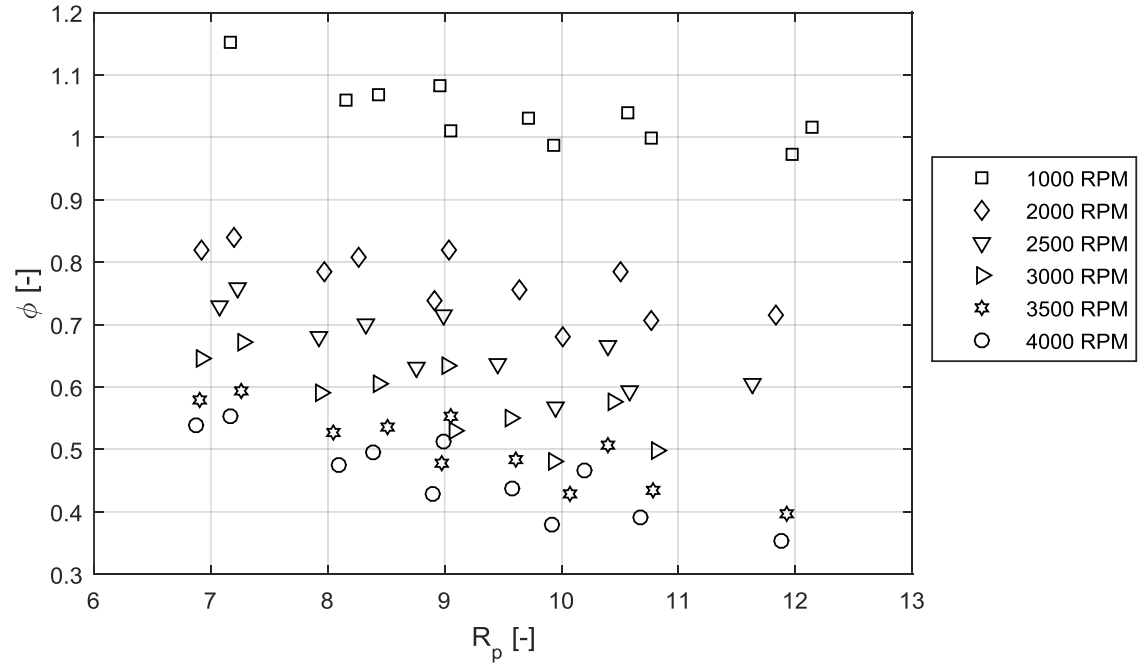

Figure 5-13: Filling Factor in term of pressure ratio

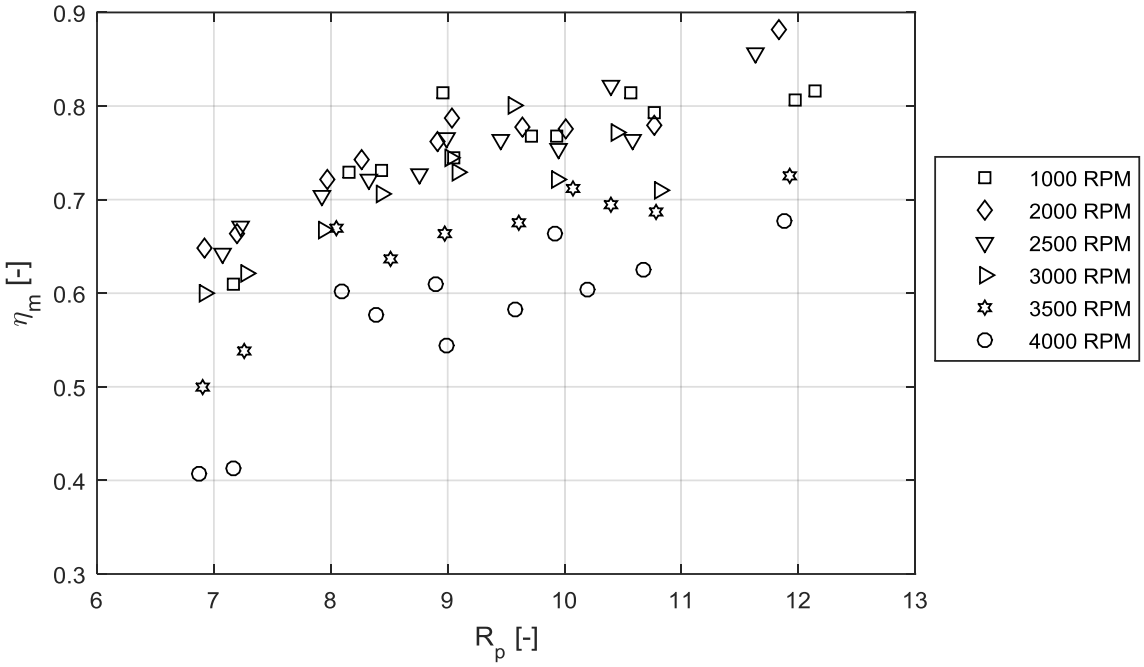

Figure 5-14: Mechanical efficiency in term of pressure ratio

3.4. Mechanical losses

As the indicated and shaft powers are both known, the mechanical friction work and power can be computed. Figure 5-15 and Figure 5-16 show the evolution of these two values in terms of rotational speed and supply pressure. It can be seen that, as for the expander investigated in Chapter 4, the mechanical friction work can increase when the rotational speed decreases. This leads to the conclusion that boundary lubrication regime is encountered, especially at low rotational speed. Moreover, it seems that the mechanical friction work is better correlated to the supply pressure (and then the load) but still scattered. This boundary regime can be explained by not appropriate oil characteristics, which are influenced by the temperature and the amount of diluted working fluid.

As in Chapter 4, it can be observed that mechanical friction power is (unlike the work) well correlated to the rotational speed. However, supply pressure seems to have a significant impact. Then, a correlation including the rotational speed and the supply pressure is proposed:

$$\dot{W}_{mf} = 0.0646\, N^2 + 0.552\, N.P_{su} \qquad (5\text{-}9)$$

where $\dot{W}_{mf}$ is the mechanical friction power in [W], N is the rotational speed in [Hz] and P_{su} is the supply pressure in [bar]. The first term accounts for the hydrodynamic friction while the second one stands for the boundary friction. This correlation predicts the mechanical friction power with a coefficient of determination of 89%. The corresponding $fmep$ is:

$$fmep = 5.5\ 10^{-5}\, RPM + 0.0283\, P_{su} \qquad (5\text{-}10)$$

whith $fmep$ and P_{su} in bar.

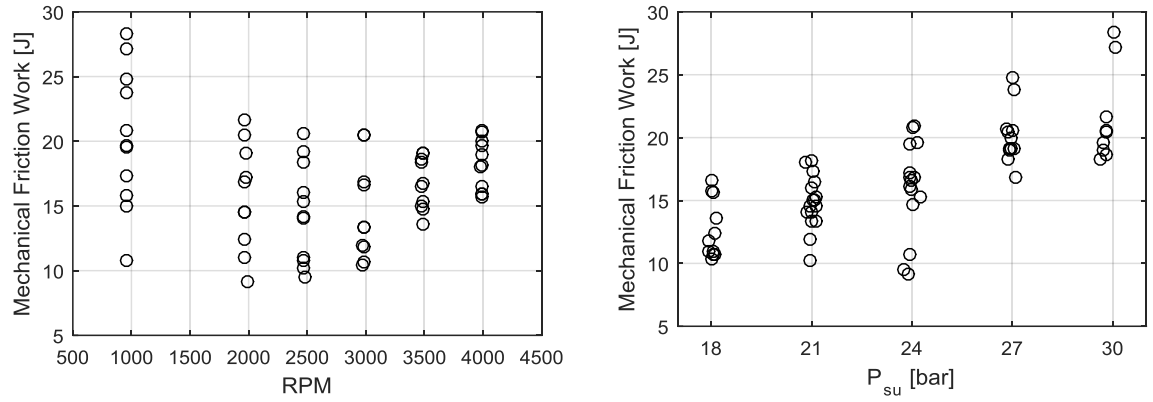

Figure 5-15: Evolution of mechanical friction work in terms of rotational speed (left) and supply pressure (right)

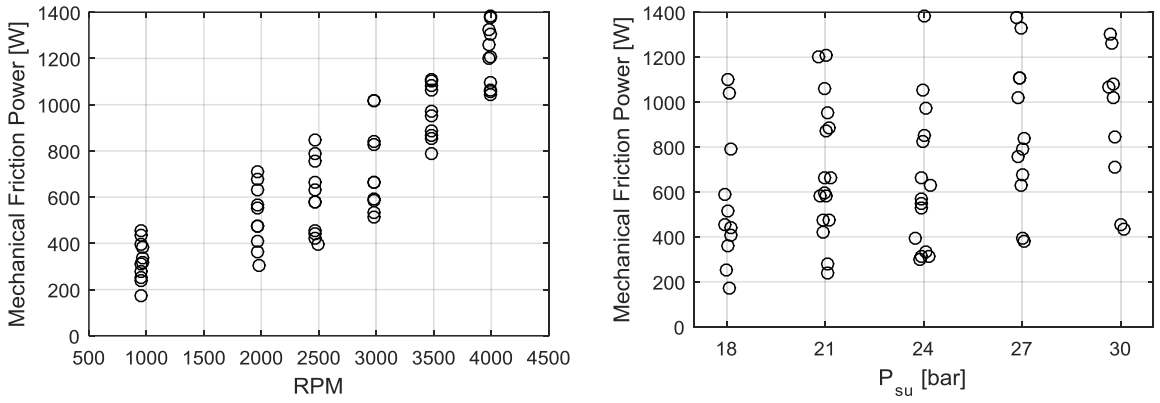

Figure 5-16: Evolution of mechanical friction power in terms of rotational speed (left) and supply pressure (right)

3.5. Indicator diagram

As mentioned in section 2.3. , in-cylinder pressure sensors allowed the measurement of the in-cylinder pressure and then, to draw indicator diagrams and compute indicated work and power. The indicated work and power was used in previous section to split the losses and compute mechanical efficiency. Over the 65 points, the indicated work of one cylinder varies from 5.3 W (for Psu=18 abr, Pex=2.5 and RPM=4000) to 27.97 W (for Psu=30 bar, Pex=2.5 bar and RPM=1000).

Figure 5-17 and Figure 5-18 show indicators diagrams for different operating conditions.

Figure 5-17 shows the effect of the rotational speed on indicator diagram for a supply pressure of 24 bar and an exhaust pressure of 2.5 bar. It can be seen that indicator diagram is pretty close to the theoretical one for 1000 RPM (ϵ_{in}between 70 % and 80 % depending on pressure ratio). Supply pressure drops are the most important losses and increase significantly with the speed. In-cylinder pressure at inlet closing volume (red circles) passes from 22 bar to 17 bar for rotational speed increasing from 1000 RPM to 4000 RPM and ϵ_{in} goes down from 78% to 43%. Exhaust pressure drops are less significant but induce a compression process at slightly higher pressure that the theoretical one. Finally early opening of supply/exhaust ports induces an early rise/fall of pressure before piston reach TDC/BDC.

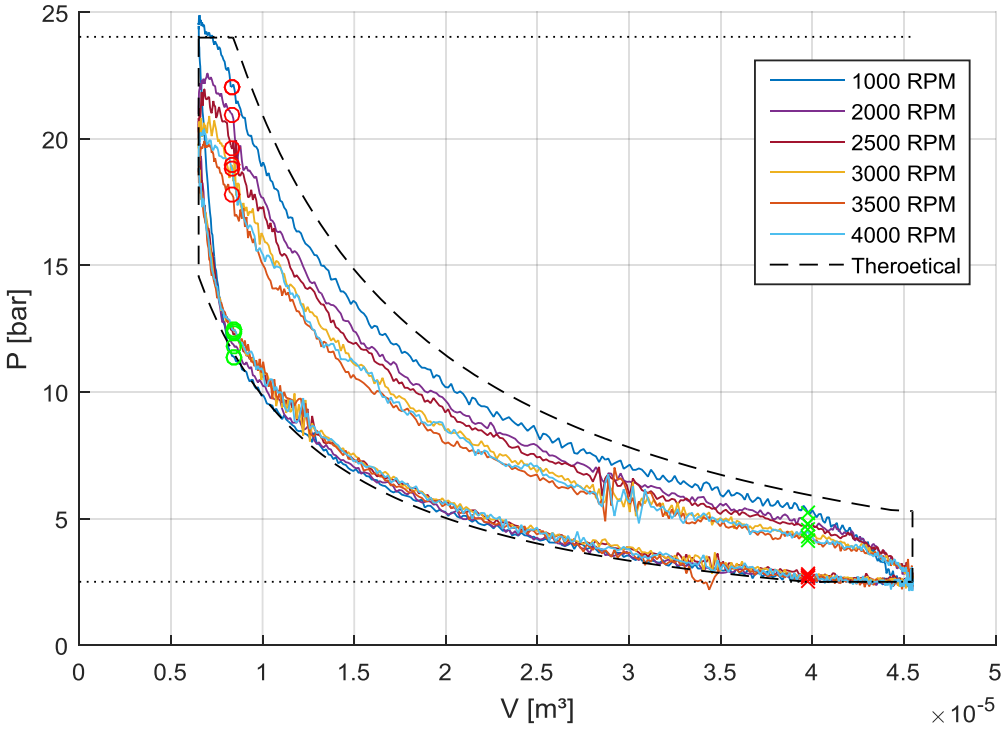

Figure 5-17: Indicator diagrams for Psu=24 bar, Pex=2.5 bar and different rotational speeds. Opening and closing volume are respectively represented in green and red

Figure 5-18 shows the effect of pressure ratio. It can be seen that supply pressure drops also increase with pressure ratio. Ratio between in-cylinder pressure at inlet closing volume (red circles) and supply pressure passes from 0.87 to 0.77 for pressure ratio increasing from 7.2 to 10.8. This increase in supply drops causes ϵ_{in} to decrease from 57 % to 54 %.

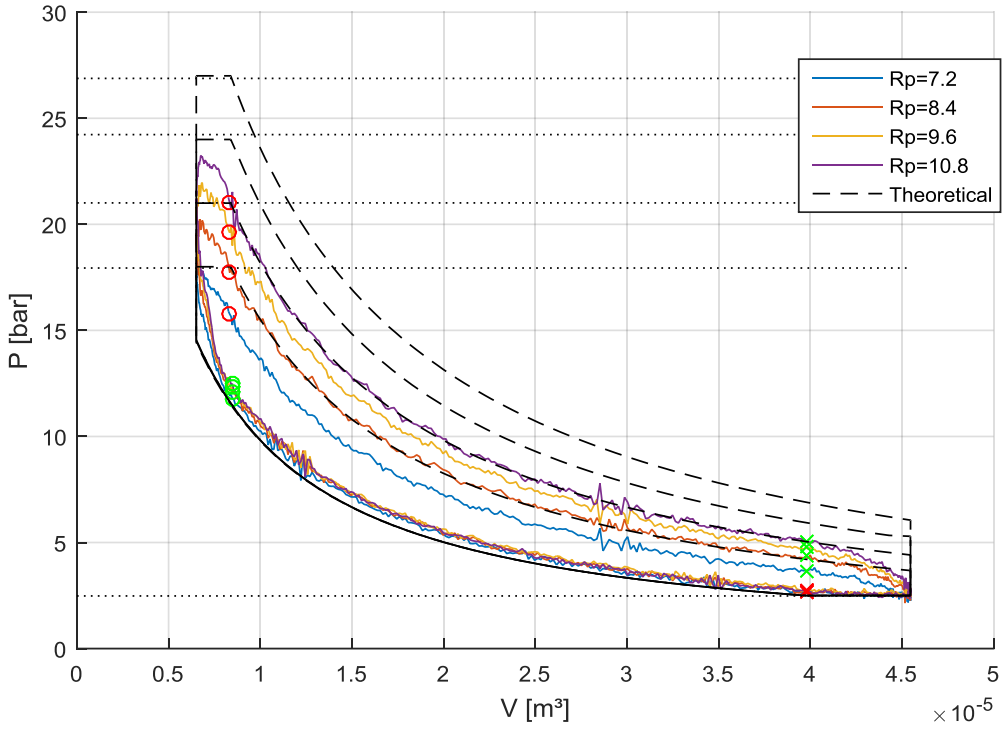

Figure 5-18: Indicator diagrams for Pex=2.5, RPM=2500 and different pressure ratios. Opening and closing volumes are respectively represented in green and red

4. Detailed model validation and analysis

In this section, the detailed model proposed in Chapter 3 is used to represent the tested expander. First, the geometrical parameters have to be described. Then, calibration parameters are adjusted to get the best fit between measurements and model outputs. Finally, once the model is validated, it is used to analyse the losses in more detail.

4.1. Geometrical parameters

The geometrical parameters that have to be defined are the evolution of the volume and surface area of the cylinder and the cross sectional areas of the supply and exhaust ports in term of shaft angle.

Evolution of the volume and the surface area are given by equations (3-1) and (3-4) given in Chapter 3. And all geometrical data needed are given in Table 5-1.

Cross sectional areas of supply and exhaust ports can be deduced from their geometrical dimensions and (due to the “piston controlled” opening and closing nature of the ports) from the kinematic motion of the piston. The evolutions of these two sections are given in Figure 5-19.

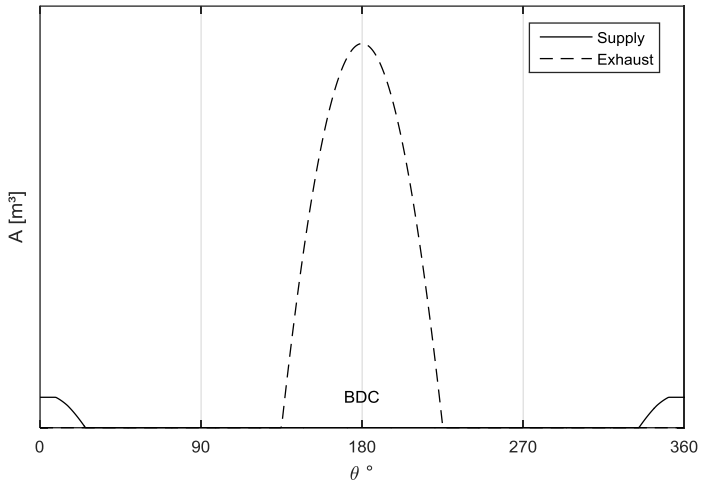

Figure 5-19: Cross sectional area of supply and exhaust port in term of shaft angle

4.2. Calibration process

Figure 5-20, Figure 5-21 and Figure 5-24 show respectively difference between some measured and simulated indicator diagrams and indicated power. Without calibration, indicator diagrams show that the model underestimates pressure drop and then overestimates the indicated power. In the calibration process, flow coefficients are set to 0.82 for the supply port and 0.6 for exhaust ports in order to obtain a good fit between measured and simulated pressure curves. With these values of flow coefficient, the model is able to predict with a good agreement the indicated power (see Figure 5-22). The mechanical losses are computed with equation (5-9) which allows for the determination of the shaft power as shown in Figure 5-23. With these values of flow coefficients, Figure 5-24 shows that mass flow rate is underestimated showing that leakages have to be added. Then, the lumped leakage cross section area is increased until the simulated mass flow rate fits with the measurement. Finally, the ambient heat loss coefficient is increased to obtain better prediction of the exhaust temperature. Table 5-5 lists the calibrated parameters.

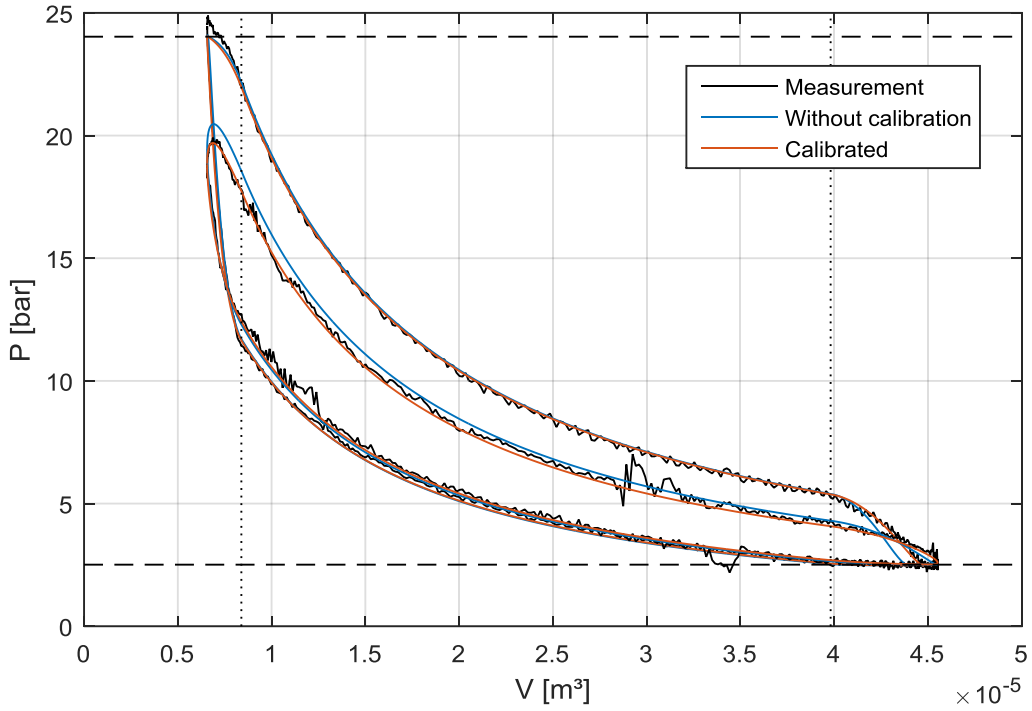

Figure 5-20: Comparison between measured and simulated indicator diagram for Pex=2.5 bar, Psu=24 bar and RPM=1000/4000 (detailed model)

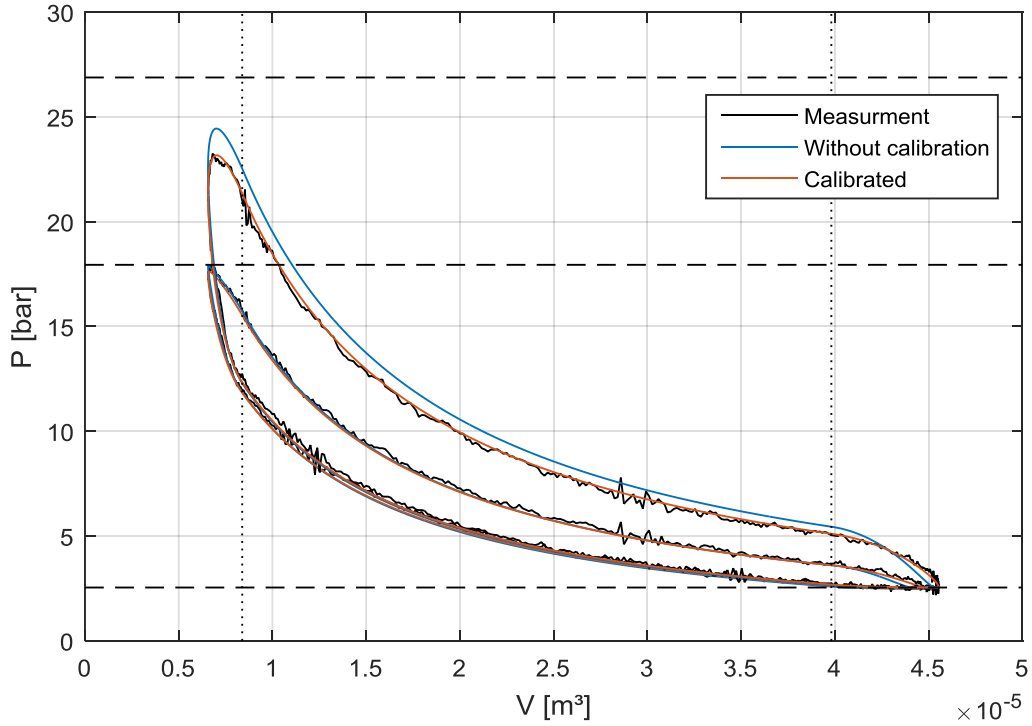

Figure 5-21: Comparison between measured and simulated indicator diagram for Pex=2.5 bar, Psu=18/27 bar and RPM=2500 (detailed model)

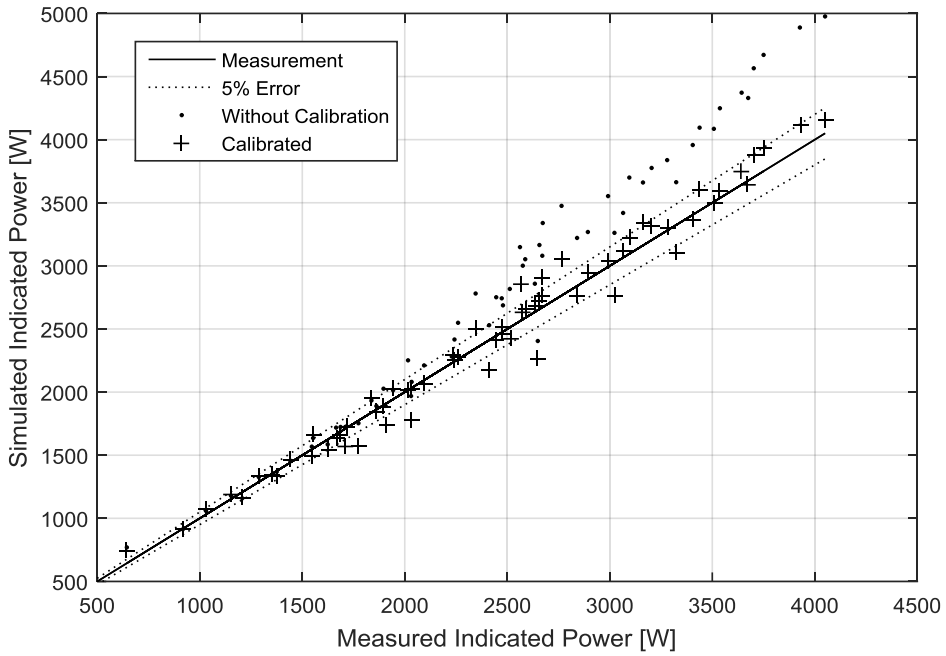

Figure 5-22: Comparison between measured and simulated indicated power (detailed model)

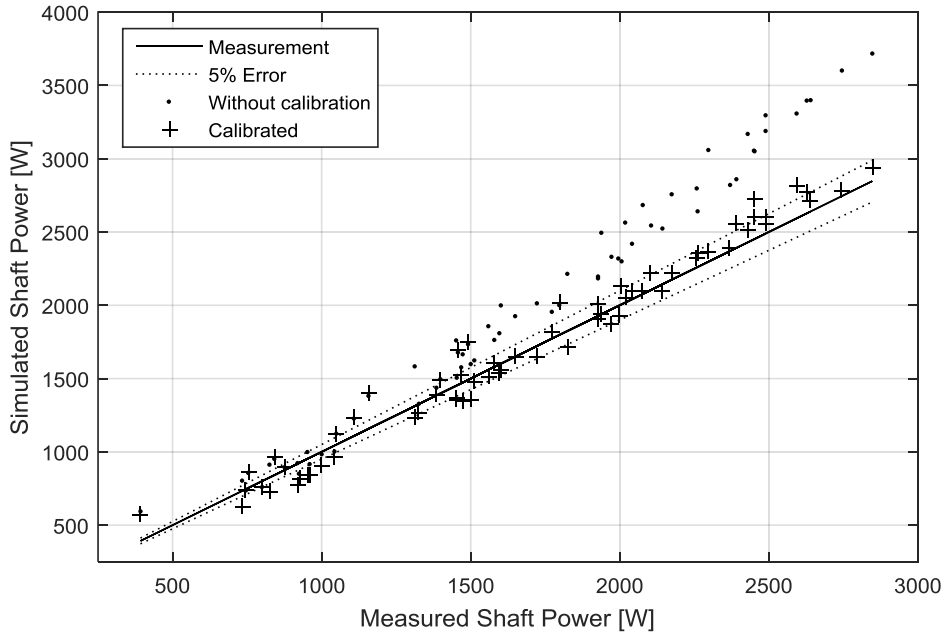

Figure 5-23: Comparison between measured and simulated shaft power (detailed model)

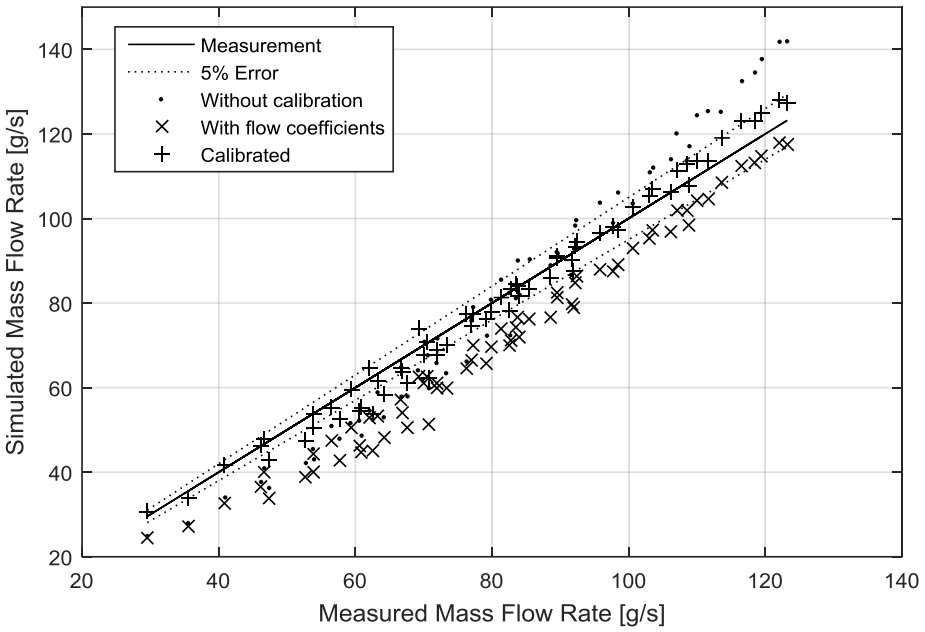

Figure 5-24: Comparison between measured and simulated mass flow rate (detailed model)

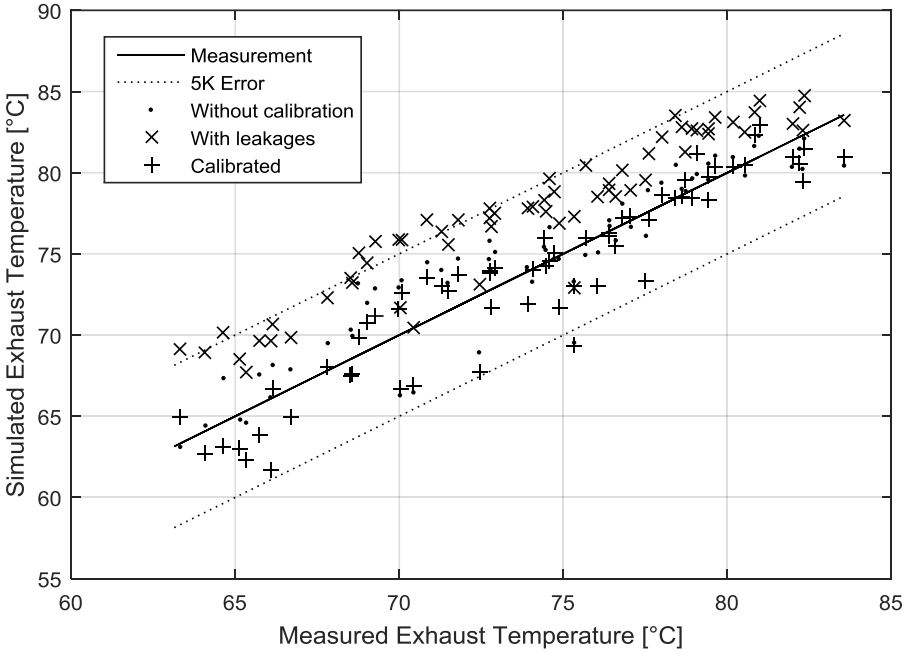

Figure 5-25: Comparison between measured and simulated exhaust temperature (detailed model)

Table 5-5: Calibrated parameters of the detailed model

$C_{d,su}$ [-]	$C_{d,ex}$ [-]	$A_{leak}[mm^2]$	AU_{amb} $[W/K]$
0.82	0.6	0.15	3

4.3. Model based losses analyses

The model allows for the simulation of the effect of the pressure drops and the leakages separately and then to finish the decomposition of the losses presented in section 4.3. Figure 5-26 shows the leakage, internal and filling factor in term of rotational speed. It can be seen that pressure drop has the bigger influence on the decrease of the filling factor with the speed. As expected, leakages tend to increase the filling factor (value>1) while pressure drops tend to decrease it.

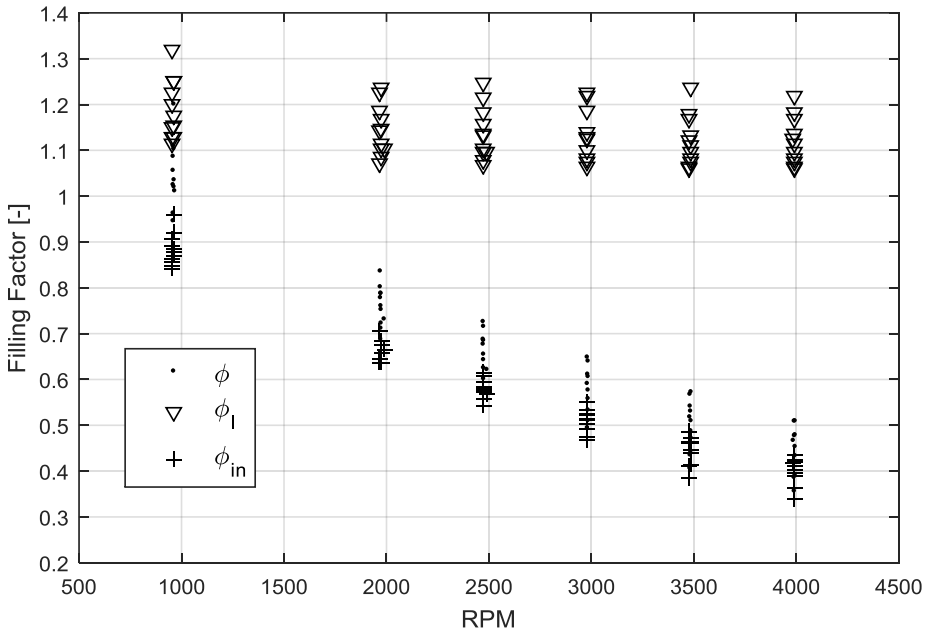

Figure 5-26: Filling Factor detachment in term of rotational speed

Figure 5-27 shows the evolution of the diagram and specific diagram factors in terms of the rotational speed. This plot shows that $\epsilon_{sp,in}$ slightly increases with the speed, showing that pressure drops affect relatively more the mass flow rate than the internal power. The value of $\epsilon_{sp,in}$ is close to one (0.86-1.06), meaning that pressure drop does not affect so much the isentropic efficiency and can even slightly increase it (when $\epsilon_{sp,in} > 1$) by reducing the reference mass flow rate. However, pressure drops affect the compactness of the expander by decreasing the power for a given cylinder volume.

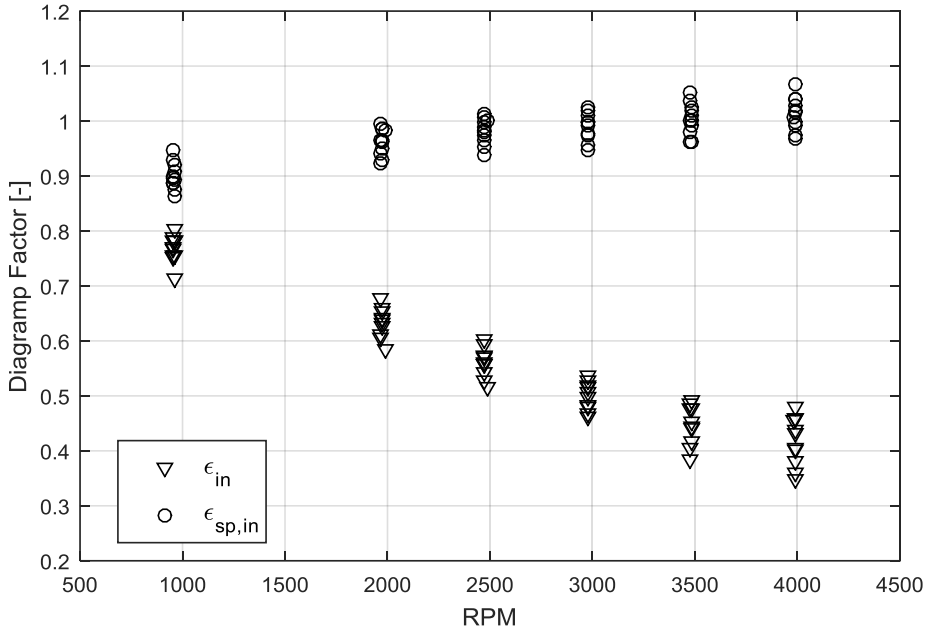

Figure 5-27: Diagram and specific diagram factor in terms of rotational speed

5. Semi-empirical model validation

Once again, the validation process is applied to calibrate the semi-empirical model with the measurement:

- Increase pressure drops (decrease supply and exhaust fictive nozzles areas A_{su} and A_{ex}) until indicated work is well predicted
- Add leakages (increase leakage fictive nozzle area A_{leak}) in order to increase the simulated mass flow rate until an agreement with the measurements is found
- Add heat transfers (increase the supply and exhaust overall heat transfer coefficients AU_{su} and AU_{ex}) until simulated exhaust temperature match with the measurements

Table 5-6 lists the calibrated parameters found with the procedure and the simulation results are compared to the measurement in Figure 5-28, Figure 5-29 and Figure 5-30. These figures show that, despite its simplicity, the semi-empirical model gives very good fit between computed and measured values.

Table 5-6: Calibrated parameters of the semi empirical model

A_{su} $[mm^2]$	A_{ex} $[mm^2]$	$A_{leak}[mm^2]$	AU_{su} $[W/K]$	AU_{ex} $[W/K]$	AU_{amb} $[W/K]$
2	78	0.23	1	2	3

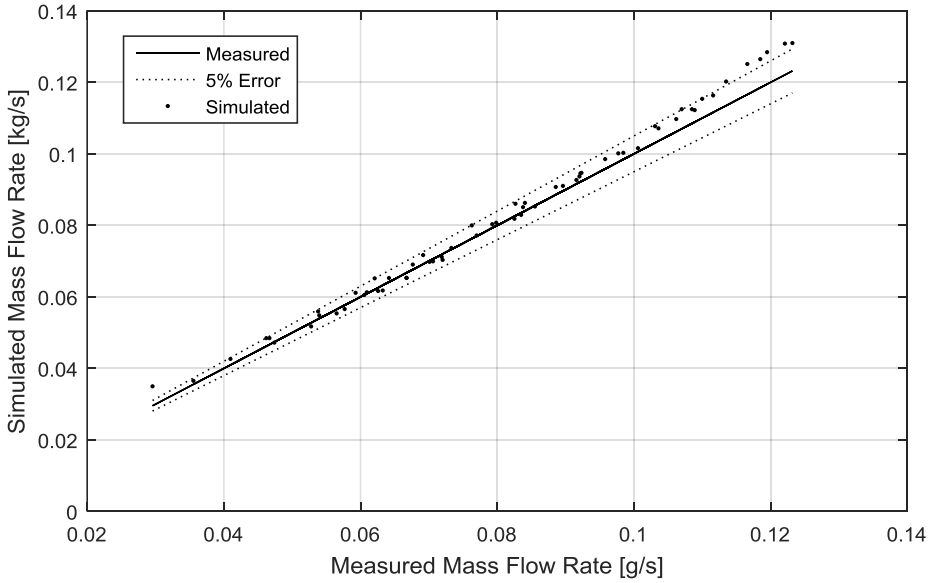

Figure 5-28: Comparison between measured and simulated mass flow rates (semi-empirical model)

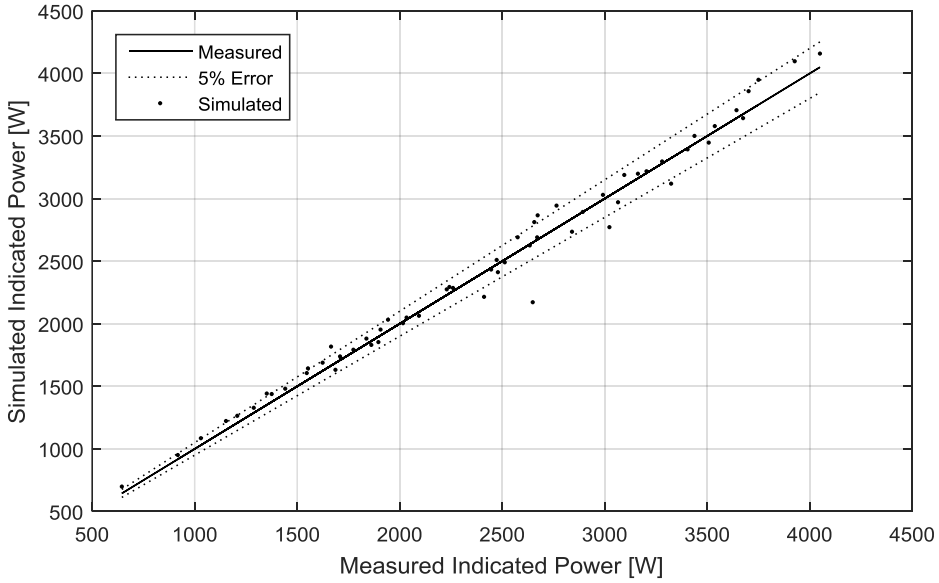

Figure 5-29: Comparison between measured and simulated indicated powers (semi-empirical model)

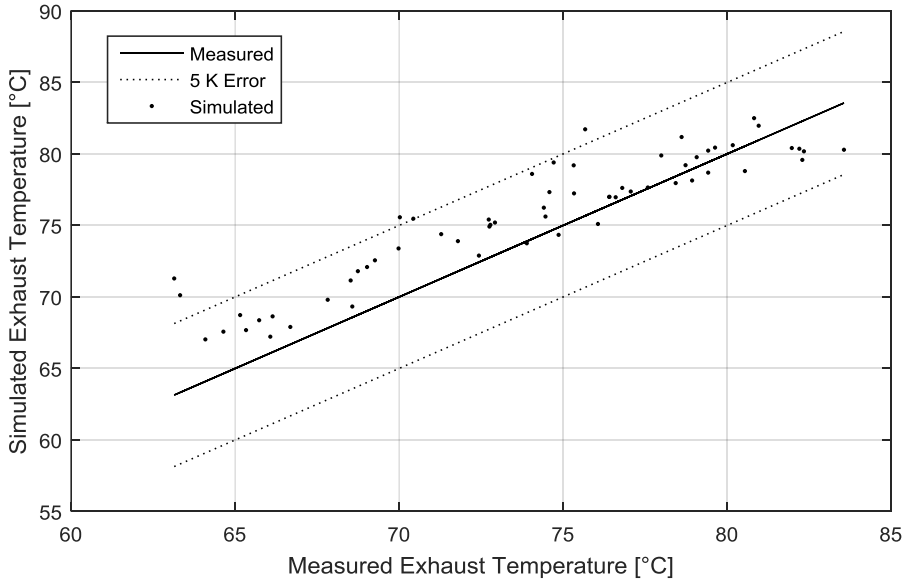

Figure 5-30: Comparison between measured and simulated exhaust temperatures (semi-empirical model)

6. Conclusions

A 195 cm³, five cylinders, swash-plate piston expander was successfully tested in an ORC using R245fa as working fluid. It was tested for rotational speed of 1000 RPM to 4000 RPM and pressure ratio varying between 7 and 12. A total of 65 steady state points was measured and the quality of the measurement was assessed in order to show their relevance. With these measurement, performances maps were generated to show influence of rotational speed and levels of pressure on mechanical power and isentropic efficiency. These maps highlighted the existence of an optimal rotational speed around 3000 RPM maximising the mechanical power but that the speed that maximises the isentropic efficiency is between 2000 and 2500 RPM. Maximal achieved mechanical power was 2.8 kW and maximal isentropic efficiency was 53%.

Then the measurements was used to analyse the losses. This analyse shows that under expansion and compression limit the theoretical isentropic efficiency at values comprise between 90% and 70% for pressure ratio of 7 to 12. Then, filling factor affect the isentropic efficiency for low rotational speed and low pressure ratio. Indeed, indicated isentropic efficiency is around 60% for 1000 RPM and around 75% for 4000 RPM. These values stay quite constant with pressure ratio. Finally, a mechanical efficiency comprised between 40% and 90% was observed which lowers the isentropic efficiency to values comprise between 30% and 53%.

Finally, a model based on energy and mass conservation into cylinders volume was successfully calibrated and is able to predict mass flow rate, mechanical power and exhaust temperature with a good agreement. This model enables to detach the influence of pressure drops and leakages on the filling factor and then on the isentropic efficiency. This analyse shows that pressure drops affect principally the compactness of the expander and not so much the isentropic efficiency (excepted for low rotational speed where pressure drops can lower by 14% the isentropic efficiency). In the other hand, leakages have strong impact. A part of this losses analysis is summarized in Table 5-7 where value of factors impacting the isentropic efficiency are listed for three rotational speeds and supply

and exhaust pressure of respectively 21 bar and 2 bar (optimal operating pressures). As for the expander investigated in Chapter 4, the importance of the different source of losses varies with the speed. For the optimal speed of 2500 RPM, the under expansion and compression have the strongest impact followed by the mechanical losses, leakages and pressure drops respectively.

Table 5-7: Summarized of the losses analysis

Rotational speed	$\epsilon_{s,th}$ [-]	ϵ_{in} [-]	$\frac{1}{\phi_{in}}[-]$	$\frac{\epsilon_{in}}{\phi_{in}} = \epsilon_{sp,in}$ [-]	$\frac{1}{\phi_{l}}[-]$	$\epsilon_{s,in}$[-]	η_m [-]	$\epsilon_{s,sh}$ [-]
1000 RPM	0.78	0.78	1.1	0.86	0.87	0.59	0.81	0.48
2500 PRM	0.78	0.56	1.64	0.92	0.91	0.65	0.82	0.54
4000 RPM	0.79	0.46	2.39	1.09	0.89	0.77	0.60	0.46

Finally, the semi-empirical model presented in Chapter 3 is validated with the same calibration process that one used for the detailed model. Despite of its simplicity, this model gives very good results and will be used in next chapter to evaluate the potential of an ORC-based m-CHP system.

7. References

Dickes, R., O. Dumont, S. Declaye, S. Quoilin, I. Bell, and V. Lemort. 2014. “Experimental Investigation of an ORC System for a Micro-Solar Power Plant.” In . Purdue, USA.

Padet, J. 2016. “Convection Thermique et Massique Principes Généraux.” *Techniques de L’ingénieur Transferts Thermiques* base documentaire : TIB214DUO. (ref. article : be8205). http://www.techniques-ingenieur.fr/base-documentaire/energies-th4/transferts-thermiques-42214210/convection-thermique-et-massique-be8205/.

Subcommittee 65B : Measurement and control devices. 2013. *Thermocouples. Part 1, Part 1,*. International Electrotechnical Commission.

8. Annexes

8.1. Gaussian regression results

Two plots are presented for each studied variable:

- The first show the values predicted by the regression model in term of the measured values. Red points (train) represents the results of the model based on all the data set. The blues points (cross validation) represents the results of a model based on all the data set except the predicted values. The MARE given in section 3.1.1. is related to the "cross validation" model.
- The second plot show the discrepancy between the measured and predicted values on a normalized Gauss curve.

8.1.1. Indicated power

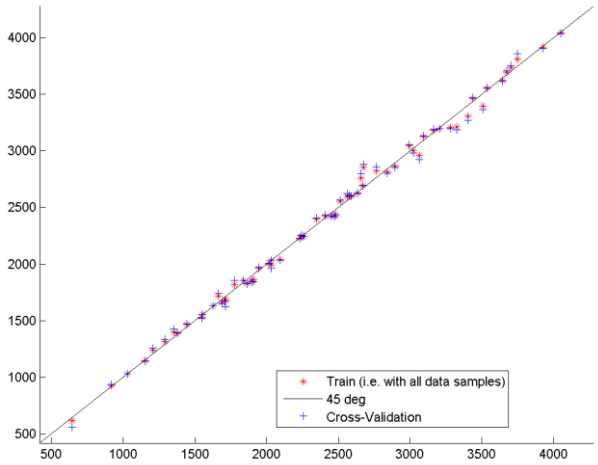

Figure 5-31 : Predicted VS measured values of $\dot{W}_i$

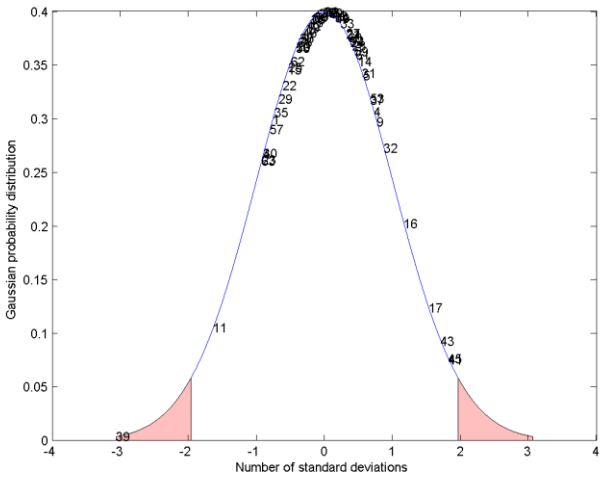

Figure 5-32 : Normal distribution of the error of $\dot{W}_i$

8.1.2. Mechanical power

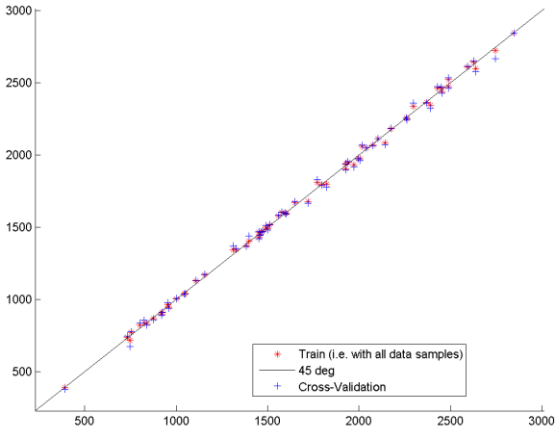

Figure 5-33 : Predicted VS measured values of$\dot{W}_m$

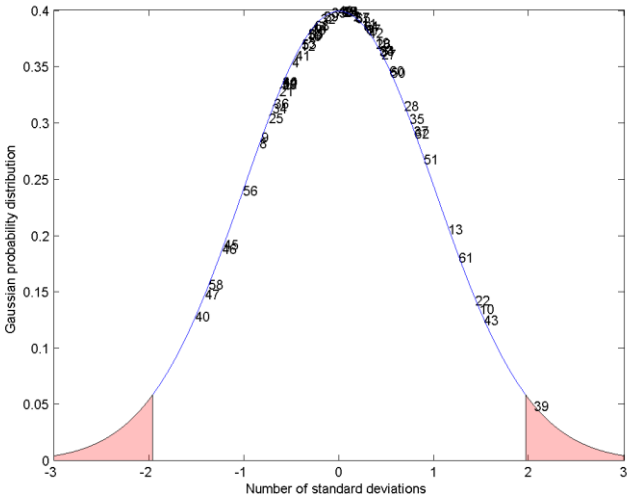

Figure 5-34 : Normal distribution of the error of $\dot{W}_m$

8.1.3. Isentropic efficiency

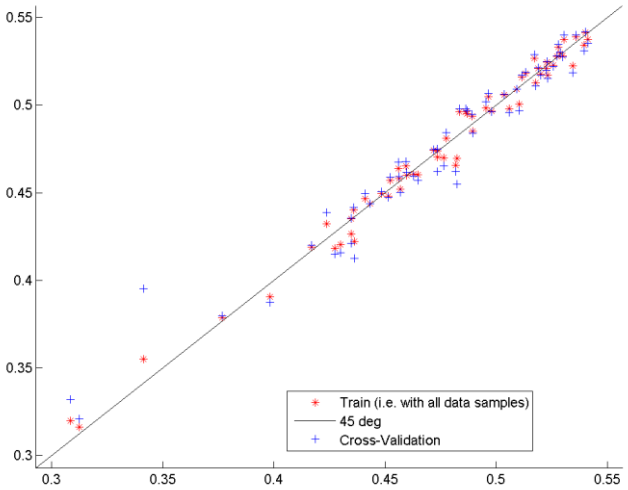

Figure 5-35 : Predicted VS measured values of de ϵ_s

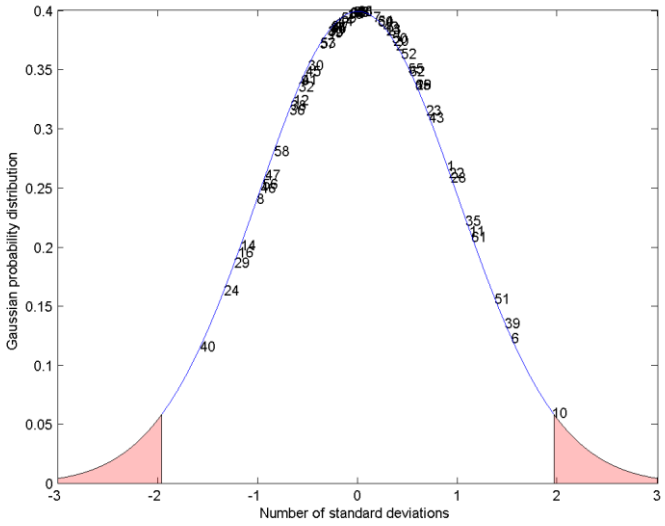

Figure 5-36 : Normal distribution of the error of ϵ_s

8.1.4. Mass flow rate

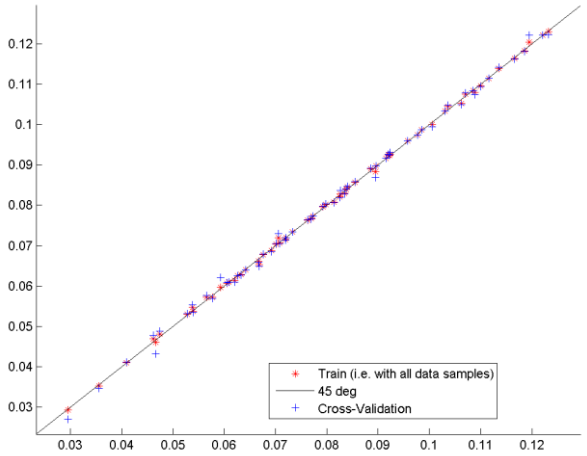

Figure 5-37 : Predicted VS measured values of $\dot{M}_{wf}$

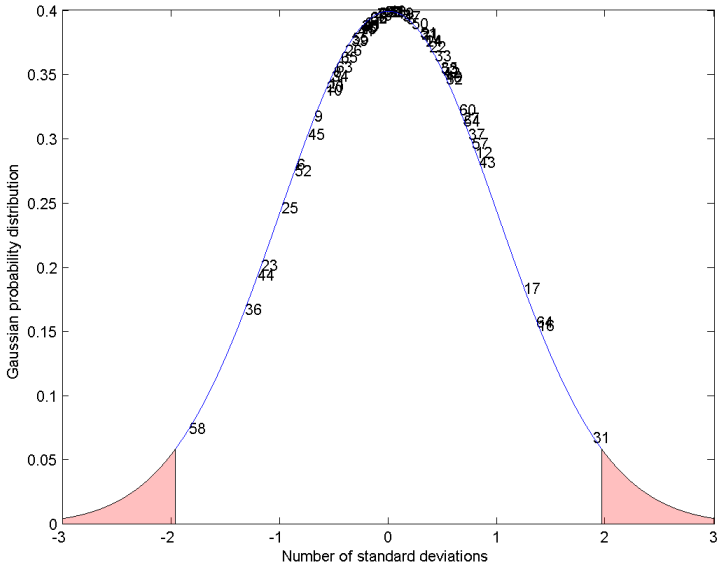

Figure 5-38 : Normal distribution of the error of $\dot{M}_{wf}$

Chapter 6: Performance evaluation of ORC-based and Ericsson engine-based combined heat and power systems

Contents

1. Introduction

Combined Heat and Power (CHP) refers to the production of electrical (or mechanical) power and useful heat simultaneously. This way to produce heat and electricity leads to a reduction of primary energy consumption and, in most cases, a reduction of greenhouse gas emissions. Therefore, in the current energy and environmental context (depletion of fossil fuels and climate change), the interest in CHP is growing. Special attention is currently paid to small scale CHP such as micro-CHP (<50kWe) because it is not widely implemented while it offers an alternative to large scale CHP (De Paepe and Mertens 2007) (Simader, Krawinkler, and Trnka 2006) (Liu et al. 2010) (Lombradi, Ugursal, and Beausoleil-Morrison 2008). Moreover, CHP is within the scope of distributed energy production, one of the key issues in the energy sectors of the European Union.

The main technologies available for micro-CHP at the present time are the internal combustion engine (ICE), the Stirling engine and fuel cells, which are already marketed and the micro-gas turbine and the ORC, which are still in development (Andlauer et al. 2010). Table 6-1 summarizes the main characteristics of each technology (in this table, electrical efficiency is the ratio between electrical power output and fuel power input, total efficiency is the sum of electrical efficiency and thermal efficiency, which is the ratio between heat power output and fuel power input). The technologies giving the best efficiencies are the ICE and the Fuel Cell but they have the drawback to be limited in fuels. Moreover fuel cell systems still show very high costs. Micro-turbines are not suitable for micro-CHP because of their poor efficiency at low scale and because the high temperature of heat generated is more suitable for industrial process than for building heating. Finally, the two external combustion engines, namely the ORC and the Stirling engines, are comparable in terms of electrical efficiency. Moreover, they show the advantage of fuel flexibility that can lead to use renewable fuels such as biomass or solar energy.

Table 6-1: Comparison of the different technologies of m-CHP

	ICE	**Micro-Turbine**	**Stirling**	**ORC**	**Fuel cell**
Electrical power	5kWe-20MWe	15kWe-300kWe	1kWe-1.5MWe	1kWe-10MWe	1kWe-1MWe
Electrical efficiency	**25-45%**	15-30%	10-20%	~10%	**30-70%**
Total efficiency	65-92%	65-90%	65-95%	~90%	90%
Fuel	Gasoline, Diesel, Gas, Biogas, etc.	Gas, Biogas, etc.	**Flexible**	**Flexible**	Hydrogen or Hydrogen-rich gas
State	**Widespread**	Uncommon	Development, early market	Development, early market	Proven technology

This chapter aims at evaluating and comparing the performances of two different kinds of CHP units based on the two technologies studied in this work: Ericsson engine-based and piston expander ORC-based CHP. For this purpose, cogeneration performance indicators are defined. Then, the Ericsson

engine performance is simulated considering potential improvements of the modified engine tested in chapter 4. Finally, fluid selection and heat exchanger design of an ORC using the piston expander tested in chapter 5 are performed in order to evaluate potential performance.

2. Interest of cogeneration and performance indicators

First, as CHP produces electrical and thermal power, two main performance indicators can be defined:

- Electrical efficiency :

$$\eta_{el} = \frac{\dot{W}_{el}}{\dot{Q}_{fuel,boil}} \quad (6\text{-}1)$$

- Thermal efficiency:

$$\eta_{th} = \frac{\dot{Q}_{heat}}{\dot{Q}_{fuel,boil}} \quad (6\text{-}2)$$

where $\dot{W}_{el}$ and $\dot{Q}_{heat}$ are the electrical and thermal powers produced by the CHP system and $\dot{Q}_{fuel,boil}$ is the fuel power consumed by the boiler of the system.

Then, other indicators related to advantages of cogeneration can be defined. The three main interests are: economy of primary energy, reduction of CO2 emission and economic interest.

2.1.Reduction of primary energy

The quality of a CHP system is generally evaluated by the Primary Energy Saving (PES) Indeed, by producing simultaneously electricity and heat, CHP allows the consumption of less energy compared to the same production by separated units, e.g. electric power plant and domestic boiler. Then, the PES represents the economy of primary energy achieved by using CHP in percent of the consumption of the separated production. It is computed by:

$$PES = \left(1 - \frac{1}{\frac{\eta_{CHP,th}}{\eta_{ref,th}} + \frac{\eta_{CHP,el}}{\eta_{ref,el}}}\right).100 \quad (6\text{-}3)$$

where:

- $\eta_{CHP,th}$ is the thermal efficiency of the CHP
- $\eta_{CHP,el}$ is the electrical efficiency of the CHP
- $\eta_{ref,th}$ is the thermal efficiency of a reference separated heat production unit
- $\eta_{ref,el}$ is the electrical efficiency of a reference separated electricity production unit

The reference efficiencies are given by (European Commission 2006) and depend on the fuel type. In the present case, wood biomass is considered. For this type of fuel, the reference thermal efficiency is 86% and the reference electrical efficiency is 33%.

2.2.Reduction of CO2 emission

The diminution of primary energy consumption and the use of alternative fuel such as biomass may lead to a reduction of CO2 emission compared to separate production. The reference installation considered for the CO2 emission is generally a gas boiler (in order to take into account the use of alternative fuel such as biomass) and a Combined Cycle Gas Turbine (CCGT) power plant (Daoud 2013). Then, the CO2 emission saving per electric megawatt hour produced is given by:

$$S_{CO2} = Em_{CCGT} + \frac{\eta_{CHP,th}}{\eta_{CHP,el}} \frac{e_{fuel,ref}}{\eta_{ref,th}} - \frac{e_{fuel,CHP}}{\eta_{el,CHP}} \quad (6\text{-}4)$$

where $Em_{CCGT} = 456\ \mathrm{kgCO2/MWh_e}$ is the specific emission of a CCGT plant, e_{fuel} is the specific emission of the fuel with respect to its lower heating value (LHV), and $\eta_{ref,th} = 90\ \%$ is the reference efficiency of a gas boiler. The two first terms of this equation represent the emission of the production of the electricity and heat separately while the third term represents the emission of the CHP plant. Table 6-2 lists the specific emissions of some fuels. As biomass fuels have much lower CO2 emission than petroleum products, they allow a significant reduction of CO2 emission.

Table 6-2: CO2 specific emission of different fuels (Daoud 2013)

Fuel	$e_{fuel}\left[\frac{kgCO2}{MWh}\right]$
Natural gas	251
LPG	267
Heating oil	306
Harvested wood	45
Wood waste	23
Biodiesel	80

2.3.Economic interest

In addition to the environmental advantages, cogeneration has an economic interest. Indeed, the user of the CHP unit has to consume a bit more of fuel to cover his heating demands compared to a classic boiler. But, in compensation, electricity is produced and this electricity has a higher added value than heat. The user has then two possibilities, either he sells the electricity on the grid to generate an income or he directly consumes it to reduce his electricity bill. The profit depends on the electricity and fuel price and increases when the price difference between electricity and fuel increases. As these prices can strongly fluctuate in the time and differ from a country to another, it is difficult to precisely evaluate the future income. Moreover, the profit depends on eventual state incentives such as investment incentive and feed-in tariff.

In order to evaluate the profitability of the investment in a CHP plant, several economical criteria can be used such as the levelized electricity cost, internal rate of return or actualized pay-back time. All these criteria depend on the investment, future profits and discount rate and are then difficult to evaluate, especially for units in development as the investment is not known.

3. Ericsson engine based CHP unit

The goal of this section is to evaluate the performance of an Ericsson engine-based m-CHP unit. Figure 6-1 shows the layout of the proposed system which is composed of the compressor and the expander of an Ericsson engine, a biomass furnace to feed the engine, eventually a recuperator if it allows an increase in the efficiency and two water-cooled heat exchangers in order to recover the heat available at the engine jacket cooler and in the hot exhaust air. The possibility to use a turbocharger in order to increase the power of the engine is considered.

As seen in Chapter 4, the valves of the engine used as compressor have a high leakage rate and the valve timings are designed for one compression ratio. This leads to a poor compressor efficiency. As air compressor is a very mature widespread technology (contrary to piston expander especially for the considered power and temperature), it is proposed to use a commercially available compressor in order to ensure the best performances of this component. For the expander, the same engine as the one tested in Chapter 4 is considered but the whole six cylinders are used as expansion machines.

It is supposed that the produced hot water feeds a hot water tank that plays the role of a buffer. This assumption has the corollary that the Ericsson engine can always run in nominal regime rather than in part-load when the heat demand is lower than the nominal heat capacity of the CHP.

The goal of this section is to evaluate the performance of this system considering improvement of the actual expander. As in chapter 4, the supply temperature of the expander is set to 800°C. For the rotational speed, 600 RPM is considered, as it is the optimal speed considering isentropic efficiency.

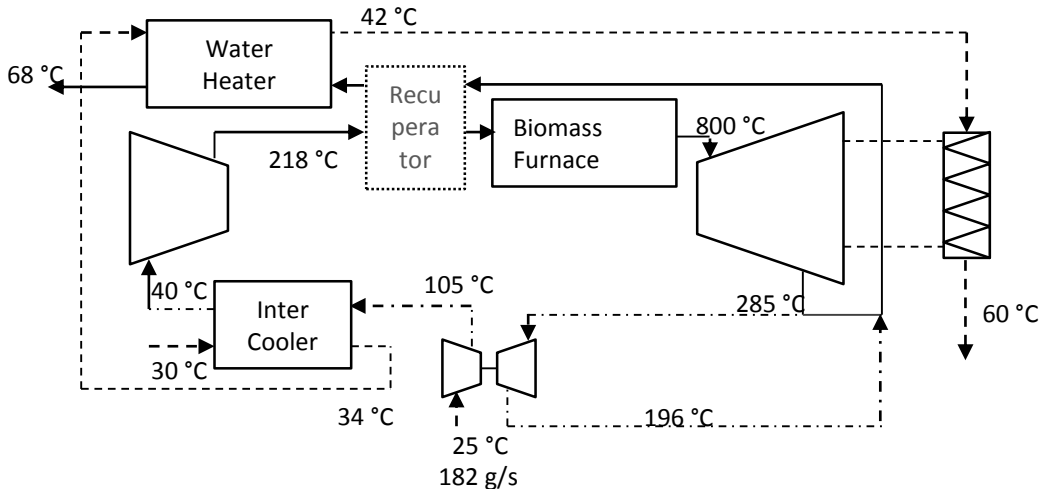

Figure 6-1: Schematic representation of the Ericsson engine based m-CHP unit

3.1. Ericsson engine improvement and pressure ratio optimization

In order to evaluate the performance of the Ericsson engine based m-CHP unit the expander is simulated with the semi-empirical model proposed in chapter 3 and validated in chapter 4. The isentropic efficiency of the commercially available air compressor is assumed to be 80% (Vittorini,

Bianchi, and Cipollone 2015). The same value is considered for the turbo compressor while the efficiency of the turbine is set to 70 % (Parois 2001)

As seen in Chapter 4, some improvements of the expander can be envisaged. These improvements are the reduction of the leakages, the attenuation of the supply pressure pulsations and the reduction of the cut-off ratio. These three improvements have been simulated and the results are shown in Figure 6-2 and Figure 6-3 where the efficiency and the power of the Ericsson engine are plotted in terms of the pressure ratio. It can be seen that in order to increase the efficiency and the net power, the best improvement is the reduction of the leakages followed by the attenuation of the supply pulsations. The reduction of the cut-off does not improve significantly the performance if it is not combined with a reduction of the leakages. By combining these three improvements, the efficiency is increased from 1 % to 7 % and the power from 500 W to 4500 W. The efficiency with a recuperator is also plotted in the figures. The improvement given by this additional heat exchanger is not significant because of the large heat losses of the expander that reduce the expander exhaust temperature.

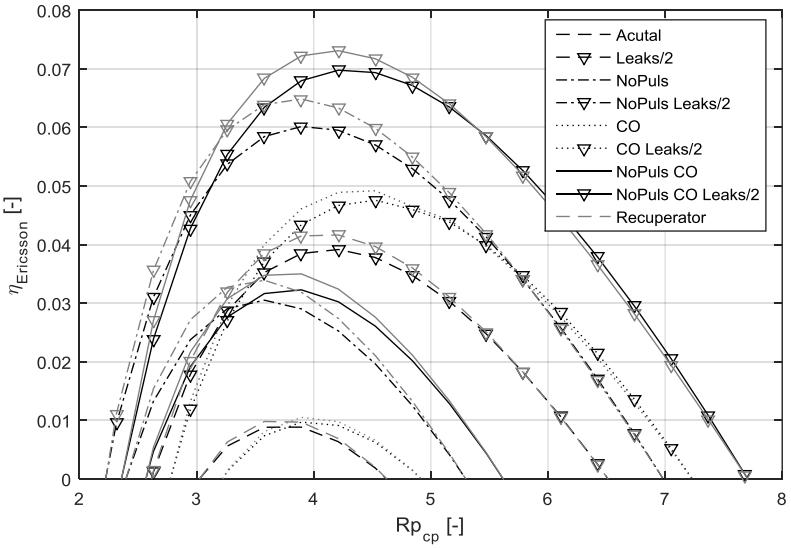

Figure 6-2: Ericsson engine efficiency in terms of compressor pressure ratio

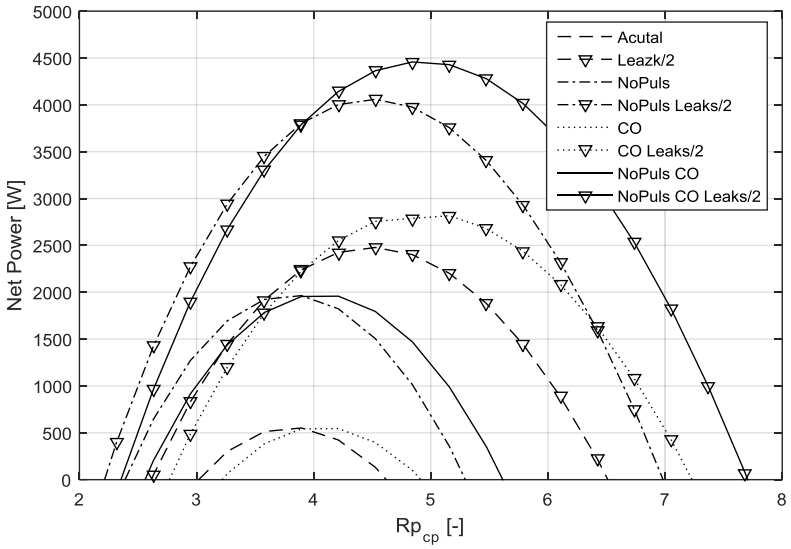

Figure 6-3: Ericsson engine net power in terms of compressor pressure ratio

Figure 6-4 and Figure 6-5 also show the evolutions of efficiency and power in terms of compressor pressure ratio but considering a turbocharged engine. The supply pressure of the compressor is set to 2 bar. It should be noted that with a turbocharger, the pressure ratio of the compressor and of the expander are not equal anymore. Indeed, the turbine induces an expander back pressure that differs from the compressor supply pressure. As expected, the turbocharger allows the available power to be increased. Moreover, it can be observed that even the efficiency is improved (about 1% point). As the expander exhaust hot gases are now cooled down by the expansion in the turbine, the use of a recuperator is not possible anymore in most cases (the efficiency with recuperator is smaller than without it).

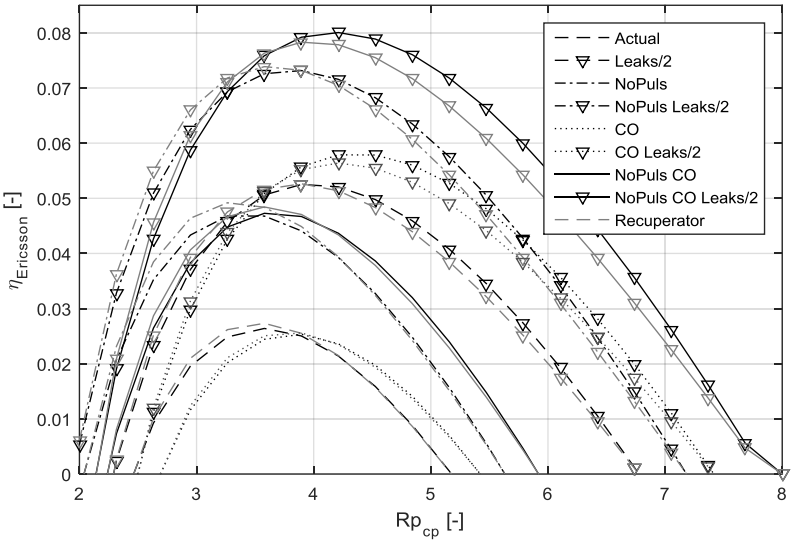

Figure 6-4: Turbocharged Ericsson engine efficiency in terms of compressor pressure ratio

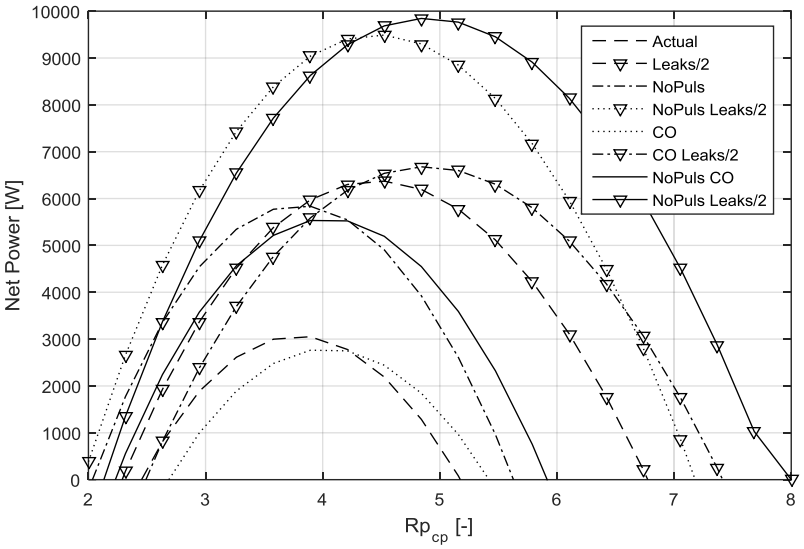

Figure 6-5: Turbocharged Ericsson engine net power in terms of compressor pressure ratio

With the three improvements and the turbocharger, the efficiency of the engine is 8 % for a pressure ratio of 4.2, which corresponds to an available mechanical power of 9.2 kW. These operating parameters are considered for the next section and some corresponding characteristics are listed in Table 6-3.

Table 6-3: Performance and characteristics of the Ericsson engine based CHP unit

$\dot{W}_{exp}\ [kW]$	43.9
$\dot{W}_{cp}\ [kW]$	34.6
$\dot{W}_{net}\ [kW]$	9.2
$\dot{Q}_{th}\ [kW]$	95
$\dot{M}_a\ [g/s]$	182
$\dot{V}_{a,su,cp}\ [m^3/h]$ $(P = 2\ bar, T = 40°C)$	284
$\dot{Q}_{furnace}\ [kW]$	115
$\eta_{el}\ [\%]$	6.5
$\eta_{th}\ [\%]$	70.5
$PES\ [\%]$	2

3.2.Recovered heat and PES

In the engine described above, there are three sources of heat losses. The first one is the heat evacuated by the coolant, the second one is the rejection of hot air at the exhaust of the engine and the third one is the heat evacuated at the intercooler. In the m-CHP unit, this available heat is recovered by the hot water through three heat exchangers, as shown in Figure 6-1.

The cooling loop of the engine evacuates the heat transferred by the air to the wall of the cylinder and the friction losses. In practice, 95 % of this heat is evacuated by the coolant and the remaining 5 % is evacuated to the ambient (Pulkrabek 1997). Then, computing the heat flux to the wall and the friction power with the model, the power available at the cooling loop can be estimated:

$$\dot{Q}_{cool} = \left(\dot{Q}_w + \dot{W}_{loss}\right) * 0.95 \quad (6\text{-}5)$$

The heat recovered from the exhaust gases can be computed considering the heat exchanger (water heater in Figure 6-1) efficiency:

$$\dot{Q}_{wh} = \epsilon_{wh}.\dot{C}_{min}.(T_{a,su,wh} - T_{w,su,wh}) \quad (6\text{-}6)$$

where ϵ_{wh} is the water heater efficiency, $\dot{C}_{min}$ is the smallest heat capacity flow rate of the two fluids and $T_{a,su,wh}$ and $T_{w,su,wh}$ are the supply temperatures of air and water respectively.

The heat available at the intercooler is known because the temperature of the air leaving this exchanger is imposed to 40 °C and the supply air temperature is the temperature at the exhaust of the turbo-compressor, computed with the help of the isentropic efficiency.

Finally, the heat power produced by the CHP is the sum of these three heat flows:

$$\dot{Q}_{heat,chp} = \dot{Q}_{cool} + \dot{Q}_{ex,hx} + \dot{Q}_{IC} \quad (6\text{-}7)$$

Considering an exhaust heat exchanger efficiency of 80%, the total available heat is 89 kW, which corresponds to a thermal efficiency of 82 %. The computed water and air temperatures are shown in Figure 6-1.

As the exhaust water temperature does influence neither the Ericsson engine efficiency nor the thermal efficiency (change of 0.7 percentage point difference for exhaust temperature varying from 35 °C to 65 °C), there is no need to perform seasonal simulations.

Finally, the proposed Ericsson engine based CHP unit shows a shaft power efficiency of 8 % and a thermal efficiency of 82%. Considering an electrical generator and a biomass boiler with efficiencies of 95 % and 86 % (biomass boiler reference efficiencies) respectively, the electrical and thermal efficiency became 6.5 % and 70.5 %. These efficiencies lead to a PES of only 2%.

4. ORC-based CHP unit

This section aims at evaluating the performance of an ORC based m-CHP unit using the axial piston expander tested in Chapter 5. The system consists of a biomass furnace coupled with an ORC unit. The selected configuration of the ORC-based CHP unit is shown in Figure 6-6: the biomass oil boiler heats up a heat transfer fluid (HTF), this HTF passes through the evaporator of the ORC where it preheats, evaporates and eventually superheats the working fluid. The superheated vapor is expanded into the expander and generates electrical energy. A regenerator is used to increase the ORC efficiency and hot water for heating purpose is produced in the condenser. As for the Ericsson engine-based CHP unit, it is supposed that the hot water produced feeds a hot water tank.

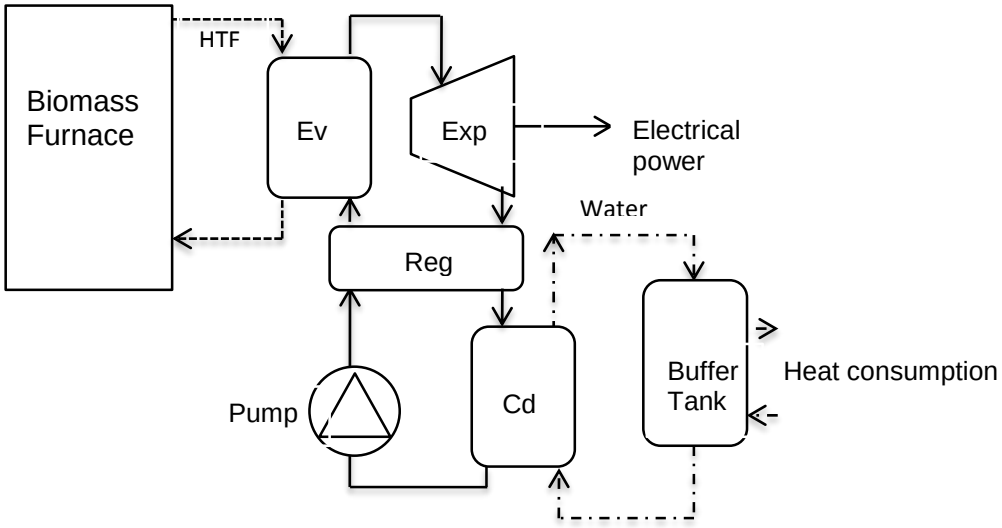

Figure 6-6: Configuration of the ORC-based CHP

The goal of this section is to optimize the operating conditions and, as the efficiency of the ORC varies with the hot water temperature, to evaluate seasonal performance of the proposed system. First, the ORC working fluid is selected by comparing performances of the ORC cycle. Then, a simulation model is built by assembling different sub-models of each component: heat exchangers, piston expander and working fluid pump.

4.1.Fluid selection

The fluid is a critical component of an ORC system since it has a strong impact on the design and on the performance of the system. Different criteria must be taken into account, such as pressure and density levels, thermodynamic performance, environmental impact, cost and security (Quoilin, Declaye, and Lemort 2010) (Aoun 2008). The selection of a given working fluid always results in a tradeoff based on selection criteria and on the constraints of the system.

In this study, a set of seven fluids, based on a previous study (Oudkerk et al. 2013) are considered (see Table 6-4, the fluid properties are provided by EES software (Engineering Equation Solver)). Non-null Ozone Depleting Potential (ODP) working fluids have not been considered in this study since they are or will be phased out by the Montreal protocol.

For the purpose of the working fluid comparison, the following conditions are imposed (T_{cd} is the condensing temperature):

- $T_{cd} = 50\ °C$ to allow the production of hot water in the condenser.
- Overheating and sub-cooling of 5K are considered to avoid droplets in the expander and cavitation in the pump.
- The isentropic efficiency of the pump is set to $\epsilon_{s,pp} = 0.7$
- The efficiency of the regenerator is set to $\epsilon_{reg} = 0.8$

Figure 6-7 shows the evolution of the net cycle efficiency with the evaporating temperature for the considered fluids. First, it can be seen that, for a given evaporating temperature, slight differences

exist between the different fluids: fluids with higher critical temperature lead to higher net cycle efficiency. Second, fluids with high critical temperature have the ability to operate with higher evaporating temperature and thus with higher net cycle efficiency.

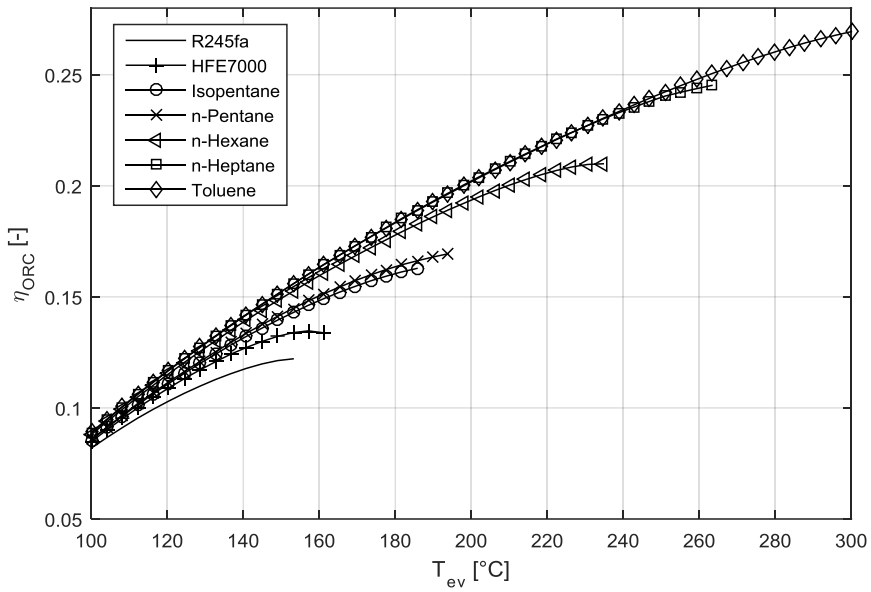

Figure 6-7: Evolution of the predicted cycle net efficiency with the evaporating temperature for different fluids with constant expander isentropic efficiency ($\epsilon_s = 0.7$) (Tcd=50°C)

These observations may lead to the conclusion that fluids with higher critical temperature are a better choice. However, for fluid selection, real characteristics of the expander have to be take into account. This can be done by using the semi-empirical model presented in Chapter 3 and validated in Chapter 5. Figure 6-8 shows the ORC net efficiency simulated using the semi-empirical model and thus, considering the real features of the expander. It can be seen that there is an optimal evaporating temperature and that fluids with high critical temperature do not show better performance, even at high evaporating temperature. Indeed, as shown in Figure 6-9, isentropic efficiency is lower for high critical temperature fluids.

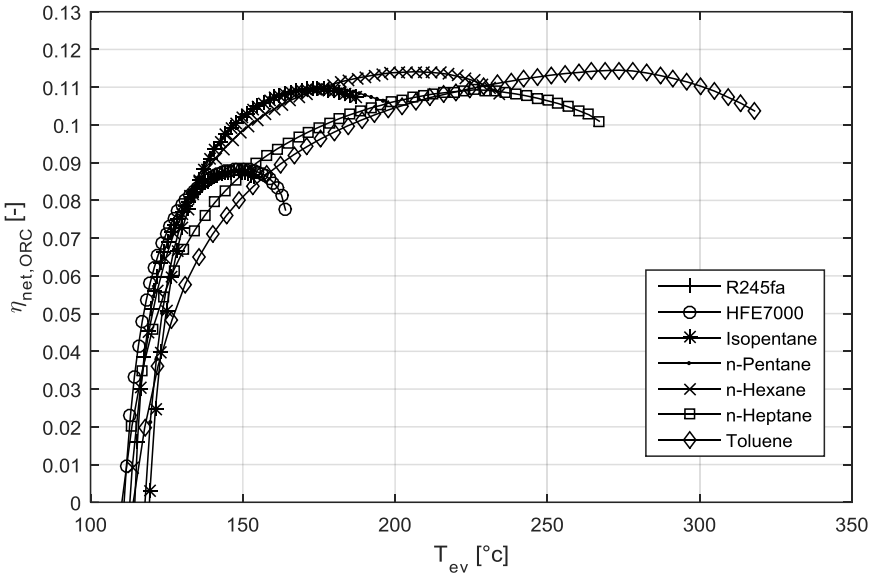

Figure 6-8: Evolution of the predicted cycle net efficiency with the evaporating temperature for different fluids using the expander semi-empirical model (Tcd=50°C)

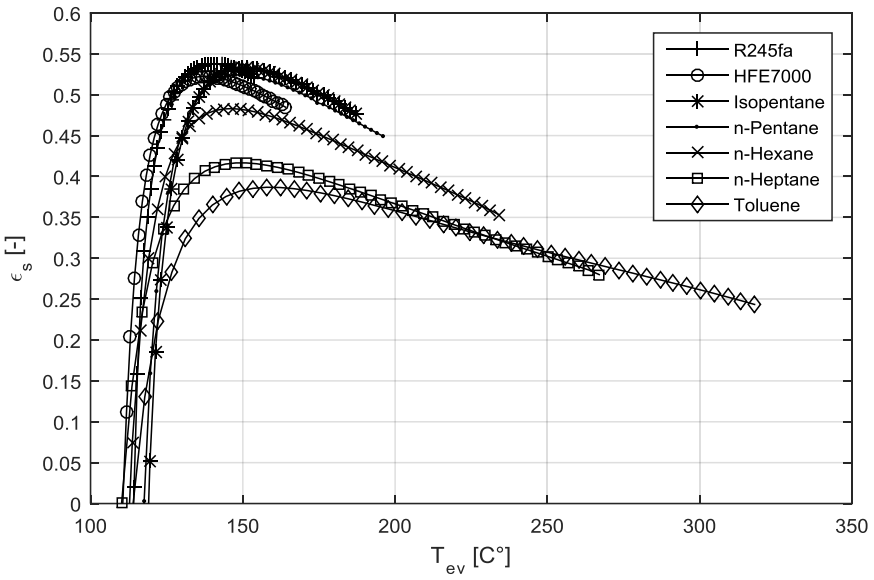

Figure 6-9: Evolution of the simulated isentropic efficiency with the evaporating temperature for different fluid (Tcd=50°C)

Table 6-4 summarizes the results of these simulations. For each fluid, the optimal evaporating temperature is given as well the resulting performances. However, as maximum supply temperature of the expander is 250°C, if optimal evaporating temperature is higher, the evaporating temperature is constrained to 250 °C (it is only the case for toluene). It can be seen that n-hexane, isopentane and n-pentane give the best net cycle efficiency and isopentane the highest net power. Considering this observation, isopentane is considered for the CHP unit.

Table 6-4 : Considered fluids, critical properties and simulation results at optimal evaporating temperature

Fluids	T_{crit} [°C]	P_{crit} [Bar]	$T_{ev,opt}$ [°c]	ϵ_s [%]	$\dot{W}_{net}$ [W]	$\eta_{cycle,net}$ [%]
R245fa	154	36.51	145	53	2410	8.7
HFE7000	164	24.78	149	51	1351	8.8
Isopentane	187	33.70	171	50	3076	10.9
n-Pentane	196	33.64	174	46	3015	10.9
n-Hexane	234	30.58	206	40	2924	11.4
n-Heptane	267	27.27	229	33	2355	10.9
Toluene	318	41.26	250	30	2584	11.3

4.2.CHP Model

4.2.1. ORC Heat exchangers

Heat exchangers of the ORC system are modeled by the ϵ-NTU method. The evaporator and the condenser are divided into three zones, each zone corresponding to a specific state of the fluid: vapor, two-phase and liquid (Quoilin, Lemort, and Lebrun 2010). Each zone is characterized by a heat transfer coefficient and a heat transfer area. The total heat transfer area is the sum of these three zones areas.

For the sizing of the heat exchangers, the pinch-point (ΔT_{pp}) is imposed and the exchanger heat transfer area is computed. For off-design simulation, the determined heat transfer area is imposed.

4.2.2. Expander

In this work, the considered expander is an axial piston machine tested in chapter 5 and modeled by the semi-empirical model proposed in Chapter 3. An electrical generator efficiency is introduced and set to 95 % in order to take into account electromechanical losses.

4.2.3. Pump

The pump is assumed to be adiabatic, and its consumption is evaluated by imposing a constant overall isentropic effectiveness (i.e. including electromechanical losses):

$$\dot{W}_{pp} = \frac{\dot{M}.(h_{ex,s} - h_{su})}{\epsilon_{s,pp}} \quad (6\text{-}8)$$

4.3.Sizing

Two main degrees of freedom on the operating conditions are available to optimize the proposed system: the evaporating temperature T_{ev} and the HTF temperature difference between the supply and the exhaust of the evaporator ΔT_{HTF} (or the HTF mass flow rate). The remaining operating

conditions are linked to design or technical constraints and do not result from an optimization. Their values are listed in Table 6-5.

Table 6-5 : Values of input parameters for simulations

$T_{w,ex}/T_{w,su}$ [°C]	40/30
$\Delta T_{sh}, \Delta T_{sc}$ $[K]$	5
$\Delta T_{pp,ev}, \Delta T_{pp,cd}$ $[K]$	10
α_{liquid} [W/m²/K]	1000
α_{vapor} [W/m²/K]	140
$\alpha_{two-phase}$ [W/m²/K]	10000

The influence of T_{ev} on the ORC efficiency has already been shown in Figure 6-7 and Figure 6-8: on one hand, the ideal cycle efficiency increases with the evaporating temperature, but on the other hand the isentropic effectiveness of the expander exhibits a maximum for a given T_{ev} (Figure 6-9). The combination of these two effects leads to an optimum value for T_{ev} that maximizes the ORC efficiency (Figure 6-8). For isopentane, the optimal evaporating temperature is 171°C.

As shown by the author (Oudkerk et al. 2013), when the ORC cycle is coupled to a boiler, ΔT_{HTF} also shows an impact on the cycle performance since it impacts the exergy destruction due to a poor matching between heating and cooling curves. The optimum value of ΔT_{HTF} corresponds to HTF temperature profile parallel to the liquid temperature profile of the working fluid (see Figure 6-10). In this case, the value is $\Delta T_{HTF} = 130\ K$.

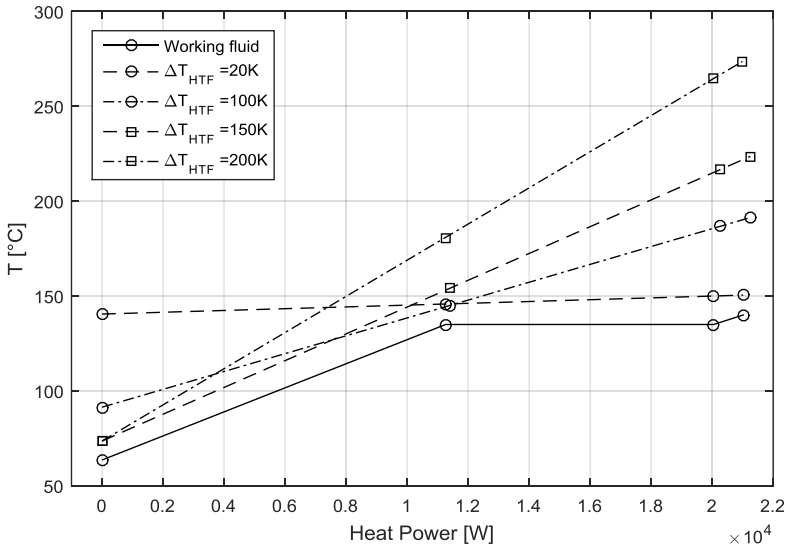

Figure 6-10: Temperature profile in the evaporator

Table 6-6 summarizes the values of the performance indicators when operating at the optimal performance point (T_{ev}=171 °C and ΔT_{HTF}=130 K). This optimal point is chosen as design point and Table 6-6 gives also the results of the sizing of the ORC heat exchangers and boiler power. The areas

of the different zones of the heat exchangers were computed with typical values (see Table 6-5) of the transfer coefficients for each zone, as recommended by (McMahan 2006)

Table 6-6 : Achieved performance and ORC parameters for the design point

Achieved performance		ORC parameters	
η_{el} [%]	10.7	A_{ev} $[m^2]$	3.8
η_{th} [%]	85	A_{cd} $[m^2]$	2.4
$\dot{W}_{net}$ $[kW]$	3	A_{reg} $[m^2]$	4.1
$\dot{Q}_{heat}$ $[kW]$	24.3	$\dot{Q}_{boiler}$ $[kW]$	29

4.4.Seasonal simulation

As the performances of the proposed system vary with the hot water temperature by modifying the condensing temperature, a seasonal performance simulation must be performed over one year. The results of simulation strongly depend on climatic conditions and thus on the location and on the control strategy regulating hot water temperatures. The climate can be defined by a "temperature bin" diagram such as the one presented in Figure 6-11 for an average European climate as defined by the standard PrEN14825. This diagram indicates the number of hours (bin hours, h_i) during which the outdoor temperature is within a range of 5 K (a bin) around the discrete central temperature (the bin temperature, $T_{out,i}$). For the purpose of the simulation, four heat emitter heating curves are considered, corresponding to very high, high, medium and low temperature heating applications according to the standard PrEN14825 (see Figure 11). These curves give the hot water temperature leaving the CHP system. This hot water temperature influences the condensing temperature and thus the operating condition of the ORC, which affects the efficiency of the system. Finally, a heating demand for each bin ($\dot{Q}_{load,i}$) must be defined. This heating demand depends on the outdoor temperature. Here, a linear profile is considered: the heat load is maximum ($\dot{Q}_{load,max}$) for an outdoor temperature of -10 °C and is null for an outdoor temperature of 20°C.

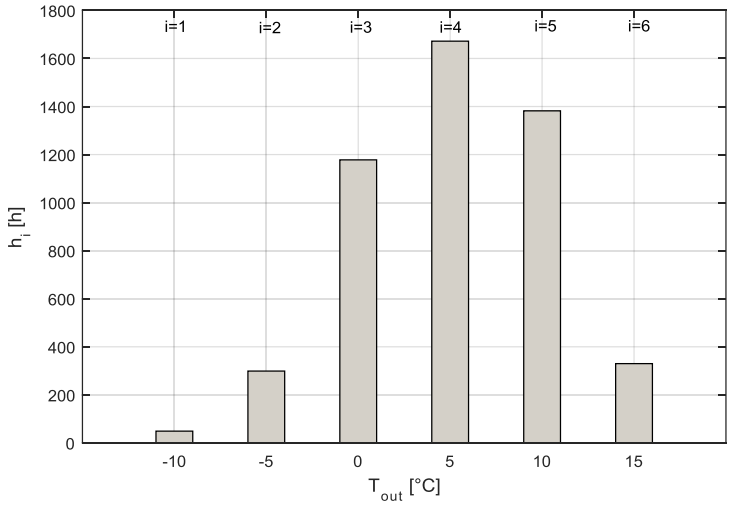

Figure 6-11 : Average European climate (PrEN14825)

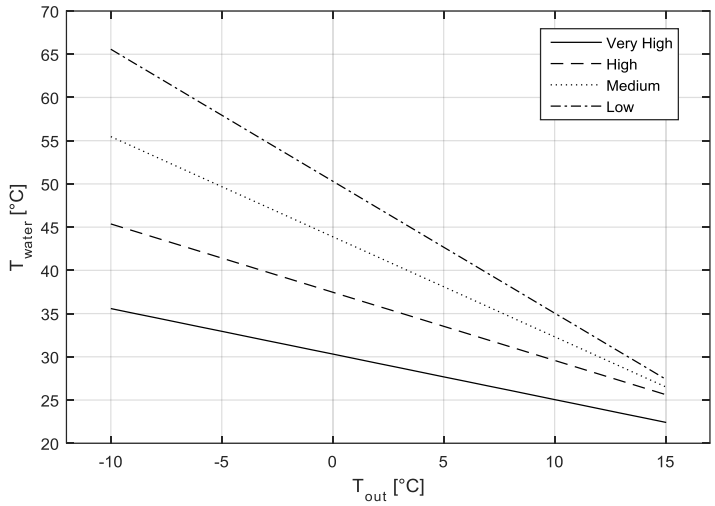

Figure 6-12: Heat emitters heating curve (PrEN14825)

For each bin, simulation is performed with design point parameters (see Table 6-6 right column). As explained above, it is also assumed that, through the use of a buffer tank, the CHP system always operates at full load.

Figure 6-13 shows the evolution of the electrical efficiency in terms of outdoor temperature for each bin. The electrical efficiency of the system varies from 9.2 % for a hot water temperature of 65°C ($T_{out} = -10°C$, bin 1, very high temperature application) to 11.2 % for a hot water temperature of 22°C ($T_{out} = 15°C$, bin 6, low temperature application). Corresponding net electrical powers vary from 1.9 kW to 3.6 kW.

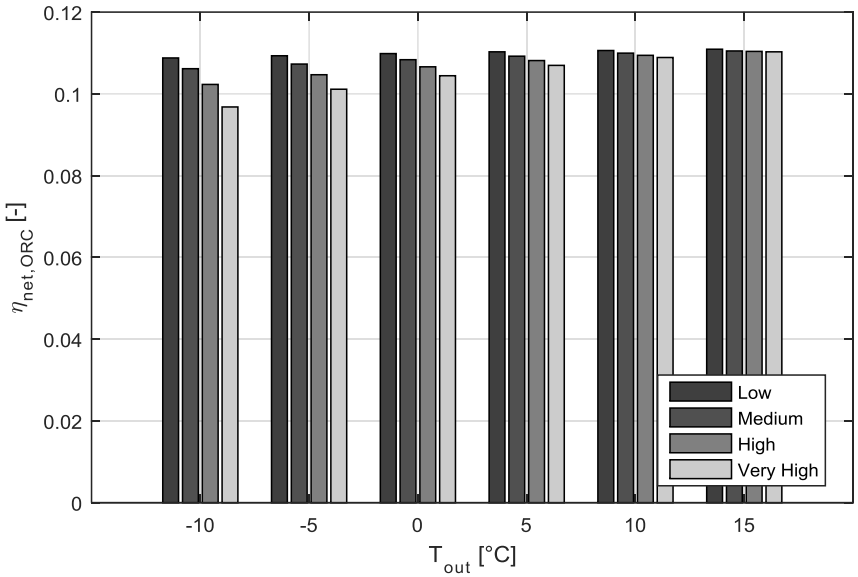

Figure 6-13: Electrical efficiency for each bin in term of outdoor temperature for four heat emitter heating curves (very high, high, medium, and low temperature application)

The overall efficiencies, which are the efficiencies of the micro-CHP system during one year, are computed as follows:

$$\eta_{el,overall} = \frac{\sum_{i=1}^{n}(RunTime_i.\dot{W}_{el,i})}{\left(\sum_{i=1}^{n} RunTime_i\right).\dot{Q}_{ev}}.\eta_{ref,th} \quad (6\text{-}9)$$

$$\eta_{th,overall} = \frac{\sum_{i=1}^{n}(RunTime_i.\dot{Q}_{heat,i})}{\left(\sum_{i=1}^{n} RunTime_i\right).\dot{Q}_{ev}}.\eta_{ref,th} \quad (6\text{-}10)$$

where n is the amount of bin (here $n = 6$), $RunTime_i$ is the necessary time to fulfill the heat demand and $\eta_{ref,th}$ is the reference efficiency for a biomass boiler (83%, see section 2.1).

The results for seasonal simulation are summarized in Table 6-7. The electrical efficiency is about 8.8 % and the variation in electrical efficiency between low and very high temperature applications is 0.4 percent point. The system allows saving about 10.3 % of primary energy compared to a separate production. The electrical efficiency is relatively low compared to ICE (about 30%) and needs to be improved to allow ORC-based CHP to be profitable. However, this low efficiency is counterbalanced by the fact that biomass fuel is used instead of hydrocarbon fuel.

Table 6-7: Results of ORC based CHP unit seasonal simulation

Application	$\eta_{el,overall}$ [%]	$\eta_{th,overall}$ [%]	PES [%]
Low temperature	9	72.8	10.8
Medium temperature	8.9	72.8	10.5
High temperature	8.7	72.9	10.1
Very high temperature	8.6	72.9	9.7

5. Potentials improvements

Figure 6-9 shows that for the higher critical temperature fluids (n-hexanse, n-heptane and toluene), the isentropic efficiency is lower compared to other fluids. For all fluids, the isentropic efficiency decreases with the evaporating temperature while the ORC efficiency increases (see Figure 6-7). Thus, in order to detect which sources of losses affect the most the isentropic efficiency, Figure 6-14, Figure 6-15 and Figure 6-16 show the evolution of the different loss factors affecting the isentropic efficiency for isopentane, n-hexane an toluene respectively (see isentropic efficiency disaggregation in Chapter 2, equation (2-16)). For the three fluids, it can be seen that it is the under expansion and compression losses (represented by the theoretical isentropic efficiency) that affect the most the performances at high temperature. This is due to a too high fluid volume ratio compared to the built-in volume ratios. At low temperature, mechanical efficiency affects the most the performances. Indeed, when evaporating temperature is lower, indicated power is lower too but mechanical friction losses remain quite constant, leading to a decrease of the mechanical efficiency. These two phenomena show the trade-off that has to be made between low under expansion/compression losses and low mechanical efficiency. In order to decrease under expansion and compression losses, two possible geometrical changes are investigated separately: the reduction of the clearance factor and the increase of the stroke.

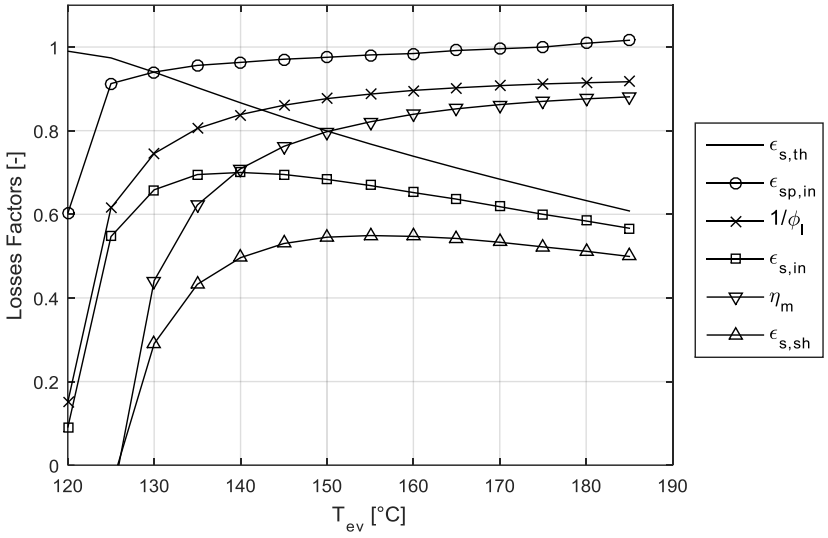

Figure 6-14: Evolution of the loss factors (isentropic efficiency disaggregation) in terms of the evaporating temperature for isopentane (detailed model simulation)

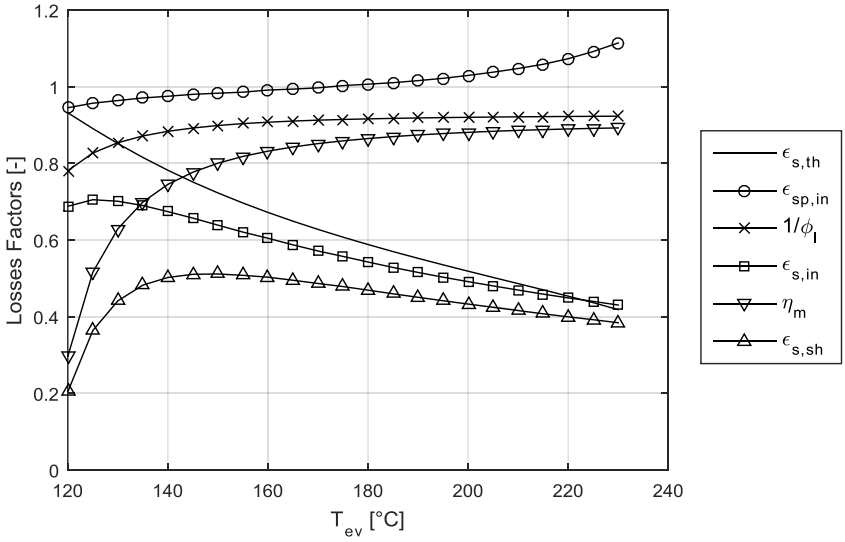

Figure 6-15: Evolution of the loss factors (isentropic efficiency disaggregation) in terms of the evaporating temperature for n-hexane (detailed model simulation)

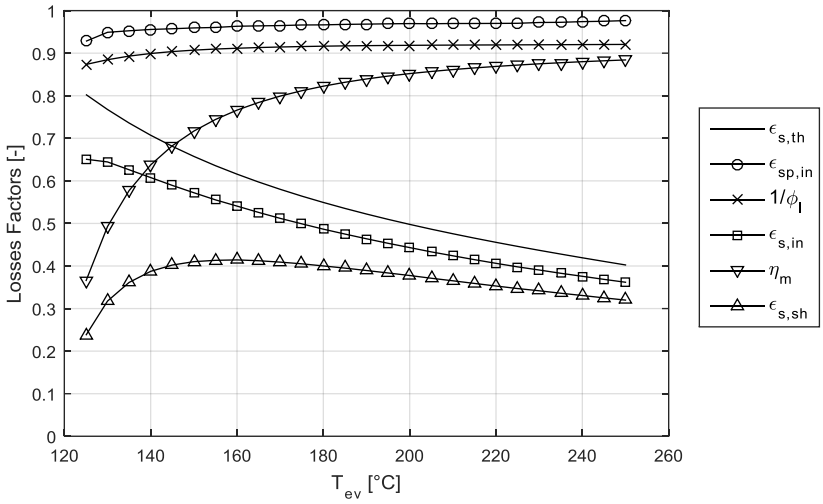

Figure 6-16: Evolution of the loss factors (isentropic efficiency disaggregation) in terms of the evaporating temperature for toluene (detailed model simulation)

5.1.Reduction of the clearance factor

In order to increase the built-in volume ratios (expansion and compression), the inlet closing volume can be decreased and the exhaust closing volume can be increased. However, even if these two volumes are respectively equal to the clearance volume and to the total volume (admission and exhaust occurring only during the equalization of the pressure), the gain in theoretical isentropic efficiency is very small (42% instead of 40% for toluene for example).

Another way to increase both built-in volume ratios is to reduce the clearance volume. Figure 6-17, Figure 6-18 and Figure 6-19 show the effect of such a reduction for isopentane, n-hexane and toluene for evaporating temperatures of 185°C, 230°C and 250°C respectively. It can be seen that a decrease of the mechanical efficiency and an increase of the leakage filling factor occur, reducing the positive effect of the clearance factor reduction on the under expansion and compression losses. Indeed, the mass flow rate and the indicated power decrease with the decrease of the clearance factor, increasing the impact of the leakages and the mechanical losses. These simulations show that a reduction of the clearance factor can lead to slight improvement of the shaft isentropic efficiency: 3% points for isopentane, 9% points for n-hexane and 7% points for toluene. With this improvement and considering a condensing temperature of 50°C, the ORC efficiency can reach values of 12%, 14% and 13.8% respectively (compared to 10.9%, 11.4% and 11.3%, see Table 6-4).

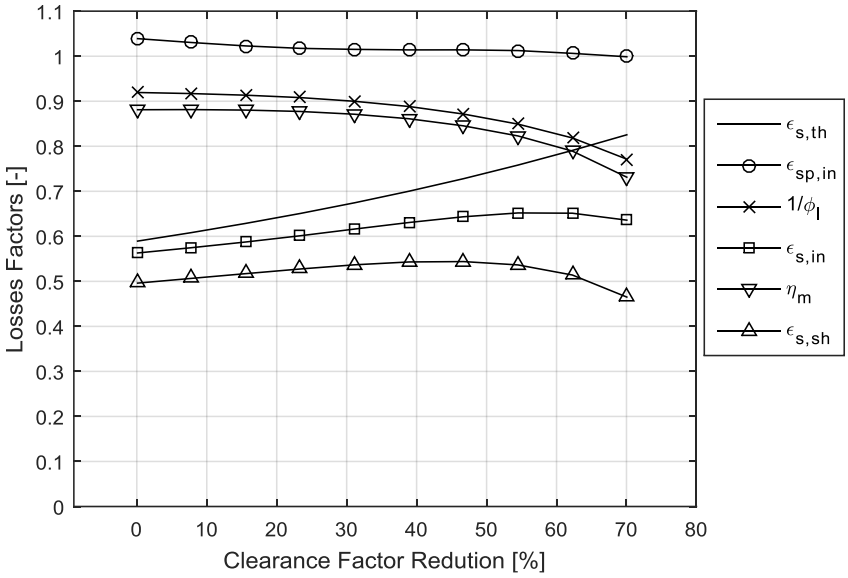

Figure 6-17: Evolution of the loss factors (isentropic efficiency disaggregation) in terms of the clearance factor reduction for isopentane (detailed model simulation)

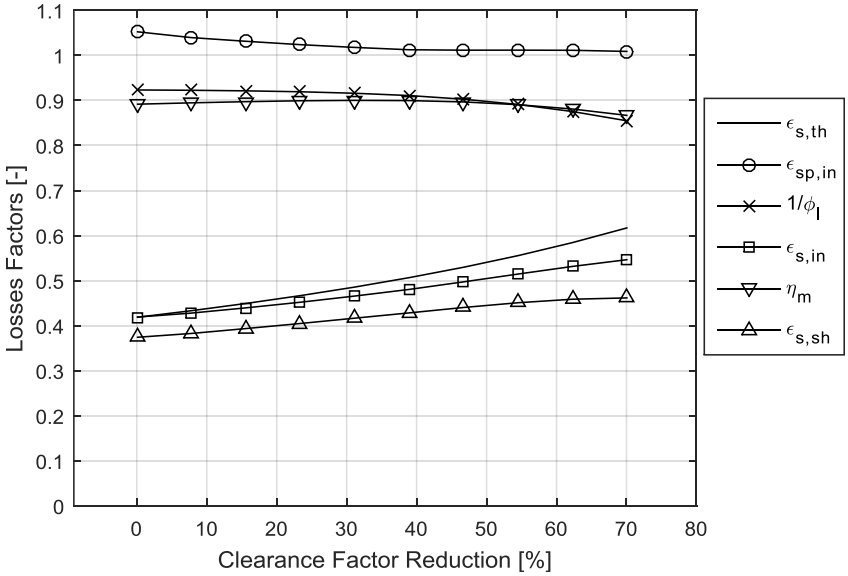

Figure 6-18: Evolution of the loss factors (isentropic efficiency disaggregation) in terms of the clearance factor reduction for n-hexane (detailed model simulation)

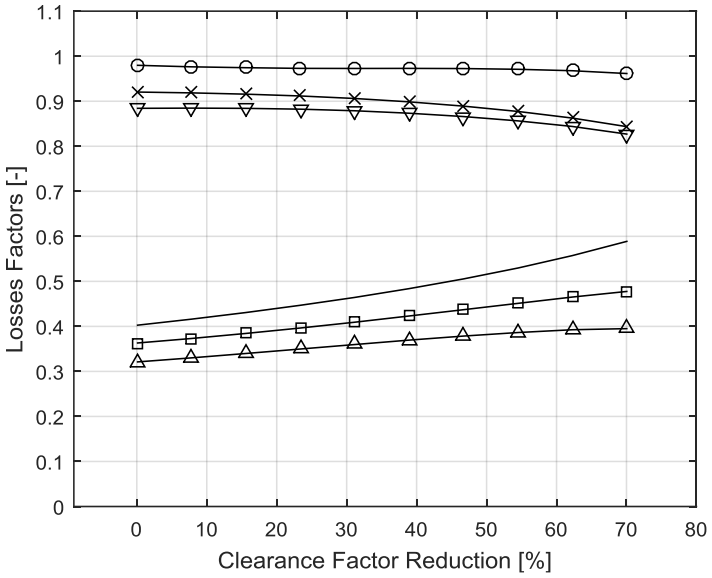

Figure 6-19: Evolution of the loss factors (isentropic efficiency disaggregation) in terms of the clearance factor reduction for toluene (detailed model simulation)

5.2.Increase in the piston stroke and speed optimization

The increase of the piston stroke, keeping the volumes V_{IC} and $V_{tot} - V_{EC}$ constant, also leads to an increase of the built-in volume ratios and then of the theoretical isentropic efficiency. But, the modification of the stroke leads also to a change in the total swept volume and mechanical losses. For the simulation results presented hereunder, it was assumed that the $fmep$ (computed with equation (5-10)) is constant, which is equivalent to consider mechanical losses proportional to the size of the expander.

5.2.1. Increase in the piston stroke at constant rotational speed

Figure 6-20, Figure 6-21 and Figure 6-22 show the simulation results of an increase in the stroke. Once again, it can be seen that a trade-off between theoretical isentropic efficiency and mechanical efficiency can be made and that the impact of leakages increases with the stroke as the internal mass flow rate decreases. This decrease in the mass flow rate is due to a higher re-compression rate as shown in Figure 6-23. This increase in the recompression rate also leads to a decrease in the indicated power. Finally, an increase of 4% points can be obtained for isopentane and 3% points can be obtained for n-hexane and toluene.

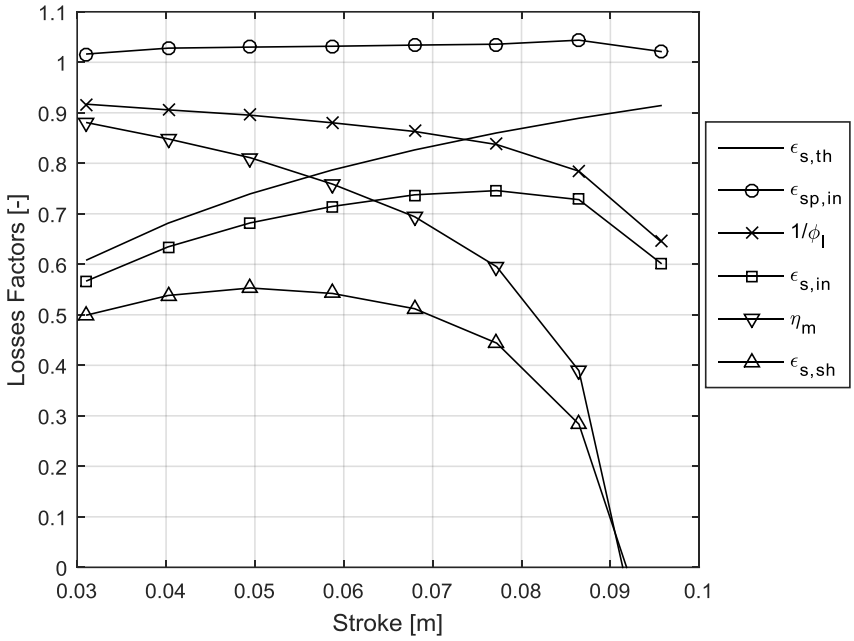

Figure 6-20: Evolution of the loss factors (isentropic efficiency disaggregation) in terms of the stroke for isopentane (detailed model simulation)

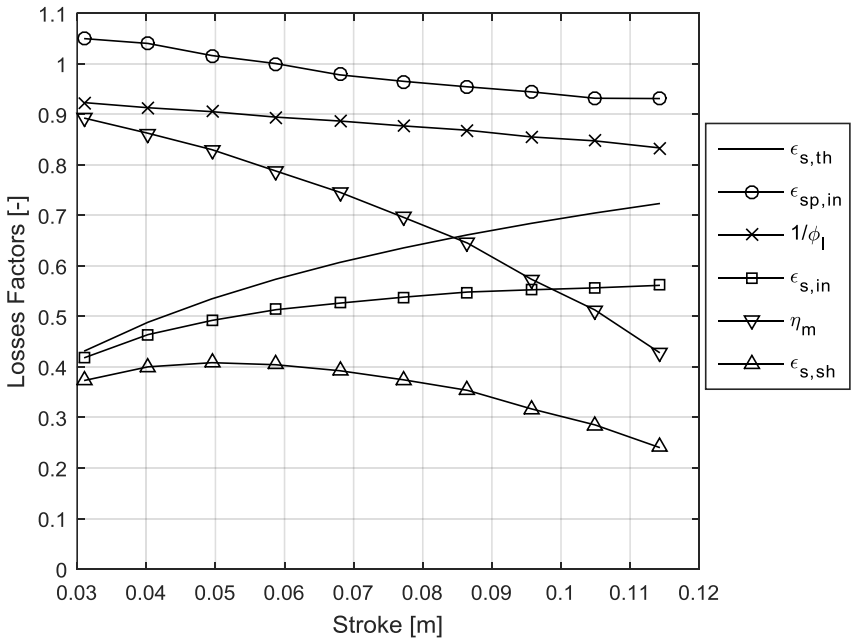

Figure 6-21: Evolution of the loss factors (isentropic efficiency disaggregation) in terms of the stroke for n-hexane (detailed model simulation)

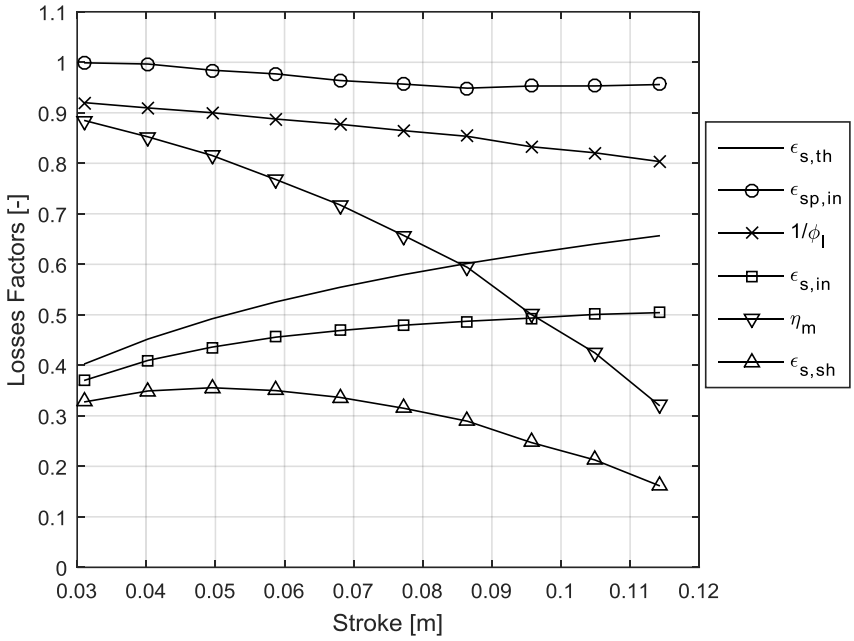

Figure 6-22: Evolution of the loss factors (isentropic efficiency disaggregation) in terms of the stroke for toluene (detailed model simulation)

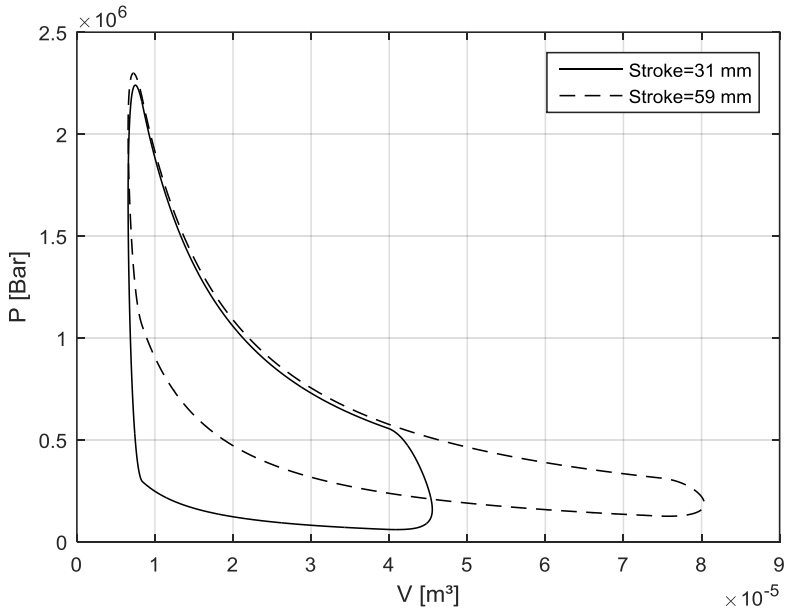

Figure 6-23: Indicator diagrams of n-Hexane for two different strokes

5.2.2. Optimisation in the rotational speed

As seen in Chapter 4 and 5, there is an optimal rotational speed that maximises the shaft isentropic efficiency. This optimum is due the increase in the mechanical losses and the decreases in the leakages with the speed that have antagonist effects. Therefore, a speed optimization can be made

for different strokes. By doing so, the results show that for each stroke, the optimal rotational speed gives the same mean piston speed (and thus, lower rotational speed as stroke increases). This result is illustrated at Figure 6-24 for toluene. With the optimization of the speed and the stroke, a gain of 5, 7 and 9% points can be obtained for isopentane, n-hexane and toluene respectively. With this improvement and considering a condensing temperature of 50°C, the ORC efficiency can reach values of 12.5%, 14.5% and 14.3% respectively (compared to 10.9%, 11.4% and 11.3%, see Table 6-4). It should be noted that with these modifications, the system is less compact as the power decreases with the stroke and the speed.

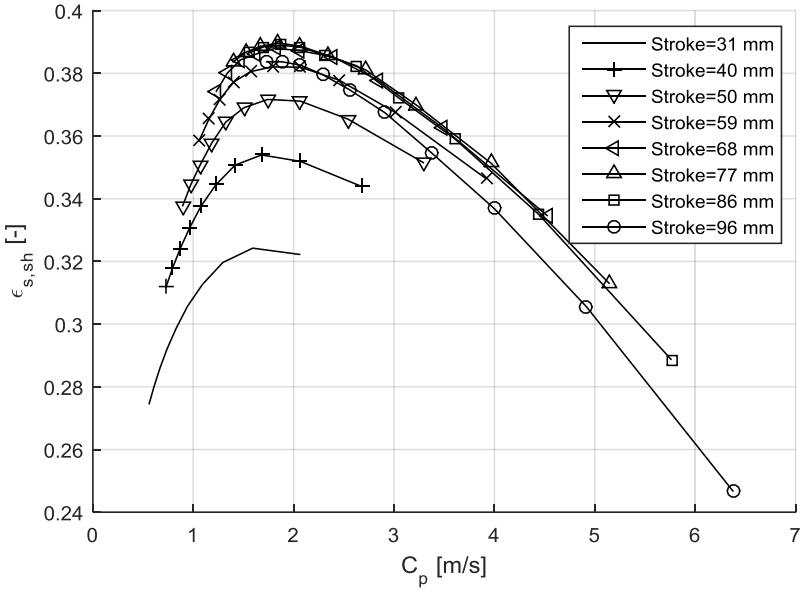

Figure 6-24: Shaft isentropic efficiency in term of mean piston speed for different strokes (toluene)

6. Conclusions

The actual prototype of Ericsson engine tested in Chapter 4 is not able to produce power. Nevertheless, some achievable improvements have been identified and simulated. These improvements are the reduction of the internal leakage flow rates, the attenuation of the supply pressure pulsations and the reduction of the cut-off. The use of a turbocharger in order to increase the power has also been investigated. The proposed Ericsson engine-based CHP unit uses a commercially available compressor in order to ensure best performance of this component. The expander considered is the modified engine tested in Chapter 4 but considering the three proposed improvements and considering that the whole six cylinders are used as expanders. A turbocharger with pressure ratio of 2 is used. Hot water is produced in the intercooler, the exhaust air heat exchanger and the expander cooling loop. This system shows electrical and thermal efficiencies of 6.5 % and 70.5 % respectively, an electrical power of 9.2 kW and allows the saving of 2 % of primary energy compared to separate production.

Then, a model of an ORC-based m-CHP unit has been developed by associating heat exchanger model and the validated model of piston expander. This model was used to optimize and size the system

and to perform seasonal simulations as the efficiency of the ORC varies with hot water temperature. These seasonal simulations were performed for an average European climate and four heat emitter heating curves according to the standard PrEN14825. The results show that the ORC efficiency varies from 9.2 % when producing hot water at 65°C to 11.2 % when producing hot water at 22°C. The system shows an overall electrical efficiency about 8.8% and a thermal efficiency about 73% without significant differences between the four heat emitter heating curves. The m-CHP system allows saving 10.3 % of primary energy compared to a separate production. Finally, potential improvements of the expanders were investigated for high critical temperature fluids. Indeed, these fluids offer the possibility to obtain good ORC efficiency but present high volume ratio and then low isentropic efficiency.

In order to reduce the under expansion and compression losses of the expander considered for the ORC system, the reduction of the clearance factor and the increase of the stroke were simulated. These simulations have shown that a trade-off can be made between, on one hand, low under expansion and compression losses and, on the other hand, high mechanical efficiency and low leakage filling factor. Indeed, by increasing both built-in volume ratios, mass flow rate and indicated power decrease, increasing the impact of leakages and mechanical losses. Moreover, when the stroke is increased, the mechanical losses rise. This trade-off shows that, even if piston expander built-in volume ratios can be high, the gain in performance is counterbalanced and the optimal built-in volume ratio is limited. Simulations have shown that by reducing the clearance factor of 70%, the ORC efficiency with n-hexane could reach a value of 14% instead of 11.4% (see Table 6-4). A value of 14.5% can be obtained by increasing the stroke from 31 mm to 86 mm with a rotational speed of 717 RPM. Finally, it has been shown that the optimal mean piston speed stays constant when the stroke varies.

By comparing the two systems, the ORC-based CHP unit shows the best performance even without improvement of the ORC piston expander while both have similar isentropic efficiency without improvement. Moreover, the Ericsson engine needs a heat exchanger that hold up 800 °C and 8 bar, which brings a technical drawback.

7. References

Andlauer, B., P. Stabat, D. Marchio, and B. Flament. 2010. “Multi-Objective Optimization Procedures for Sizing Operating Building-Integrated Micro-Cogenration Systems.” In *Proc. 8th International Conference on System in Buildings*. Liège, Belgium.

Aoun, B. 2008. “Micro Cogénération Pour Les Batiments Residentiels Fonctionnant Avec Des Energie Renouvelables.” PhD Thesis, France: Ecole des Mines de Paris.

Daoud, I. 2013. “Installer Une Cogénération Dans Votre Établissement.” Wallonie: DGTRE-Division de l’Energie.

De Paepe, M., and D. Mertens. 2007. “Combined Heat and Power in a Liberalised Energy Market.” *Energy Conversion and Management* 48 (9): 2542–55. doi:10.1016/j.enconman.2007.03.019.

European Commission. 2006. *Commission Decision of 21 December 2006 Establishing Harmonised Efficiency Reference Values for Separate Production of Electricity and Heat in Application of Directive 2004/8/EC of the European Parliament and of the Council*. Vol. OJ L 32, 6.2.2007.

Liu, H., G. Qiu, Y. Shao, F. Daminabo, and S. B. Riffat. 2010. “Preliminary Experimental Investigations of a Biomass-Fired Micro-Scale CHP with Organic Rankine Cycle.” *International Journal of Low-Carbon Technologies* 5 (2): 81–87. doi:10.1093/ijlct/ctq005.

Lombradi, K., V.I Ugursal, and I. Beausoleil-Morrison. 2008. “Performance and Emissions Testing of 1kWe Stirling Engine.” In *Proc. Micro-Cogeneration*. Ottawa.

McMahan, A. 2006. “Design & Optimization of Organic Rankine Cycle Solar-Thermal Powerplants.” PhD Thesis, University of Wisconsin-Madison.

Oudkerk, J.-F., S. Quoilin, S. Declaye, L. Guillaume, and V. Lemort. 2013. “Evaluation of the Energy Performance of an Organic Rankine Cycle-Based Micro Combined Heat and Power System Involving a Hermetic Scroll Expander.” *Journal of Engineering for Gas Turbines & Power* 135 (4). doi:10.1115/1.4023116.

Parois, A. 2001. “Suralimentation Des Moteurs de Véhicules Par Turbocompresseur.” BM 2 631. Techniques de l’Ingénieur.

Pulkrabek, W. 1997. *Engineering Fundamentals of the Internal Combustion Engine*. Prentice Hall. New Jersey.

Quoilin, S., S. Declaye, and V. Lemort. 2010. “Expansion Machine and Fluid Selection for the Organic Rankine Cycle.” In *Proc. 7th International Conference on Heat Transfer, Fluid Mechanics and Thermodynamics*. Antalya, Turkey.

Quoilin, S., V. Lemort, and J. Lebrun. 2010. “Experimental Study and Modeling of an Organic Rankine Cycle Using Scroll Expander.” *Applied Energy* 87 (4): 1260–68. doi:10.1016/j.apenergy.2009.06.026.

Simader, G., R. Krawinkler, and G. Trnka. 2006. “Micro CHP Systems: State-of-the-Art.” Deliverable 8 (D8). Green Lodges Project. Austrian Energy Agency.

Vittorini, D., G. Bianchi, and R. Cipollone. 2015. “Energy Saving Potential in Existing Volumetric Rotary Compressors.” *Energy Procedia* 81 (December): 1121–30. doi:10.1016/j.egypro.2015.12.137.

Chapter 7: Conclusion

The piston expander is one of the oldest expansion machines. It was already used in late 19th century in Brayton (Ericsson engine) and Rankine cycle heat engines, but has been replaced in such engines by turbines. However, this type of volumetric expander regains interest for few years for small scale (<50kW) decentralized power generation. Indeed, Ericsson engine and (O)RC offers, contrary to ICE engines, the possibility to use renewable heat sources such as biomass, solar, but also waste heat. Moreover, the ORC offers the possibility to use low temperature heat sources.

This work aimed at better characterizing this type of expander in order to improve its performance when used in Ericsson and ORC heat engines for CHP applications. The work methodology was based on modeling, simulation and experimental approaches.

Modeling

Two main kinds of model can be found in the literature. The first type describes the shaft angle (or time) evolution of the state of the fluid in the control volume limited by the cylinder. The second type of model is based on theoretical indicator diagram. In this work, both types of model have been proposed, denoted as “detailed” and “semi-empirical” models. In the detailed model, all sources of losses are described taking into account effects of main influent variables (e.g; with correlation) while other models found in the literature use simplification such as constant heat transfer or incompressible fluid (see Table 1 in Chapter 3). In the same way, the semi-empirical model describes all physical phenomena instead of using constant losses factors.

The advantage of the detailed model compared to the semi-empirical one is that it can be used as first approximation without calibration. Indeed, it is based on a detailed geometrical description and describes the actual indicator diagram. In the other hand, it requires more computational effort for similar results if both models are calibrated. Then, the semi empirical model is more suited for system level simulation.

First, the detailed model was used to evaluate potential performances of an Ericsson engine. Then, both models were validated with experimental results (from an ORC and Ericsson engines test benches). The detailed model was used for the losses analyses while the semi empirical model was used to simulate performances of the two different CHP systems (operating with the ORC and Ericsson engines, respectively).

Preliminary design and prototype development of an Ericsson engine

Simulation of an Ericsson engine was performed with the help of the detailed model. With this model, heat losses and pressure drop were taken into account but leakages were at this stage, wrongly, neglected. It has been shown that, for a given expander supply temperature, pressure ratio depends only on the ratio between the swept volumes of the expander and of compressor. An optimization of this ratio was then performed and optimal volume ratio of 2.2 (leading to a pressure

ratio of 5) was found to give the best efficiency. Expected efficiency, without considering leakages and mechanical losses, was 24%.

The investigated Ericsson engine prototype has been built from a commercially available ICE. The main modifications made to turn the ICE into an Ericsson engine were the change of the manifold, the design of a new camshaft and modification of the valves trains. This prototype has 6 cylinders, 2 used as compressor and 4 as expander. Each cylinder has a swept volume of 2 l. Unfortunately, the prototype did not run as expected and was not able to produce power. The reasons of this dysfunction are the too low temperature reached (450°C instead of 800°C), too high leakages and too high cut-off ratio. Indeed, these three features led to a decrease of the high pressure. The too low temperature was caused by a lack of heat transfer in the electrical heater. High leakage rate is due to unsuited valves. Indeed, the ICE valves were not changed while the pressure gradient is inverted for high-pressure valves. Finally, the too large cut-off is due to a non-adapted camshaft design. Nevertheless, the engine was tested with an extra compressor allowing to reach pressure up to 7 bar in order to characterize the expander with the methodology explained below.

Experimental work

In order to evaluate real performance of piston expander, two experimental campaigns were performed on two different piston machines. The first campaign was performed on the Ericsson engine prototype while the second one concerns a swash-plate piston expander integrated into an ORC.

For both experimental campaigns, the same methodology was applied to characterize the piston expanders. First, measurements over a wide range of operating conditions were collected. These measurements include at least: supply and exhaust temperatures and pressure, mass flow rate, rotational speed, mechanical or electrical power and in-cylinder pressure. Quality of the measurements is then evaluated through a statistical method based on Gaussian regression allowing to detect outliers and uncertainties calculation of variables depending on measurement. If redundancies measurements are available, reconciliation method can also be applied in order to assess the quality and coherence of the measures. Once measurements have been collected and assessed, they were used to perform a losses analysis based on the isentropic efficiency disaggregation. Theoretical isentropic efficiency (accounting for under/over expansion and compression) is simply evaluated knowing the geometry of the engine and the operating conditions. Measurement of the in-cylinder pressure was used to draw indicator diagram and determine indicated power and then indicated isentropic efficiency while measure of the mechanical power was used to compute shaft isentropic efficiency. The comparison of the indicated mechanical power gives the mechanical efficiency and correlations to compute mechanical friction power in terms of rotational speed and supply pressure have been proposed. Finally, these measurements allowed to compute diagram and filling factor. But, in order to complete the disaggregation, the leakage and internal filling factor had to be evaluated. As no efficient way to measure the leakage flows was available, this evaluation was carried out by model simulations. Therefore, a calibration process has been proposed and applied to calibrate the detailed model. Once the model has been calibrated, it was used to determine leakage filling factor and specific diagram factor and then, to complete the losses analyses. The last factor, the specific diagram filling factor was defined by the authors in this

thesis and allows to quantify the impact of pressure drops and heat transfer on the isentropic efficiency.

The first investigated piston expander is the Ericsson engine expander. This expander is an 8000 cm^3 four-cylinder engine using a crank mechanism. It was tested with pressure ratio ranging from 2 to 5 and rotational speed from 300 RPM to 900 RPM.

The second piston expander is a 195 cm^3, five-cylinder machine using a swash-plate mechanism. This expansion device was integrated into an ORC system using R245fa as working fluid. It was tested for pressure ratio ranging from 7 to 12 bar and rotational speed from 1000 RPM to 4000 RPM.

Table 1 shows a comparison of the two investigated piston expanders considering the point that maximize the shaft isentropic efficiency. First, the large difference between total swept volumes should be noted, the Ericsson expander being 40 times larger. Optimal operating conditions (rotational speed, and pressure levels) are also different. Then, it can be seen that the Ericsson expander shows a slightly better isentropic efficiency. This difference is due to a better theoretical isentropic efficiency. Indeed, the Ericsson engine has a very small clearance factor leading to small under compression losses. Otherwise, the swash plate piston expander seems less affected by pressure drops and leakages as it has higher specific diagram factor and lower leakage filling factor. Finally, Ericsson engine expander has better mechanical efficiency but is less compact. The better compactness of the swash plate is mainly due to its higher optimal rotational speed.

Simulation of CHP applications

The validated semi-empirical model was used to simulate two m-CHP systems, one using the prototype of the Ericsson engine, but with the whole six cylinders used as expander, and the other the swash-plate expander integrated into an ORC.

For the Ericsson engine system, potential improvements were investigated as the prototype did not run as expected. The first one would consist in using a commercially available compressor in order to ensure to have the best performances of this component and in using the turbocharger in order to increase the power. Then three potential improvements of the expander were considered: reduction of the supply manifold pressure pulsations, smaller cut-off ratio and decrease of the leakages. With all these improvements, the optimal pressure ratio found is 4.2, the electrical and thermal powers are 9.2 kW and 95 kW while the electrical and thermal efficiencies are 6.5% and 70.5%. This m-CHP unit allows to save only 2% of primary energy compared to a separate production.

For the ORC system, first a fluid selection was performed and resulted in the selection of isopentane to maximize the efficiency of the cycle using the swash-plate expander. The evaporating temperature has been optimized and a value of 187°C was found. Then, as the ORC efficiency depends on the condensing temperature, varying with the hot water temperature, a seasonal simulation was performed to take into account heat emitters heating curves influences. Results show that this system is able to produce 3.3 kW of electrical power and 24 kW of thermal power with overall efficiencies of 8.2% and 73 respectively allowing to save 9% of primary energy. Fluid selection has shown that fluids with higher critical temperatures could offer better ORC efficiencies but show lower isentropic efficiencies. Simulations have shown that these low efficiencies are principally due high fluid volume ratios and then low theoretical isentropic efficiencies (high under expansion and

compression losses). Therefore, the impact of an increase of both built-in volume ratios was investigated with the detailed model. The existence of trade-off between high built-in volume ratio and high mechanical efficiency has been shown. This trade-off limits the optimal built-in volume ratio which can be theoretically higher.

Table 1: Comparison between the two investigated piston expander at optimal (maximal shaft isentropic efficiency) operating conditions (rotational speed, pressure ratio and supply pressure) *

	Ericsson engine expander	Swash plate expander integrated into an ORC
Total swept volume	8000 cm³	195 cm³
Optimal rotational speed	600 RPM	2500 RPM
Optimal mean piston speed	3 m/s	2.6 m/s
Optimal pressure ratio	4.5	10.5
Optimal supply pressure	5	21
$\epsilon_{s,sh}$	59%**	54 ±0.6 %
$\epsilon_{s,in}$	67±0.9 %	66 ±1 %
$\epsilon_{s,th}$	89±0.1 %	78±0.3 %
$\epsilon_{sp,in}$	89%	92%
$\frac{1}{\phi_l}$	84%	91%
η_m	88%**	82 ±0.8 %
C_{ness}	2 kW/l **	9.8 ± 0.03 kW/l
$imep$	2.25±0.01 bar	2.9±0.07 bar
$fmep$	0.28 bar **	0.51±0.03 bar

* Underlined values are computed with the help of the calibrated detailed model.

** Values computed with the hypothesis made in Section 5.3.2 of the Chapter 4 i.e. considering the mechanical losses of the Ericsson engine but assuming that all the six cylinders work as an expander.

Perspectives

The detailed simulation model validation process has shown that it can be used to a first estimation of the performance of piston expanders using usual flow coefficient values (between about 0.8 and 0.6). Nevertheless, it was also shown that leakages are difficult to quantify without experimental data while they have a strong impact on the performances. Then, leakage modeling and prediction should be more investigated.

The parameters of the semi-empirical model cannot be directly set for a given expander (while the detailed model is based on detailed geometrical description). However, once calibrated, this model

gives as good results then the detailed one and is more suited for system simulation. A methodology to find these lumped parameters without calibration would then be useful for prospective works.

While the Ericsson engine did not work as expected, the feasibility to turn an available ICE into a piston expander is proven. This expander has comparable performance to the dedicated swash-plate prototype and some potential improvements are possible. Then, production of piston expanders built from ICE can be envisaged, allowing the development effort and production cost to be reduced.

The evaluation of the performance of an ORC-based m-CHP system has shown that this system has low electrical efficiency compared to ICE or fuel cell based m-CHP. But, in the other hand, the ORC system offers the possibility to use alternatives heat sources such as biomass, counterbalancing this low efficiency. Futures works should investigate the entire system with biomass boiler in order to better evaluate environmental and economic profitability of such a system.